Engineering Models of Aircraft Propellers at Incidence

Harry Redgrave Smith

Submitted in partial fulfilment of the requirements for the
Degree of Doctor of Philosophy

Aerospace Sciences Research Division
School of Engineering
College of Science and Engineering
University of Glasgow

January 2015

"The literature of propeller aerodynamics is scattered and in some respects is inconsistent and incomplete."

– Quentin Wald (2006)

PREFACE

This dissertation presents work carried out by the author in the Aerospace Sciences Research Division at the University of Glasgow in the period from March 2011 to September 2014, supervised by Dr. Eric Gillies and Dr. Richard Green. The work is part of an EPSRC CASE Ph.D. studentship between the University of Glasgow, the Engineering and Physical Sciences Research Council (EPSRC), Dowty Propellers (GE Aviation) and the Aircraft Research Association (ARA). Industrial supervision has been provided by Dr. Josef Trchalík and Dr. Angela Knepper (GE Aviation) and Mr. Peter Wong (ARA). The content is original except where otherwise stated.

ACKNOWLEDGEMENTS

I would like to extend my deepest gratitude to my academic supervisor, Dr. Eric Gillies, for his continued hard work and patience throughout my doctoral studies. He's taught me how to be a worthy aerodynamicist and all-round scientist with integrity - and he's pulled me out of a few research 'flat spins' with a dram or two along the way. I wouldn't have made it anywhere near this far without his guidance. My sincere gratitude is also due to Dr. Richard Green for his input throughout my work - and for his undergraduate lectures on propeller aerodynamics, which put me in excellent stead for this project. A big thank you is also due to Dr. Stewart Houston for his patience when helping me to understand inflow (particularly dynamic inflow!).

My viva voce was challenging but fair, and I'm proud to have gotten through the four-and-bit hours. Thank you to Dr. Douglas Thomson for his role as the internal examiner, with fair criticism of my work. Thank you also to the external examiner, Mr. Allan Bocci for significantly more criticism (still fair, though!), and for helping me steer this work towards the version printed today. In addition, thank you to Dr. Marco Vezza for his hard work at my viva to keep things on track and stopping Allan and I from getting lost in technical debate.

Dr. Josef Trchalík, Dr. Angela Knepper and Mr. Paul Methven at Dowty Propellers have been integral to the success of this project - without their support, the project wouldn't have been possible. Thank you, also, to Mr. John Dunn at Dowty for pushing the dissertation through review! Mr. Peter Wong at ARA has provided support and guidance along the way - and eagerly took on the role of industrial supervisor at short notice. I would like to express my appreciation for the support all four have provided, and to take the opportunity to formally say 'thank you' here.

My colleagues in the Aerospace Sciences Research Division have helped provide a productive research environment, and provided engaging conversation (and entertainment!) along the way. A big thank you is due to many other staff members within the division for help with niche questions - too many to name here.

Thank you to all my friends for your continued support along the way - you know who you are, and I'll always remember what you've done. Also, my heartfelt thank you to my family who have supported me along the way. Thank you, Katy, for always being supportive and thank you, Grandad, for the bookstand you made - I use it every day and hope I always will.

Particularly, I am sincerely grateful to my parents who have always supported me, and let me live at home whilst writing up. Thank you Mum for always understanding. Thank you to my father, for his diligent proofreading (he loved the word 'vorticity') and for refraining from asking '*have you figured it out yet?*' as much as possible. Thank you, Dad.

To my parents, and to Kaya.

ABSTRACT

Aircraft propellers in any flight condition other than pure axial flight are subject to an incident flowfield that gives rise to time-varying forces. Means of modelling these time-dependent forces have been presented in the literature, to varying degrees of success - but a review of the different models is missing, and there is a need for an instructive means of simulation using physically realistic but computationally light methodologies. This dissertation provides a comprehensive overview of the relevant work to date, in addition to providing a logical framework in which the problem of propeller blade cyclic load variation may be assessed. Through this framework, the importance of different aerodynamic features pertinent to this problem are compared, and a new solution methodology based on adaptations of existing models is presented. This research project was commissioned by Dowty Propellers (DP), who chose Glasgow University and the supervisors for their rotorcraft simulation experience.

Prediction of the propeller induced flowfield is shown to be of importance for the calculation of blade cyclic loads. Momentum models are fit for purpose owing to relative computational simplicity - this dissertation suggests a new radially-weighted implementation of momentum theory that provides better correlation with wind tunnel data than existing models.

Swept propeller blades are discussed and the inherent problems faced by a designer or performance engineer are highlighted. An Euler transform to resolve velocities and forces between disc and blade element axes is presented, along with the assertion that 'simple' sweep correction methods can be deleterious to propeller aerodynamic simulation if used naïvely. Fundamentally, representation of a swept propeller blade by a blade element model is described as wholly more problematic than a straight propeller blade owing to the displacement of blade elements with respect to the blade pitch change axis - and that flow information will always be lost with such a representation.

Installation effects are simulated and installed load fluctuations are predicted to a reasonable degree of accuracy compared to what little data is available. Different means of resolving installation velocities to disc and, subsequently, blade element axes are compared, and it is shown that representing installation effects by an effective incidence angle as is 'standard practice' will most likely underpredict installed load fluctuation.

In addition to a varying blade root bending load caused directly by load fluctuation on a propeller at an angle of incidence, the reacted net loads at a propeller hub may include a constant yawing moment and in-plane force. This in-plane force has been well documented in the literature, but the equations for its calculation may miss a component of force due to a tilting of the blade tangential force. New equations for this additional force term are presented that validate well to legacy experimental data.

CONTENTS

LIST OF FIGURES

LIST OF TABLES

Nomenclature

Abbreviations

AMT/DMT/WMT	(Annular/Differential/Weighted) Momentum Theory
BE	Blade Element
BEMT	Blade Element Momentum Theory
CCW	Counter-Clockwise
CFD	Computational Fluid Dynamics
CW	Clockwise
DP	Dowty Propellers
ESDU	Engineering Sciences Data Unit
GDW	Generalised Dynamic Wake
IDE	Integrated Development Framework
LDV/A	Laser Doppler Velocimetry/Anemometry
NACA	National Advisory Committee for Aeronautics
NASA	National Aeronautics and Space Administration
ODE	Ordinary Differential Equation
PCA	Pitch Change Axis
PIV	Particle Image Velocimetry
PSP	Pressure Sensitive Paint
QS	Quasi-Steady
RPM	Revolutions Per Minute
URANS	Unsteady Reynolds-Averaged Navier-Stokes
US	Unsteady
VLM	Vortex Lattice Method
wrt	with respect to

Greek Symbols

α_R	Resultant blade element AoA $\triangleq \beta - \phi$
β	Blade setting angle - wrt disc plane $\triangleq \beta_{tw} + \beta_0$
β_0	Blade root setting angle
$\beta_{.7}$	Blade setting angle as defined at $0.7R$
β_{tw}	Blade structural twist angle
$\delta\psi$	BE azimuthal shift due to sweep
ϵ	Upwash angle into propeller disc
γ	Propeller disc inclination angle wrt freestream
κ	BE dihedral angle
Λ	Blade element sweep angle - definition dependent on context
Ω	Rotational speed - RPM
ω	Angular frequency - rad/s
ψ	Azimuthal angle on propeller/rotor disc.
ψ'	Effective azimuthal angle - based on the projection of blade quarter-chord in the disc plane
σ	Solidity $\triangleq \frac{Bc}{2\pi r}$
τ	Sidewash angle
θ	Angle between projection of two points in disc plane in Appendix B
θ	BE built-in twist in Appendix B

Roman Symbols

$()'$	Fluctuating component, Chapter 6.
$\bar{x}$	BE mid-chord position in lead/lag direction
$\bar{z}$	BE mid-chord position out of disc plane
$\overline{()}$	Mean component, Chapter 6.
a_ω	Tangential induction factor $\triangleq \frac{v_t}{V_\infty}$
a_a	Axial induction factor $\triangleq \frac{v_a}{V_\infty}$
B	Number of blades
c	Blade chord.
C_Q	Torque coefficient $\triangleq \frac{Q}{\rho n^2 D^5}$
C_T	Thrust coefficient $\triangleq \frac{T}{\rho n^2 D^4}$

D	Propeller diameter
dC'_T	Radial thrust coefficient gradient $\triangleq \frac{dC_T}{dx}$
$\hat{J}$	Normal advance ratio $\triangleq J \cdot \cos\gamma$
J	Advance ratio $\triangleq \frac{V}{n \cdot D}$
k	Reduced frequency $\triangleq \frac{\omega_f c}{2V}$
L_{QS}	Quasi-steady lift, Theodorsen.
L_{US}	Unsteady lift, Theodorsen.
n	Rotational frequency - rev/s
R_e	Effective blade radius (Prandtl)
V_ω	Blade element rotational velocity $\triangleq \omega \cdot r$.
V_p	Incident velocity normal to blade PCA.
V_R	Resultant blade element velocity
V_T	Blade total tangential velocity $\triangleq \omega \cdot r + V_p$.
x	Nondimensional radial ordinate $\triangleq \frac{r}{R}$.
$\begin{bmatrix} U_B \\ V_B \\ Z_B \end{bmatrix}$	Velocity field in blade axes, see Equation 2.7 on page 44
$\begin{bmatrix} U_D \\ V_D \\ Z_D \end{bmatrix}$	Velocity field in disc axes, see Figure 2.1 on page 38

CHAPTER 1

INTRODUCTION

Aircraft propellers have been in use since the birth of powered aviation, and continue to be utilised on both contemporary aircraft and conceptual future designs. Fossil fuels are running out and becoming more expensive, and there is an increased awareness of environmental responsibilities for big industry. The efficiency gains that aircraft propellers have over turbofans mean that they are being re-explored by aircraft manufacturers - they can potentially provide the abilities that consumers have come to expect at a reduced cost, both in fiscal and environmental terms.

The theory and methodology used for engineering-level design and aerodynamic simulation has remained largely unchanged since 'Theory of Propellers' (Theodorsen, 1948) - published forty-five years *after* the birth of powered aviation, but still closer in time to that day at Kitty Hawk than to the present day. Figure 1.1, overleaf, shows the significant milestones in propeller aerodynamic theory. At the time of Theodorsen, the typical propeller planform was similar to that of the propeller on the Wright Flyer - straight, rectangular and with two to four blades.

Modern propellers have a greater number of blades with more complex geometries and look far removed from the paddle-type propeller on the Wright Flyer. Modern blades are slender, highly twisted and incorporate sweep, dihedral and variable pitch. Efficiency gains may be made by adjusting the aerodynamic properties of the blade, and by making them more slender and reducing weight. In order for this to be feasible, though, they need to be designed to cope with any forces liable to arise in a flight. The flight environment of a modern propeller blade is also far removed from the propellers of early aircraft - with rotational speeds of thousands of revolutions per minute (RPM), and high angle of attack (AoA) flight (*e.g.,* see Figure 1.2), a propeller blade on a modern aircraft may be

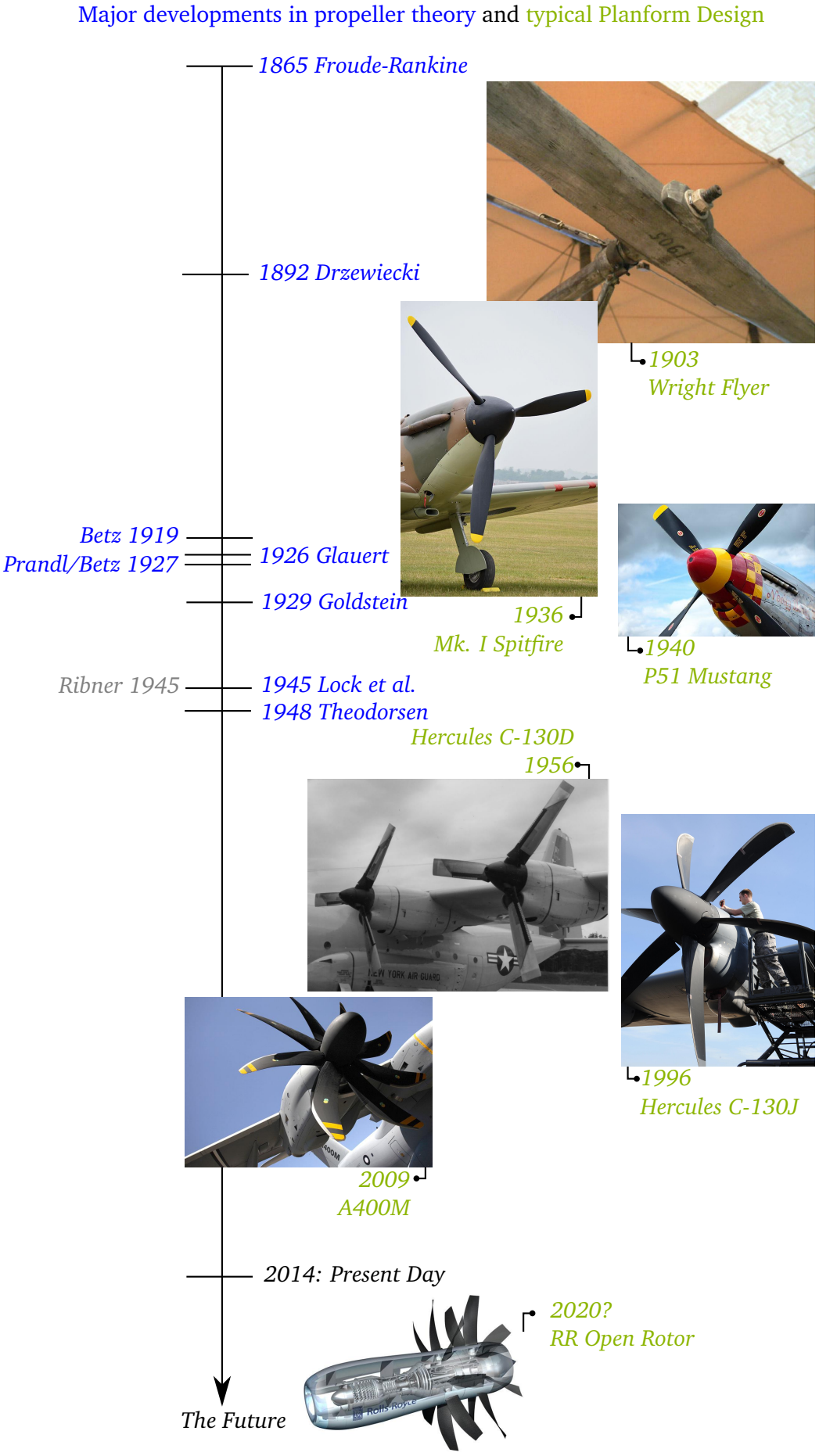

FIGURE 1.1: SIGNIFICANT MILESTONES IN PROPELLER AERODYNAMIC THEORY AND CHANGES TO TYPICAL PLANFORM DESIGN IN PAST 150 YEARS.

FIGURE 1.2: C-27J SPARTAN AT NONZERO ANGLE OF ATTACK

subject to large local aerodynamic perturbations within a single revolution. With any local aerodynamic changes comes a local force change, and this means that the load on a propeller blade may be *cyclic*, and hence oscillating hundreds of thousands of times for any flight. Figure 1.2 shows a propeller-driven aircraft at nonzero angle of attack. An exaggeration of this flight regime at the propeller plane is shown in Figure 1.3 - **the key aspect is that for non-axial flight, the incident velocity and the thrust axis are not coaxial**. There is an in-plane velocity, V_p - this is summed with the velocity due to blade motion to determine the total effective velocity at a propeller blade. The downgoing and upgoing blades will have the in-plane velocity added and subtracted from their tangential velocity, respectively.

Chiefly, **the disc-normal velocity, V_n, is effected equally at every azimuthal position, whilst the in-plane velocity, V_p, is not - this gives rise to an aerodynamic environment on the blades that changes with azimuthal position**. For a typical propeller aircraft, high AoA flight is common during take-off and landing. During these regimes, however, the forward velocity is small and so the in-plane velocity is small compared to the tangential velocity due to blade rotation. For this reason, it must be possible to determine where the greatest load fluctuation is likely to occur - this may not be at the greatest angle of attack, but where the aircraft flight conditions have the greatest total effect on local blade aerodynamics. *i.e., at high advance ratio, a small angle of attack may lead to a greater propeller blade load fluctuation than a high aircraft angle of attack at low advance ratio flight.*

With any change to blade aerodynamic loads, the *stress* on the blades is changed, and thus so is the structural response - the *strain* in the blades materials.

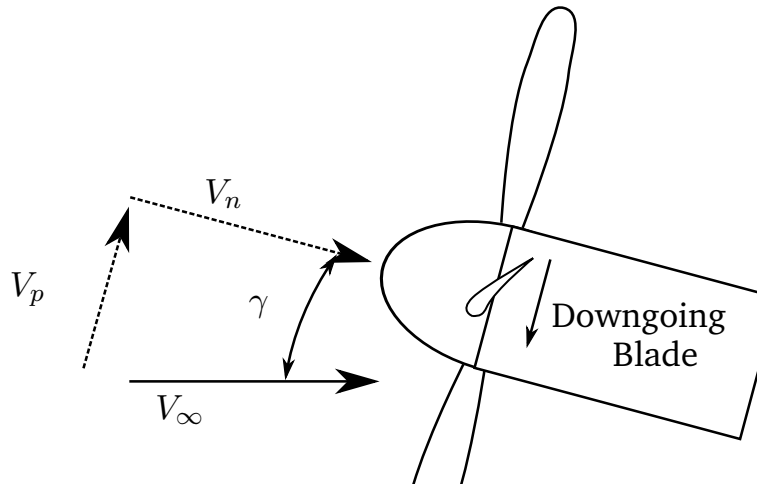

FIGURE 1.3: REPRESENTATIVE FLIGHT ENVIRONMENT AT PROPELLER DISC PLANE ON AIRCRAFT AT INCIDENCE

Materials subject to time-varying strain suffer fatigue damage due to repeated loading/unloading, and this can have disastrous consequences as demonstrated by the Comet aircraft. Clearly the fluctuating loads need to be predicted so blades can be designed to withstand them and so service intervals can be set. Whilst for axial flight the means of determining the aerodynamic forces has been reasonably well-established through the 1940's-1950's, an instructive means of determining the variation of force on the blades of a propeller subject to a non axial incident flow is less clear. Different approaches to this problem have been used and discussed in the literature, but the assumptions and validity of different methods have not been compared and contrasted, to this author's knowledge - hence that comparison shall be part of the contribution of this dissertation to the wider literature. In recent years flow phenomena on aircraft propellers at an angle of incidence have been explored using Reynolds-Averaged Navier-Stokes Computational Fluid Dynamics (RANS CFD), and these works are discussed in the literature survey. Whilst these methods are useful for investigation of detailed flow physics, simpler methods are needed at the design stage and for routine performance calculations. Computational complexity will be of paramount importance in this dissertation - the computational power needed for many higher order methods is several orders of magnitude above that available to the average designer[1]. For this reason, a range of calculation methods that have been used in both propeller and rotorcraft fields will be explored. Each methods' applicability to this problem will be discussed.

To elaborate on the computational cost aspect, the likely use of any industrial code will be briefly explained here. The periodic loading a blade will be subject to for a given portion of an aircraft's flight will be of interest for industry during the design phase - *i.e.,* a designer will need to determine likely load cycle

[1]For the foreseeable future at the time of writing.

stresses for any given configuration in order to ensure that a production blade will be strong enough. In addition, a rotary aerodynamicist or performance engineer will likely want to perform routine performance calculations, including 1P load determination, on an in-service propeller. That is, for a given aircraft in some configuration and attitude, it will be necessary to be able to determine the forces and moments the blades of a propeller are subject to within each revolution - *i.e., cyclic* or *fluctuating* stresses. For a comprehensive analysis, such work requires individual calculations for a given aircraft attitude and velocity to be performed many times for a given aircraft flight. Whilst some mid-level computation methods (*e.g.,* Euler/Panel codes) can produce results in less than an hour, it is the necessity for repeat calculations that sets a strict limitation on the computational cost of any design-level code.

This dissertation focusses on *once-per-revolution*, or 1P-loading. These loads are defined as having a single fluctuation with the azimuthal position of the rotor, and may be caused by non-axial velocity perturbations at the propeller disc. The physics behind 1P loading and why they have been focussed on instead of higher-harmonic loading is discussed in Chapter 2.

1.1 LITERATURE REVIEW

The timeline of key discoveries in propeller aerodynamics that are relevant to this dissertation is given in the timeline in Figure 1.4, overleaf. This figure is not intended to be a comprehensive overview of *all* propeller literature, instead it is aimed to chronologically display the sources that have been particularly useful in the writing of this dissertation. The last major propeller-specific publication which was arguably Theodorsen's in 1948, which was published closer to the birth of powered aviation than to the present day. There have been recent developments and new applications of existing theory for propellers at incidence, but a review of the different models used for such analysis and a discussion of the assumptions made between different techniques is missing from the literature. The literature review presented over the following section aims to provide that critical review.

More recent developments for simulations of propellers at incidence tend to be using higher-order models, and there appears to be a lack of a suitable engineering-level model for load determination. Owing to the similarity of the flight environment of the blades of a propeller at an angle of incidence to helicopter rotor blades in forward flight, or wind turbine blades in skewed incident flow, this dissertation has borrowed theory from across the entire field of rotary aerodynamics, and has not solely used propeller-based literature.

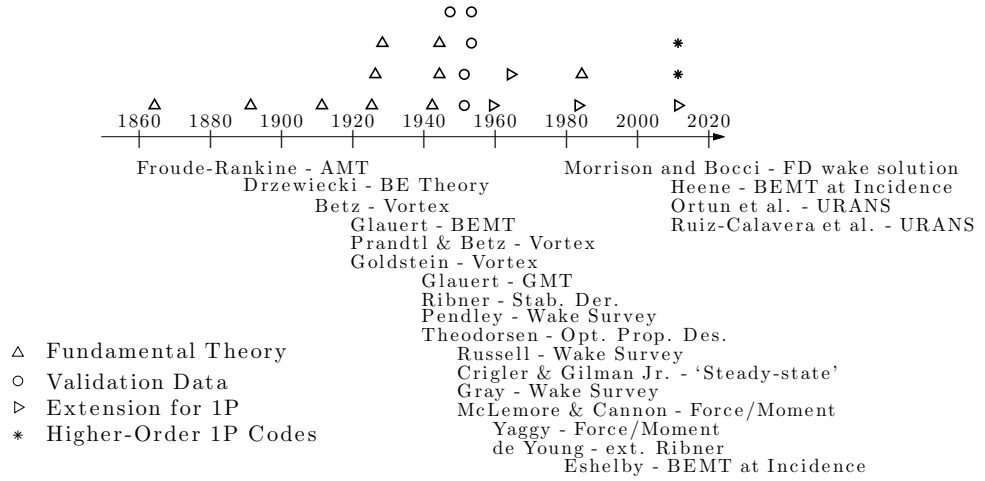

FIGURE 1.4: TIMELINE OF KEY PROPELLER DEVELOPMENTS RELEVANT TO THIS DISSERTATION

Whilst literature on the aerodynamics of propellers at an angle of incidence is demonstrably lacking - literature regarding propellers in axial flight (*i.e., at zero incidence*) has also been described as 'scattered', 'inconsistent' and 'incomplete' (Wald, 2006). Another field of rotary aerodynamics, helicopter theory, has been developed almost in parallel with propeller theory and is relatively well-documented with a myriad of textbooks devoted to the subject. Helicopters may be seen as an offshoot of the early autogyros - though autogyros are conceptually more removed from propellers than helicopter rotors. The same theorists worked on problems in both fields of rotary aerodynamics, but helicopter and propeller aerodynamics have developed into separate fields with different methods and nomenclature (Prouty, 2009). Since there has been relatively little comparison between the fields of propeller and helicopter aerodynamics, despite the similarities, this dissertation shall serve as a comparison in places and provide a discussion of which modelling techniques may be utilised between both fields, and which may not.

Propellers and helicopter rotors serve fundamentally different purposes - a rotor is designed to provide lift, thrust and control whilst a propeller is designed to provide thrust alone. A helicopter rotor, by nature, is more likely to spend a portion of any given flight with a large component of in-plane freestream velocity - else a helicopter is constrained to little other than vertical take-off, hover and landing. A propeller, by comparison, is designed to thrust in the axial flight direction and in-plane components of freestream velocity are likely to be much smaller than the component in the axial direction.

Both the physical geometry of the blades, and the ways in which they are arrange and operate can be significantly different between propeller blades and helicopter rotor blades;

- Propeller blades tend to have larger chord at the root with taper towards the tip. Rotor blades tend to have near constant spanwise chord.
- The thickness of propeller blades can vary from 30% in the root, to 3% at the tip. The thickness of rotor blades tends to be more constant.
- Propeller blades are usually highly twisted, with 40-50° of twist from root to tip being common. The twist of propeller blades can often be non-linear, whereas the twist of rotor blades is usually lesser over the span and linear in variation.
- Modern propellers are usually variable-pitch, with thrust/power controlled by pitch for a constant motor RPM[2]. Rotor blades have both collective and cyclic pitch control, enabling control but also forcing a 1P load variation.
- Propeller blades are almost universally hingeless and very stiff. Rotor blades have flapping/lagging degrees of freedom (out of plane and in-plane, respectively), or are designed to be flexible enough to allow effective flapping/lagging.

Care has been taken in the writing of this dissertation not to draw too many parallels with the propeller and rotor fields of rotary aerodynamics - but it should be self evident that there are clear aerodynamic similarities between the two disciplines. Unaddressed load fluctuations on propeller blades can cause issues with blade longevity and blades can simply be designed *stronger*. Unaddressed load fluctuations on helicopter blades, however, can have fatal consequences. It is perhaps the inherent criticality of the rotor system vs. the propeller system that has provided the impetus for helicopter research into a range of suitable models for edgewise flight. Moreover it is likely a combination of the criticality and the fact that edgewise flight is of fundamental importance for a useful helicopter. Because of these considerations, helicopter theory has a range of models and nomenclature that serve use in this dissertation, though the focus in this work is on propeller blades. For example - traditionally, laterally opposing propeller blades are distinguished in discussion by the terms ‘upgoing’ and ‘downgoing’, but these terms are not descriptive of the aerodynamic phenomena key to load fluctuations on a propeller at an angle of incidence. The ‘advancing/retreating’ distinction is common in use for discussion of helicopter forward flight, and will be used in this dissertation - defined in Chapter 2. Throughout this dissertation in all cases where helicopter-specific nomenclature and theory is used, references

[2]As engines tend to operate most efficiently at a given RPM.

and distinction shall be made. This dissertation remains focussed on propeller application and aims to use propeller terms throughout.

1.1.1 ROTARY NOMENCLATURE CLARIFICATION - 'INFLOW'

An area for potential confusion in discussion between propeller/rotor aerodynamics is the term 'inflow'. In rotorcraft literature, 'induced flow' and 'inflow' are used semi-interchangeably - hence Pitt & Peters *Dynamic Inflow* model is often used to describe what is technically a Finite-State *Induced Flow* model. In propeller nomenclature, 'inflow' definition depends on the source - sometimes it is the flow at the disc *without* induced flow which in turn is termed 'incremental inflow', and in other sources it is the whole flowfield at the propeller disc including the induced flow. To avoid confusion, the following definitions of "*Induced Flow/Velocity*", "*Incident Flow/Velocity*" and "*Inflow*" are used in this dissertation:

Induced flow/velocity is the velocity increment effected at the propeller disc plane as a result of thrust produced by the propeller. For use in a blade-element analysis, the induced velocity is resolved into axial and tangential velocities which contribute to the wake axial and angular momentum, respectively, and hence propeller thrust and induced power. The induced flow may be due to both steady and unsteady loading, discussed in Chapter 3.

Incident flow/velocity is the velocity, $\vec{V_D}$, at the propeller disc plane *without the effect of the propeller itself - i.e.,* incident velocity is the combination of freestream velocity and installation (*i.e.,* airframe) effects with no propeller-induced velocity.

Inflow is the combination of incident flow and induced flow. Since induced flow is a function of incident flow and, to some extent, vice versa[3] - (see Veldhuis, 2004), the inflow distribution may be converged upon through momentum/vortex methods as part of the aerodynamic model. The inflow velocity is resolved into blade/blade-element fixed axes for determination of resultant angle of attack and velocity at a blade element, α_R and V_R.

1.2 HISTORY OF PROPELLER THEORY

Despite the main principles of propeller design being over sixty years old, they have enabled designers and blade manufacturers to produce efficient and powerful propellers. Where there has been a lack of propeller-focussed research, and where there are gains to be made in terms of reduced fatigue *etc.*, is in the propeller off-design and potentially *unsteady* aerodynamics. By analysing how the

[3] Though this effect is much lower order in terms of its effect on blade forces.

blade forces and moments change with respect to time due to non-axisymmetric incident flow, correlation between cyclic loading and design features may be determined and blades designed/adapted for maximum life between service intervals.

Before developing a model for a propeller at an angle of incidence, however, a designer needs to have an appreciation of the aerodynamics in play on a propeller in steady axial flight. The history of propeller theory and design for optimum efficiency is laid out chronologically in great detail in a 2006 review of propeller aerodynamics (Wald, 2006). This work provides an overview of not only the key developments, but goes into detail on the theory of propellers and shows the different means via which propeller calculations have been performed through different flight regimes; *propeller*, *vortex-ring* and *windmill* states. Some of the works and citations discussed in the following section are taken directly from Wald (2006), as the works themselves are not written in English and no translations readily available.

The earliest applicable theoretical work on propellers was performed by Froude and Rankine and Rankine (1865), working on marine propellers. They formulated the basic theory of the propulsive fluid momentum equations, and thus created actuator-disc theory - or axial momentum theory. Although this crude approximation allows designers to set performance and sizing requirements, it involves no real detail on actual propeller aerodynamics, instead proposing an infinitesimal imaginary disc through which there is a discontinuity in pressure and momentum, resulting in thrust.

1.2.1 AXIAL MOMENTUM THEORY

Rankine and Rankine (1865) developed *1D/Axial Momentum Theory*, which is based on the following assumptions:

- The propeller may be represented by a disc imparting momentum to the flow through it - the **actuator disc**, which is a circular disc of infinitesimal thickness with a radius equal to that of the propeller.
- The axial force effected by a propeller is equal to a pressure discontinuity through the disc, multiplied by area (*i.e.,* $F = \Delta P \cdot A_{disc}$).
- The axial force may also be determined from momentum considerations and application of Newton's second law (*i.e.,* $F = \dot{m} \cdot dv$).
- The flow through the disc is uniform and irrotational, incompressible and inviscid.
- Far upstream and far downstream (at undefined distances), the pressure returns to freestream conditions.

By applying Bernoulli's equation upstream and downstream separately, and considering Newton's second law at the disc, Rankine showed that the velocity increment at the disc is half that in the far slipstream. For a given thrust, T, and freestream velocity, V_∞, axial momentum theory enables calculation of induced axial velocity, v_a, due to a propeller of disc area, A_{disc}:

$$v_a = \sqrt{\frac{V_\infty^2}{4} + \frac{T}{2\rho A_{disc}}} - \frac{V_\infty}{2} \tag{1.1}$$

Drzewiecki (1900, 1901) is credited as being the first to discretise a blade into a number of elements and treat them as isolated lifting surfaces - thus formulating *blade element theory*, but he made no account for the velocity field induced by the propeller itself.

1.2.2 GENERAL MOMENTUM THEORY

Glauert (1943) extended the axial momentum theory by considering the tangential/rotational velocity induced in the slipstream - whereas in axial momentum theory, irrotationality is assumed. Otherwise the assumptions of general momentum theory include those of axial momentum theory in addition to the following:

- The angular velocity in the slipstream upstream of the disc is zero.
- The disc imparts an instantaneous angular momentum to the flow.
- Conservation of angular momentum applies everywhere in the slipstream *except* across the disc, where there is a discontinuity.

Both the general momentum model, and an extension for a propeller at incidence are presented in Appendix A, but the governing equations axial and tangential induced velocity with the aerodynamic forces on the blades:

$$\frac{a_a}{1+a_a} = \frac{\sigma\left[dC_l \cdot \cos\phi - dC_d \cdot \sin\phi\right]}{4 \cdot \sin^2\phi} \tag{1.2}$$

$$\frac{a_\omega}{1+a_a} = \frac{\sigma\left[dC_l \cdot \sin\phi + dC_d \cdot \cos\phi\right]}{2 \cdot \sin^2\phi} \tag{1.3}$$

with axial and tangential induction factors defined as

$$a_a \triangleq \frac{v_a}{V_\infty} \tag{1.4}$$

$$a_\omega \triangleq \frac{v_\omega}{\omega \cdot r} \tag{1.5}$$

General momentum theory models the rotational velocity downstream, whereas the simpleraxial momentum theory assumes irrotationality in the fluid domain surrounding the propeller. The axial induced velocity is determine using the same

relationships, hence Equations 1.1 and 1.2 are equal. Equation 1.3 is derived from the relationship between the angular momentum imparted to the fluid, and the tangential force acting on the blades.

Momentum theory in both formulations is a simple analysis in which the propeller/rotor is modelled by an actuator disc that imparts momentum to a bounding streamtube, thus effecting the thrust of the propeller. It can be extended by applying the method to annular elements, giving a spanwise discretisation, but this inherently couples the flow at laterally opposing sides of the propeller disc, which is physically unrealistic for any non-axial flight condition. This will be discussed in Chapter 3.

1.2.3 VORTEX THEORIES

Implicit in the coupling of blade element element and momentum theory is an assumption of *infinite blades*. The nomenclature is slightly misleading, however; at no point is the number of blades stated to be infinite, rather that the ΔP is continuous in azimuth as per momentum theory. The only blade element case that could provide such a pressure discontinuity is the case of an infinite number of blades. Prandtl and Goldstein both present relationships between induced flow/disc loading from vortex theory. Though these relationships are derived from different principles than momentum theory, the governing equations are identical except for a factor that gives a radial distribution of induced velocity. Goldstein's solution relies on modelling the helical wake, whereas Prandtl's solution models the wake as a series of two-dimensional vortex sheets. Owing to the similarity between the momentum equations and vortex theories, Prandtl's function can be viewed as a *correction* to momentum theory due to a finite-radius and finite number of blades. Sometimes it is erroneously called a "*tip-loss*" correction - though it predicts a circulation reduction towards the tip of the blades, it does not account for three-dimensional tip-losses. The benefit of Prandtl's function is that it is closed-form in solution, whereas Goldstein's relies on interpolation between tabulated values from lookup tables (Tibery and Wrench, 1964), which means Prandtl's correction factor is more often used due to its simplicity. The origin of both Prandtl and Goldstein's functions will be described below, and a comparison between the two will be presented.

In 1919, Betz (reprinted in Prandtl and Betz, 1927) showed that the loading distribution for *'lightly-loaded'*[4] propellers is such that the shed vorticity forms regular helicoidal sheets moving aft uniformly from the propeller at freestream velocity (*i.e.,* the induced velocity is not considered in wake convection. For the fixed-wing, it is well-known that the induced drag will be minimum when the induced velocity is constant along the span. For this minimum loss case, at a

[4] A lightly loaded propeller is described as one where the induced velocities are small compared to the propeller velocity (Makinen, 2005).

sufficient distance behind the wing (the far wake), the induced velocity becomes independent of the distance from the wing, and the flow can be modelled by a two-dimensional strip of equal span (see Bramwell et al., 2001, pg. 60). It may be shown by considering the velocity potential above and below the wing that the circulation for a two-dimensional strip is elliptical distributed along the span with a maximum at the wing centre:

$$\Gamma_0 = 4ws \tag{1.6}$$

where s is the span, and w is the uniform induced velocity.

The equivalent for the rotary wing is to model the wake as a set of regular helicoidal sheets - Betz's ideal wake. The solution for the velocity potential at the disc has been tackled by both Prandtl (in Prandtl and Betz, 1927), and Goldstein (1929). Prandtl modelled the helicoidal wake as a series of planar sheets, utilising the assumption that the helix curvature for the outer sheets is large enough for the two cases to be comparable. A detailed derivation is found in (Prandtl and Betz, 1927, in German) or in (Bramwell et al., 2001, pages 61-63), but the important detail is by using blade element and Kutta-Joukowski, Prandtl showed that the velocity potential across the disc, or the circulation distribution for minimum loss is can be shown in a similar form to Equation 1.6:

$$\Gamma = kws \tag{1.7}$$

where

$$k = \frac{2}{\pi}\cos^{-1} e^{-\frac{B(1-x)}{2\sin\phi}} \tag{1.8}$$

with the induced velocity at the disc given by

$$v_i = \frac{\Gamma}{4\pi rk}\frac{B}{\sin\phi} \tag{1.9}$$

for any radial point on the disc ($x = \frac{r}{R}$). B is the number of blades, and B where ϕ' is the advance angle (the angle between the resultant flow and the disc plane), which will be covered in further detail later. Equation 1.8 is sometimes referred to erroneously as Prandtl's "tip-loss" factor in the literature. Whilst it adequately predicts the loss of thrust near the blade tips, Prandtl devised a simpler tip-loss factor giving the ratio of the mean induced velocity over the disc to the effective velocity at the blades (see Bramwell et al., 2001, pg. 111). This factor is based on finite number of blades giving rise to a finite number of vortex sheets. Such a system allows fluid to pass around the edges of the sheets, thus altering the effective velocity at the disc. Prandtl's methodology modelled this as an effective shortening of the vortex sheets in radius - equivalent to an effective loss of blade

span from R to R_e. Prandtl showed that:

$$R - R_e = \frac{1.386}{B} x R \sin\phi \tag{1.10}$$

since close to the tip, $x \to 1$ (Bramwell et al., 2001)

$$R_e/R \simeq 1 - \frac{1.386}{B}\sin\phi \tag{1.11}$$

For rotorcraft problems, Equation 1.11 is often approximated as $R_e/R = 1 - \sqrt{C_T}/B$, using a mean induced velocity calculated from 1D axial momentum theory. Owing to its lack of common usage on propeller calculations, Prandtl's tip-loss factor will not be used in this dissertation, but is discussed here to highlight the potential confusion in nomenclature between Prandtl's vortex model, Equation 1.8, Equation 1.11.

The tip losses on a propeller have been described in detail by Bocci (as referenced by Bocci and Morrison (1988)), and this will be discussed in Section 2.6 on page 78.

Goldstein tackled the vortex problem of the induced velocity at the propeller disc, but did not use the simplifying assumption of modelling the wake as planar sheets, instead solving for the helicoidal vortex structure. His methodology produced the same formulation as Equation 1.9, noting that he used a function $G(\mu)$ in place of k, where μ is a function of ϕ. His function is actually a function of B, x and ϕ, but has no closed form solution. Goldstein presented tabulated solutions of G for two and four-bladed propellers, for different radial locations. Goldstein's loading function gives the ideal circulation distribution - *i.e.,* one that induces a uniform velocity field at the propeller disc. Propeller design via Goldstein's function is thereby a procedure to fit this ideal circulation distribution by altering blade design characteristics (twist, chord, camber). The reverse problem *i.e.,* to predict the performance of a propeller of known design characteristics under non-ideal loading is more complex. For a propeller at incidence, the shed wake structure will not be a regular helicoid - this is problematic when attempting to adapt/utilise Goldstein's function for the propeller at incidence.

Lock extended Goldstein's method to include blade numbers up to six, expressing the Goldstein function in terms of his own κ-function (Lock, 1932; Lock et al., 1945). He chose a different formulation than the Goldstein function as it allows presented of the κ-function in a nondimensional form.

$$\kappa = \frac{\Gamma}{v_a \cdot x} \cdot \frac{B}{4\pi \sin\phi} \tag{1.12}$$

$$\Rightarrow \sigma \cdot C_l = 4\kappa \cdot \frac{v_a}{V_\infty}\sin\phi \tag{1.13}$$

Goldstein's methodology, as extended by Lock is referred to as the Lock-Goldstein method - and remains to be the de-facto standard in many industrial codes to the present day. The need for tabular interpolation, the reliance on an assumed ideal wake are troublesome for modelling a propeller at incidence - and in the following chapter, the suitability of using Prandtl's simpler function will be explored. Prandtl's function has been used in rotorcraft blade-element codes, with a clear lift asymmetry, so it has proven usage for an azimuthal variation of lift.

Although the work by Betz, Prandtl, Goldstein and Lock marked the development of a better understanding of propeller aerodynamics via vortex theory, work continued on the refinement of Blade Element Momentum Theory (BEMT), notably by Glauert. This development by Glauert (1926b, 1943) is still applied in practical calculations today, despite the assumption of an "*independence of blade elements*", which was shown to be without physical justification[5]. Owing to the continued use of the blade element method for high accuracy predictions in wind turbines, propellers and helicopter rotors, the validity of the independence of blade elements assumption is not discussed in this dissertation and taken to be suitable for an engineering-level model. Whilst there is certainly potential to extend Lock's methodology to a propeller at an angle of incidence, it is more rigorous to derive a model from the ground-up from first principles. In addition - the model implicitly relies on Goldstein's vortex model, which has a simple helical structure, non-representative of the likely wake of a propeller at an angle of incidence.

The Goldstein correction factor is difficult to compute as it requires modelling of the vortex system for the relevant number of blades. Goldstein only presented the function in tabulated form for two and four-bladed propellers. Applied mathematicians Tibery and Wrench (1964), used modern computational and mathematical techniques to tabulate accurately functions related to the Goldstein function over a wider range of parameters than had previously been attempted. This work has been summarised and presented in a form more suitable for propeller design by Wald (2006) - though it appears neither Tibery and Wrench nor Wald were aware of the developments of Lock.

'*Theory of Propellers*' (Theodorsen, 1948) is essentially a collection of NACA Technical Notes (TNs) 775-778 (Theodorsen, 1944a,b,c,d) - Theodorsen followed from Goldstein's ideal circulation distribution and studied the shed wake far downstream, rather than at the propeller itself and as such was able to negate the need for the lightly-loaded condition that had previously been invoked. Arguably, Theodorsen's work marks the most recent major presentation of propeller vortex theory. Like Goldstein's method, Theodorsen's theory relies on the ideal wake of Betz with perfectly uniform and rigid vortex sheets - it is relatively unused in

[5]Taken from Wald (2006).

modern industrial codes, and will not be further explored in this dissertation for both these reasons.

Morrison and Bocci (1985) used a finite-difference solution to provide a solution to Goldstein's loading function for arbitrary blade number, and solving for the helix angles such that the methodology was not restricted to light loading. The solution enables relatively easy calculation of the influence of the vortex wake, but in the form presented is restricted to a uniform wake convecting downstream at a uniform velocity. Extension of the methodology to a propeller at incidence either requires invoking a 'steady-state' assumption[6], or a much more elaborate wake structure that would require a thorough re-working of the methodology, and greatly increased computational complexity.

The use of vortex theory to determine the forces on a propeller at an angle of incidence requires determination or prescription of the geometry of the wake - which is orders of magnitude above BEMT in terms of calculation cost. Since BEMT appears to be the most suitable tool for an engineering-level model of a propeller at an angle of incidence, its inception will be explored in more detail. The 'Blade Element' model has its roots in aerodynamic strip theory, whereby spanwise elements of a propeller blade may be assumed to act independently as elements of a uniform, infinite span lifting surface. Extension of this method to a propeller at an angle of incidence involves careful resolution of velocities into the correct axis system. From this point, a lifting model may be applied that has the potential to include unsteady effects. The pertinent work in both propeller and rotorcraft fields will be discussed further in Sections 1.2.4 (lifting models) and 1.2.7 (unsteady aerodynamics).

The vortex methods as presented in the preceding sections amount to numerical or analytical solutions of Prandtl's lifting line with a prescribed helical or planar wake structure - and all reduce to the general momentum model for the case of infinite blades. No actual vortex calculations are performed with their usage, rather the relationship between wake and disc loading is used, as determined by Prandtl's, Lock/Goldstein's or Theodorsen's model. By comparison, a propeller *lifting-line* model can afford the ability to use either a prescribed/semi-free/free wake. In theory this would enable the calculation of induced velocity at the propeller disc due to a non-axisymmetric wake. However, it has been shown that such methods have significantly larger computational cost and no better performance for the axisymmetric case (Gur and Rosen, 2008). Extension to the non-axisymmetric case would involve a massive computational cost increase (as symmetry cannot be utilised), and a greater uncertainty. Accordingly, the aim of this dissertation is to use a momentum model with a vortex correction of possible. The nonuniform azimuthal distribution of thrust on a propeller at an angle

[6]The 'steady-state' assumption is elaborated further in this chapter, but essentially invokes the assumption that individual azimuthal points may be treated in isolation, as part of a hypothetical propeller on which all other azimuthal points are subject to those local conditions.

of incidence requires a reworking of the momentum model - and this will be discussed in Chapter 3 and Appendix A.

1.2.4 PROPELLERS IN NON-AXIAL FLIGHT

Ribner and Ribner (1945) presented a method to determine the hub forces and moments on a propeller in an angle of yaw, with the method being extensible to pitch. His work is based on the derivatives of the propeller performance equations for C_T and C_Q with respect to changes in inclination angle, γ. Ribner assumed a sinusoidal distribution of induced flow, and a linear variation with radius. To afford calculation, Ribner's method uses only the chord at 75% radius, and assumes linear aerodynamics. Small angle assumptions in the analysis also mean that Ribner's method is only suitable for small inclination angles. His method showed reasonable validation for small inclination angles vs. the test data available at the time.

To date, there are not many experiments that have been published on isolated propellers at angles of incidence, and most are from the 1950's. A series of wind tunnel tests were performed to determine the effect of an angle of incidence on aircraft propellers (Gray et al., 1954), (Russell, 1952), (Pendley, 1945), (Yaggy and Rogallo, 1960) and (McLemore and Cannon, 1954). Semi-empirical means of calculating the thrust variation were presented by Gray et al., requiring knowledge of the radial thrust gradients and how they change with advance ratio and rotational speed - *i.e.,* the methods presented are a means of extrapolating axial test data to predict the forces of a propeller at an angle of incidence.

Ribner's method was extended by de Young (1965) by simplifying the evaluation of the functions required, removing the small angle assumption and extending the application of the model to higher inclination angles. In this work de Young did not take into account the effect of the induced flow perturbation on the distribution of advance angle over the disc, implying a uniform induced flow over the propeller disc.

ESDU Data Sheet 89047 (Chappell, 1989) utilised de Young's method, and presented correlation of the method with legacy experiments - with the caveat "*The data are intended primarily for aircraft stability and control calculations at the project stage; more detailed methods will usually be required for load calculations, such as propeller blade stresses and powerplant mounting loads.*".

The equations for the normal force and yawing moment derivatives with disc inclination angle as presented by de Young and in ESDU 89047 are only loosely coupled with blade solidity, σ, which by definition means that they are only loosely coupled with blade number as $\sigma \triangleq \frac{Bc}{2\pi r}$. This makes little sense physically, as the equations used to determine in-plane force and yawing moment in

Ribner and Glauert (1943, 1926b) (and most other texts with discussion of in-plane force and yawing moment) show that for disc inclination, both the in-plane force and yawing moment are *directly proportional* to blade number. This loose coupling is highlighted in ESDU 89047 - "*Analysis of these equations shows that for practical ranges of* σ_e*,* J *and* C_T *the derivatives are comparatively insensitive, within a few per cent, to variations in B over the range* $2 \leqslant B \leqslant 10$".

This is particularly fallacious for the case of $B = 2$, for which the total normal force and yawing moment will be a function of blade position (*i.e.,* time-varying) - hence there is a time-varying nodding moment on two-bladed wind turbines in non axial inflow, and why a teetering hub can work for a two-bladed helicopter rotor. For $B > 2$, the harmonic loads on the separate blades lead to a *constant* moment and in-plane force. Equations for hub moments and in-plane force are discussed further in Chapter 6 on page 192

Though the work contained in this thesis focusses on the variation of blade-loading and its radial variation, a successful methodology *should* capture related phenomena that are dependent on blade load fluctuation. The predictions from the method presented in ESDU 89047 for yawing moment are presented and compared in Chapter 3, but prediction of the in-plane load requires a re-working of the fundamental equations, and this is discussed in Chapter 6.

Methods presented for determination of the force variation on propellers at an angle of incidence have been presented in conjunction with some of the experimental work listed above. The bulk of the theory is based on the so-called 'steady-state' method.

STEADY-STATE METHODS - IMPLICIT

Crigler (1944) developed a procedure based on BEMT to determine the performance of a given aircraft propeller in axial flight. These equations were subsequently utilised by Crigler and Gilman Jr (1952) on a propeller at an angle of incidence utilising an azimuthal independence assumption, and that each position on the propeller at an angle of incidence would act as though it were on a propeller for which its own local conditions existed uniformly in azimuth.

> "*Forces* [...are calculated...] *under the assumption that the existing propeller theory* [Crigler (from 1944)] *may be used in conjunction with the instantaneous angles of attack and resultant velocities along the blades of the pitched propeller at successive blade positions around the periphery*"
>
> Crigler and Gilman Jr (see 1952, introduction, pg. 2)

The so-named 'steady-state' propeller theory introduces an implicit azimuthal independence in the momentum equations - *i.e.,* that each azimuthal position

may be treated independently from other positions. Since the performance equations as derived by Crigler (1944) are for a B-bladed propeller in axial flight, however, it also implies that for a given blade at some azimuthal position, the remainder of the blades are producing the same thrust/torque. This is clearly not the case, but the validity of this assumption is not questioned in the literature concerning steady-state propeller theory.

For a propeller in axial flight, annular momentum theory also implies that the conditions within an annular area of the propeller disc are constant and that the thrust of each blade is summated and contributes to the annular induced flow. Any application of the momentum equations to a propeller at an angle of incidence, where flow conditions change with azimuthal position, has to provide a means of using either the local 'steady-state' induced flow, or by summating the induced flow produced by all the blades around the azimuth. To date, to this author's knowledge, a discussion of the validity of either assumption is not present in the literature.

Steady-state propeller theory has been used to determine the load variation on a propeller at an angle of incidence, with reasonable prediction (Roberts and Yaggy, 1950), but although this approach implicitly models the induced flow, the implied steady-state distribution is not discussed in their paper. Notably, the method also relies on linear aerodynamics. Roberts and Yaggy also found that by taking into account the nonuniform incident flow at the propeller plane due to installation, as measured through a pitot survey, the peak-to-peak propeller thrust variation could be increased by around 75% as opposed to simply looking at geometric angle of attack. Again, in this referenced work, only the *thrust variation* was taken into account due to the ability to measure it from wake survey.

STEADY-STATE MOMENTUM METHODS

The blade-element momentum theory with vortex correction factors from Prandtl or Lock/Goldstein is computationally light in axial flight, as the axisymmetric flowfield means that determination of the blade element aerodynamic environment is needed only for a single azimuthal position. For a propeller at an angle of incidence, the change in incident flow with azimuthal position means that some azimuthal discretisation is required in a model - for a 10° step size, the BEMT equations must be solved $36\times$ more than they need to be solved for the axial case. The coupled blade-element momentum equations can be solved in a few seconds for a propeller in axial flight, but this time is multiplied for each increase in azimuthal discretisation. Additionally, with an increase in blade loading and sections encountering aerodynamic nonlinearities at different points around the disc, the iterative solution of the BEMT equations also takes longer.

Eshelby (1985) proposed a mathematical formulation of momentum theory for a propeller at an angle of incidence. In his formulation, he resolved part of the axial induced velocity, v_a, in the disc plane. He provided an installation model for the wing and showed predictions of reacted hub loads, but without validation.

Heene (2012) developed a BEMT model for determining load variation on a propeller at an angle of incidence. He showed good correlation with the load variation at $60\%R$, but does not discuss whole blade loading or look at inboard or tip sections. He also looked at unsteady aerodynamics with an implementation of the Theodorsen function, but he used the argument of $C(k)$ to simply determine the phase shift in the steady-state load, and did not take account of lift deficiency or impulsive load. His extension of BEMT to incorporate azimuthal variation is also performed without discussion of the physical implication thereof, and used a B multiplication factor in the blade element equations to determine the force at a point, which is without physical justification. The validity of this approach will be discussed in Chapter 3, section 3.2.1.

Veldhuis and Veldhuis (2005) presented a model for a propeller at an angle of incidence, as part of a work looking at the effect of the propeller on the wing, and utilised steady-state effects with the assertion that such methodology is adequate for determining the net propeller effects on the airframe. He relies on the work of de Young (1965) to determine the net forces and moments reacted on the nacelle by the propeller.

HIGHER-ORDER METHODS

The phenomena of both in-plane loading and blade cyclic loading has been explored recently using high-fidelity methods. Ortun et al. (2011) utilised an approach based on the Unsteady Reynolds-Averaged Navier-Stokes (URANS) equations and also coupled vortex/lifting-line models to determine the in-plane forces on a propeller at an angle of incidence. Their method showed reasonable accuracy when compared to wind-tunnel results, but is of considerable computational complexity. ONERA's parallel supercomputer with 256 high-speed processors is quoted as taking over ten hours for convergence during simulation. As such, the use of such a method for design purposes on even a high-end desktop computer is not feasible at the time of writing this dissertation.

A similar study was performed by Ruiz-Calavera and Perdones-Diaz (2012) but again, the computational complexity of their method precludes use in this dissertation.

UNSTEADY PROPELLER AERODYNAMICS

None of the methodologies discussed thus far have considered the effect of the dynamic flowfield at the blade element level, and its impact on a methodology - aside from an addition of a Theodorsen-based method to the steady-state method by Crigler and Gilman Jr (1952).

The addition of unsteady aerodynamics to any methodology is not a simple task. The problem of unsteady stall is one of considerable complexity that is the subject of ongoing research, and will not be considered in this work. Steady stall and the potential model modifications that would be necessary for more detailed modelling of static *and* dynamic stall are discussed in Section 2.5.1 on page 53.

Accordingly, when determining the magnitude and significance of unsteady aerodynamic phenomena of propellers at an angle of incidence, this dissertation focusses on methods which are available for *unsteady attached flow* - which is still a formidable problem. There is a potential for C_{Lmax} to increase in unsteady blade motion, which could lead to increased blade loads. Modelling of this effect could be the work of an entire Ph.D. dissertation, and whilst it is briefly discussed in Section 1.2.7, it will not be included in the model developed herein.

> "*While the absence of significant flow separation reduces somewhat the complexity of the problem,* ***a complete understanding of unsteady aerofoil behaviour even in attached flow has not yet been obtained.***"
>
> Leishman (2006, *Unsteady Airfoil Behavior*, pg. 423)

In terms of engineering/design-level models, little has been presented for unsteady *propeller* aerodynamics due to non-axial incident flow, aside from "*ESDU 96027: Estimation of the lift coefficient of subsonic propeller blades in non-axial inflow.*" (Chinoy, 1992). This data sheet aims to predict the aeroacoustics of rotating propeller blades, and its formulation is based on the work of TH. Von Karman and Sears (1938) - which looks at an aerofoil in a sinusoidal vertical gust field, (described in Leishman, 2006, Sec. 8.9). A validation of ESDU 96027 for blade load variation is not presented in the literature, and the theory behind the data sheet is only referenced in personal communications nearly twenty years old. It is difficult to determine the suitability of the method and as such it is not explored in this dissertation.

The bulk of the literature concerning unsteady blade element methods come from rotorcraft and wind turbine literature, and the pertinent sources are described in Section 1.2.7.

1.2.5 SWEPT PROPELLER BLADE AERODYNAMICS

Modern turboprops are highly different in flight environment and shape than the early straight-bladed propeller blades. The blades of modern propellers are often 'scimitar'-shaped - including large amounts of compound sweep along the blade axis, increasing towards the tip.

Early implementations of sweep on propellers was researched by German researchers during WWII, prompting a perceived impetus at NACA to research sweep in the mid-1940's (Becker, 1980). The most significant test of swept propellers (as noted by Becker, 1980) was by Evans and Liner (1951), who tested a highly-swept (45° at the tip) propeller based on the design procedure of Whitcomb (1950). They noted that the swept propeller showed delay in compressibility losses, but "*only about a quarter of what might be expected from the simple sweep theory*" (Becker, 1980).

Whilst sweepback was initially explored to reduce compressibility losses using 'simple sweep' relationships (*i.e.,* reducing the component of Mach number parallel with blade chord), it has the additional effect of sweeping the shock that may form along the blade span. This reduces the losses associated with the shock - the mechanisms behind this are best modelled with CFD (*e.g.,* Denton, 2002).

Simple sweep theory, noted by Whitcomb, has its roots in fixed wing sweep corrections. Despite these sweep corrections showing poor behaviour on the swept propellers tested, they find common usage in the literature and in engineering-level codes to this day. This will be discussed in Chapter 4. The addition of sweep makes definition of blade geometry far more involved, as blade sections may be oriented in the disc plane at different angles. The different approaches to the definition of section geometry - and even to the definition of the sweep angle itself are discussed in Chapter 4. Aside from the original definitions of Whitcomb (1948, 1950), a discussion of the problems surround the introduction of sweep to a propeller aerodynamic model are not discussed in the literature.

Discussions of the structural complexity of swept propeller blades are given by Bielawa et al. (1983) and Kosmatka (1986), with the focus on vibrational models. The model in Bielawa utilises an aerodynamic model created for helicopter rotors, and no large discussion of aerodynamic sweep corrections is provided.

1.2.6 ROTARY AERODYNAMICS - FORWARD FLIGHT

The pertinent literature related to propellers at an angle of incidence has been presented in the section above. The governing equations that formed BEMT that find use in practical propeller design tools were defined before the first gyroplane or helicopter flight, and propeller theory and rotorcraft theory have been

developed somewhat in parallel, with little comparison in the literature.

A propeller at an angle of incidence is subject to a velocity in the disc plane, and this is the flow situation present for any autogiro or a helicopter in forward flight. Formulations of momentum and vortex theories have been developed to simulate this problem and engineering-level models find common usage.

It is known that the helicopter in forward flight has an asymmetric induced flow distribution - and many attempts have been made to provide closed-form solutions for the distribution of induced flow (see Leishman, 2006, 3.5.2, pg. 158).

Glauert (1926a) suggested a sinusoidal distribution of the induced flow of the rotor in forward flight that provided an upwash at the rotor leading edge and a downwash at the rotor trailing edge - relative to the average value. This methodology was based on the chordwise downwash distribution of a fixed wing.

Two-harmonic distributions of induced flow have been suggested that have longitudinal and lateral variations based on wake skew - but these are largely based on the pressure distribution due to translational lift. The lift asymmetry present on a propeller at an angle of incidence is not present on any advancing helicopter as it is alleviated by blade flapping (or more complex cyclic control) in order to afford stable helicopter forward flight.

Two-harmonic solutions for the induced flow distribution on a helicopter rotor have been presented by Pitt and Peters (1981) - whereby the induced flow distribution is coupled to the reacted axial force and pitching and rolling moments at the helicopter hub. These models were developed to investigate dynamic wake motion following impulsive hub load/moment variation due to control inputs - based on the observations and theory of Carpenter and Fridovich (1953).

Generally, the lower order models for rotorcraft aerodynamics do not have provision for tangential induced velocity. The tangential velocity on a rotorcraft blade due to blade rotation will be much larger than the axial velocity due to forward flight, so the lift produced by the blades is predominantly in the shaft-wise direction and hence so is the velocity increment effected in the disc plane (the *induced velocity*). For propeller blades, the root sections will experience a much larger axial velocity compared with a relatively low tangential velocity. The accounts for the much larger twist in the root sections of propeller blades, and why tangential induced velocity is included in propeller-based methods.

FINITE-STATE INDUCED FLOW MODELS

Somewhere between the simplistic but well-validated momentum theories, and the much more complex but more physically realistic vortex methods lies the work of Peters et al. (1989, 1995); Peters and He (1995); He (1989); Morillo

(2001); Murakami (2008).

With their roots in the work of Pitt and Peters, these methods are termed 'Finite-State induced flow Models'. Referred to more colloquially as the 'dynamic inflow' models, they are fundamentally based on an actuator disc - whereby the pressure distribution and induced flow solution are represented by an infinite series of radial and azimuthal shape functions (truncated). Using the linearised Euler equation, a set of first-order differential matrix equations are obtained which are solved for the induced flow solution. The model is denoted as the Generalised Dynamic Wake (GDW) in the literature. The GDW has been modified for use on aircraft propellers by Makinen (2005). Makinen added extra terms in the mass-matrix of the GDW (both He's and Morillo's formulations) that more accurately model the large swirl velocity added to the propeller wake by the blade root sections. Makinen showed good correlation for low tip speed to the exact circulation distributions of Prandtl and Goldstein for the optimum, infinite-bladed rotor.

Whilst the work of Makinen shows that the GDW is extensible to the propeller problem in theory, he worked only on propellers in purely axial flight. The large lift asymmetry on a propeller at an angle of incidence is beyond the intended scope of his additions, and the implications of the large azimuthally-varying load on the GDW will be compared and discussed in Section 3.9 on page 144.

1.2.7 UNSTEADY ROTARY AERODYNAMICS

Leishman (see 2006, Chapter 8) goes through the development of *unsteady attached* theory, *quasi-steady thin-aerofoil theory*, *Theodorsen's theory/function* with returning-wake additions by *Loewy* and *Jones*, and through other frequency-domain theories. These methods are only valid for aerodynamic forcing that can be written as a harmonic series (that is, a mean and a fluctuating component), as this is integral to the frequency-domain based solution having applicability in the time-domain (*i.e.,* one which has relevance outside of determining stability boundaries). The aerodynamic forcing of the blades of a propeller at an angle of incidence may be represented by a harmonic function, so these methods will be investigated.

Theodorsen based-methods have found use in propeller literature, as discussed in the preceding sections - though their coupling with a steady-state momentum method has not been researched or discussed, and will be in Chapter 3. Loewy's lift deficiency function is a more realistic representation of the unsteady rotary wake, but has its roots in the Theodorsen method, so both will be explored. Loewy's method has found use when coupled with a blade element method in wind-turbine aerodynamics (Silva and Donadon, 2013).

Other first-generation 2D unsteady aerofoil methods are defined via Laplace transform methods of the indicial response - *e.g.,* (Beddoes, 1984). The attached unsteady model of Beddoes is easy to implement, but requires indicial coefficients that are particular to the aerofoil section in use. These are commonplace for thin rotorcraft sections and for standard research aerofoils (*e.g.,* NACA 0012), but are not available for thicker, propeller-type aerofoils[7] - at least not in the public domain. Such coefficients would need to be determined from experimental work or, less preferably, from unsteady CFD - both methods are beyond the scope of this present work.

1.2.8 PROPELLER STRUCTURAL-DYNAMIC MODELLING

Owing to the stiffness required for structural integrity at high rotational speeds, blade torsional and bending deflection can be of high frequency. Whether the related unsteady loads are of importance for this problem will be discussed separately, but the magnitude of blade deflections needs to be determined for the propeller at an angle of incidence.

The majority of propeller structural-dynamic models in the literature are constructed to determine the mode shapes of the blades (Kosmatka, 1986) or for building an unsteady aeroelastic model (Yadykin et al., 2006). There appears to be no freely-available data for blade deflection measurements with azimuth on a propeller at an angle of incidence at the time of writing. Kurkov (1988) presents a set of experiments on an advanced turboprop, highlighting the complexity of the measurement system for determining the steady deflections of a propeller in axial flight - determining the change in deflection with azimuthal position would be markedly more complex.

Dunn and Farassat (1992) presented a finite-element structural dynamic model coupled with an Euler-based aerodynamic method to predict the deflections of a scale turboprop with high success. They noted that though the blade torsional deflections were of significant magnitude, the centrifugal contribution to twist was much greater than the aerodynamic contribution. This will be discussed in Section 2.5.4.

1.2.9 INSTALLATION EFFECTS

Wing, nacelle and fuselage interference produce a variety of in-plane and disc-normal velocities at the propeller plane. A method, presented by (Yaggy, 1951) is used as part of ESDU 90020 - "*Airframe-induced upwash at subsonic speeds*" (Chappell, 2009). It is based on a lifting line model to determine the flow around

[7] The thickness-to-chord ratio, t/c, can range from 30% to 6% for propeller blades, from root root to tip.

the wing, and a nonlifting axisymmetric potential model for determination of the flow around the fuselage and nacelle.

The methodology of Yaggy is elegant but simplistic, and offers little scope for progression in terms of aerodynamic research. It is suggested in ESDU 90020 to determine the mean upwash angle at the 70% radius, and use this as an equivalent inclination angle for determination of blade cyclic loading. Since this is not physically realistic, the propeller model in this dissertation has been written from the outset to be able to accept a fully nonuniform incident flow in the calculations, rather than a single inclination angle. Extension of their method by using a surface panel method in place of the axisymmetric potential model should afford the ability to model more complex geometries, without altering the fundamental model operation.

Unfortunately, there exists little validation data for the flowfield at the propeller plane due to installation effects - aside from that referenced in the report (Roberts and Yaggy, 1950). Installation effects will not form a large part of this dissertation owing to the sparsity of validation data - but the steps that must be taken to accommodate installation in the model presented will be included in Chapter 5, and the model is formulated for their inclusion from the outset.

1.2.10 PROPELLER BLADE AEROFOILS

The early propellers comprised Clark-Y or RAF 6 aerofoil sections (Korkan et al., 1980). Both of these aerofoils have flat lower surfaces - hence the geometric pitch of the lower surface is equal to the blade pitch giving rise to the "pitch surface" and "camber surface" propeller nomenclature referring to the pressure/lower and suction/upper surfaces, respectively.

During the mid 20^{th}, NACA 16-series aerofoils gained popularity in propeller design, still finding use in many aerofoils to this day. The NACA 16-series is a subset of the NACA 1-series, with the 6 referring to the location of minimum pressure - 60% back from the leading edge of the aerofoil (stack, 1940). These aerofoils were the first NACA series to use aerofoil theory to dictate the shape rather than simple geometric relationships. The design concept of these aerofoils is to specify the pressure distribution and hence the lift, and derive the geometric shape that provides such a distribution. The aerofoils have the assignation NACA 16-XXXX, where the first two digits refer to the design lift coefficient in tenths, and the last two digits refer to the maximum thickness percentage. Hence a NACA 16-0212 aerofoil has a design lift coefficient of 0.2 and a maximum thickness of 12% - shown in Figure 1.5. The two-dimensional geometry of a NACA 16-profile is defined by a camber line and the thickness distribution with chordwise location. The defining equations are found in the literature (Lindsey et al., 1948), but are included here for completeness. The aerofoil geometry is defined by the

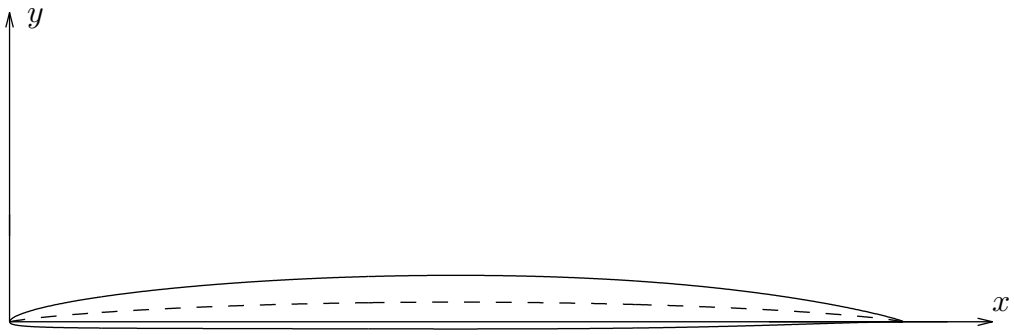

FIGURE 1.5: NACA 16-0212 AEROFOIL SECTION

design lift coefficient, C_{l_d}, and the maximum thickness $\frac{t}{c}$:

$$y_c = -0.079577 \cdot C_{l_d} \cdot [x \cdot \ln x + (1-x)\ln(1-x)] \tag{1.14}$$

where

$$x = \frac{x}{c} - \text{nondimensional chordwise position} \tag{1.15}$$

with upper and lower surfaces defined by

$$y_{upper} = y_c + \delta y \tag{1.16}$$

$$y_{lower} = y_c - \delta y \tag{1.17}$$

$$\delta y|_{x<.5} = 0.01 \cdot \frac{t}{c} \cdot \left[0.989665 \cdot \sqrt{x} - 0.239250 \cdot x \ldots \right. \tag{1.18}$$
$$\left. -0.041000 \cdot x^2 - 0.559400 \cdot x^3 \right] \cdot c$$

$$\delta y|_{x>.5} = 0.01 \cdot \frac{t}{c} \cdot [0.01 + 2.325000\,(1-x) \ldots \tag{1.19}$$
$$\left. -3.42\,(1-x)^2 + 1.46\,(1-x)^3 \right] \cdot c$$

The aerodynamic advantages of the NACA 16-series aerofoils is that they avoid pressure peaks and have a high drag divergence Mach number but they produce relatively low lift compared to other NACA sections.

An improvement to the NACA 16-series is offered by the ARA-D series aerofoils, presented by Bocci (1977). Bocci noted that the 16-series aerofoils tend to have reduced efficiency at higher lift owing to leading-edge flow separation which causes a drag rise. He designed a family of profiles with modifications including a increased lower-surface camber, a dropped leading edge and an increased leading-edge radius. Compared with the NACA-16 series, these aerofoils delay stall at high C_l, and show greater efficiencies. The ARA-D and ARA-D/A families of aerofoils are the standard used at Dowty Propellers. Owning to the lack of public-domain validation data for ARA-D and ARA-D/A aerofoils, they will not be directly compared in this dissertation. However, the methodologies presented that have been developed for NACA-16 series aerofoils should be trans-

ferable to other propeller aerofoil sections..

1.2.11 INDUSTRY DOCUMENTS

Outside of that referenced above, there has been little in terms of engineering-level propeller fluctuating load prediction codes in *published sources*. However, some proprietary methods are used in industry.

Documentation of the methodology of a 1P prediction code has been reviewed and proven to be useful. It is of particular relevance in Chapter 4, and is referenced and discussed therein. It should be noted that both the information in this industrial document and its title are commercially sensitive and thus unpublishable in this document.

1.2.12 LITERATURE SUMMARY

Although the aerodynamic environment of propellers has been well explored throughout the years, the problem of a propeller at an angle of incidence has tended to be one of stability and control in terms of the entire aircraft. Methods have been presented by utilising noninclined methodologies for use on a propeller at an angle of incidence, with little consideration of the validity of the assumptions therein.

Little work has been performed on the unsteady aerodynamics of propellers at an angle of incidence outside of aeroacoustic investigation. A comparison of the methods that have shown use in conjunction with first-order unsteady rotorcraft-based methods will prove of use in characterisation of this problem, and in determining the most efficient engineering solution.

The aerodynamics of swept propeller blades has been relatively unexplored in the literature, with it being commonplace to apply fixed-wing sweep corrections to a swept propeller blade, with little or no discussion of the suitability of such methods. This, along with a brief look at the history of swept propeller blades, is included in Chapter 4.

There is little open-source information available for installation effects at the propeller disc. There have been some more recent higher-order computational methods presented in research papers, but there are only a few sources of validation data, all from the mid 20^{th}-Century.

1.3 DISSERTATION OBJECTIVES

The governing objective of this work is to **determine the model of lowest computational cost that can determine the once-per-revolution (1P) load variation on an installed aircraft propeller at an angle of incidence.** The project behind this dissertation, therefore, must evaluate the physical insight that different model aspects give and the impact that any particular phenomena may have on prediction of loads - and it must be mindful of unnecessary computational cost for little change in loading prediction. Hence a full RANS CFD calculation may give more physical insight into the minutiae of blade aerodynamics, but when integrated to provide root bending loads, such a solution may provide a only a modest improvement to load prediction. When weighed up against the computational cost, such a model may prove unfeasible.

It has been noted in the literature review that the bulk of the work on propellers at incidence in the mid 20^{th}-Century was either from empirical methods or by extension of propeller performance calculations - leading to the so-called "steady-state" methods. The physical implications of the steady-state methods will be explored and their validity questioned. Though the steady-state methods have been shown to produce reasonable but inconsistent predictions of inclined propeller load fluctuation, their physical basis has never been justified. This will be explored in Chapter 3.

Modern analyses of aircraft propellers at incidence tend to use higher-order computational methods that provide reasonable predictions and match wind-tunnel results. However, such methods are unsuitable for use in the design stage owing to the large computational costs involved. Additionally, whilst the higher-order techniques may capture the salient flow features and get the correct result, they arguably remove some of the physical insight into a problem in that that can be troublesome to separate the mechanisms behind different flow phenomena when using RANS CFD - and that can be a tendency for a CFD user to simply 'trust what the computer says', without applying basic 'sanity checks' from fundamental aerodynamic theory.

To fulfil the objectives discussed above, the key aims of this dissertation can be briefly summarised overleaf.

- Provide a comprehensive overview and critical review of the published works available for the loading of aircraft propellers at an angle of incidence.
- Formulate a modelling framework for an aircraft propeller at incidence from the ground-up - flexible so that it can include different physical modelling technique.
- Explore the different physical phenomena present for an aircraft propeller at incidence and perform and order of magnitude analysis to determine which effects are important for this problem and which effects are small by comparison. Hence, this objective aims to answer the question *'what is important to model for a propeller at incidence, and what is less important?'*.
- Review the different techniques that have been utilised for modelling sweep on propellers, and discuss the limitations thereof.
- Discuss how sweep affects the load distribution on a propeller at incidence.
- Determine the requisite fidelity required in an aircraft installation model. Owing to a lack of validation data, this exercise will be a comparison of industry-standard assumptions and the implications thereof.

Throughout this dissertation, an importance is placed on computational cost. "Computational cost" is a relative term, but the benchmark used in this dissertation is to aim to formulate a method that takes < 10 minutes from input to output on the machine used for this Ph.D. Project[8]. MATLAB has been chosen as the code development environment due to the ease of data import and presentation of results. In addition, MATLAB is optimised for matrix calculations and this affords strip methods with a large number of azimuthal stations to be calculated as a single matrix calculation rather than using loops. Though a compiled language such as FORTRAN/C# may be faster for a production code, the speed of various computational techniques in MATLAB will be taken as representative of their numerical efficiency. In addition, techniques suitable for usage in MATLAB are amenable to the open-source platform PYTHON, which is advantageous for a low-cost code. For the purposes of developing and comparing numerical techniques, an Integrated Development Framework (IDE) such as MATLAB is ideal.

[8]iMac 2.8 GHz i7, 20GB RAM, OS X 10.9.2, running MATLAB R2013a. Representative of medium-spec desktop computer at time of writing.

1.4 CONTRIBUTION AND SCOPE

This dissertation comprises a survey of existing modelling techniques and a determination of the respective advantages and disadvantages of each. This project may be regarded as an academic perspective on an industrial problem, providing a new comparison of legacy methods and extensions to existing tools.

In line with the objective stated, this dissertation is focussed on physical effects (aerodynamic, structural) on a propeller at an angle of incidence that contribute to once-per-revolution loading. A propeller at an angle of incidence may produce more noise than one in axial flight due to aeroacoustic considerations, but if these effects are non-contributory to physical loading, they will not be considered. Models utilised in this dissertation will be chosen based on computational cost and suitability. To this end, a justification for including or neglecting physical phenomena needs to be laid out. This dissertation will describe an order of magnitude analysis via which effects on once-per-revolution loading may be compared quantitatively, and hence legitimately ranked in terms of importance in an engineering-level once-per-revolution model.

This dissertation aims to formulate an *efficient* model in that it requires the lowest computational cost without sacrificing the quality of results. The results of interest are the fluctuating loads on aircraft propeller blades when subject to a non-uniform incident flow field - *i.e.,* due to incidence. This dissertation shall not be an overview of propeller performance calculations nor will it attempt to provide detailed modelling techniques for physical phenomena that are beyond the scope of modelling the load fluctuation.

Through research of the salient literature it is apparent that flows near the tips of propeller blades are highly three-dimensional and no one solution exists to simulate these effects in a model that otherwise uses two-dimensional aerodynamics. To this end, this dissertation is provided with the caveat that except for the discussion and incorporation of standard techniques for approximating three-dimensional effects (*e.g.,* Goldstein and Prandtl), they are explicitly not modelled by the techniques presented herein - and no greater discussion of their effect on 1P loading is included.

1.5 DISSERTATION STRUCTURE

The theme through all the chapters is a focus on once-per-revolution loading, and an overview of the topics covered is included below. In addition, the key contributions of each chapter is included in the following descriptions.

Chapter 2 - Modelling Propellers at Incidence:
This chapter serves as an introduction to the flowfield of an aircraft propeller at an angle of incidence, and the aerodynamic environment experienced by a rotating blade. A description of the model formulation is included; the axes systems used and blade element equations are presented. A discussion is provided as to why looking at the *isolated* propeller at an angle of incidence is a valid means to formulate a mathematical model for the general case of a propeller at incidence. The relative magnitude of different factors - *induced flow, unsteady aerodynamics*, *blade deformation* and *incident flow* - are compared, providing the reasoning for the chapters that follow.

Chapter 3 - Induced Flow and Unsteadiness:
Following from the conclusions of Chapter 2, a physically-realistic model of the induced flowfield of an inclined propeller is formulated and validated to experimental data from legacy NACA tests. The means via which the induced flow field has been determined in the literature are compared, and the assumptions in each dicsussed. Different induced flow models and unsteady models are compared and a combinatory model, *steady weighted momentum theory (qsWMT)*, is formulated in this dissertation. The qsWMT model is shown to be most fit for purpose on the 1P problem in comparison to the test results available and is used for the remainder of this dissertation. A discussion of the future validation work that needs to be performed is provided.

Chapter 4 - Swept Blade Elements:
The extension from straight to swept bladed propellers is not simple - a straight blade will have defined parallel sections that are coincident with the respective onset flow, enabling simple blade-element models to be used. A discussion of why this is not possible with a swept propeller blade is provided and the changes that must be made to a blade element model are highlighted. Additionally, the definition of 'sweep' and its effect on sectional aerodynamics is discussed, and it is argued that the blades of an aircraft propeller are not swept in a traditional aerodynamic sense, and hence that 'simple sweep' corrections are deleterious to propeller performance predictions. Since no results are available for validation of 1P loads on a propeller at an angle of incidence with *swept* blades, the validation criteria laid out in Chapter 2 are utilised, and comparisons of 1P loading presented for two different blade element definitions.

Chapter 5 - Installation Effects and Model Predictions:
The model as presented in Chapters 2-4 meets the validation criteria laid out at the start of Chapter 3. Such a model should be able to predict 1P load variation due to any superposition of velocity perturbations at the propeller disc, provided they are correctly resolved into the blade element axes. Detailed solutions for the flowfield at the disc plane due to a combined fuselage/wing/nacelle is a highly complex problem, and beyond the scope of an engineering-level model and by extension, this dissertation. Current industry practice, however, is to determine the mean flowfield (*i.e.,* averaging the effects from individual aircraft elements) and model the propeller 1P loading as due to an equivalent inclination angle. The validity of this approach is discussed in place of any suitable validation data.

Chapter 6 - In-Plane Forces:
A model for blade oscillatory forces that is rigorously formulated and well validated *should* encompass lower-order modelling techniques. That is, the steady in-plane force effected in inertially-fixed axes on a propeller at an angle of incidence *should* be predicted well by such a model - as this effect is governed by the same loading fluctuation, but dominated by blade drag and not lift. A naïve implementation of the model presented in Chapters 2 and 3 will appear to *underpredict* the in-plane forces of a straight-bladed propeller at an angle of incidence, whilst proving most fit for calculating the thrust variation. Confusingly, a uniform induced flow model will appear to perform slightly better predicting in-plane loads whilst shown to be poor at determining thrust fluctuation. The physical reasoning for this is discussed, and a new set of equations to determine in-plane intertially-fixed forces from a blade element model presented, along with good validation to experimental data. The additional equations presented in this chapter can be seen as an extension of the original method presented by Glauert, and it is shown that they predict the magnitude and trends of forces better than industry-standard methodologies based on performance derivatives.

Chapter 7 - Conclusions and Future Work:
A full discussion of the findings in Chapters 2 through 6 is summarised, explained, and the implications thereof presented. A look at potential future theoretical and experimental work is presented.

CHAPTER 2

MODELLING PROPELLERS AT INCIDENCE

This chapter provides the fundamental formulation of the model presented in this dissertation, and is formulated to model the load fluctuation due to an arbitrary incident flow distribution. This chapter also provides justification for simulating an isolated propeller at incidence as the basis for model validation. An order of magnitude analysis technique is presented to determine the respective magnitude of different physical effects.

2.1 PROBLEM STATEMENT

During any given flight, the velocity field at a propeller may be nonuniform - that is, varying in azimuth, radius or both. The reasoning for this is simple - the basic aircraft angle of attack, sideslip and the combination of interference from wing, nacelle and fuselage will likely lead to an incident flowfield that is non-axisymmetric. As a consequence of the azimuthal variation of incident velocity, the blades will experience an aerodynamic environment that varies with blade position - hence loads will vary within a single rotation, and these varying loads have already been described as the 1P loads. There are many time-dependent phenomena as a consequence; *e.g.,* aeroacoustic effects, changes to propeller efficiency and time-dependent strains that may lead to fatigue problems.

These phenomena are documented in the literature and some measurements of 1P loads have been published (Rogallo et al., 1951; Ribner and Ribner, 1945; Crigler and Gilman Jr, 1952). Different engineering level models have been formulated for propellers at incidence - however, these methods have largely been focussed on simulating the reacted loads at the propeller hub in inertially-fixed axes (*i.e.,* the constant vertical force and yawing moment for a propeller at incidence). The loads in inertially fixed axes are important for modelling overall

aircraft stability and control, but the methods presented to calculate them involve assumptions that may not be suitable for blade stress determination. A quote from ESDU 89047, below, shows the impetus for a review of methods for propeller blade load calculations.

> "[this method is] intended primarily for aircraft stability and control calculations at the project stage; more detailed methods will usually be required for load calculations, such as propeller blades stresses and powerplant mounting loads."
>
> Chappell (1989) - ESDU 89047 In-Plane Forces and Moments on Installed Inclined Propellers at Low Forward Speed

There is difficulty in validating a 1P model owing to the overall complexity ofthe problem and the lack of suitable validation data. An industry document presents of measured strains on an installed aircraft propeller in flight and compares them to an engineering model based on the steady-state assumption (Methven, 1998). The comparison showed that the error in prediction vs. measurement was significant and fairly unpredictable - this led to safety factors being introduced to provide conservative load estimates.

It is difficult to draw firm conclusions from the industry document - and detailed discussion of it within this work is not possible due to commercial issues. It will be argued in this dissertation, however, that to validate a research code straight to flight test data would be foolhardy. The problem involves too many variables to reliably observe trends with modelling techniques. Instead, for a design and research code, a rigorous way to build an aerodynamic model is to remove as many extraneous phenomena, and validate for the simplest case of cyclic loading. This validated model may be extended to more complex propeller geometries and to installation on an airframe. The issues of *blade-level aerodynamics*, *installation aerodynamics* and *aeroelasticity* may be explored independently.

The simplest case of propeller cyclic loading is a straight-bladed, isolated propeller at an angle of incidence. For such a propeller, the flow around an airframe and its influence at the propeller disc is not an issue, and the complex geometry of modern, scimitar-type propeller blades is removed from the problem. This chapter discusses the isolated propeller at an angle of incidence, and determines the magnitude of different effects that may contribute to cyclic loads - introducing the *first order* load variation and *higher order* sources of cyclic load variation. Building upon the model developed in this chapter, the steps that must be taken to include effects due to blade sweep are discussed in Chapter 4 and potential extension of this model to incorporate installation effects is discussed in Chapter 5.

The underlying philosophy of this dissertation is key to its structure - that is, the model is developed in this chapter and is formulated to be flexible and easily extensible. Through the chapters that follow, it is used to compare different modelling techniques and those that prove important are presented in a means such that they can be easily adopted into the aerodynamic model.

Note 2.1.1
Design philosophy for a once-per-revolution aerodynamic model:

- At a blade radial station, the local aerodynamic environment and its change with azimuth is fundamentally similar for both uniform and nonuniform incident flow. *i.e., a quasi-sinusoidal forcing with a period of* 2π *with extrema at laterally opposite positions.*
- An aerodynamic model constructed to capture once-per-revolution load fluctuation and validated for an inclined, isolated propeller can be extended to a nonuniform incident flow, provided that a suitable co-ordinate transform is applied.
- The magnitude of different factors contributing to once-per-revolution forcing may be compared with such a model and the conclusions extended to nonuniform incident flow.
- The model presented should encompass related physical phenomena - *i.e.,* it should be able to accurately predict the forces in inertially-fixed axes.

2.2 AN ISOLATED PROPELLER AT INCIDENCE

Figure 2.1a shows an isolated propeller at zero incidence (*i.e.,* pure axisymmetric incident velocity). The incident velocity, V_∞, is parallel with the rotation axis and as there is no component of incident velocity in the disc plane (defined as the $X_D - Y_D$ plane), the incident velocity in a blade-fixed reference frame is constant with azimuth/time. Consequently the blades produce forces and moments that are constant with azimuthal position. For a propeller of known geometry, the total propeller forces and moments may be determined by considering a single blade at an arbitrary azimuthal position, and multiplying by the number of blades to determine the forces reacted at the hub. Only a few operating parameters are required to determine the blade element and total blade forces:

$$\vec{F_{BE}}, \vec{F_B}\Big|_{\gamma=0} = f\left(J, n, r, \beta\right) \tag{2.1}$$

where the subscripts $()_{BE}$ and $()_B$ refer to blade element and blade quantities, respectively. Blade element forces are the elemental forces in element axes, and blade forces are the total integrated forces on a single blade. J is advance ratio and is defined,

$$J \triangleq \frac{V}{n \cdot D} \tag{2.2}$$

where n is rotational speed, r is radial position and β is the blade setting angle.

Figure 2.1b shows a propeller inclined to the freestream at angle γ. The fundamental point is that **a component of freestream velocity, $V_\infty \cdot \sin\gamma$, is now parallel to the disc plane**. This component of velocity is the excitation that causes the aerodynamic phenomena previously mentioned - the 1P aerodynamic forcing. That is, **the incident velocity in a blade-fixed axes system now varies with azimuthal position/time**.

Since the component of velocity that the blades encounter now varies with position around the disc, this introduces a dependency in Eq. 2.1 on the azimuthal position, ψ, and the disc inclination angle, γ. As the sectional aerodynamics are altered azimuthally so is the aerodynamic response of the blade sections:

$$\vec{F_{BE}}, \vec{F_B}\Big|_{\gamma\neq0} = f\left(J, n, r, \beta, \gamma, \psi\right) \tag{2.3}$$

This *cyclic loading* gives rise to a time-dependent strain whereby the blades oscillate around some mean deformation. Historically, propeller blades have been made from wood[1] and metal - more recently, they may be manufactured from carbon-fibre composites. All of these materials suffer to varying degrees from material fatigue[2] and hence the magnitude of any fluctuating loads must be pre-

[1] Arguably making the first propellers *composite* propellers.

[2] Metal fatigue has more notoriety due to the *Comet* disasters, but wood and modern composites suffer from fatigue stress (Clorius, 2001; Tomblin and Seneviratne, 2011).

dicted in order to ensure blade operating safety.

Cyclic loading on propellers may be described as NP loading, where N is any integer - standing for N-per-revolution loading. This dissertation aims to specifically investigate the aerodynamics of 1P or once-per-revolution loading as for any realistic flowfield this component of cyclic loading will be the largest. This may be shown from simple aerodynamic considerations which will be outlined in the next section.

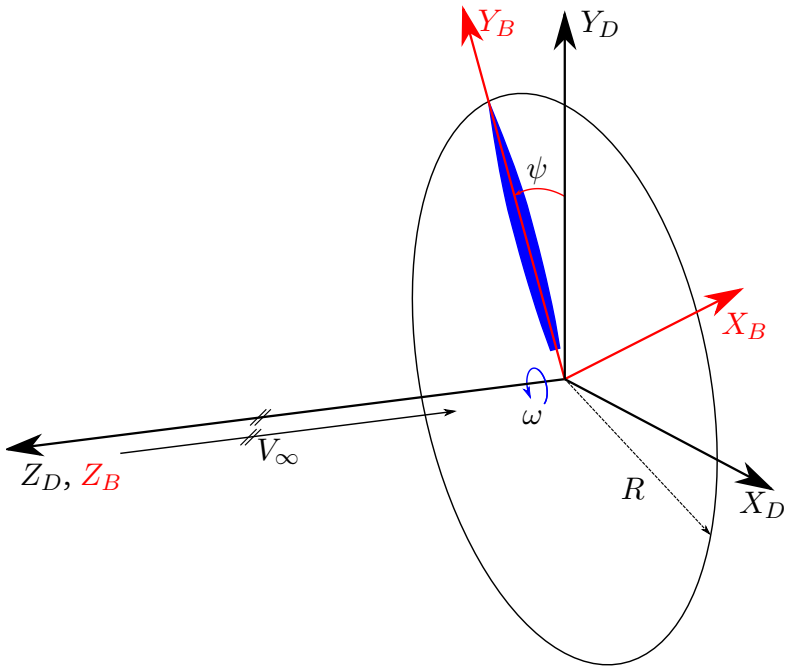

(A) PROPELLER DISC/BLADE AXES IN AXIAL FLIGHT

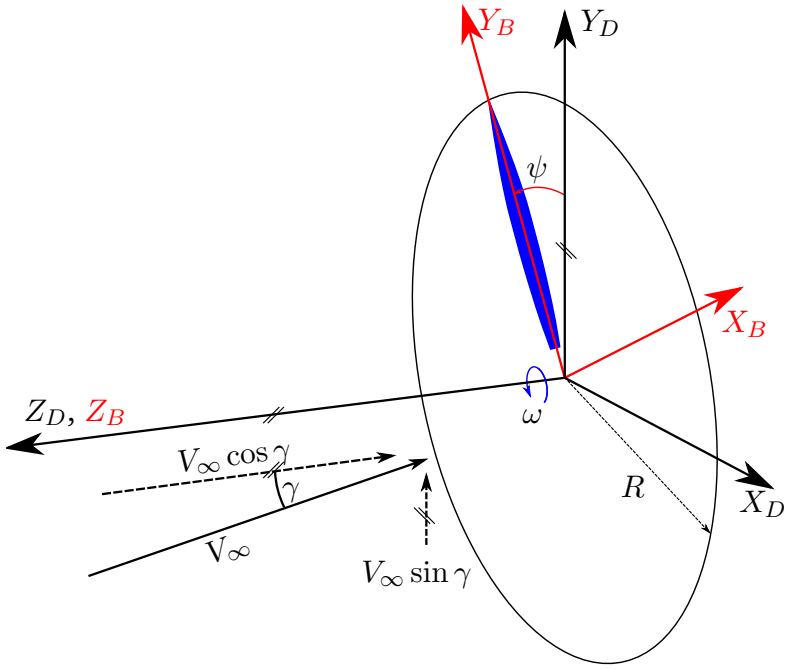

(B) PROPELLER DISC/BLADE AXES IN NON-AXIAL FLIGHT

FIGURE 2.1: DISC AND BLADE AXES - AXIAL AND NON-AXIAL FLIGHT. *Note:* $V_\infty \cdot \sin\gamma$ *is aligned along* Y_D.

2.3 THE PHYSICS OF 1P AIRLOADS

The primary source of cyclic loading may be broadly defined as being due to incident flow velocity parallel to the disc-plane. This is analogous to a helicopter flying at low forward speed[3] - see Figure 2.2. For a helicopter in forward flight, shown in Figure 2.2a, the total velocity in blade-fixed axes is the sum of the tangential velocity due to blade rotation, and the flight speed resolved in the blade X axis (chordwise direction). The tangential velocity, V_T, at any blade position is a function of radial and azimuthal position.

$$V_T(r, \psi) = \omega \cdot r + V_\infty \cdot \sin\psi \tag{2.4}$$

where ω is angular velocity (rotation speed) in SI units of rad/s.

The variation in tangential velocity gives rise to a variation in the lift around the azimuth. In the development of functional helicopters, this variation of lift necessitated the development of blade flapping hinges to afford stable forward flight. Helicopter blades have a 'flapping' degree of freedom, hinged so they can move around X_B, out of the disc plane. An increase in lift causes the blades to be displaced upwards from an equilibrium position, which causes an effective downwash over the blade, thus attenuating the angle of attack and hence attenuating the lift increase that caused the displacement.

Propeller blades are generally unable to flap to attenuate their own angle of attack, but the nomenclature in rotorcraft analysis is useful for this dissertation. The 'advancing' side of the disc is defined as the half of the propeller/rotor disc where the in-plane component of freestream velocity resolved into disc axes has the same sign as the tangential velocity due to blade motion. The 'retreating' side of the disc is defined as the half of the propeller/rotor disc where this component of in-plane velocity is in the opposite direction to the tangential velocity. For the propeller disc at an angle of incidence, γ, the disc axes are defined with X_D parallel with the axis of inclination, Figure 2.1b. The advancing and retreating sides may be defined for the propeller at angle of incidence, γ. Note that combinations of angle of attack and sideslip can be resolved into a single inclination angle about some azimuthal position.

$$0 < \psi < \pi \quad - \text{Advancing Side}$$
$$\pi < \psi < 2\pi - \text{Retreating Side}$$

[3] At *low advance ratio* in rotorcraft nomenclature noting that rotorcraft advance ratio, $\mu \triangleq \frac{V \cdot \sin\alpha}{\Omega \cdot R}$ with α being rotor disc inclination from a 'wings level' orientation, has a different definition to the propeller definition, $J \triangleq \frac{V}{n \cdot D}$.

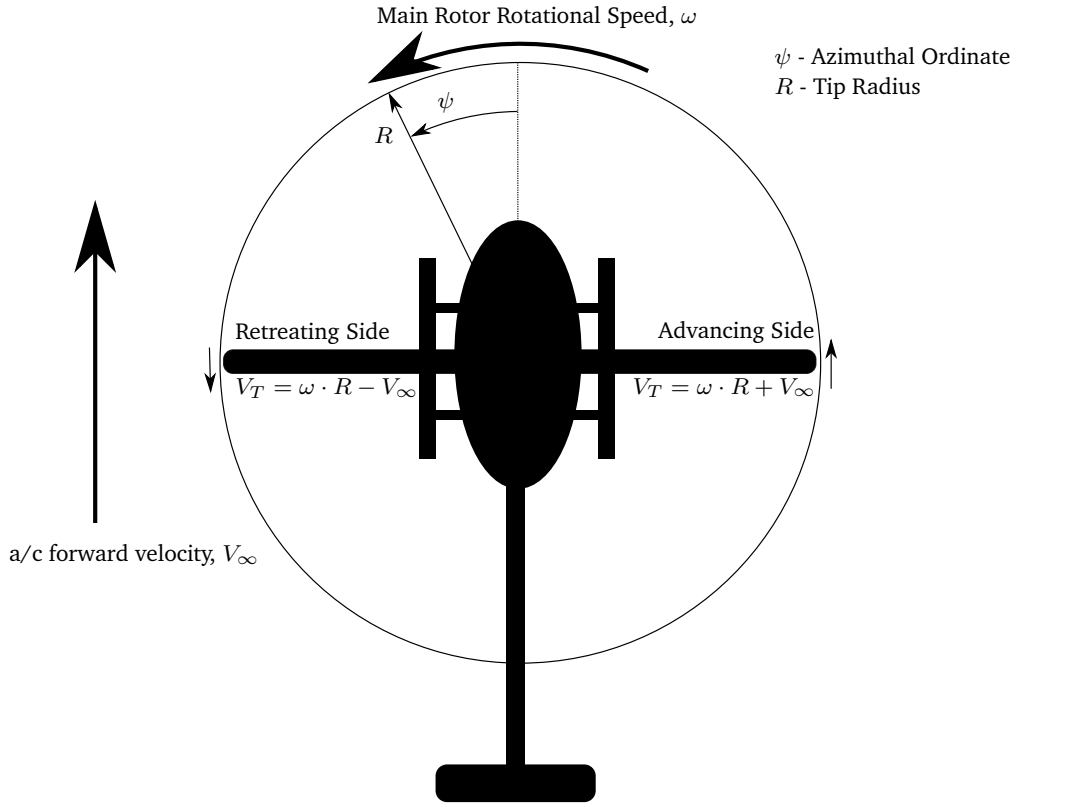

(A) HELICOPTER IN FORWARD FLIGHT.

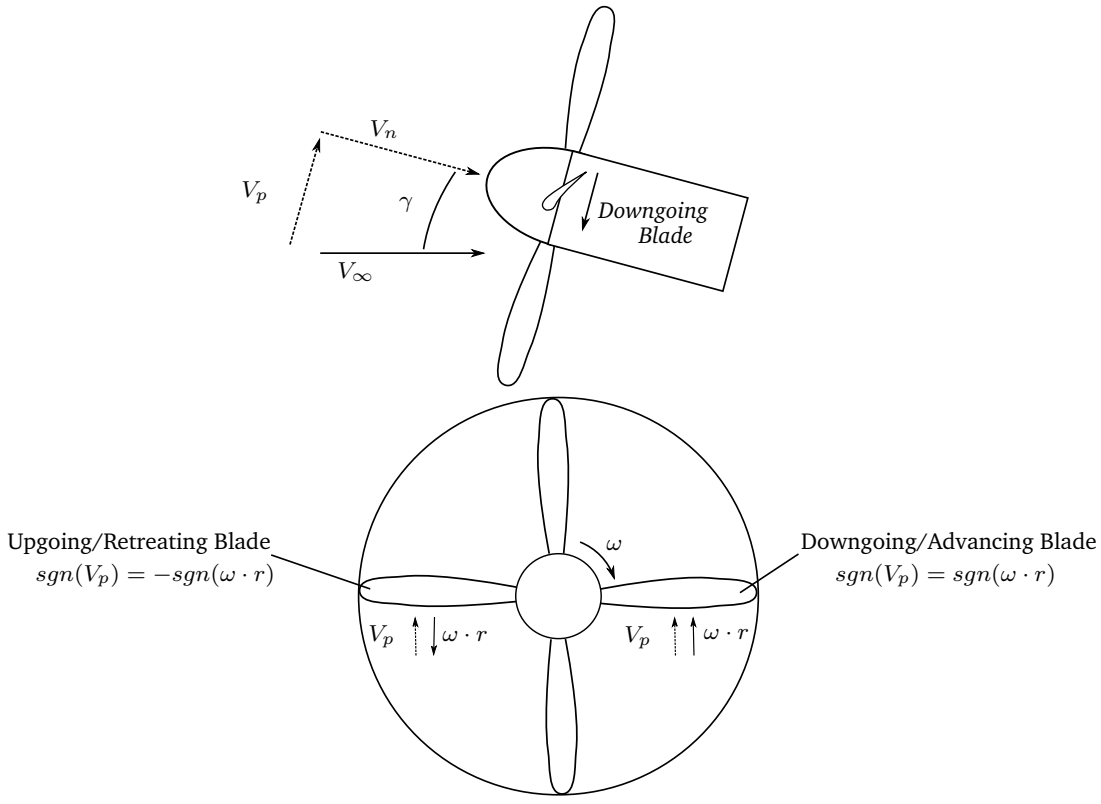

(B) AIRCRAFT PROPELLER AT INCIDENCE - *note: Signum operator* $sgn(x) \triangleq \frac{(x)}{|(x)|}$.

FIGURE 2.2: ADVANCING AND RETREATING SIDES OF PROPELLER AT INCIDENCE AND HELICOPTER IN FORWARD FLIGHT.

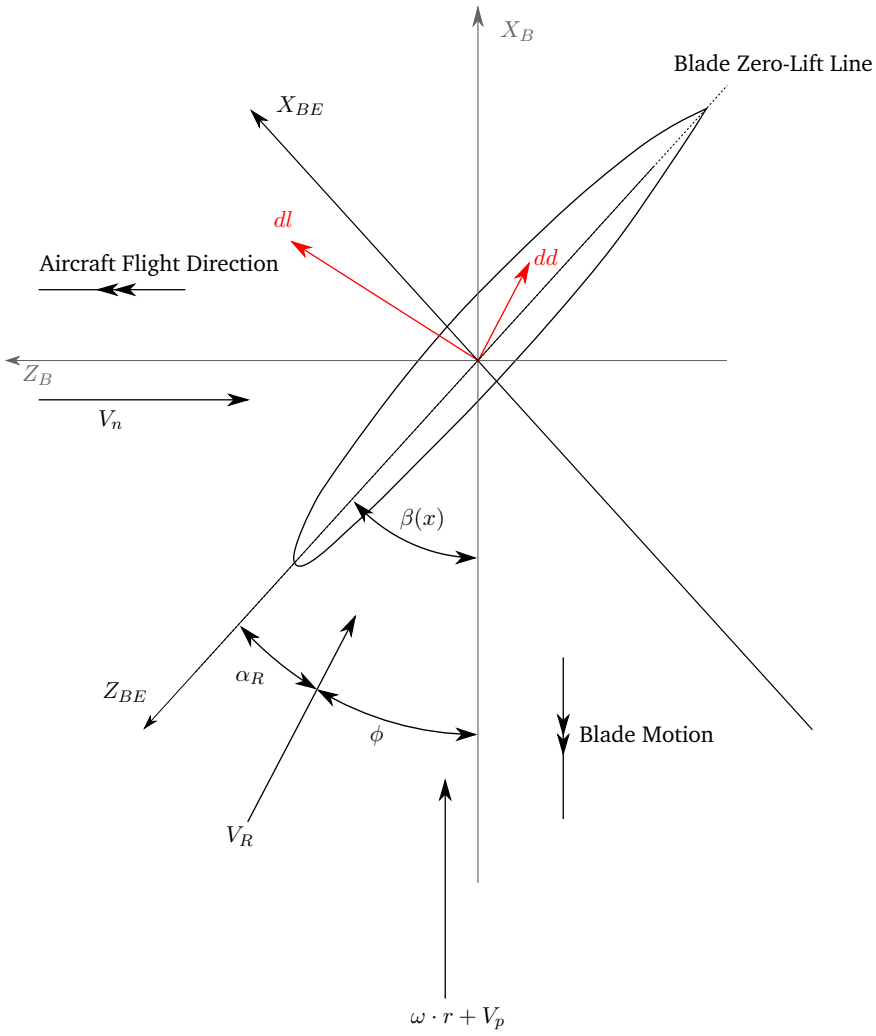

FIGURE 2.3: BLADE AND BLADE ELEMENT ELEMENT AXES, VELOCITIES AND ELEMENTAL FORCES. Y_B IS $+ive$ OUT OF PAGE. VALID FOR STRAIGHT BLADES ONLY.

Figure 2.3 shows a blade element at a radial station on a propeller. The relationships will be defined in Section 2.4, but is can be seen from the geometry that the sectional angle of attack, α_R, and resultant velocity, V_R, are both a function of V_p which varies in azimuth. There is an increase in both α_R and V_R on the advancing side, and a respective decrease in both on the retreating side - **hence a 1P aerodynamic forcing**. This 1P variation in α_R and V_R effects a 1P variation in sectional lift, drag and pitching moment.

As mentioned, propeller blades are rigid and unable to flap out-of-plane, so this *force* asymmetry remains a 1P oscillatory loading on the propeller blades - whereby the lift and drag will theoretically be maximum at the advancing side and minimum at the retreating side. Accordingly the forces in blade and blade element axes will vary proportionally. It is the requisite model fidelity needed to accurately determine these oscillatory forces that this dissertation aims to determine. For an engineering model of 1P loading, it is sufficient to model only the significant sources of loading. Hence this model may be limited to the largest

source of azimuthally-varying aerodynamic excitation, which will be caused by in-plane velocity for a propeller at an angle of incidence. Higher order excitation such as *blade-vortex interaction (BVI)*, *turbulent incident flow* and *wake dynamics* - where the unsteady development of the wake and its movement effect a transient velocity increment at the disc - are beyond the scope of this dissertation.

On an installed aircraft propeller, there may be a combination of aircraft angle of attack, $\alpha_{a/c}$, sideslip $\beta_{a/c}$, and a combination of in-plane velocities from wing, nacelle and fuselage interference at varying incidences, ϵ_w, ϵ_n, ϵ_f - all of which will cause some 1P variation of α_R and V_R with varying magnitudes and at different phase positions. To demonstrate that a combination of multiple out-of-phase periodic functions of the same period can always be reduced to a single function, it will be shown for the general case, below. Take two functions, f_1 and f_2, with different magnitudes and phases *e.g.,* :

$$f_1 = A \cdot \sin(\psi)$$
$$f_2 = B \cdot \sin(\psi + \delta)$$

where in this instance, δ refers to an arbitrary but constant value. The sum of the two functions may be written as a single sinusoid with a different phase:

$$\begin{aligned} F &= f_1 + f_2 \\ &= A \cdot \sin(\psi) + B \cdot \sin(\psi + \delta) \\ &= C \cdot \sin(\psi + \Delta) \end{aligned}$$

where the coefficient C is the magnitude of the combined equivalent function, F, and Δ is the phase offset of F with respect to the first function, f_1. These coefficients may be determined from the following

$$C = \sqrt{A^2 + B^2 + 2AB\cos\delta}$$
$$\Delta = \sin^{-1}\frac{B\sin\delta}{C}$$

Hence, **any combination of in-plane velocities may be represented by a single equivalent in-plane velocity at a phase angle**. Another way to summate 1P aerodynamic forcing components is to resolve vector quantities at the propeller disc, and create a single incident velocity vector - though that approach is only valid for uniform incident velocity - whereas by considering the sum of periodic functions, a radially nonuniform incident flowfield with a 1P azimuthal harmonic will still be representable as a single periodic forcing at each radial station. This means that an aerodynamic model capable of modelling the load variation of an inclined isolated propeller should be suitable to determine the 1P load variation due to a more complex incident flowfield - provided the model is formulated to correctly resolve disc velocities into blade element axes.

Blade radial stations are regularly treated in isolation for performance and design codes in the form of blade-element or strip analysis, invoking the so-

called 'independence of blade-elements assumption', which is noted as being without physical justification (Wald, 2006). Though the three-dimensional behaviour of a lifting surface is generally different to its two-dimensional behaviour, particularly looking at aerodynamic nonlinearities, the two-dimensional behaviour is generally suitable for strip analysis of high aspect ratio lifting surface - *i.e.,* wings and propeller blades. Vortex corrections such as Goldstein's/Lock-Goldstein's/Prandtl's circulation distribution function enforce a spanwise loading more representative of a working propeller subject to the assumptions within (*e.g.,* light loading). The finite-difference solution of Morrison and Bocci (1985) removes the light loading assumption, but the wake is still helical in structure - which it will not be for a propeller at an angle of incidence.

It is known that close to the root and tip of a propeller blade, the isobars will not follow the wing sweep line - hence the flow will be 'sheared' (ESDU, 1978). Though various correction factors exist for approximating three-dimensional effects as a change in the sectional geometry (*e.g.,* an industrial source as referenced by Bocci and Morrison (1988) - as described in Section 2.6), the extension of these methods to a propeller at an angle of incidence is a considerable task and will not be considered in this dissertation but would be a good avenue for future research and a potential extension of the methods developed in this present work.

The 'advancing' and 'retreating' halves of the propeller disc have been described - with the extrema being the $\frac{\pi}{2}$ and $\frac{3\pi}{2}$ positions, respectively. For a given propeller at known J, n and γ, the geometric angle of attack change due to the summation of in-plane velocity and rotation may be determined easily - this will be defined as the **first-order angle of attack (AoA) change**.

This definition serves as a useful metric; *higher order physical effects that may be present on a propeller at an angle of incidence (e.g., aeroelasticity, wake skew), but cause an AoA change that is an order of magnitude below the first order AoA change, may be justifiably disregarded for an engineering-level model.*

Definition 2.3.1

The **first order angle of attack change** is defined as the range of effective angle of attack at a given radial position, $\Delta\alpha_R|_{1^{st}}$, due to the vector resolution of V_n, V_p and $\omega \cdot r$ at that station. No higher order effects taken into account.

To quantify these effects, the model formulation needs to be developed and described. The method used in this model is based on fundamental blade element theory, which is described in many sources (*e.g.,* Gur and Rosen, 2008; Ingram, 2011; Heene, 2012). The formulation of such a model for a propeller at an angle

of incidence has been described much less frequently, and semi-inconsistently so will be laid out rigorously in this chapter. The formulation of a blade element model for a propeller at an angle of incidence is as follows.

2.4 MODEL FORMULATION AND FIRST ORDER 1P LOAD

The velocity field at the propeller in *disc axes*, X_D, Y_D, Z_D (see Figure 2.1 on page 38), for pure disc inclination is:

$$\vec{\mathbf{V_D}} = \begin{bmatrix} U_D \\ V_D \\ Z_D \end{bmatrix} \tag{2.5}$$

$$= \begin{bmatrix} 0 \\ V_\infty \sin\gamma \\ -V_\infty \cos\gamma \end{bmatrix} \tag{2.6}$$

which may be resolved into blade axes, dependent on azimuthal position:

$$\vec{\mathbf{V_B}}(\psi) = \begin{bmatrix} U_B \\ V_B \\ Z_B \end{bmatrix} \text{ or } \begin{bmatrix} V_p \\ V_r \\ -V_n \end{bmatrix} \tag{2.7}$$

$$= \begin{bmatrix} U_D \cdot \cos\psi + V_D \cdot \sin\psi \\ U_D \cdot \sin\psi + V_D \cdot \cos\psi \\ W_D \end{bmatrix} \tag{2.8}$$

which, since equation 2.6 has shown for pure disc inclination, $U_D = 0$, becomes

$$= \begin{bmatrix} V_D \cdot \sin\psi \\ V_D \cdot \cos\psi \\ W_D \end{bmatrix} \tag{2.9}$$

V_p and V_n refer to the velocity components parallel to axes X_B and Z_B ($= Z_D$)[4], and V_r refers to the radial component of velocity, parallel to Y_B. If, instead of pure disc inclination in a uniform freestream, the incident flow distribution is nonuniform and defined over the disc as $\vec{\mathbf{V_D}}(r,\psi)$:

$$\vec{\mathbf{V_B}}(r,\psi) = \begin{bmatrix} V_p \\ V_r \\ -V_n \end{bmatrix} = \begin{bmatrix} U_D(r,\psi) \cdot \cos\psi + V_D(r,\psi) \cdot \sin\psi \\ U_D(r,\psi) \cdot \sin\psi + V_D(r,\psi) \cdot \cos\psi \\ W_D(r,\psi) \end{bmatrix} \tag{2.10}$$

So for uniform incident flow, Eq. 2.9 determines the disc to blade transformation, whereas Eq. 2.10 determines the disc to blade transformation for any dis-

[4]Note that V_n is defined as positive towards the disc, whereas the Z_D is defined in the opposite direction.

tribution of incident velocity defined at the propeller disc. For a straight-bladed propeller, this is enough information to determine sectional aerodynamic properties - as the blade elements are defined along the pitch change axis (PCA), and hence in blade axes. Referring to Figure 2.3, the advance angle is defined:

$$\phi = \tan^{-1} \frac{V_n}{V_\omega + V_p} \tag{2.11}$$

and the incident flow magnitude, V_R:

$$V_R = \sqrt{V_n^2 + (V_\omega + V_p)^2} \tag{2.12}$$

at effective angle of attack, α_R:

$$\alpha_R = \beta - \phi \tag{2.13}$$

where the tangential velocity due to blade rotation is defined as

$$V_\omega \triangleq \omega \cdot r \tag{2.14}$$

The effective angle of attack and resultant velocity may be used to determine the lift and drag from a variety of methods (see Section 2.5.1). The elemental lift and drag, dl and dd, may be resolved into the elemental thrust and tangential force contributions due to a single blade element:

$$dT = \sum F_{ZB} = dl \cdot \cos\phi - dd \cdot \sin\phi \tag{2.15}$$

$$\tfrac{dQ}{r} = \sum F_{XB} = dl \cdot \sin\phi + dd \cdot \cos\phi \tag{2.16}$$

Integration of Equations 2.15 and 2.16 and summation over blade index, b, determine the propeller performance characteristics - the reacted thrust and torque in addition to pitching and yawing moments (T, Q, L and M, respectively) at the hub:

$$\text{Thrust:} \qquad T = \sum_{b=1}^{B} \int_{r_{hub}}^{R} dT_b \, dr \tag{2.17}$$

$$\text{Torque:} \qquad Q = \sum_{b=1}^{B} \int_{r_{hub}}^{R} dQ_b \, dr \tag{2.18}$$

$$\text{Pitching Moment:} \qquad L = \sum_{b=1}^{B} \int_{r_{hub}}^{R} dT_b \cdot r \cdot \cos\psi \, dr \tag{2.19}$$

$$\text{Yawing Moment:} \qquad M = \sum_{b=1}^{B} \int_{r_{hub}}^{R} dT_b \cdot r \cdot \sin\psi \, dr \tag{2.20}$$

Similar expressions exist for the in-plane force reacted at the hub, but these may not fully capture the total contributions to in-plane force, and this is discussed in Chapter 6.

To determine the load fluctuation on the blades, it is useful to resolve the forces in the directions in which blade structural characteristics are determined

i.e., out-of-plane, defined positive towards the suction surface and *in-plane*[5], defined as positive in the chordwise direction. The blade element axes are not pictured in Figure 2.3, but are defined in these directions, that is, with Z_{BE} normal to the chord line, and X_{BE} parallel to the chord line. It follows that:

$$F_{ZBE} = F_{XB} \cdot \sin\beta + F_{ZB} \cdot \cos\beta \qquad \text{(Out-of-plane Force)} \tag{2.21}$$

$$F_{XBE} = F_{XB} \cdot \cos\beta - F_{ZB} \cdot \sin\beta \qquad \text{(In-plane Force)} \tag{2.22}$$

The bending moment experienced at a given blade element will be due to be the sum of elemental forces from blade elements outboard of that point, resolved into the axis of the first element, and multiplied by the moment arm. For the moments at blade element e, it may be written for out-of-plane moment, L, and in-plane moment, N:

$$L|_e = -\sum_{i=e}^{nr} [F_{XBi} \cdot \sin\beta_e + F_{ZBi} \cdot \cos\beta_e] \cdot (r_i - r_e) \tag{2.23}$$

$$N|_e = \sum_{i=e}^{nr} [F_{XBi} \cdot \cos\beta_e - F_{ZBi} \cdot \sin\beta_e] \cdot (r_i - r_e) \tag{2.24}$$

For a given propeller at an angle of incidence the sectional velocities and angle of attack may be determined all over the propeller disc. When combined with a suitable lifting model, the forces and moments at any point may be calculated using equations 2.6 through 2.24. To extend this model, a suitable lifting model needs to be identified, and the respective magnitude of higher-order 1P loading sources needs to be determined. For the purposes of determining the 1P loading, parameters introduced by Gray et al. in the 1950's will prove useful.

2.4.1 EFFECTIVE ADVANCE RATIO AND ROTATIONAL SPEED

Gray et al. (1954) used an empirical method to estimate 1P load variation. In their analysis, they measured the thrust gradings (the spanwise variation of thrust) from a noninclined propeller over a large range of advance ratio and rotational speed and presented them in coefficient form - $\frac{dC_T}{dx}$. Their measurements were taken with a set of total pressure probes mounted fixed on a rake that extended along the propeller radius, capable of measuring several radial positions at one time, and moveable to different azimuthal locations. They used these values from the noninclined propeller to interpolate for the local thrust gradings for the same propeller at incidence. To achieve this, they introduced two new parameters, described in the following section.

[5] *In-plane* here refers to the plane in which the blade element chord is defined, not the disc plane. Since the stiffness in this direction is usually very high, only the out-of-plane force is likely of interest.

Over the disc of a propeller at incidence, the distribution of normal and in-plane incident velocity give rise to a tangential velocity field that varies with azimuthal and radial position. The tangential velocity experienced by a particular blade station is equivalent to that that which would be experienced in steady axial flight at *some* advance ratio and *rotational speed - i.e.,* the advancing blade is operating under local conditions equivalent to some effectively higher rotational speed, n, than the physical RPM and a corresponding lower advance ratio, J. The retreating blade will similarly be operating under conditions equivalent to a lower n and a higher J. These *effective* values of n and J, which will not be the same as the operational advance ratio and rotational speed are defined as the **effective advance ratio**, J', and the **effective rotational speed**, n':

$$J'(\gamma, \psi, x) = \frac{\pi \cdot x \cos\gamma}{\frac{\pi \cdot x}{J} + \sin\gamma \sin\psi} \tag{2.25}$$

$$n'(\gamma, \psi, x) = n + \frac{V \sin\gamma \sin\psi}{\pi D x} \tag{2.26}$$

From basic physical reasoning, and inspection of 2.25 and 2.26, it can be seen that for $\gamma > 0$, on the advancing side of the propeller disc:

$$J' < J \tag{2.27}$$

$$n' > n \tag{2.28}$$

and for the retreating side

$$J' > J \tag{2.29}$$

$$n' < n \tag{2.30}$$

whilst at the top and bottom of the disc ($\psi = 0, \pi$):

$$J' = J \tag{2.31}$$

$$n' = n \tag{2.32}$$

such that the uppermost and lowermost positions of the propeller disc are unaffected by the disc inclination in this simple case - though Chapter 6 will demonstrate a means via which this assumption is not wholly correct.

The work in this dissertation will utilise the effective advance ratio and the effective rotational speed as the basis for an order of magnitude analysis. The methodology as described by Gray et al. goes further and assumes that the aerodynamic response of the blades would be exactly the same as for the effective conditions. Implicit in this is a reliance upon the so-called **steady-state assumption**. This assumption will be fully explained in the next chapter, but the pertinent detail is that the thrust on the propeller blades is assumed to react instantaneously to the change in J' and n'. This enfores an azimuthal independence of blade elements in that the local thrust is assumed to be dependent on local conditions *only*. Gray et al. cite Crigler and Gilman Jr (1952) as the basis for the steady-state assumption, whose description of the steady-state method is given below:

> "In steady-state calculations of the forces and moments on the blade of a pitched propeller, a change in time (blade position) is treated simply as a change in the operating V/nD of the propeller in accordance with equation (3)[6]. The complete propeller is assumed to operate successively at different blade positions under the instantaneous condition at each particular position."
>
> Crigler and Gilman Jr (1952) - Calculation of Aerodynamic Forces on a Propeller in Pitch of Yaw.

Discussion of the validity of this assumption will be left until the next chapter - the use of the effective conditions does not invoke the steady-state assumption and this work will use J' and n' for the model as a benchmark for the range of aerodynamic conditions experienced at the propeller disc.

The range of J' and n' over the disc may be determined from the difference from the extrema positions $\psi = \frac{\pi}{2}, \frac{3\pi}{2}$:

$$\Delta J'(\gamma, x) = \frac{2 \cdot \pi x \cos\gamma \sin\gamma}{\left(\frac{\pi x}{J} + \sin\gamma\right)\left(\frac{\pi x}{J} - \sin\gamma\right)} \tag{2.33}$$

$$\Delta n'(\gamma, x) = 2 \cdot \frac{V \sin\gamma}{\pi D x} \tag{2.34}$$

Equations 2.33 and 2.34 may be used to determine the effective range of advance ratio and rotational speed experienced on a propeller at an angle of incidence. For conditions of $J = 1.5$ and $D = 3$m the following spanwise ranges for J' and RPM' may be calculated for different inclination angles, γ - see Figure 2.4.

A large change in both J' and RPM' may be seen in the inboard sections, with the change getting smaller and staying roughly constant towards the outboard sections. A good first approximation of what any 1P model needs to be able to predict, therefore, is the steady blade forces for these given advance ratios and rotational speeds. The influence of other phenomena on the prediction of these characteristics will give a good indication of what needs to be included in an industrial 1P code, and what may be justifiably disregarded. To this end, performance predictions of axial flight may be compared - since the performance parameters of Thrust Coefficient, C_T, Torque Coefficient, C_Q, and Power Coefficient, C_P, are the product of elemental forces integrated along the span. Figure 2.4 indicates that the range of flow conditions will vary the most in the inboard sections - however the inboard sections will contribute the *least* to 1P bending stress, due to the smaller moment arm. In addition, the dynamic pressure will be considerably lower in the inboard sections, so even if the ΔC_l is larger in the root sections, the Δl will likely be smaller.

[6] *Equation (3) in Crigler and Gilman Jr (1952) is equation 2.25 is this dissertation*

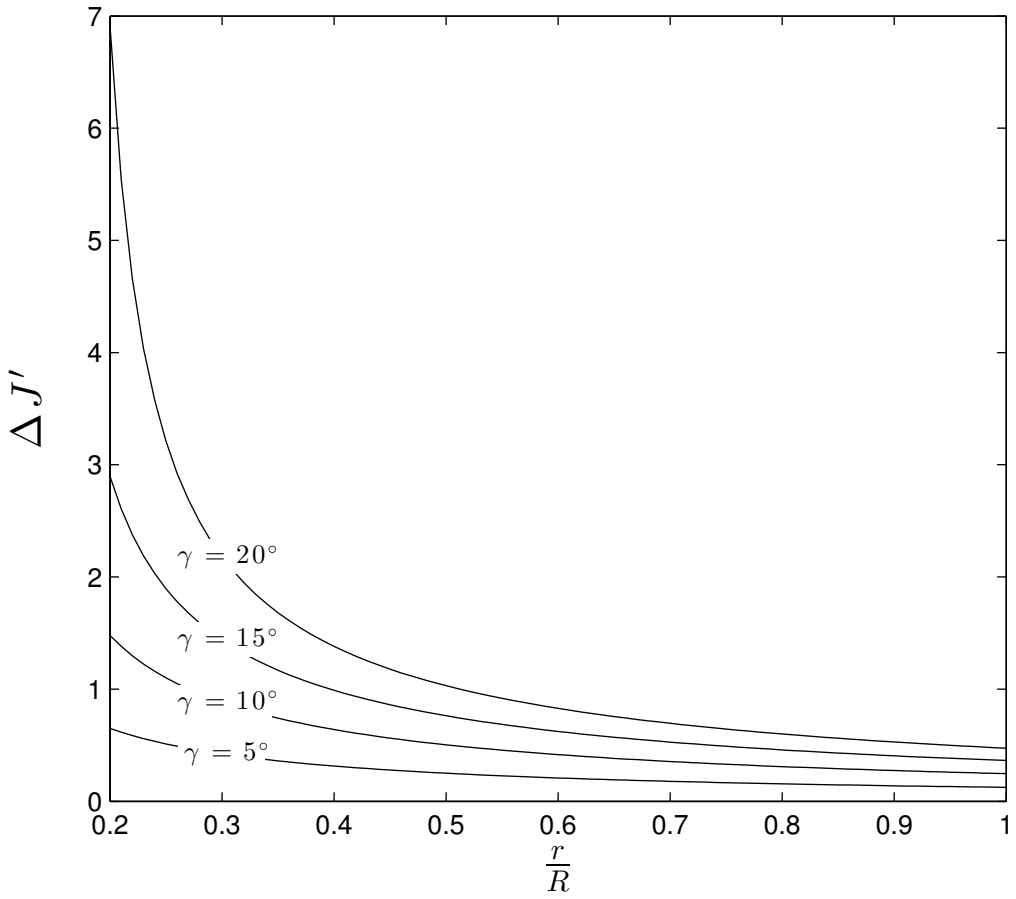

(A) RANGE OF EFFECTIVE J

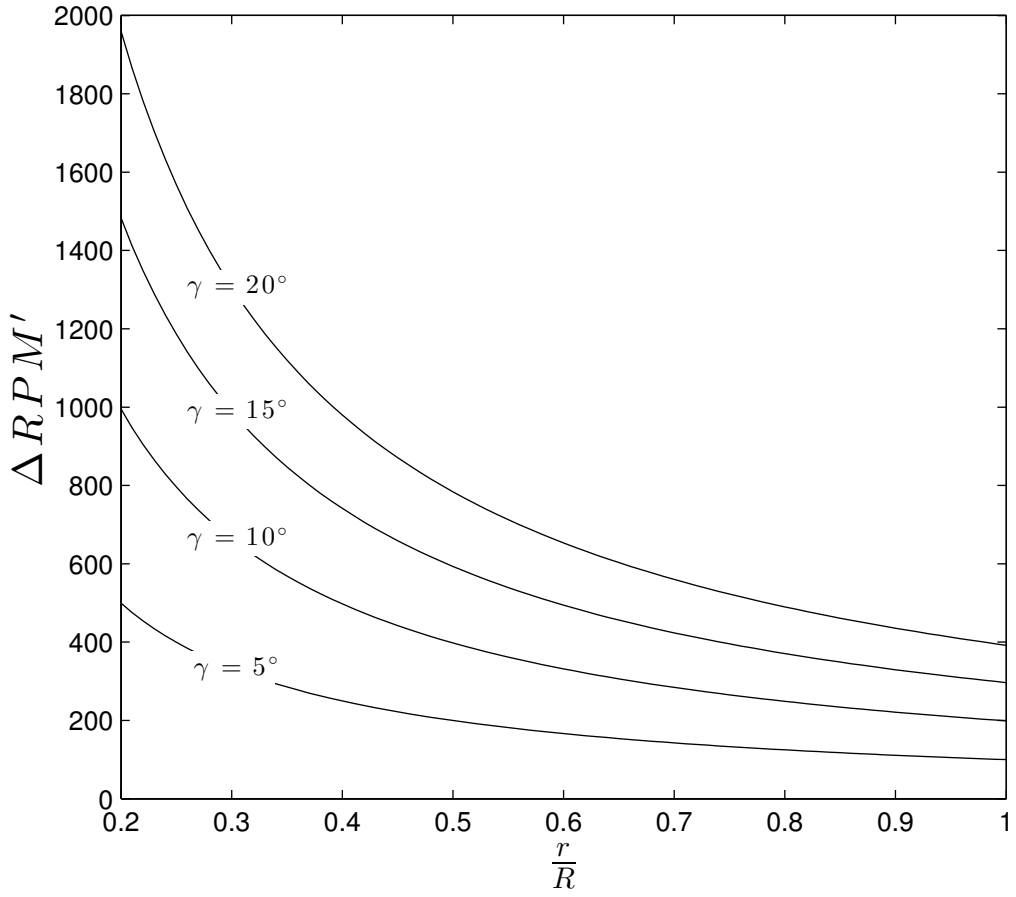

(B) RANGE OF EFFECTIVE RPM

FIGURE 2.4: J' AND RPM′ VS x FOR DIFFERENT γ. $J = 1.5$, $D = 3m$

Even for the largest disc inclination shown, $\gamma = 20°$, the $\Delta J'$ at the 30% radius is ~ 2, whilst at 70% radius is < 1. As a crude first approximation it can be expected that the local elemental force variation, $\Delta\vec{F_{BE}}$ for the inboard stations would be an order of magnitude above those of the outboard stations. However, the respective radial positions means that the moment arm of the inboard section is $\frac{1}{6}^{\text{th}}$ that of the outboard section[7]. It follows that the range of $\Delta J'$ over the outboard sections is going to be more important in determining a given modelling technique's validity for prediction of integrated moment at the root.

The reasoning presented above means says that modelling techniques capable of predicting the variation of C_T and C_Q or C_P over a range of J and n equivalent to the range of J' and n' will provide the minimum fidelity needed in a 1P model. In order words, if a model cannot adequately predict the performance over this range, it clearly cannot be used to give reliable 1P load estimates.

Once a model achieves the necessary condition above, it may be used and extended to incorporate other effects. The steady state change to sectional angle of attack was defined in on page 43 as $\Delta\alpha_R|_{1^{\text{st}}}$. This parameter can be determined in terms of radial position, advance ratio and disc inclination. From equations 2.11 and 2.13, it may be defined:

$$\begin{aligned}\alpha_R(\gamma,\psi,x) &= \beta - \phi \\ &= \beta - \tan^{-1}\frac{V_n}{\omega\cdot R\cdot x + V_p}\end{aligned} \tag{2.35}$$

and the range of α_R may be determined:

$$\begin{aligned}\Delta\alpha_R|_{1^{\text{st}}} &= \left[\beta - \phi|_{MIN}\right] - \left[\beta - \phi|_{MAX}\right] \\ &= \Delta\phi \\ &= \tan^{-1}\frac{V_n}{\omega\cdot R\cdot x - V_D} - \tan^{-1}\frac{V_n}{\omega\cdot R\cdot x + V_D}\end{aligned} \tag{2.36}$$

using the arctangent addition formula:

$$\tan^{-1}A \pm \tan^{-1}B \equiv \tan^{-1}\frac{A\pm B}{1\mp A\cdot B}, \qquad (A\cdot B \neq 1)$$

equation 2.36 may be written as

$$\begin{aligned}&= \tan^{-1}\frac{2V_D V_n}{(\omega\cdot R\cdot x)^2 + V_n^2 - V_D^2} \\ &= \tan^{-1}\frac{2V_\infty^2\cos\gamma\sin\gamma}{(\omega\cdot R\cdot x)^2 + V_\infty^2\left(\cos^2\gamma - \sin^2\gamma\right)}\end{aligned} \tag{2.37}$$

in nondimensional form:

$$\Delta\alpha_R|_{1^{\text{st}}} = \tan^{-1}\frac{J^2\sin(2\gamma)}{(x\pi)^2 + J^2\cos(2\gamma)} \tag{2.38}$$

Equation 2.38 provides the magnitude of the geometric angle of attack variation due to in-plane velocity for pure disc inclination, and it can be seen that it is a

[7]This analysis is only looking at the $.7R$ section, and obviously the $.95R$ section will have an even larger moment arm.

function of advance ratio, radial position, and disc inclination angle. This first order angle of attack variation is plotted for low and high advance ratio over a range of disc inclination angles in Figure 2.5. The first order angle of attack change is largest at the inboard sections, and smaller at the outboard sections. For cruise-type advance ratios, Figure 2.5b, from the $x = 0.4$ station the $\Delta\alpha_R|_{1^{st}}$ is about the order of magnitude of the disc inclination, with the range being reduced to about half this value at the tips.

With this range of first order angle of attack change, second order effects on the 1P load may be quantified - and the requisite fidelity in different model components determined. Two criteria to justify inclusion/exclusion of physical flow effects in a 1P prediction model have been defined in this chapter and discussed in the introduction. They are formally outlined below:

Note 2.4.2
Model 1P Prediction Criteria:

1. The *minimum criterion* for a 1P prediction model is **accurate prediction of propeller performance over a range of effective advance ratio and rotational speed**, J' and n'. These are defined in Equations 2.25 and 2.26 for a given J, n, D and γ. If a model fails to capture this variation, then it cannot accurately predict the first order angle of attack or force variation due to disc inclination.

2. To determine the respective magnitude of physical effects on 1P load, the second criterion is defined. If **a physical effect or modelling technique causes a 1P AoA change that is an order of magnitude equal to or larger than the first order 1P AoA change (definition 2.3.2), then it must be included in an engineering-level 1P prediction model**. *Effects that cause an AoA change smaller than this* may be physically present and offer an insight into detailed flow physics, but their effect on reacted 1P bending load will be small, and *may be disregarded in an engineering level 1P prediction model.*

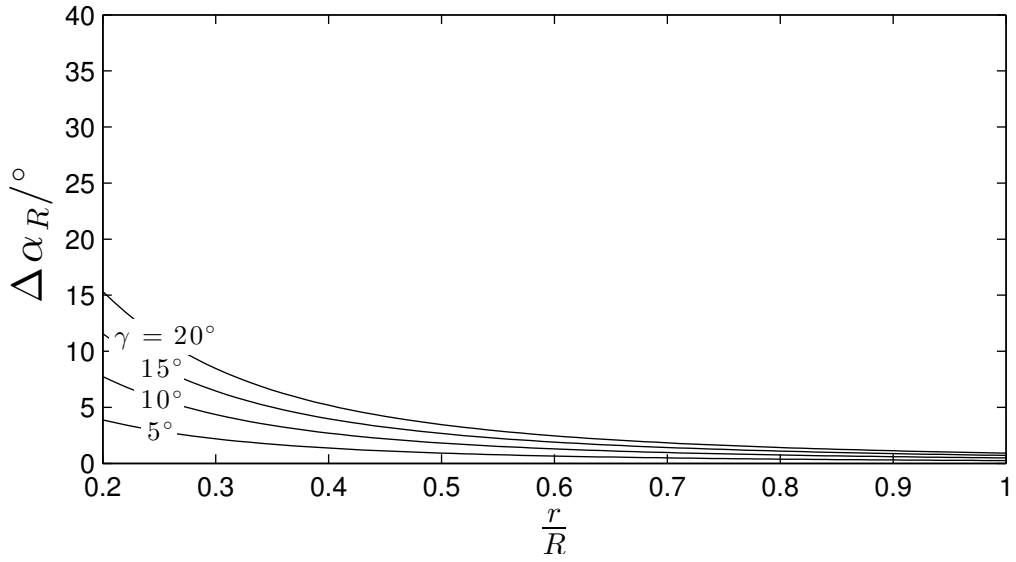

(A) $J = 0.5$

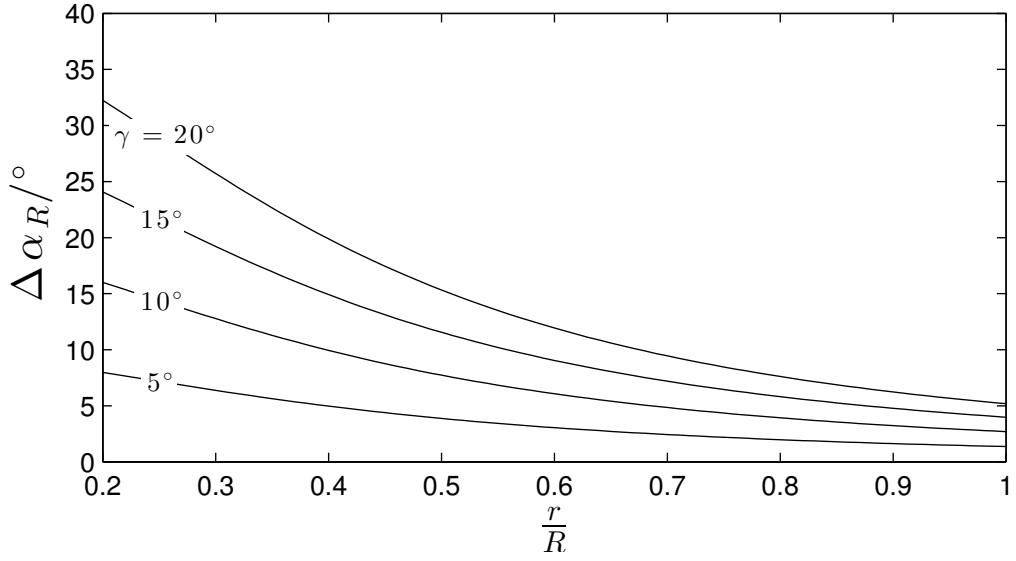

(B) $J = 1.25$

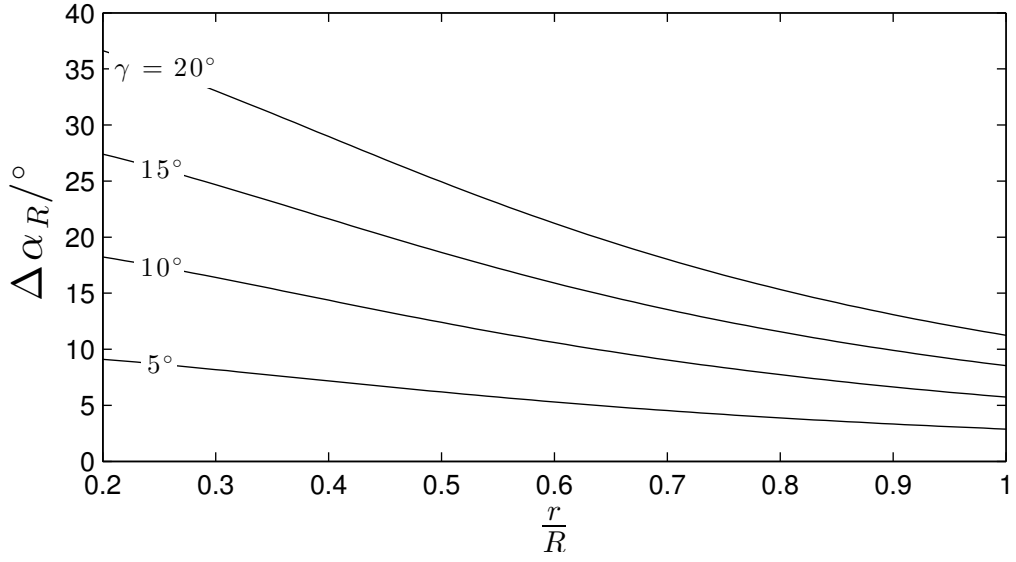

(C) $J = 2.0$

FIGURE 2.5: SPANWISE FIRST ORDER ANGLE OF ATTACK RANGE DUE TO DIFFERENT DISC INCLINATION ANGLES, γ, FOR LOW, MED AND HIGH ADVANCE RATIO.

The first is the 'necessary' criterion for elements that should be included in a 1P blade element. If a model cannot determine the performance characteristics over a range of onset flow/operating conditions as defined by equations 2.33 and 2.34, then it will fail to capture the first order fluctuating load. To determine whether a model can meet the necessary criterion, the gradients $\frac{dC_T}{dJ}$ and $\frac{dC_Q}{dJ}$ or $\frac{dC_P}{dJ}$ for different rotational speeds should be compared to test results - which are easily obtainable from performance data.

The second criterion determines the justification for what *else* should be included in an efficient 1P model. It is clearly possible to use the most physically rigorous and complex simulation technique for every step - but that is not the purpose of this model. For a computationally efficient solution, the order of magnitude of different physical effects are considered. Flow features and physical effects that change the 1P AoA prediction by an order of magnitude less than the range of first-order AoA prediction may be justifiably disregarded in an engineering-level aerodynamic 1P prediction code.

2.5 LIFTING MODEL AND HIGHER ORDER EFFECTS

The model as described up to this point is capable of determining the variation of both angle of attack and resultant velocity over the disc of a propeller at an angle of incidence - subject to either uniform or nonuniform incident flow. In order to determine the forces on the blades using equations 2.15 and 2.16, the sectional lift and drag, dl and dd, need to be calculated. With $\alpha_R(r,\psi)$ and $V_R(r,\psi)$ known, a suitable lifting model may be used to determine dl and dd.

2.5.1 LIFTING MODEL

Many propeller blade element models utilise table-lookup for sectional lift/drag based on the profile shape at each spanwise ordinate - either through empirical formulae[8] or through interpolation of test data (*e.g.,* Korkan et al., 1980). Neither of these methods is particularly computationally expensive in an axial performance calculation - as only a single azimuthal position is required. For a propeller at an angle of incidence, however, calculations need to be performed at a range of points around the azimuth. For a 5° step size in azimuthal discretisation, this raises the number of computations required $\times 72$, and it may be advantageous to use a simpler lift/drag calculation method.

Some forward flight rotorcraft models utilise linear aerodynamics, using $\bar{a} = 5.7/rad$, or using $\bar{a} = 2\pi$ with a Prandt-Glauert compressibility correction (Leishman, 2006; Prouty, 2002). Figures 2.6 and 2.7, overleaf, show propeller

[8] A commercially-sensitive reference of such a method is made in an industrial document discussed earlier, but cannot be included in this document.

performance predictions using a linear lifting model with a Prandtl-Glauert compressibility factor, and also using an interpolation databank made from experimental tests. Calculations were also performed using a simple linear lift curve slope without the compressibility correction, but have not been included on these plots as there was only a slight difference between the two models owing to the low rotational speed.

These figures show that when compared to experimental data, calculations using an experimental databank are more accurate than simple linear aerodynamic methods. Over a range of J and n simple linear aerodynamics are unsuitable for accurate performance determination, and hence will be unsuitable for determining the 1P load variation. The model developed in this dissertation assumes that a suitable means of determining dl and dd is available.

In addition, the utilisation of two-dimensional lift and drag data affords some estimation of stall characteristics - as these will be included implicitly with any two-dimensional data. This can be seen as the aerodynamic nonlinearities at low J in the results using the aerodynamic databank, which shows better correlation with experimental data than the purely linearly $\frac{dC_T}{dJ}$ prediction of the linear databank. Whilst three-dimensional stall will be different from the two-dimensional properties of the sections that make up a blade, if the two-dimensional data predict that stall is likely to occur, then it will give an indication that a higher-order modelling technique needs to be utilised. It is likely that a model based on two-dimensional data will predict that sections stall *too early*, as Coriolis effects in the boundary layer of inboard sections will delay separation (Snel et al., 1994; Rosen and Gur, 2005). The model of Snel et al. can be included easily in this model, as it is a closed-form correction to the lift curve slope based on the ratio of chord to radius, but is not discussed further in this dissertation as static stall is unlikely to be present for a 1P loading condition. Further modelling of stall would require the implementation of a dynamic-stall model such as ONERA's or the Beddoes-Leishmann model (Hansen et al., 2004).

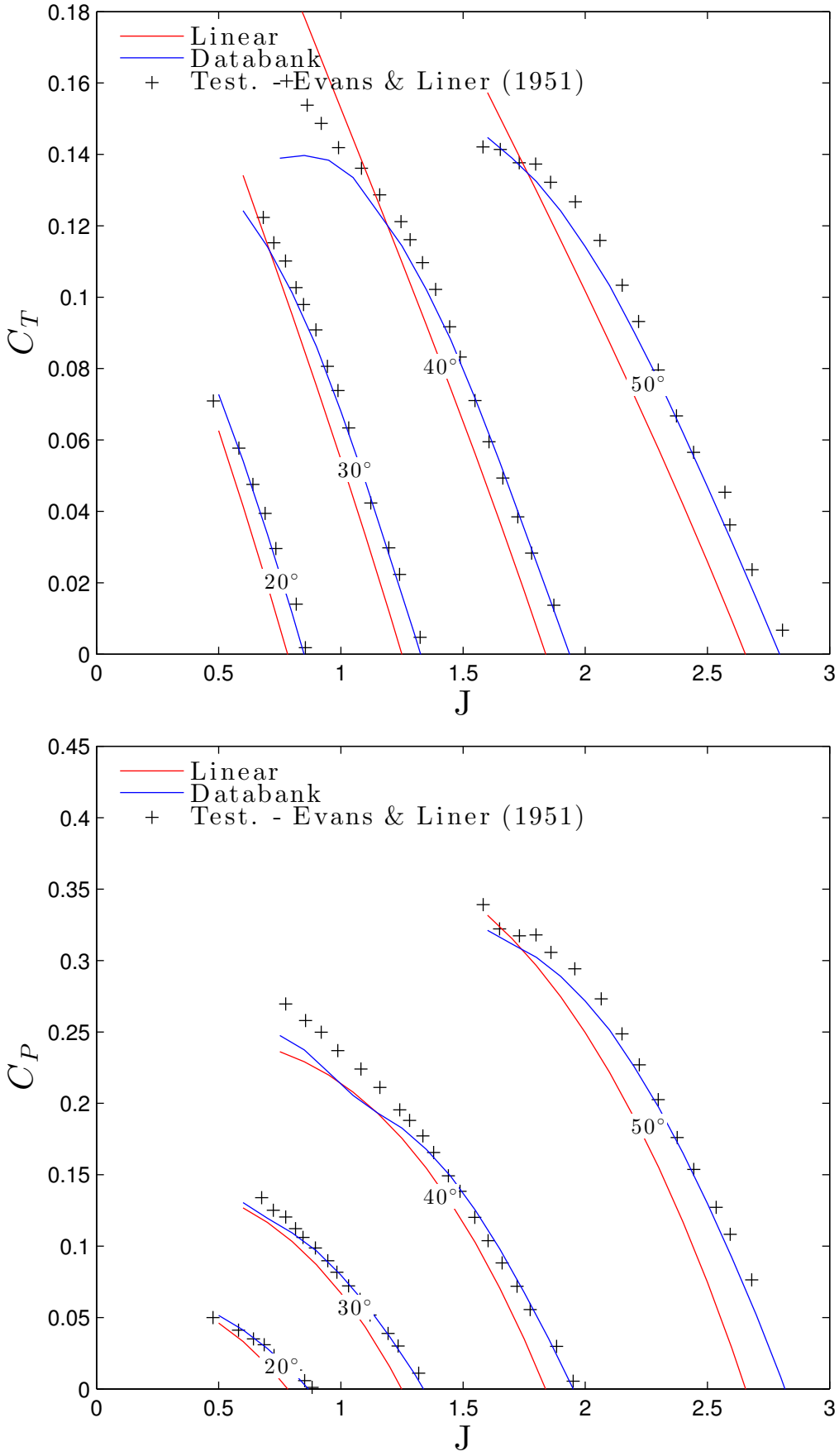

FIGURE 2.6: PERFORMANCE PREDICTIONS WITH TWO DIFFERENT LIFTING MODELS - 1140 RPM. TEST DATA FROM EVANS AND LINER (1951)

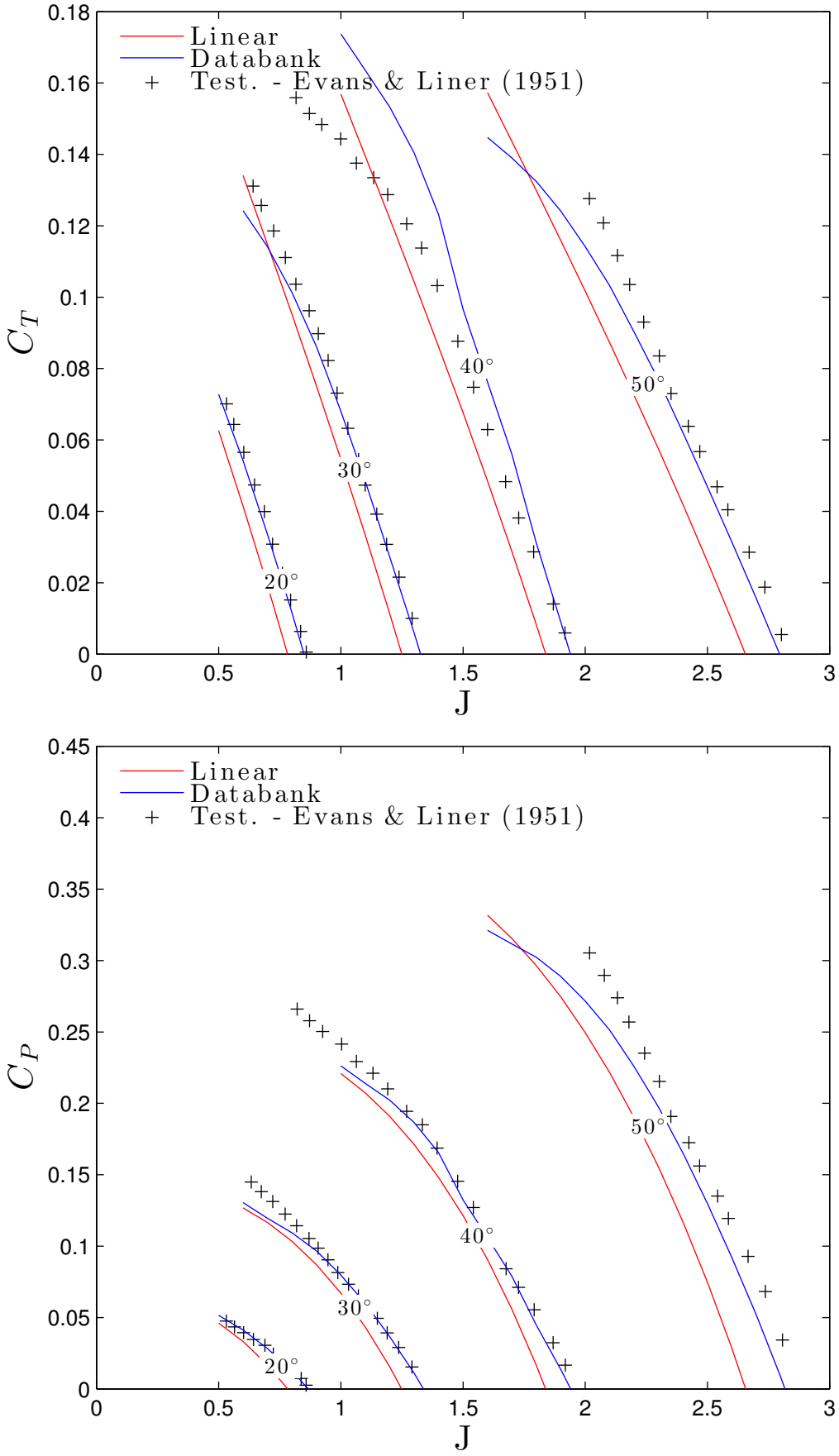

FIGURE 2.7: PERFORMANCE PREDICTIONS WITH TWO DIFFERENT LIFTING MODELS - 1350 RPM. TEST DATA FROM EVANS AND LINER (1951)

2.5.2 HIGHER ORDER EFFECTS

With the first-order 1P aerodynamic load defined, higher order effects may be considered and compared. "Higher order" in this sense should be taken to refer to any physical effect requiring further modelling techniques. This does not mean that such effects are higher order in terms of their influence on 1P loading. The effects that are considered here are:

- ***Induced Flow:*** The lifting blades have an associated bound vorticity that varies with radius and hence sheds vorticity into the wake. The bound vorticity at the blades and the shed helical wake induces an axial and tangential velocity at the propeller disc plane, thus changing the aerodynamics. The actual wake geometry will be highly complex, but there are many different engineering models that may be considered. If the distribution of induced flow is deemed to be an important effect, then what needs to be determined is the minimum fidelity required to accurately resolve *the velocity at each blade element due to the lift on the blades themselves, and its distribution around the disc.*

- ***Unsteady Aerodynamics:*** The propeller blades will be subject to an incident velocity and angle of attack that varies with time. The aerodynamic response of any lifting or non-lifting body to a time-varying flowfield is based on the entire time history of incident flow, and may not be assumed to be effected instantaneously. Furthermore, exact solutions for unsteady aerodynamic behaviour are only available for harmonic aerofoil motion (Theodorsen and Mutchler, 1935). The effect of unsteady aerodynamics on the 1P propeller problem must be determined, and a suitable aerodynamic model chosen for this purpose. Care must be taken when using an unsteady model in conjunction with a wake/induced flow model to ensure that the same features of the induced flowfield are not accounted for twice by two separate models. Most first order unsteady models (*e.g.,* Theodorsen, Loewy, Sears, Beddoes) utilise mathematical formulations that approximate the unsteady lift hysteresis and attenuation, including the effect of induced flow implicitly.

- ***Structural Deformations:*** Subject to aerodynamic and centrifugal forcing, the blades will deform and hence effect a change in sectional angle of attack. Blade elements moving within blade axes with respect to time will effect not only a change in angle of attack, but also a change in the *rate* of angle of attack. The respective magnitude of propeller blade static and dynamic deformations must be determined and accounted for by coupling with an unsteady model if deemed necessary. Higher order structural effects such as cross-sectional warping are of much lower aerodynamic magnitude and will not be discussed in this dissertation.

- ***Simple Installation:*** Extension of an inclined model to full aircraft installation will be discussed in Chapter 5, but the effect of a nacelle/spinner at incidence must be determined. Since a blade element model essentially models the spinning blades with no hub, spinner or nacelle, is not a true representation of a real life propeller at incidence - even in a wind tunnel 'isolated' setup. The effect of the flow around the spinner/nacelle at incidence must be determined. Even if a simple installation model does not largely change the predictions of $\frac{dC_T}{dJ}$, it may still change the distribution of sectional angle of attack due to in-plane acceleration.

2.5.3 INDUCED FLOW/UNSTEADINESS

Figures 2.8 and 2.9, overleaf, compare the effect of using the General Momentum Model (in an annular formation) on blade element calculations. Discussion of the momentum model and its formulation for a propeller at an angle of incidence is included in Chapter 3, but results for axial flight are shown here simply to demonstrate what effect induced flow may have on 1P load prediction. When induced flow is taken into account, the model predicts the gradients $\frac{dC_T}{dJ}$ and $\frac{dC_P}{dJ}$ much more accurately than the model without the induced flow. This highlights the importance of induced flow in determining the first order 1P load.

What cannot be determined without further investigation, is how the azimuthal distribution of the induced flow affects the 1P load prediction. It is postulated that the distribution of induced flow may lie somewhere between a 'steady-state' distribution, where the induced flow at the disc matches local loading conditions, and a distribution where the induced flow is azimuthally uniform over the propeller disc. The reasoning for this is that in a steady-state distribution, the azimuthal variation of circulation over the disc is taken into account in the induced flow distribution, but it also implies complete azimuthal independency in the solution (*i.e.,* that neighbouring azimuthal positions cannot affect one another), whilst a uniform distribution assumes the opposite (*i.e.,* that all azimuthal positions must be taken into account equally to determine the induced flow solution at a given point). Neither of these situations is physically realistic, and it is proposed that they form the likely bounds of the real induced flow distribution.

The level of unsteadiness in the flow will also contribute to the induced flow distribution. In a blade element model, the physical blade is represented by a bound vortex. It is the bound vortex that sustains the pressure discontinuity across the propeller disc, effecting the thrust. In a momentum model, the velocity induced by the pressure discontinuity is found from momentum balance in a bounding streamtube. In a vortex model, the induced velocity at the disc is found via Biot-Savart calculations on the shed vortex associated with spanwise variation

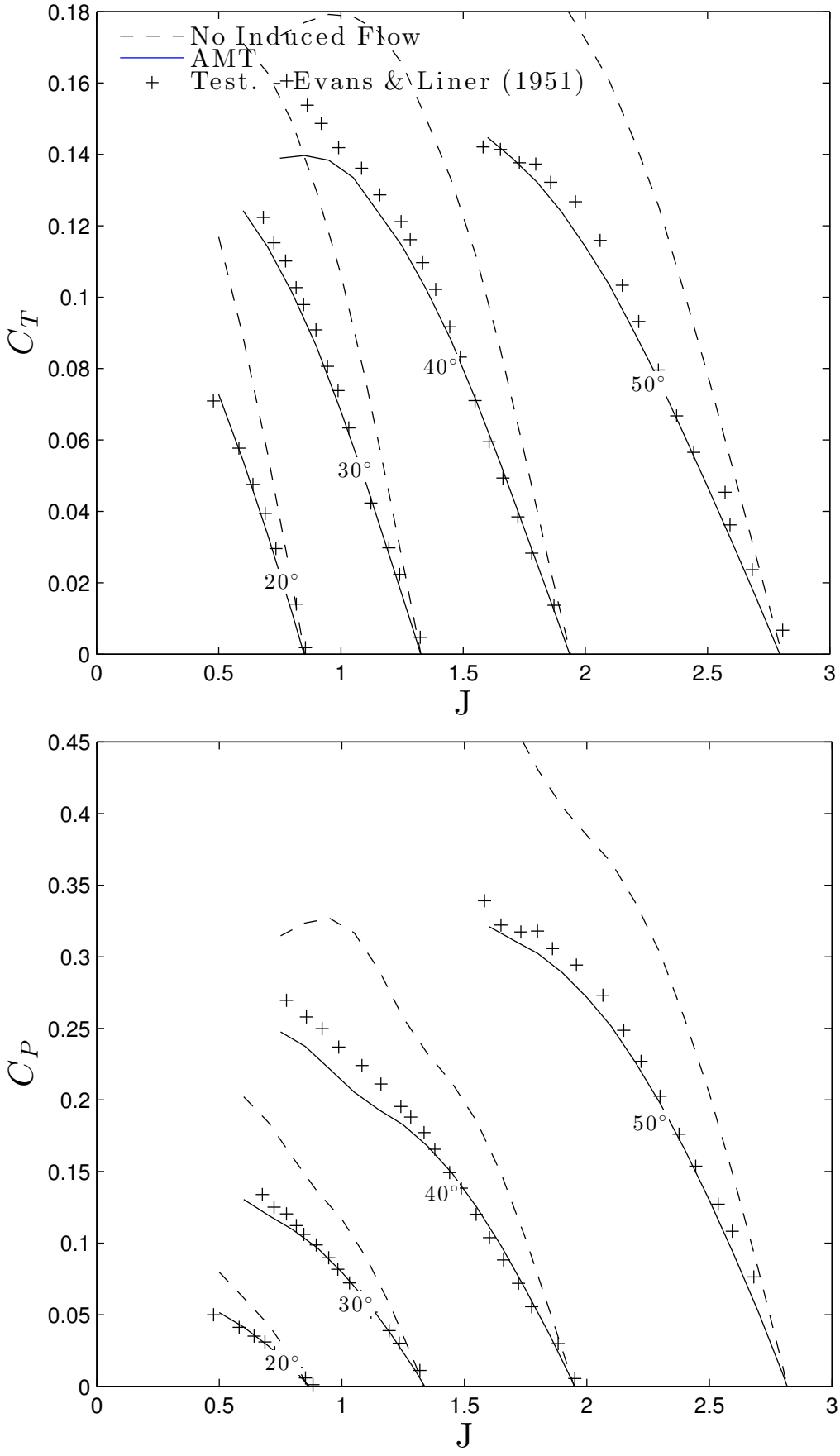

FIGURE 2.8: PERFORMANCE PREDICTIONS WITH THE EFFECT OF INDUCED FLOW INCLUDED/NOT INCLUDED - 1140 RPM. TEST DATA FROM EVANS AND LINER (1951)

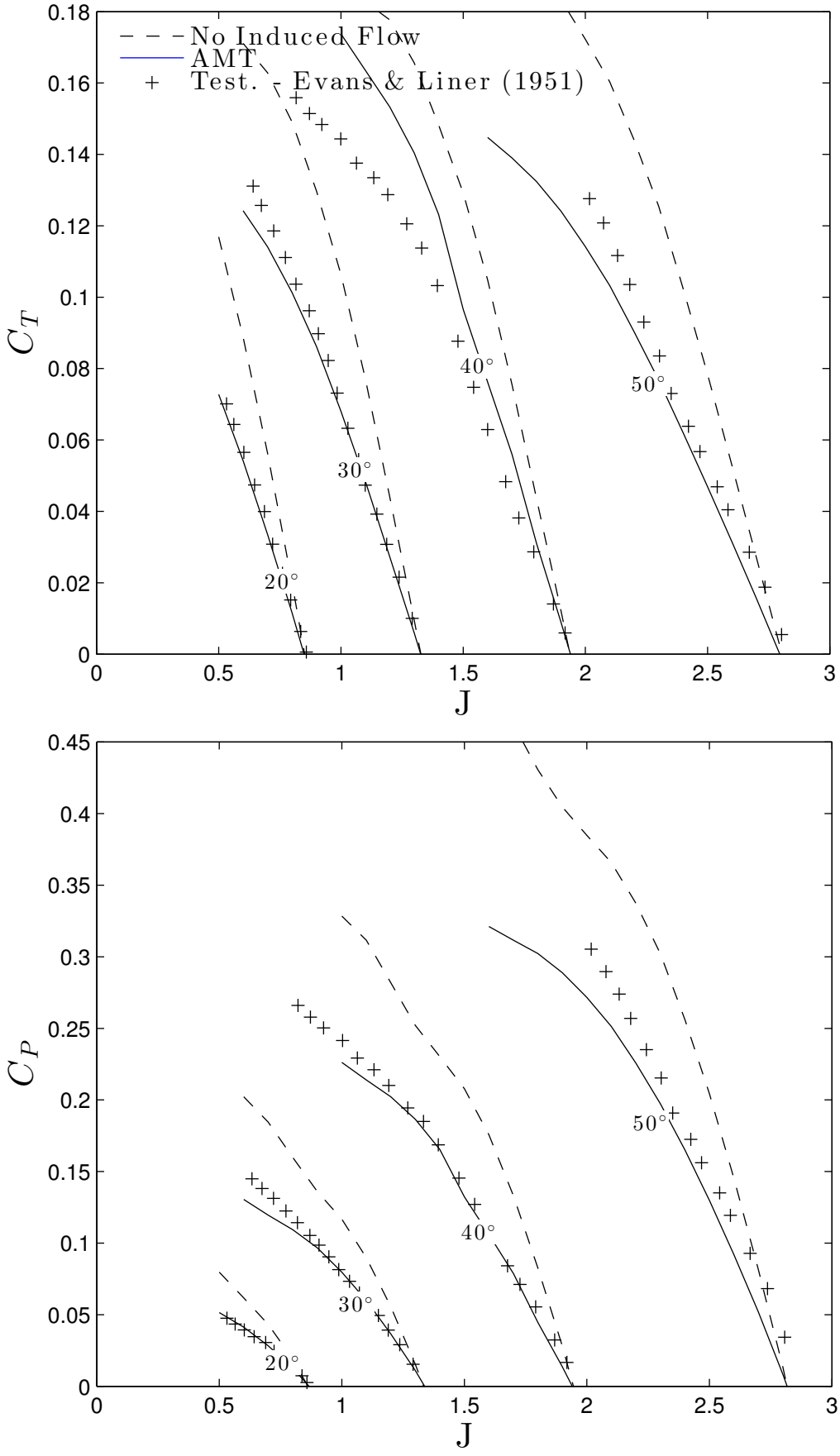

FIGURE 2.9: PERFORMANCE PREDICTIONS WITH THE EFFECT OF INDUCED FLOW INCLUDED/NOT INCLUDED - 1350 RPM. TEST DATA FROM EVANS AND LINER (1951)

of lift. Although these two modelling techniques have very different roots and inception, they produce identical results for the case of infinite blades, and may be considered to be modelling the same phenomenon - the **steady induced velocity field at the disc due to the steady thrust produced by the propeller**. This is valid for steady blade element conditions. With blade element lift that varies with azimuthal position, the strength of the bound vortex changes with time (*i.e.,* with azimuth) and conservation of vorticity from Kelvin's theorem means that any change needs to be balanced into the wake - this is in addition to the wake shed by the quasi-steady variation of lift being included in a steady-state induced flow model. This adds an extra component of induced flow at the disc; full discussion of the source of this effect and modelling techniques will be discussed in the following chapter. To see if unsteady aerodynamics are important for a given aerodynamic problem, an indication of the magnitude of unsteady effects may be determined from the *reduced frequency*, k. This parameter is widely-used and is gives an indication of the magnitude of fluctuating velocity components with respect to freestream parameters.

$$k \triangleq \frac{\omega_f c}{2V} \tag{2.39}$$

ω_f is the frequency of any forcing, c is the local chord, and V is the onset flow speed. The factor of two comes from the fact that the characteristic length for aerofoil oscillatory motion is the semi-chord, not the chord. Note that for 1P loading, the forcing frequency will be the same as the rotational frequency *i.e.,* $\omega_f = \omega$. To determine the extent of unsteady aerodynamic influence, the following definitions of flow regimes are taken from Leishman (2006, pg. 427):

$$\begin{aligned} k &= 0 && - \text{Steady Flow} \\ 0 < k &\leqslant 0.05 && - \text{Quasi-Steady} \\ 0.05 < k &< 0.2 && - \text{Unsteady} \\ 0.2 &\leqslant k && - \text{Highly Unsteady} \end{aligned}$$

Leishmann writes that flows in the quasi-steady regime do not require an unsteady model - unsteady instantaneous values of angle of attack and velocity may be assumed to effect the local lift and drag in phase with the forcing. For the regime $0.05 < k < 0.2$, the unsteady effects must be considered in any analysis. For the regime with $k \geqslant 0.2$, the unsteady terms are of considerable magnitude.

For a propeller in forward flight at some angle of incidence, Eq. 2.39 may be written, recalling that for this case $\omega_f = \omega$:

$$k = \frac{\omega c}{2\sqrt{\left[\omega r + V_p\right]^2 + V_n^2}} \tag{2.40}$$

and for an order of magnitude analysis, the *maximum* reduced frequency may be considered, which will be on the retreating side:

$$k_{max} = \frac{\omega c}{2\sqrt{[\omega r - V_D]^2 + V_n^2}} \tag{2.41}$$

For rotorcraft, generally $V_n << \omega r$, so Eq. 2.41 can be reduced to a nondimensional form by neglecting products of small quantities. However for a propeller at an angle of incidence, this is not the case.

Figure 2.10, overleaf, plots Eq. 2.41 over low, medium and high advance ratios at disc inclination angles of $\gamma = 5, 20°$. For the lower advance ratio, the reduced frequency of the inboard sections is in the *highly unsteady* regime - where "*unsteady terms...will begin to dominate the behaviour of the airloads*". However, for low advance ratio, the magnitude of the in-plane velocity will be the lowest, so the unsteady effects will likely be smaller in magnitude. For medium and high advance ratios, the whole disc is in the *unsteady* but not *highly unsteady* regime. According to the definition from Leishman (2006), "*unsteady terms in the governing equations cannot be routinely neglected*" for these sections.

As mentioned previously, many unsteady models have a formulation that determines the magnitude/phasing of the unsteady lift due to the induced flow distribution. Consequently, it is logical to research the effect of different induced flow models at the same time as exploring the effect of unsteadiness to ensure that models are compatible and the same effects are not erroneously included twice.

Bramwell et al. (2001, reproduced in Leishman (2006)) presents a breakdown of the sources of unsteady aerodynamic loading that may be found on helicopter rotor, and by analogy, a propeller at an angle of incidence. Figure 2.11 is an adaptation of these sources of unsteady aerodynamic loading, put into context on a propeller. Since propeller blades generally are not able to move freely out-of-plane and there is no cyclic control, these are removed from the problem. Looking at the flowfield structure, only the periodic terms are of consideration in this dissertation as the fuselage/nacelle in a steady freestream at an angle of incidence will give rise to a steady flow at the disc plane, and hence a periodic perturbation for the propeller blades. Since the proposed model is for propeller *cyclic* loading, only excitation terms that can cause periodic effects are considered. The 'fuselage flowfield' term may be considered a periodic effect on the propeller, as the equivalent effect in this problem is the flowfield around the nacelle, wing and body - which for steady flight conditions, will result in an asymmetric incident flow field, hence a periodic forcing on the propeller. Wake distortion is highly complex and beyond the scope of an engineering-level model. Due to its low amplitude and the complexity of the problem it will not be considered in this dissertation. Additionally, wake distortion is more of a problem in manoeuvring flight or for large dynamic pitch motions of a tiltrotor (*e.g.*, HaiLong and PinQi, 2009). This dis-

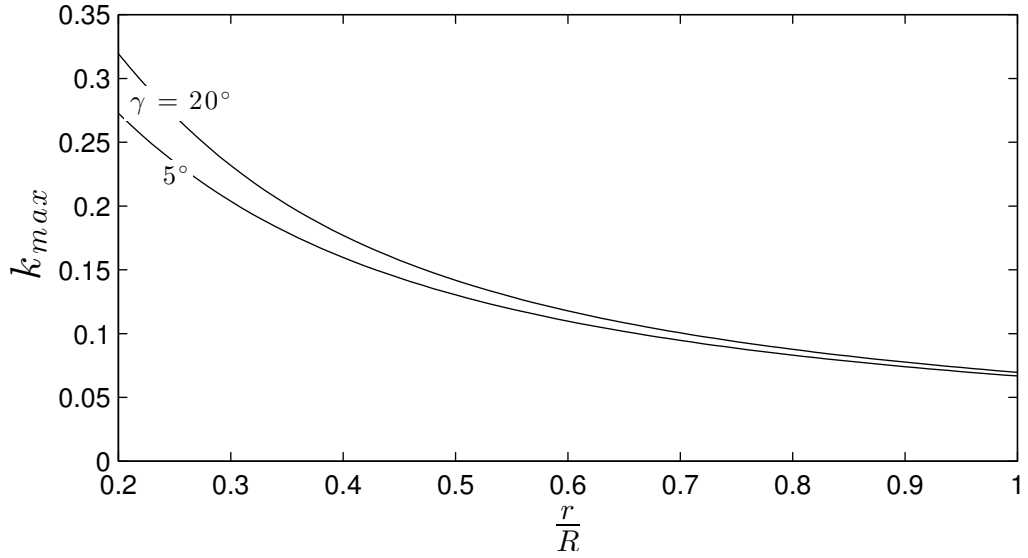

(A) $J = 0.5$

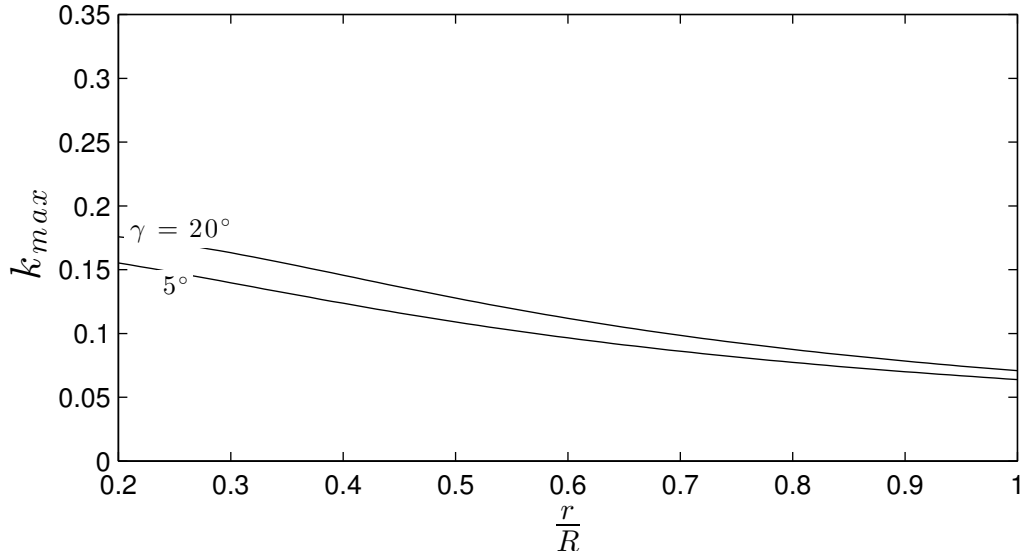

(B) $J = 1.25$

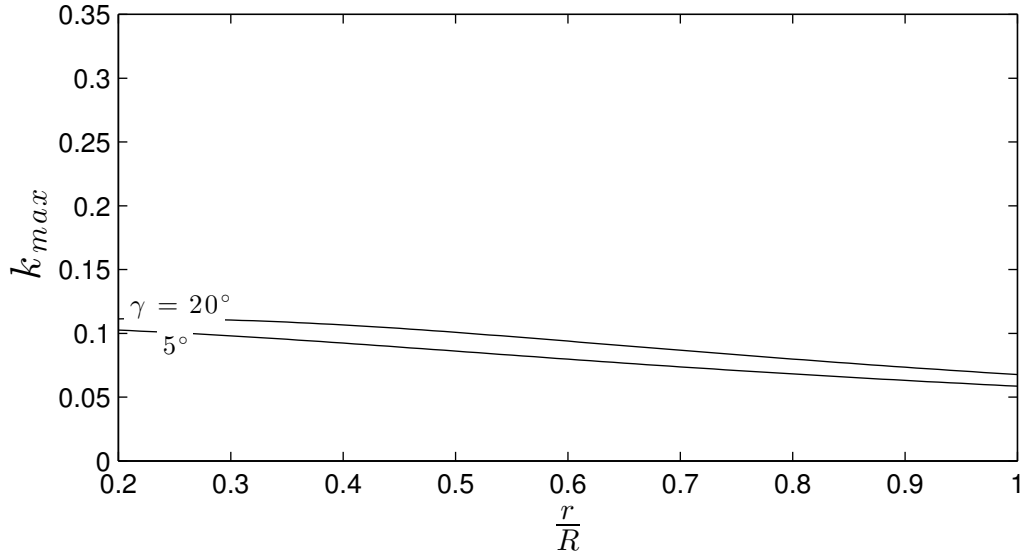

(C) $J = 2.0$

FIGURE 2.10: SPANWISE MAXIMUM REDUCED FREQUENCY RANGE DUE TO DIFFERENT DISC INCLINATION ANGLES (γ) FOR LOW, MED AND HIGH ADVANCE RATIO. $D = 3m$, $RPM = 1200$, $c = 0.2m$.

sertation is focussed on the aerodynamic phenomena of an aircraft propeller in steady flight conditions, so the problem is beyond the scope of this dissertation. Discrete vortices are unlikely to affect the steady incident velocity at an aircraft propeller. They may arise during takeoff/landing but will be short in duration. Again, as this dissertation is focussed on cyclic loading (*i.e.,* the load fluctuation due to steady incident flow) they will not be considered.

Leishman (2006) lays out the requisites of any useful unsteady aerodynamic model, for use in practical rotary aerodynamics. The following are largely common sense, but fundamental to choosing any aerodynamic model to be used as part of a larger calculation procedure and hence are included here.

1. The **assumptions and limitations** of any model need to be fully assessed, understood and justified if invoked. *e.g.,* for an unsteady model, the *incompressibility assumption* requires not only local $M \ll 1$ but $Mk \ll 1$
2. The model must be **written in a form that is easily coupled with structural dynamic model**. *e.g., the model may be in terms of ODEs at radial blade elements, or written in state-space form at the disc level.*
3. If choosing an integral approach, *i.e., a BE model*, the discretisation scheme in use places a strict limit on the computational cost of any unsteady model.

These considerations have guided the choice of unsteady models that have been utilised in discussion in Chapter 3.

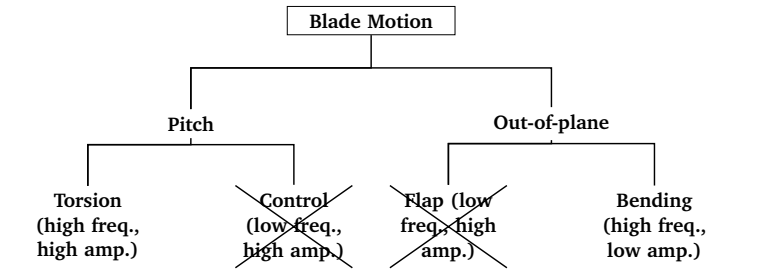

(A) UNSTEADY AERODYNAMICS DUE TO BLADE MOTION

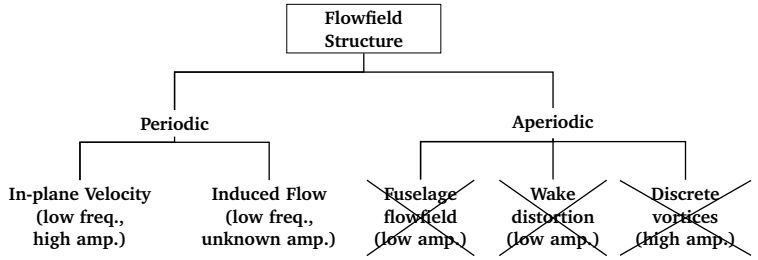

(B) UNSTEADY AERODYNAMICS DUE TO FLOWFIELD

FIGURE 2.11: UNSTEADY AERODYNAMIC SOURCES ON A PROPELLER; ADAPTED FROM (LEISHMAN, 2006)

2.5.4 STRUCTURAL DEFORMATIONS

Aeroelastic effects have the potential to change loads on a propeller at an angle of incidence through the interdependence of structural deformations and applied aerodynamic (and centrifugal) load. Gray et al. (1954) noted that blade flexibility may be significant for a propeller at an angle of incidence. They modelled out-of-plane deformation, and neglected blade twisting due to the relative complexity of the problem. If a 1P aerodynamic load is exciting either the torsional or out-of-plane displacement mode of a propeller blade, then a full structural-dynamic analysis would need to be undertaken to ascertain the effect of blade dynamics and 1P loading.

In any vibrating system, the frequency of excitation forces must be compared to the natural frequencies of the system to determine if any resonance problems are likely to occur. In a rotating frame, centrifugal effects mean that the stiffness of a system is a function of the rotational speed - and so is the natural frequency. To determine if/where resonance problems are likely to occur, a Campbell diagram[9] is used, plotting the natural frequency of different free vibration modes, ω_n against rotational speed, Ω. Since on a propeller/rotor the forcing frequencies of interest (*i.e.,* aerodynamic, but also mechanical such as gearbox vibration) will be related to the rotational speed, lines of constant $\omega_N = N \cdot \Omega$, for $N = 1, 2, 3, ...$ are overlaid. The intersection of these straight lines with the natural frequency curves shows regions of likely resonance problems - any potentially problematic forcing frequency and relevant mode can be linked to a given rotational speed by consideration of such diagram.

A Campbell diagram for a composite propeller blade representative of a modern turboprop is shown in Figure 2.12. This diagram shows that the out-of-plane natural frequency is well above the 1P forcing frequency through the range of operational rotational speeds - though the 2P forcing frequency is potentially close to the first out-of-plane natural frequency in the cruise and climb speeds. Industry reports listing frequencies of vibrational modes show the torsional frequency is four to five times higher than the out-of-plane mode natural frequency (Jayne, 2002).

[9] Sometimes referred to as a Southwell diagram/plot/chart.

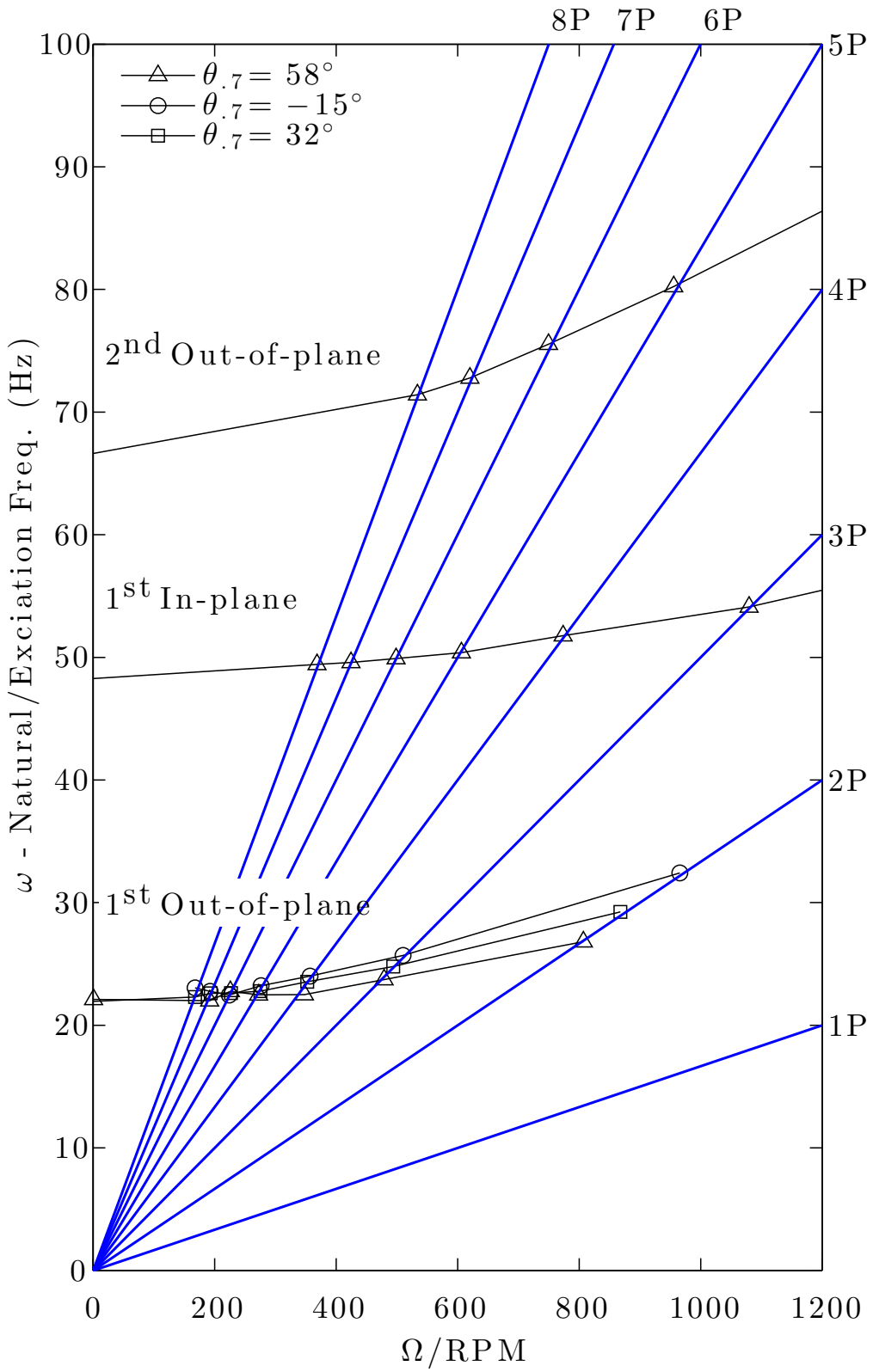

Figure 2.12: Campbell Diagram of a representative composite propeller blade. Reproduced from Jayne (2002).

To determine the likely effect of forcing an out-of-plane vibration mode, the following is a look from first principles following methodology for rotor dynamics (Bramwell et al., 2001). An out-of-plane displacement, h, will effect a *plunge velocity*, $\dot{h}$, which may be added to the expression for effective angle of attack.

$$\begin{aligned}\alpha_R &= \beta - \phi \\ &= \beta - \tan^{-1}\frac{V_n + \dot{h}\cos\beta}{\omega r + V_p - \dot{h}\sin\beta}\end{aligned} \tag{2.42}$$

For a propeller/rotor, the out of plane displacement will be a function of the structural properties, and the aerodynamic environment. A valid first approximation for a propeller at an angle of incidence is that the out of plane (flapping) displacement is proportional to the lift and consequently angle of attack.

$$h \propto \alpha_R \tag{2.43}$$

$$\dot{h} \propto \dot{\alpha_R} \tag{2.44}$$

Equations 2.42 and 2.44 show that any out-of-plane bending displacement caused by aerodynamic forcing (*i.e.,* a change in α_R, V_R) will effect a change to the angle of attack that **positively damps the angle of attack variation**. Even if the out-of-plane mode were being excited by some twice-per-revolution (2P) forcing as indicated by the Campbell diagram, this out-of-plane displacement would only serve to *attenuate* any aerodynamic forcing. Another simple reasoning to explain the positive damping of such blade motion may be considered from rotorcraft theory, whereby a once-per-revolution out-of-plane mode is deliberately forced through the flapping hinge/blade flexibility, with the purpose of attenuating a lift asymmetry due to in-plane velocity.

Since out of plane displacement cannot serve to largely increase 1P load then it may be disregarded. The blade torsional mode may, however, potentially lead to an increased 1P load. Using reasoning similar to that for h and $\dot{h}$ as above, but instead affecting a change to β and $\dot{\beta}$, the torsional deflection could serve to increase 1P loading. The change in pitching moment due to in-plane velocity will be largely dominated by the lift-dependent pitching moment - which is in the direction of β. This would serve to increase the first term in Eq. 2.42. Since the frequencies are so well-removed, however, a quasi-static analysis should suffice to determine the magnitude of any potential torsional deflection on 1P load. To determine the order of magnitude of the effect of blade torsion, it will be presumed that the blades react instantly to applied load - which is justifiable considering that $\omega_{n\theta} >> \Omega$.

A beam-type finite-element model has been formulated based on the work of Kosmatka (1986); Kosmatka and Friedmann (1987). This model was chosen initially due to the ability to determine full structural-dynamic effects on a swept,

composite blade - and if preliminary results showed that torsional deflections due to aerodynamic forcing were significant, a full dynamic analysis would need to be performed. The model has been validated against empirical formulae for curved beams (Young and Budynas, 2002) and matches very well, and validated to reasonable accuracy vs. torsional deflections of JORP blades which were taken from optical deflection measurements (unpublished data). As the FE model is not used in the final presented model formulation in this dissertation, details of its operation and validation is not included in this dissertation. For details of the model, refer to the original work of Kosmatka.

Figures 2.13 and 2.14 show two different methods of calculating torsional deflection - results being shown for the 75% and 95% radius stations in the two figures, respectively. The two methodologies compared are:

- **No Aeroelasticity:** The induced flow/aerodynamic model is run to convergence, then the final loads are used to determine the torsional deformation. The calculated deformations are not taken into account in the aerodynamic model.
- **Static Aeroelasticity:** After the induced flow/aerodynamic model has run to convergence, the torsional deformation is then calculated. The change in structural twist is included in the next iteration of the aerodynamic model, and the procedure is iterated until the maximum change in torsional deformation is $< \frac{1}{100}^{\circ}$.

There is negligible difference between the 'No Aeroelasticity' and the 'Static Aeroelasticity' models shown in Figures 2.13a and 2.14a. The observed difference is more marked on the retreating side for $\gamma = 10^{\circ}$, where the model using static aeroelasticity predicts a slightly larger torsional deflection than the model incorporating no aeroelastic effects. The difference is very small, though, amounting to an increase in torsional deflection of $< 2\%$ for both γ values. The range of torsional deflection prediction for the $\gamma = 10^{\circ}$ case is $\sim 0.2^{\circ}$ and $\sim 0.35^{\circ}$ for the two radial stations. When this is compared to the first-order α_R change - Figures 2.13b and 2.14b, $\sim 11^{\circ}$ and $\sim 10^{\circ}$ respectively - it can be seen that the change to α_R due to torsional deflection is roughly twenty times smaller than the 1$^{\text{st}}$-order α_R change. Since the change to torsional deflection is an order of magnitude smaller than the angle of attack change, it fails to meet the second criterion for inclusion in an engineering-level 1P code. This also serves as reasoning for the negligible difference between the two models shown.

Further support for this assertion can be taken from results from the unpublished JORP tests which showed that torsional deflection was largely independent of pressure distribution on the blades. This suggests the torsional deflection is largely dominated by the centrifugal load. Similar observations were shown by Dunn and Farassat (1992) using a coupled NASTRAN/Euler method, showing

that the centrifugal contribution to torsional deflection was much larger and that "*the aerodynamic loads produced only a small additional untwist*".

The results shown in Figures 2.13 and 2.14 are based on the JORP blades, which are a scaled set of Dowty propeller blades. The tests performed by Dunn and Farassat, however, were on a full-sized set of blades. Their FE code was also more complex, taking into account the enhanced flexibility afforded by a central aluminium spar whereas the FE code produced for this analysis assumes isotropic section properties. The fact that their analysis led to similar conclusions as those from this present work affords confidence in the extensibility of the conclusions of the scale simulations to full-size propeller blades. To further justify these conclusions, simulations of the JORP blades scaled up approximately three times to a 3m diameter propeller have been performed at similar J, γ and β values as the tests of the scale propeller. With these parameters, the FE code predicted a larger total torsional deflection at both angles, due to the larger centrifugal load - Figures 2.15 to 2.16 show the FE results from the scaled-up propeller. Again, the effect of quasi-static aeroelasticity provided a change of $< 1\%$ to the torsional deflection at both the sections displayed, and much less inboard.

With the dynamic effects of deflections show to be non-contributory to 1P load, and the effect of static deformation shown to be very small over the range tested, this provides confidence in not including any structural model in an engineering-level 1P code.

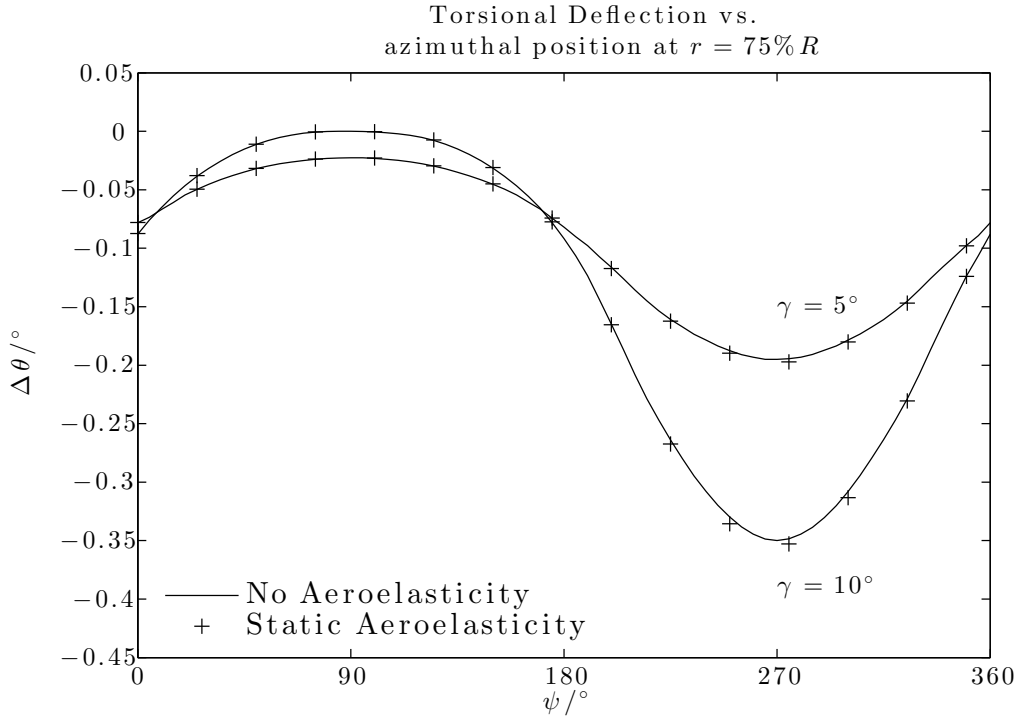

(A) TORSIONAL DEFLECTION AT $75\%R$

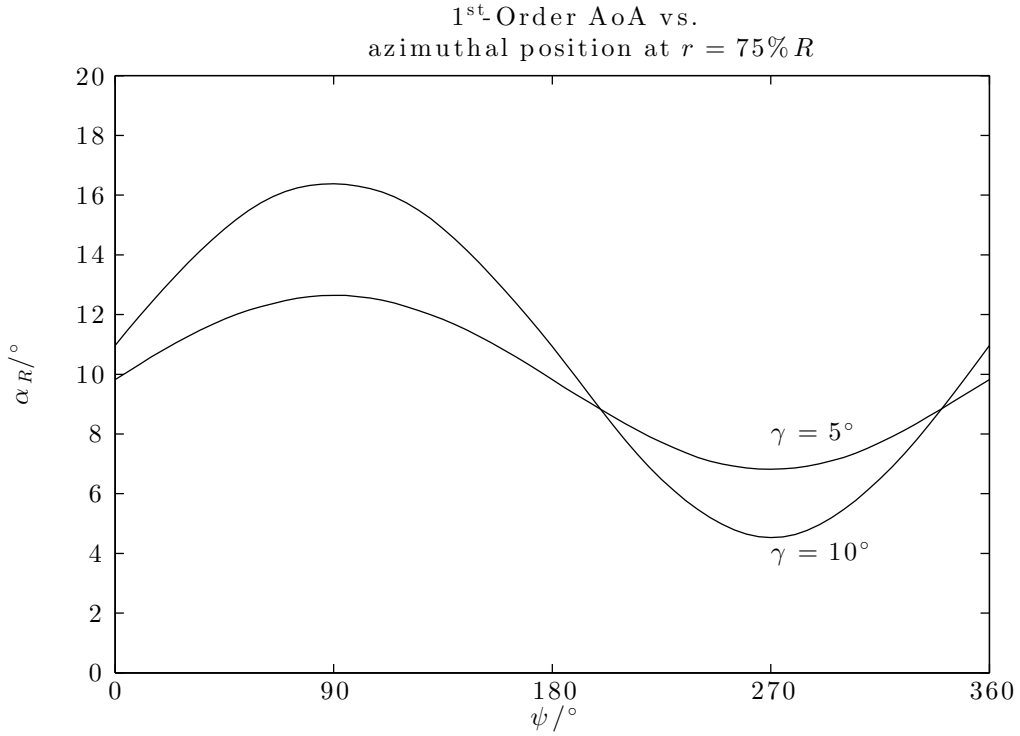

(B) FIRST ORDER α_R CHANGE AT $75\%R$

FIGURE 2.13: PREDICTIONS OF CHANGE TO TORSIONAL DEFLECTION AND 1ST ORDER AOA VS. AZIMUTHAL POSITION AT $75\%R$ STATION - ORIGINAL JORP BLADES (D=3FT)

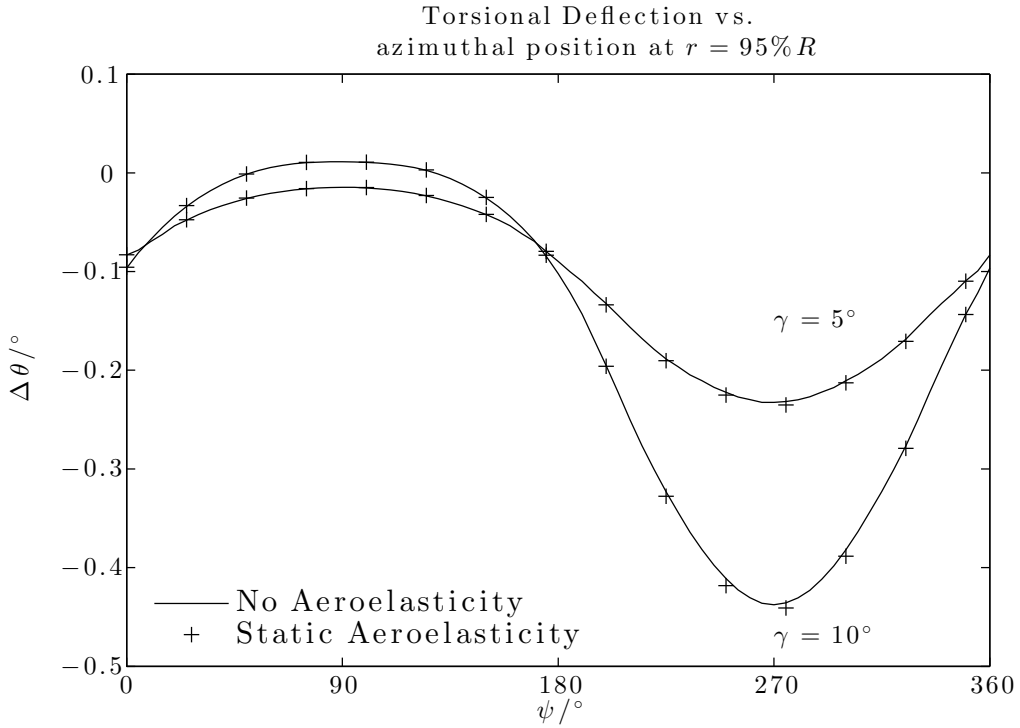

(A) TORSIONAL DEFLECTION AT $95\%R$

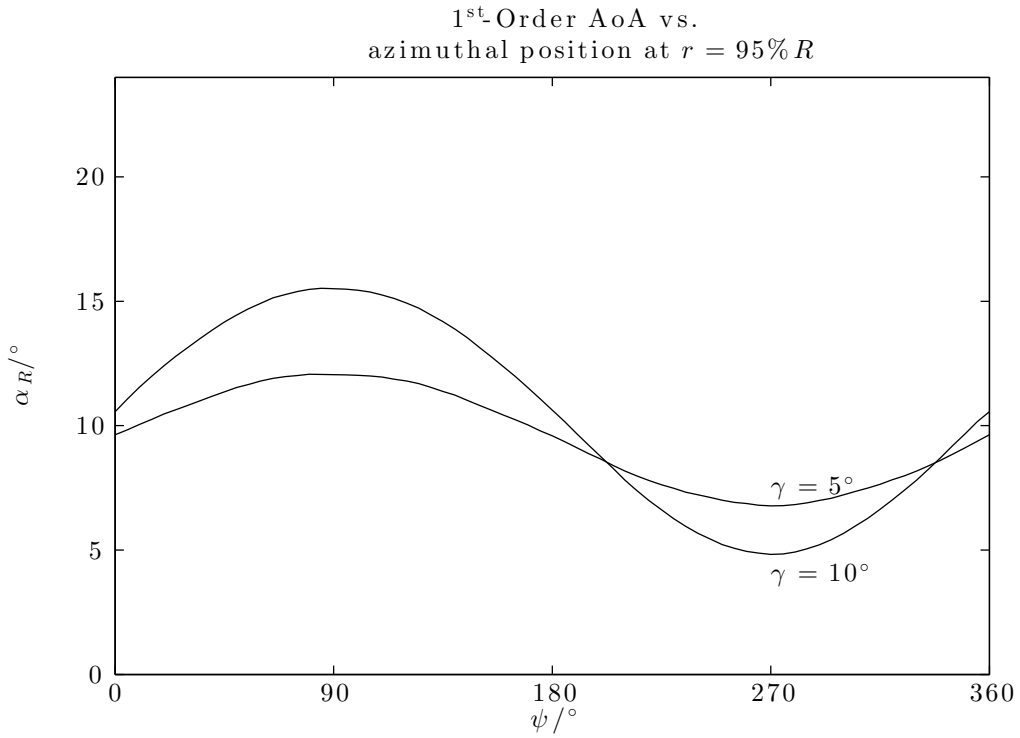

(B) FIRST ORDER α_R CHANGE AT $95\%R$

FIGURE 2.14: PREDICTIONS OF CHANGE TO TORSIONAL DEFLECTION AND 1ST ORDER AOA VS. AZIMUTHAL POSITION AT $95\%R$ STATION - ORIGINAL JORP BLADES (D=3FT)

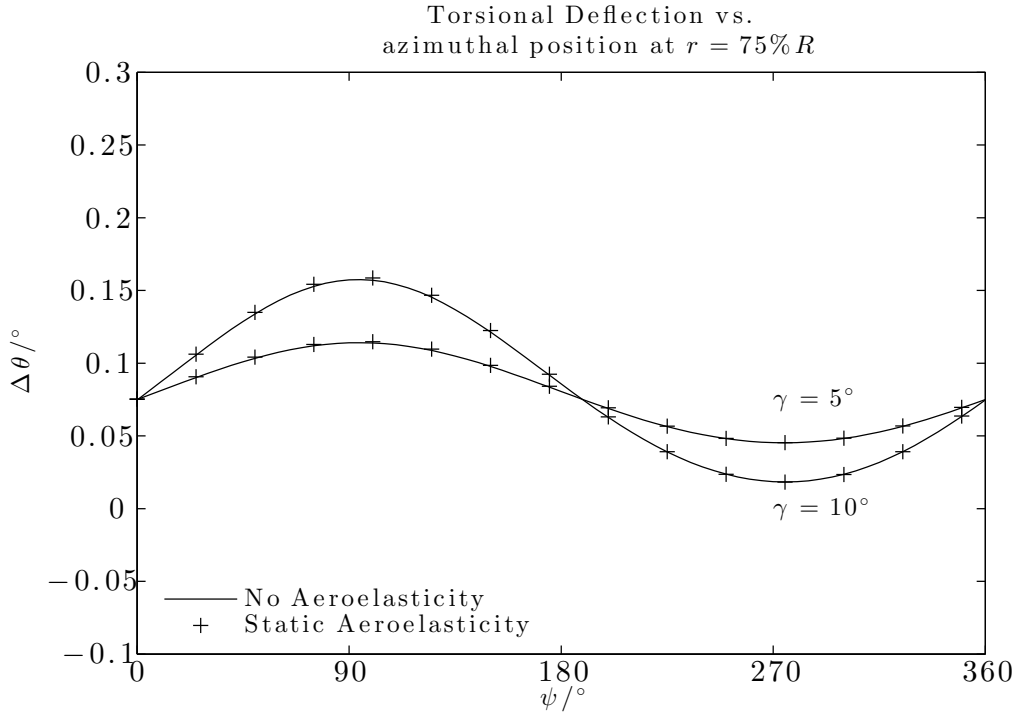

(A) TORSIONAL DEFLECTION AT $75\%R$

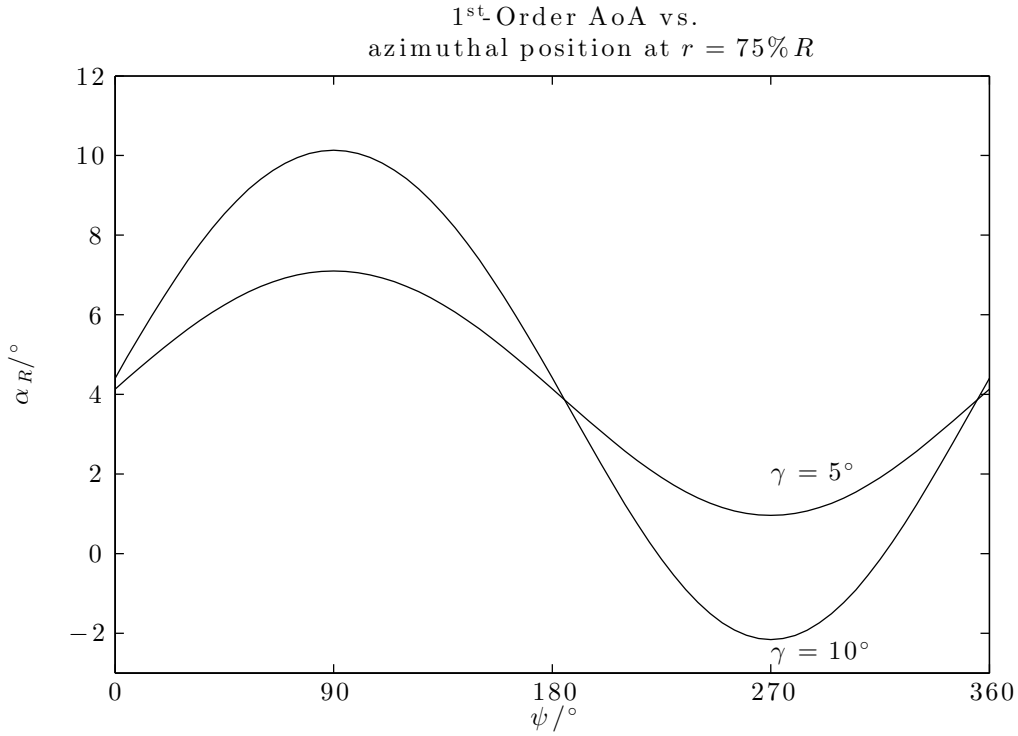

(B) FIRST ORDER α_R CHANGE AT $75\%R$

FIGURE 2.15: PREDICTIONS OF CHANGE TO TORSIONAL DEFLECTION AND 1ST ORDER AOA VS. AZIMUTHAL POSITION AT $75\%R$ STATION - SCALED-UP JORP BLADES (D=10FT)

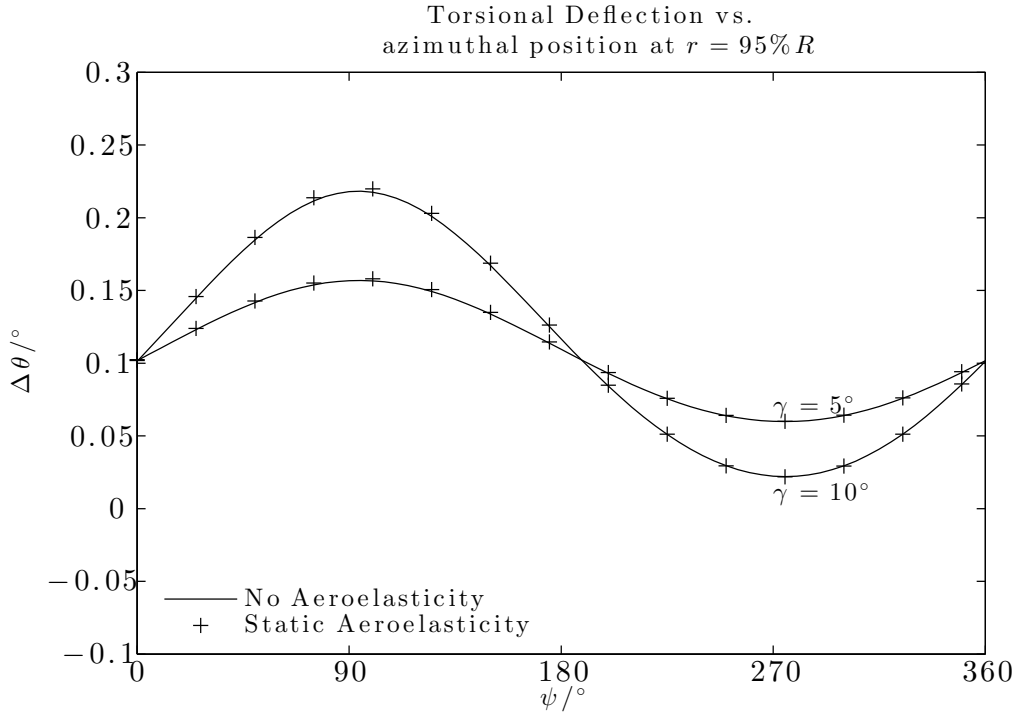

(A) TORSIONAL DEFLECTION AT $95\%R$

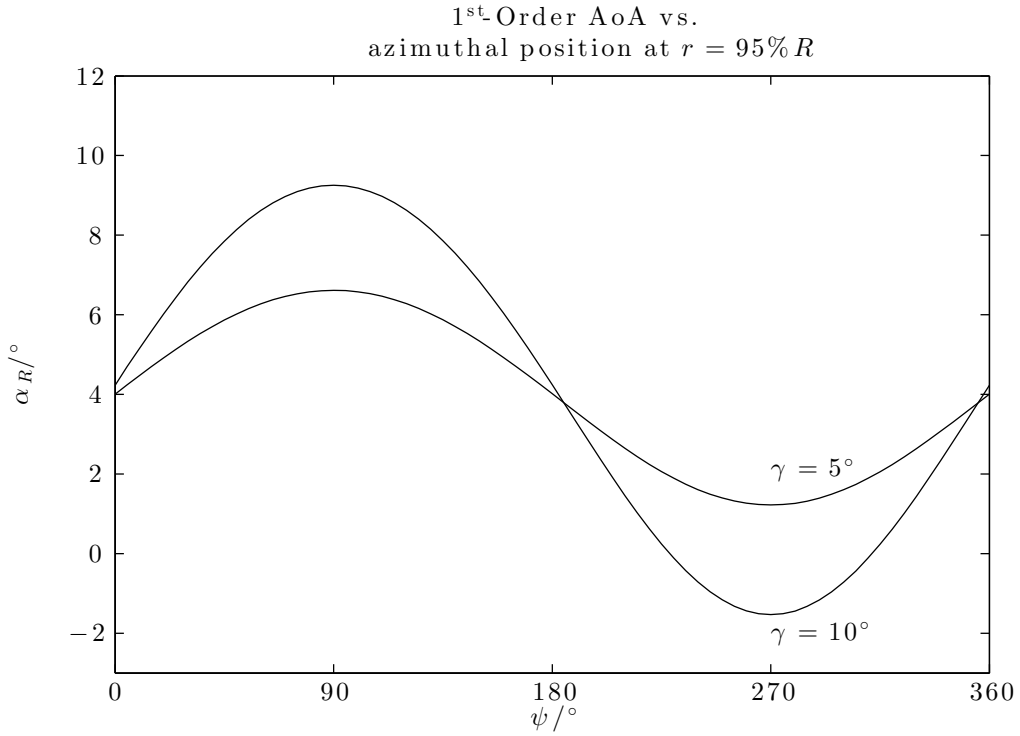

(B) FIRST ORDER α_R CHANGE AT $95\%R$

FIGURE 2.16: PREDICTIONS OF CHANGE TO TORSIONAL DEFLECTION AND 1ST ORDER AOA VS. AZIMUTHAL POSITION AT $95\%R$ STATION - SCALED-UP JORP BLADES (D=10FT)

2.5.5 SIMPLE INSTALLATION

Whilst means of utilising a fully nonuniform incident flowfield will be described in Chapter 5, an 'isolated' propeller (*i.e.,* one in a wind tunnel) is subject to a flowfield that is not truly isolated from installation effects. There will be a spinner and a nacelle in the centre of the propeller disc, and flow around these needs to be calculated and the effect quantified in terms of the criteria laid out in Note 2.4.3. An axisymmetric potential code has been written to determine the flow around the spinner at incidence based on superposition of axial and in-plane velocity solutions. The variation of the in-plane velocity is given by the 'Yaggy-Rogallo' method (Chappell, 2009), and the axial perturbation is included with theory taken from Katz and Plotkin (2001) as the estimates of the nacelle upwash shown by Yaggy (1951) tended to overestimate the upwash near the nacelle, likely due to disregarding the axial velocity perturbation. Description of the model and validation is given in Appendix C.

Using a representative ellipsoidal spinner of radius $R_{spin} = 0.2 \cdot R$ with a cylindrical afterbody, the spinner/nacelle model has been compared in axial performance with the completely isolated propeller - shown in Figure 2.17. The effect of the spinner in terms of integrated blade loads is small in axial flight - the flow acceleration around the nacelle causes an increase in effective J and M_R, which alters not only the angle of attack but the compressibility-related lift/drag characteristics. This is most observable at the high advance ratios. The spinner/nacelle model as implemented in the axial case does not largely alter the variation of $\frac{dC_T}{dJ}$ or $\frac{dC_P}{dJ}$ for axial flight, indicating that the fractional increase in V_n due to the spinner is not large enough to change the overall performance of the propeller.

At incidence, however, the flow around the spinner/nacelle will alter in-plane velocity at the disc plane. To determine the magnitude of this effect on an isolated propeller with a small spinner/nacelle[10] the change in first-order angle of attack with/without the spinner has been calculated over a range of $800\Omega \leq n \leq 2000$RPM, $0.75 \leq J \leq 1.5$ and $5^\circ \leq \gamma \leq 20^\circ$. Little change was seen with change in rotational speed, as would be expected, and only results for a single rotational speed are shown in this dissertation. Figure 2.18 shows the percentage increase in the range of first-order angle of attack variation for different J and γ for $\Omega = 800$RPM. The angle of attack change is large in the blade root (up to$\sim 12\%$ increase at $x = 0.2$), but decreases rapidly - this predicted trend is fairly insensitive to changes of operating conditions, and no obvious trend has been found with changes in n, J or γ. At $x = 0.3$, the variation is reduced to $< 10\%$, and from $x = 0.4$ and outboard the change to section angle of attack is $< 5\%$ - *i.e.,* an order of magnitude lower than the first order angle of attack

[10]Representative of the spinner used by Gray et al. (1954), based on diagram $R_{spin} = 0.18 \cdot R$.

variation. As this is an inviscid model, it is likely to overestimate the flow acceleration, but this will occur equally in axial and in-plane directions, and this model has shown good validation for determination of the upwash at the horizontal centerline - shown in Appendix C. Again, as this effect is only of significant magnitude in the blade root, it is likely to contribute *less* to total bending loads than outboard effects. In addition, the aerodynamic behaviour in the blade root sections is likely to be more three-dimensional and a blade element representation is less valid. Over the range of operating conditions given above, the maximum change to root bending load due to the flow around the spinner was $< 1\%$[11]. For the results in the following chapter, where possible, the effect of flow around the spinner is discussed, but detailed spinner geometry is unknown for the range of propellers simulated, and inferences have been made.

It should be noted that this present discussion concerns only the flow around a spinner with slim afterbody, as found on 'isolated' propellers in wind tunnel tests. With a larger spinner and/or nacelle, the change to the velocity at the propeller disc may be large. Discussion of the flow around a larger nacelle is included in Chapter 5.

[11] Calculated with no induced flow model, but including change in sectional Mach number due to spinner/nacelle.

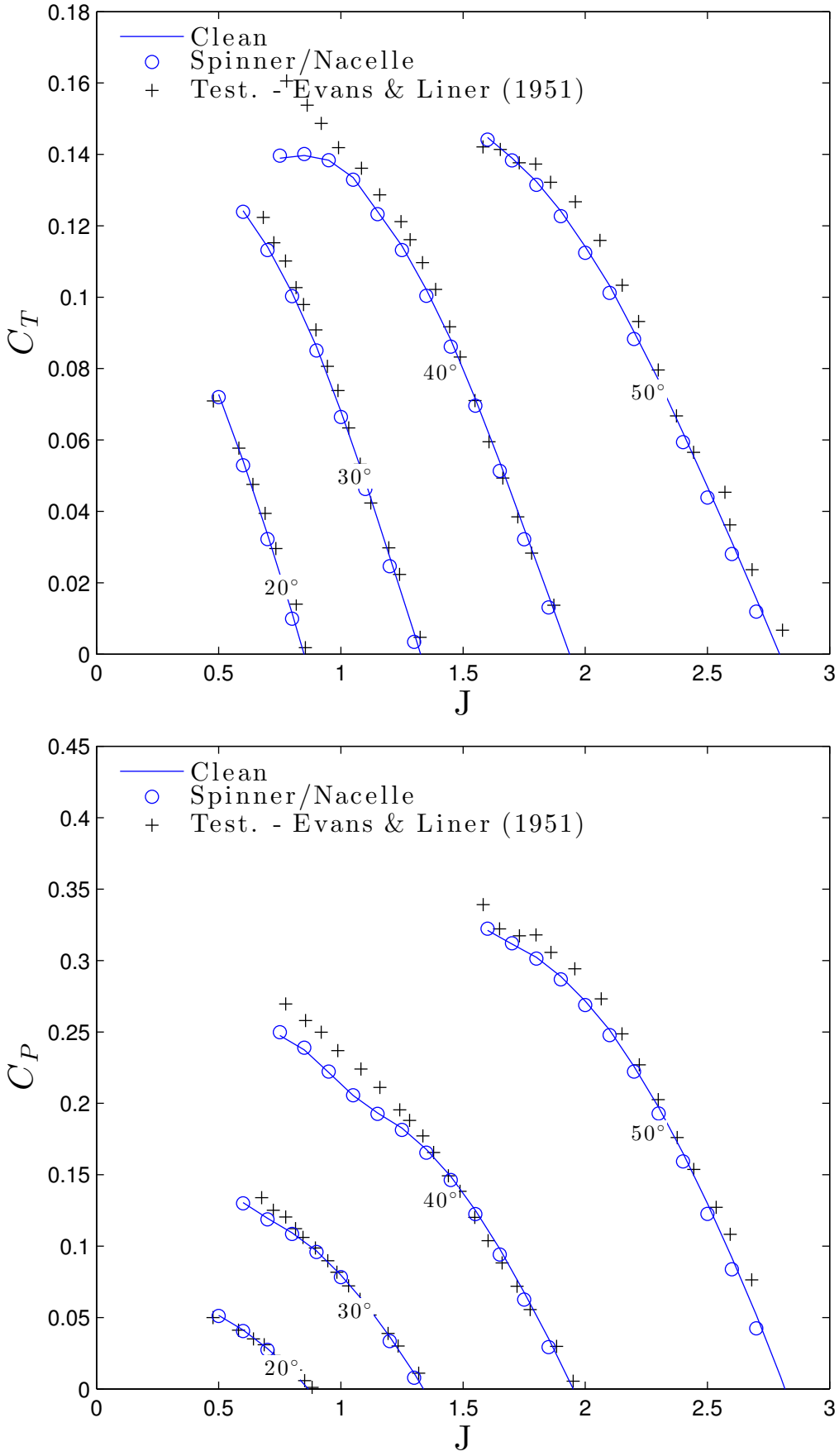

FIGURE 2.17: PERFORMANCE PREDICTIONS WITH 'CLEAN' CONFIGURATION VS. INCLUDING SPINNER/NACELLE EFFECT - 1140 RPM. TEST DATA FROM EVANS AND LINER (1951)

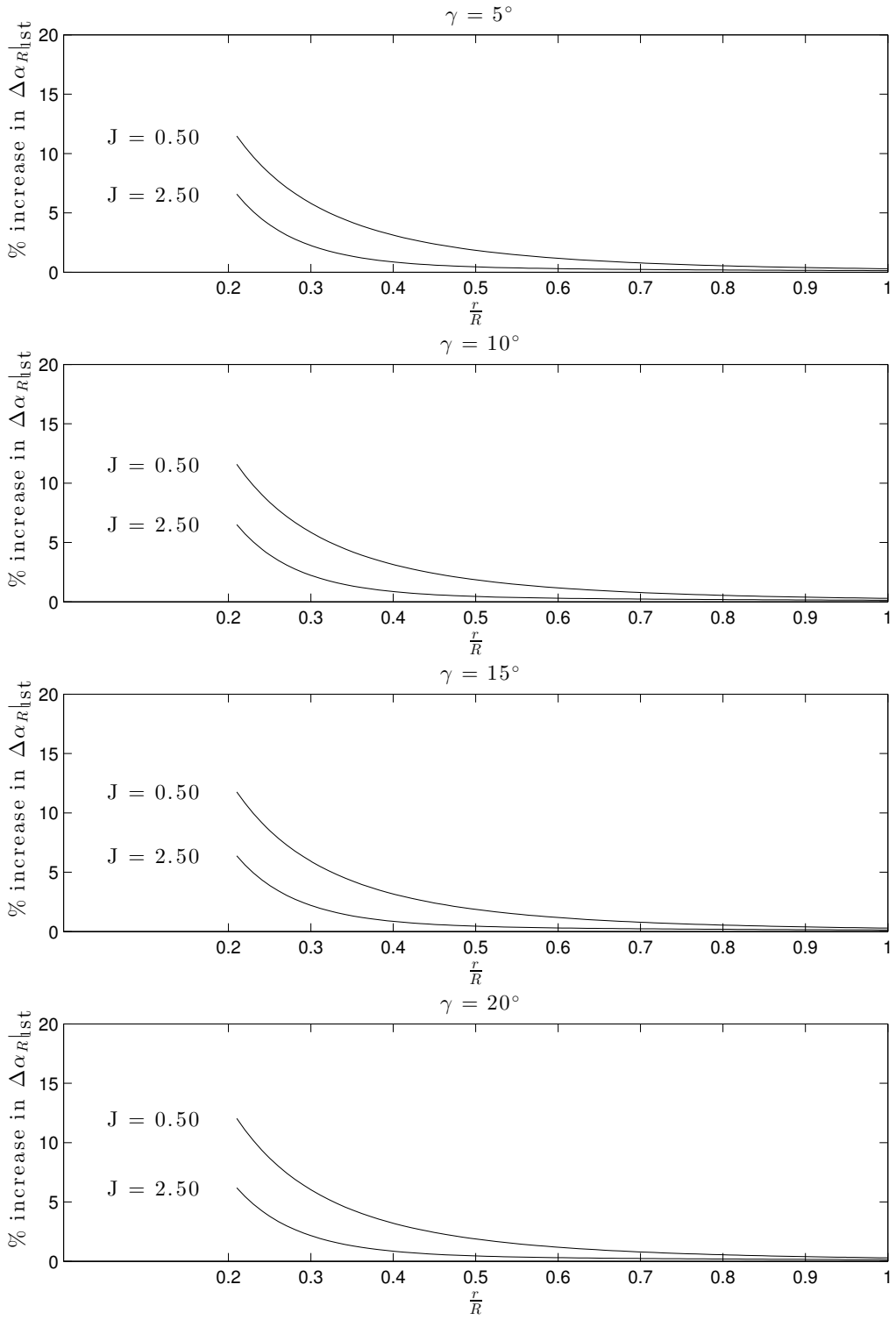

FIGURE 2.18: SPINNER/NACELLE EFFECT ON $\alpha_R\big|_{1^{ST}}$ OVER DIFFERENT γ. Ω=1500RPM.

2.6 THREE-DIMENSIONAL EFFECTS

Without modification, any blade element model explicitly disregards three-dimensional effects. Approximation of a three-dimensional lifting surface by superposition of two-dimensional equivalent aerofoils is the basis of many design and simulation codes, but three-dimensional behaviour means that such models have different predictions during certain flight regimes (*i.e.,* low advance ratio (Rosen and Gur, 2005)). Three-dimensional stall at low advance ratio has been discussed in the previous section, but in all flight regimes the root and tip of the propeller are subject to a flow that is different from the idealised, two-dimensional approximation, and this may have an effect on once-per-revolution loading. Fluctuations in root load will have a smaller effect on root bending load than tip effects due to the smaller moment arm. Additionally, Gur and Rosen (2008) compared BEMT with lifting-line vortex models in axial flight of propellers, comparing both the total performance against experiment and the spanwise variation of load between different models. The lifting line model will model these three-dimensional root effects, whilst the BEMT model will not. Overall, the predicted root loading between models was negligible - and the magnitude of the root load was small compared to the tip sections in all cases. In formulation of the model of this dissertation, root effects will be neglected unless significant deviation from experimental results are found.

Three-dimensional effects can be large towards the tip of a propeller - modelling may be important for 1P load prediction. The lift on a thrusting propeller reduces towards the tip, like the lift distribution of an ideal finite wing. There are different means to simulate this effect - the simplest being enforcing a reduction in lift from a particular radial station. Gur and Rosen (2008) utilise a reduction in the effective blade radius to $R' = 97\%R$, presenting a discontinuous and a smoothed correction factor. Prandtl's correction factor as shown by Glauert (1935) is a correction to the circulation for a finite-bladed rotor, and amounts to a loss in circulation towards the tip, applied in solution of the momentum equations. Described in more detail in the following chapter, its calculation is dependent on radial position, number of blades and local advance angle, ϕ, and is included in calculation of the BEMT equations. Prandtl's, Goldstein's and Lock's vortex models have been discussed in the previous chapter - Prandtl's in particular is often referred to as a "tip-loss" method, though the distinction is made in the previous chapter between his actual tip-loss method and his circulation distribution function, as both are often referred to as his "tip-loss" function. Although these methods accurately describe the drop-off in lift due to three-dimensional loading, there are higher-order effects on a thrusting propeller.

Higher-order three-dimensional effects include the fact that the tip vortex induces a highly three-dimensional velocity field - this effect cannot be modelled

as a simple change to the spanwise loading distribution. Bocci (as referenced by Bocci and Morrison (1988)) developed a methodology to change the sectional properties to better match the *chordwise* loading distribution towards the tip of a thrusting propeller. This methodology is based on wind-tunnel tests of pressure-tapped NACA blades, and amounts to a correction to the effective thickness and camber of sections towards the tip. Bocci's method provides good correlation with the NACA tests, also with a 3D Euler-based computational method, and with further tests on JORP blades. In this methodology, the change in effective camber changes the lift curve slope of the sections towards the tip, whilst keeping the same zero-lift angle. This gives the desired effect of changing the spanwise blade lift to match three-dimensional behaviour, intended for axial flight. Application of this methodology for dynamic aerofoil motion is beyond the scope of its original inception, and to validate this method for the case of a propeller at incidence would require significant experimental investigation or numerical simulation[12], beyond the scope of this dissertation.

Although there are higher-order three dimensional effects, it will be taken as sufficient to alter the spanwise loading distribution and to neglect the more complex chordwise changes. Prandtl's tip loss function has been implemented successfully on yawed wind turbines (Silva and Donadon, 2013) and finds common usage in helicopter BEMT methods (Bramwell et al., 2001; Leishman, 2006). Still, Lock-Goldstein remains the 'standard' for engineering-level propeller aerodynamic calculations, certainly within the UK. Since Prandtl's, Goldstein's and Lock's functions all modelling the same effect - they will be compared over a range of onset conditions in the following section, in order to determine which is more suitable for the problem at hand.

2.6.1 PRANDTL'S, GOLDSTEIN'S AND LOCK'S FUNCTIONS FOR A PROPELLER AT INCIDENCE

The origin of these methodologies has been explored in the preceding chapter, and will not be included here. Suffice to say that Prandtl's is arguably the simplest as it involves modelling the wake as planar sheets and is closed-form in solution, whereas Goldstein/Lock's method is based on the helical wake, and requires interpolation of the function from pre-calculated tables.

Clearly it would be preferable to use the simpler solution for an engineering-level model, but the differences between the models needs to be evaluated in terms of the 1P load - in line with the order of magnitude scheme introduced in this chapter.

Lock's model is essentially the Goldstein function with an increased range of applicability. For the purposes of this analysis, the Goldstein function will be com-

[12] Although validation to CFD is arguably not validation at all.

pared with the Prandtl factor since order of magnitude results shall be extensible to the Lock-Goldstein function. Bramwell et al. (2001, see table 2.2, pg. 65) has shown a comparison between the Lock-Goldstein method and Prandtl's method of determining the so-called 'interference factor', k, in Bramwell's nomenclature.

> " [Figure 2.24, Bramwell] *also shows clearly that the difference between the Prandtl and the Goldstein-Lock analyses is very small."*
>
> Bramwell et al. (2001, 2.10 Rotor wake models)

For the propeller at incidence, the parameter of interest in this chapter is the first order angle of attack variation. Since the vortex models modify the induced velocity distribution, which has shown to be of importance for once-per-revolution loading, it is important to compare the different models.

An implementation of the Goldstein function as tabulated by Wald (2006) based on work by Tibery and Wrench (1964) has been compared with Prandtl's closed-form function for a propeller at incidence over a range of advance ratios. Since both factors are a function of blade radial position, advance angle and blade number, the radial variation of $\alpha_R|_{1^{st}}$ will be compared for a range of J and at two different values of disc inclination, $\gamma = 5^\circ, 10^\circ$ for a two, three and six-bladed propeller.

Figures 2.19 to 2.21 show the overall first order angle of attack variation vs. radial station. The uppermost plots are at $\gamma = 5^\circ, 10^\circ$ at $J = 1.25$ and the lowermost plots are the same inclination angles at $J = 1.75$. The figures represent a two, three and six-bladed propeller, respectively. The units on the y-axis are degrees of $\alpha_R|_{1^{st}}$ for the solid line, and then the percentage change to this value for the results with Prandtl and Goldstein.

Fundamentally, it can be seen that the maximum change to angle of attack at any given radial station is of maximum order 5%, which is second order compared to the overall local change to induced velocity. In addition, the basic trends with both Prandtl and Goldstein are fairly similar - though the Prandtl factor tends to attenuate to affect the angle of attack variation about half as much as the Goldstein factor, particularly towards the blade roots.

Whilst this analysis shows that there is a difference in the local lift variation using the two vortex models, it also shows that the difference using *either* Goldstein's or Prandtl's model is small, and the trends are broadly similar. Clearly a more detailed analysis would be required to fully justify using either Goldstein or Prandtl on a propeller at incidence, as the assumptions made in the derivation of both are not wholly extensible to the propeller at incidence with its complex wake structure.

Such a comparison presents an opportunity for significant future research,

but is beyond the scope of this dissertation as the potential for either model to significantly alter once-per-revolution loading has been shown as small. In addition, the numerical work required to extend either model for a more complex wake structure is likely to be highly involved. This work would either dominate a Ph.D. dissertation for little insight in an Engineering-level model, or would result in a methodology too computationally complex to be of merit for this research project.

Prandtl's factor is closed-form in solution and shows the same rough trends as Goldstein's factor. In addition, it is used on rotorcraft models for forward flight, despite the inapplicability of the planar wake assumption. Accordingly, Prandtl's factor will be used for the remainder of this dissertation with the caveat that further research is required in order to wholly justify the usage of either.

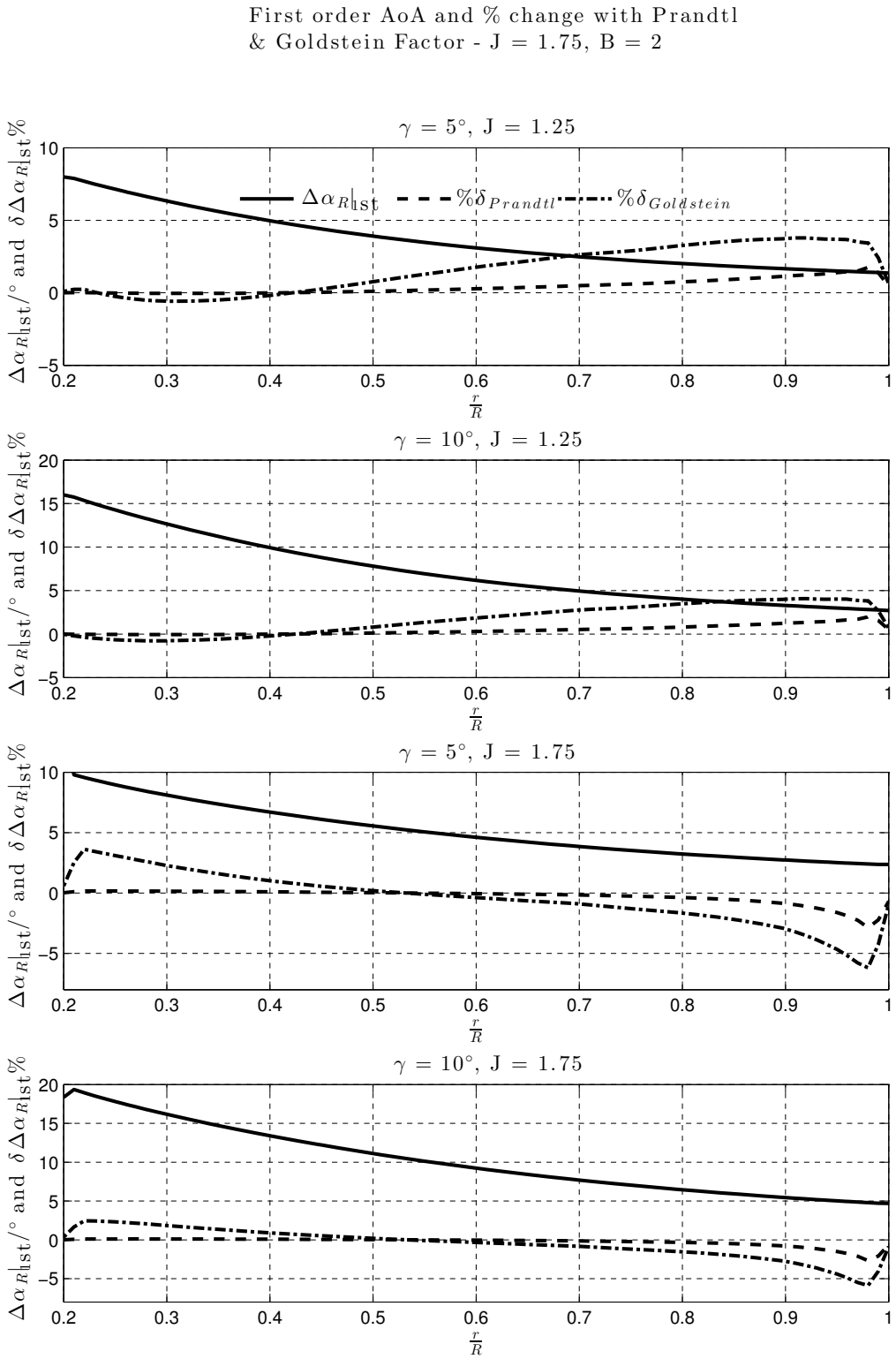

FIGURE 2.19: PRANDTL/GOLDSTEIN FACTOR EFFECT ON $\alpha_R|_{1^{ST}}$ OVER DIFFERENT γ AND J. B=2.

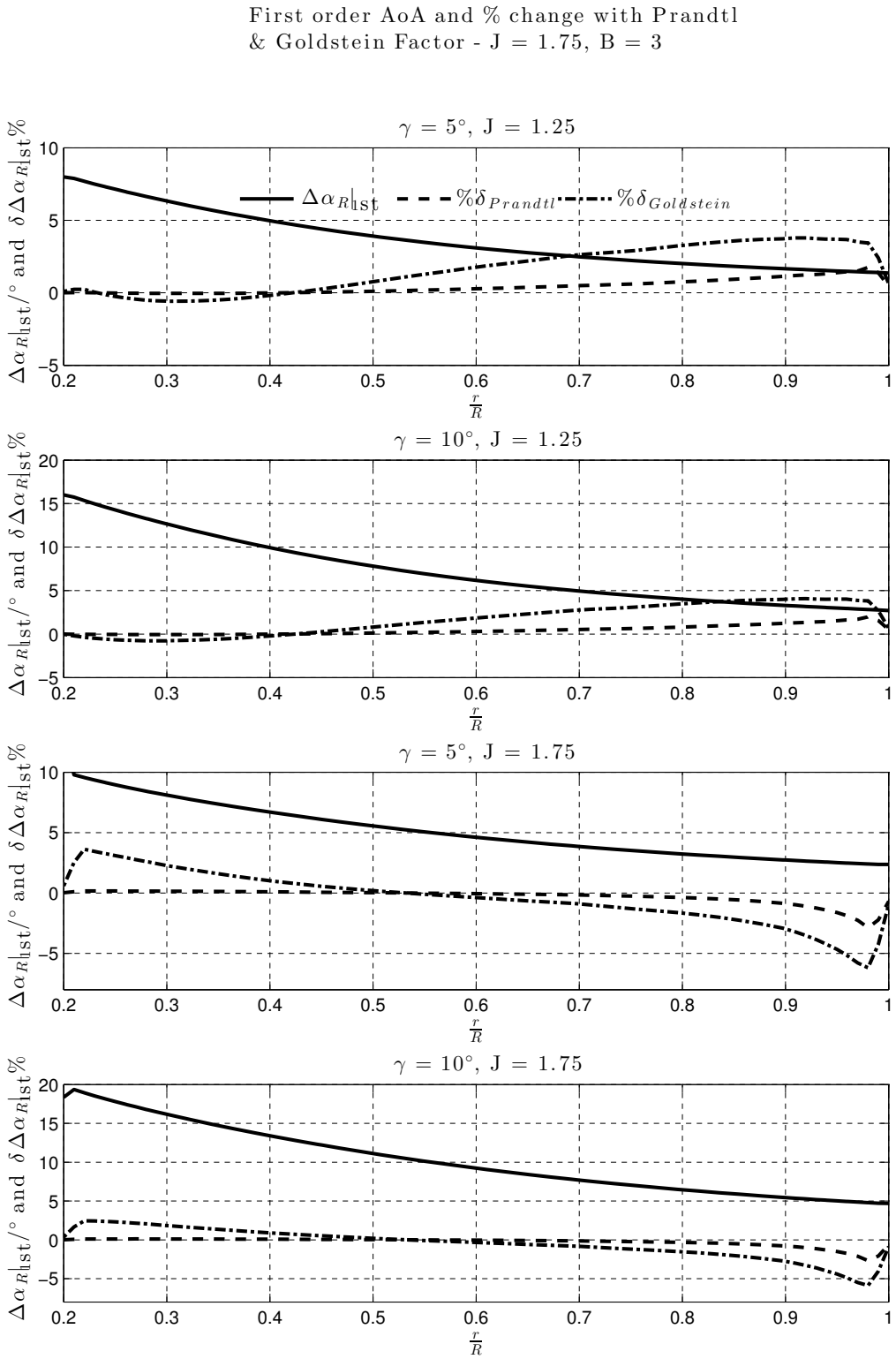

FIGURE 2.20: PRANDTL/GOLDSTEIN FACTOR EFFECT ON $\alpha_R|_{1^{ST}}$ OVER DIFFERENT γ AND J. B=3.

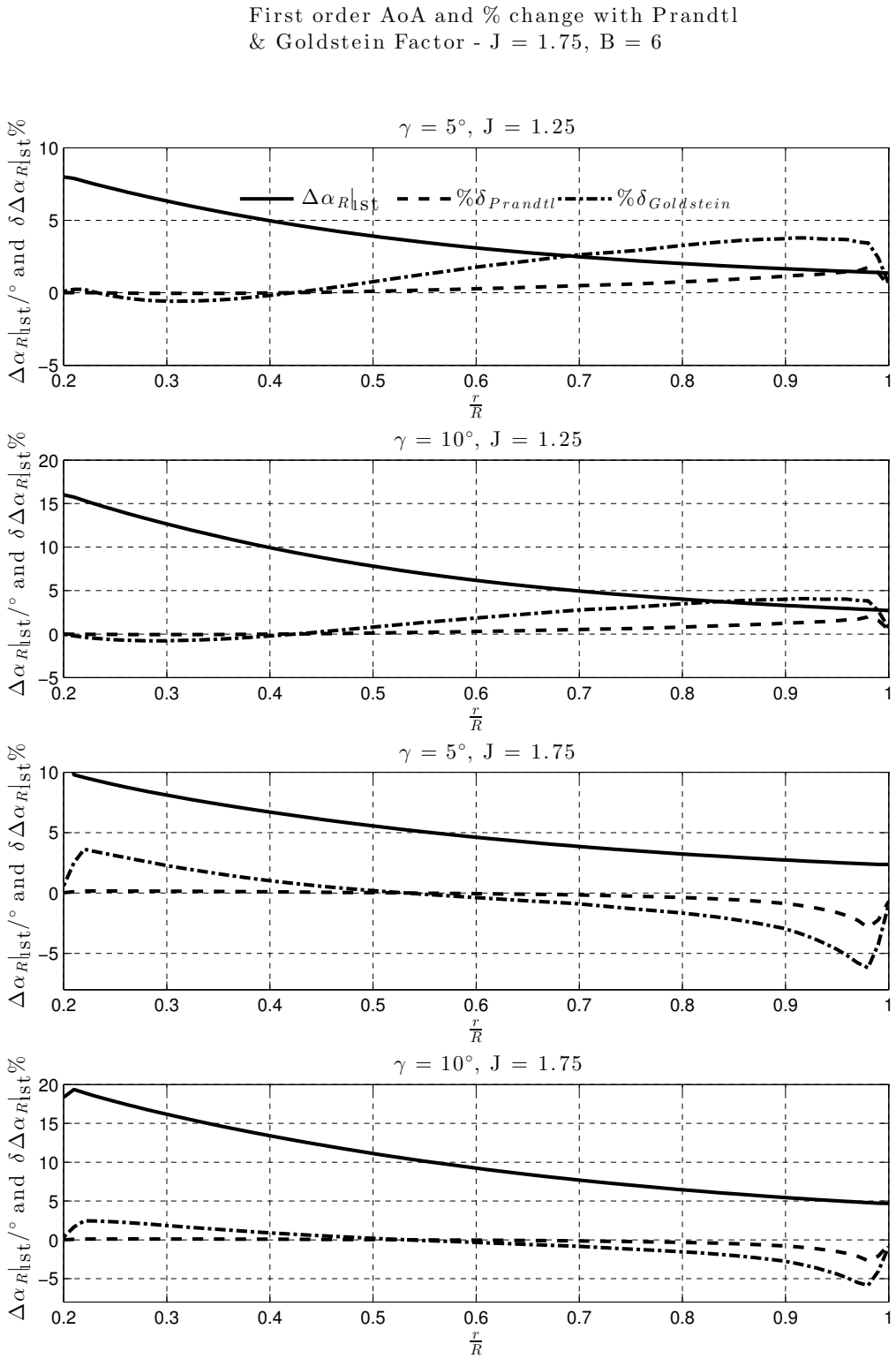

FIGURE 2.21: PRANDTL/GOLDSTEIN FACTOR EFFECT ON $\alpha_R|_{1^{ST}}$ OVER DIFFERENT γ AND J. B=6.

2.7 CONCLUSIONS

A model for a propeller at an angle of incidence with arbitrary incident flow has been presented and has been used to define the effective advance ratio, rotational speed and first-order angle of attack variation. These definitions have been used to determine the criteria via which physical phenomena contribute to once-per-revolution loading.

Through an order of magnitude analysis of different effects, it has been shown that suitable choice of lifting model is of importance for accurate prediction of 1P aerodynamic load. As a consequence, the most accurate two-dimensional data available will be used for the remainder of this dissertation[13]. As stated previously, the model as presented assumes that two-dimensional lift/drag data will be available.

The induced flow is of significant effect in prediction of 1P aerodynamic load. It has shown to affect the sufficient criteria for 1P load - prediction of $\frac{dC_T}{dJ}$ and $\frac{dC_Q}{dJ}$ or $\frac{dC_P}{dJ}$. For a propeller at an angle of incidence, the flow is unsteady (though not *highly unsteady*) and the induced flow at any point on the disc needs to be determined involving both steady and unsteady effects. Due to the interaction of the two effects and to ensure that there is no redundant description of the induced flow field, these two phenomena will be investigated and discussed fully in Chapter 3 - Induced Flow and Unsteadiness.

The out-of-plane displacement has been shown from first principles to positively damp the 1P aerodynamic forcing. Using a quasi-static aeroelastic model, the angle of attack change due to torsional deflection has been shown to be an order of magnitude below the first order angle of attack change. According to the criteria laid out in this chapter, it may be disregarded in an engineering-level 1P aerodynamic model for a propeller at an angle of incidence.

The model as described in this chapter, when combined with an accurate two-dimensional lift and drag databank, should be suitable for determination of 1P fluctuating blade forces. Its formulation allows a fully nonuniform incident flow to be used, and means of including this are described in Chapter 5.

Equations 2.9 and 2.10 are valid only for straight blades - as they implicitly assume that the blade element chord is normal to the pitch change axis, and that the blade element sections are defined parallel to one another, at the same azimuthal position. Chapter 4 provides a discussion of why this is not suitable for blades of swept geometry. A clarification of the confusing definition of geometric 'sweep' along with a derivation of an Euler transform that serves in place of Equations 2.9 and 2.10 is also included.

[13] A NACA-16 lift/drag databank has been written for this model based on two-dimensional test results supplied by DP. Information on the databank is not included in this dissertation.

CHAPTER 3

INDUCED FLOW AND UNSTEADINESS

The previous chapter explored different physical phenomena, and compared their effect on 1P loading. The velocity field induced by a working propeller, and how it varies with thrust was shown to be important in determining a propeller's gradients of performance coefficients with advance ratio, $\frac{dC_T}{dJ}$ and $\frac{dC_P}{dJ}$. It has also been shown that the effective advance ratio and rotational speed varies over the disc of a propeller at an angle of incidence - accordingly, the distribution of the induced velocity must be determined, as it will affect the 1P load prediction. In addition, it has been shown that there is a degree of unsteadiness in the flow, and this must be accounted for in a 1P model.

3.1 INTRODUCTION

With the lift distribution calculable from the equations given in the preceding chapter, the distribution of the induced velocity on a propeller at an angle of incidence remains to be determined. Referring to Figure 3.1, it is logical to assume that a propeller at an angle of incidence will have some distribution of lift that is a function of both radial and azimuth position. For a propeller at an angle of incidence, the extrema of the loading will be at laterally opposing positions[1] - the advancing and retreating extrema described in the previous chapter. This lateral lift asymmetry is shown in Figure 3.1a.

The velocity induced at the disc plane by this lift distribution will be some function of the loading. A non-inclined propeller is subject to axisymmetric incident velocity and hence axisymmetric lift/thrust - the induced velocity is azimuthally-constant. On a propeller at angle of incidence, the lift varies azimuthally and it follows that the induced velocity will also vary azimuthally.

[1] Neglecting, for this discussion, unsteady lift phase lag.

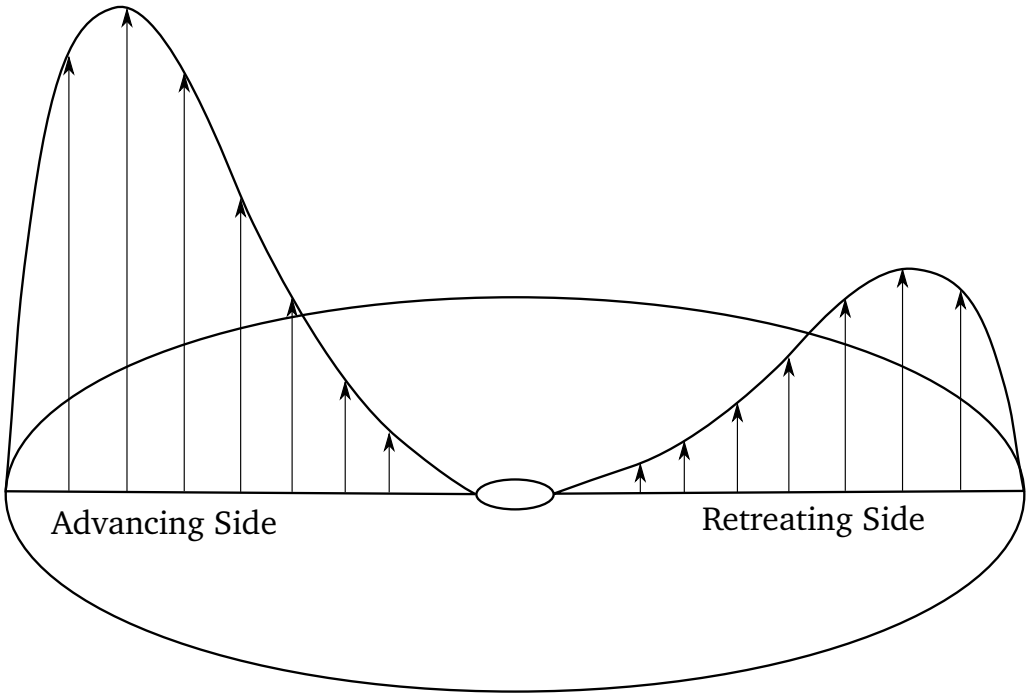

(A) LIFT ASYMMETRY ON PROPELLER AT INCIDENCE

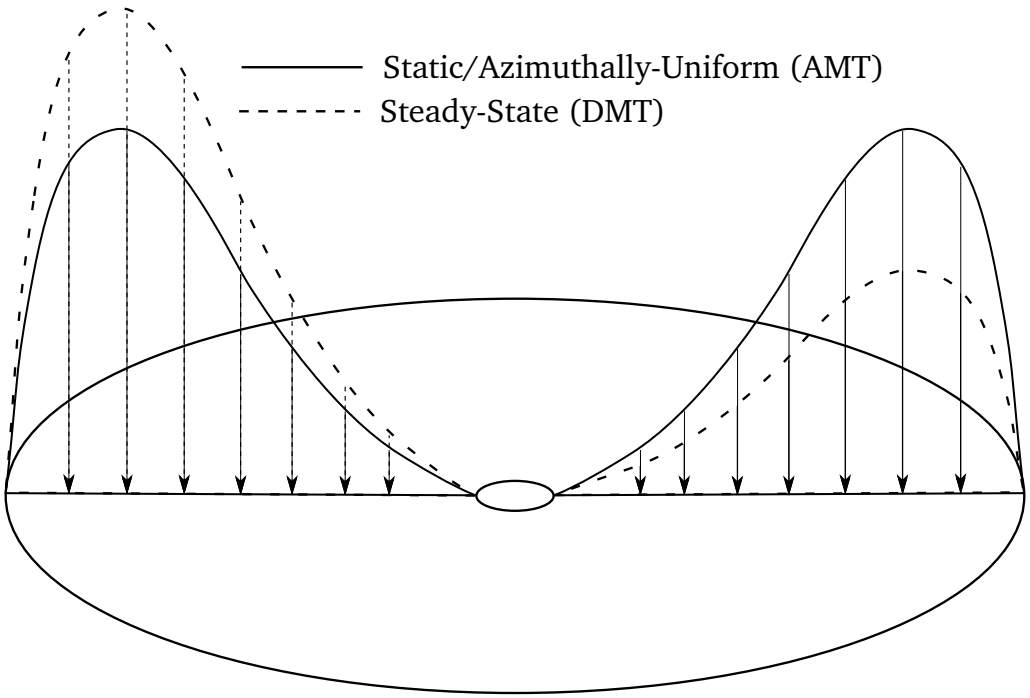

(B) STEAD-STATE VS. STATIC DISTRIBUTION OF AXIAL INDUCED VELOCITY

FIGURE 3.1: PROPELLER DISC AT INCIDENCE - LATERAL LIFT DISTRIBUTION AND PROPOSED RANGE OF INDUCED FLOW DISTRIBUTION

*Note, Figure 3.1 is **qualitative only**.*

For a propeller at an angle of incidence, there are two sources of induced velocity caused by the propeller blades; *steady* and *unsteady* induced velocity:

- **Steady Induced Velocity:** The propeller blades have a bound vorticity sustaining the pressure difference providing thrust. Actuator disc theory dictates that this pressure difference is proportional to the momentum difference in a bounding streamtube around the entire propeller disc (or annuli thereof) - and from this relationship the induced velocity perturbation may be determined. Alternatively, the bound and shed vorticity can be analysed with the Biot-Savart law to determine the induced velocity at the propeller disc. For a propeller at an angle of incidence, this steady induced velocity will be some function of the *total load*.
- **Unsteady Induced Velocity:** The spanwise blade elements of a propeller at an angle of incidence have a resultant angle of attack and velocity, α_R and V_R, that varies with azimuthal position - the lift will also vary accordingly, dl. Consequently, the strength of the bound vortex changes with azimuth (*i.e.,* with time). In accordance with Kelvin's theorem, an equal and opposite amount of vorticity is shed into the trailing wake for any change in the bound vortex (Bramwell et al., 2001), convected along the propeller slipstream. This change in vorticity is a function of the azimuthal variation of blade load, and induces a velocity at the propeller disc that is some function of the *varying load*.

To ensure these effects are modelled adequately, and to demonstrate that they are separate but related, they are described in the following section. Figure 3.2a shows a lifting surface in freestream velocity, V_∞. There will be a spanwise distribution of lift that is a function of the incident flow and the velocity induced by every position. For a wing, the lift distribution is calculable by a variety of methods, the simplest being Prandtl's lifting line theory; application of this method for the propeller is the basis of the vortex theories. Though they will not be used in this dissertation directly, vortex theory adds to the discussion in this chapter. Three-dimensional flowfield effects are highly complex and detailed discussion is beyond the scope of this dissertation aside from utilising existing three dimensional methods that couple with blade element models.

In a blade element or strip theory model there is no physical blade that interacts with the freestream. Instead the blade is represented by a lifting line along its quarter chord, and spanwise elements are presumed to act as sections of an infinite span lifting surface. The spanwise lift may be represented by a bound vortex, which sustains the pressure difference across the disc and thus creates the lift (and hence thrust) of a propeller blade. This bound vortex is also what causes the induced velocity. In a momentum analysis, the pressure difference across the blades, sustained by the bound vortex, is equated with the momentum flux in a

bounding streamtube to determine the induced velocity. In a vortex model the bound vortex and shed vortices induce a flow at the disc determined by the Biot-Savart law. Either approach is modelling the same effect - the induced velocity at the disc due to the steady circulation created by the rotating blades. Figure 3.2a on page 91 shows a blade element representation of a lifting surface in incident flow, and Figure 3.2b shows the system of equivalent horseshoe vortices - the basis of a lifting line or panel method. In such a model, the streamwise arms of the horseshoe vortices extend downstream to infinity - this is a reasonable model for a wing in steady flight. For a propeller or rotor, the vortex system cannot be described as extending in the axial direction to infinity as the blades do not translate in axially. It has been mentioned previously that the vortex system is helical in its initial stages. A representation of a trailing vortex sheet is shown in Figure 3.2c[2] - the helical wake has been coloured to qualitatively show the variation of shed vorticity due to the 1P lift variation on a propeller at an angle of incidence.

The momentum and vortex models described are means of determining the steady induced velocity as a function of the distribution of lift/thrust. For a propeller at an angle of incidence, the induced velocity field will be some function of the disc loading - potentially somewhere between a steady-state distribution and azimuthally-uniform distribution as shown in Figure 3.1b. In the steady-state distribution, the induced velocity is based on local loading. In an azimuthally-uniform distribution, the induced velocity is based on the azimuthally-averaged load. Different means of determining steady induced velocity from momentum considerations will be discussed in Section 3.2.

The unsteady induced velocity is separate to the steady induced velocity. The vortex system trailed by the lifting surface shown in Figure 3.2b shows the *fully developed* system, free from any unsteady effects. In the vortex theory of lift, an aerofoil with camber and/or incidence impulsively started in two-dimensional flow generates a bound vorticity in the aerofoil. Kelvin's theorem states that the fluid domain containing the aerofoil and its wake must contain zero net vorticity/circulation (Bramwell et al., 2001). The bound vortex created within the aerofoil must be balanced by a vortex of opposite strength in the fluid domain - the *starting/shed vortex* shown in Figure 3.3a and experimentally verified by Prandtl. The starting vortex is at the opposite end of the freestream arms of the horseshoe vortex in the system shown in 3.2b. Whilst Figure 3.2b shows the fully developed system, Figure 3.3b shows the shed vortices before they are convected away. On a propeller at an angle of incidence, the strength of the bound vortex (the lift/thrust) is changing continuously with time, which means that an equal and opposite *change in vorticity* must also be shed into the wake, which

[2]For a bound vortex of strength Γ the strength of the vortex sheet is $\left(-\frac{\partial \Gamma}{\partial r}\right)$ - the colouring to show vortex strength only refers to the **qualitative** azimuthal variation, and no radial variation is included.

will induce a velocity at the propeller disc. This is the unsteady induced velocity, and is separate to the steady induced velocity. This will be further discussed and modelled in Section 3.3.

The azimuthal pressure distribution on a propeller at an angle of incidence will be approximately harmonic, as will be the unsteady shed wake. Neglecting unsteady lift hysteresis/phasing effects, the two effects will be in-phase - it is fair to assume that the maximum steady induced velocity is at the maximum lift position, and the maximum unsteady induced velocity will also be found at this position.

An unsteady panel or lifting-line method would implicitly model these two effects simultaneously. Such methods are more computationally expensive than a steady prescribed wake model and consequently far above a momentum model. Whilst the steady and unsteady induced velocity will always both be present on a propeller at an angle of incidence, and are both caused by freestream velocity in the disc plane, they can be separated for the purposes of an engineering-level model, even if they cannot be separated in the real flow. This chapter will look at means of modelling the steady and unsteady induced velocity separately, and combine them in a series of models for comparison. The next section looks at different momentum models that have been used in other implementations in rotary aerodynamics.

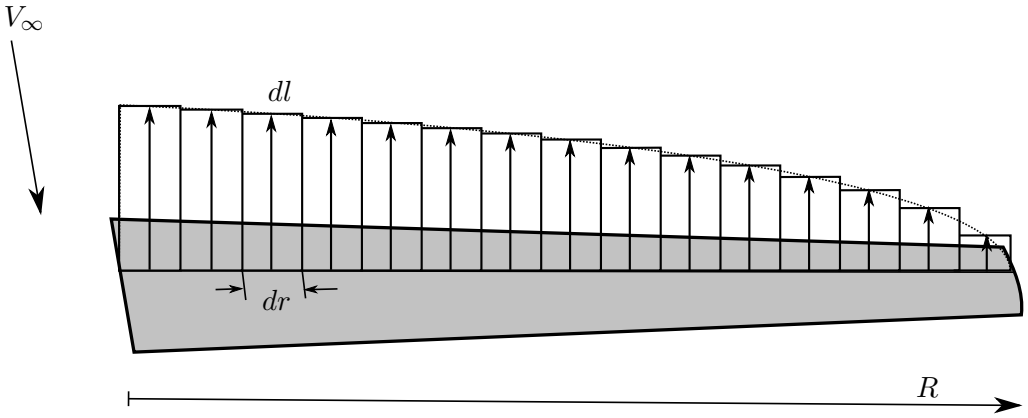

(A) LIFTING SURFACE IN INCIDENT FLOW - BLADE ELEMENTS.

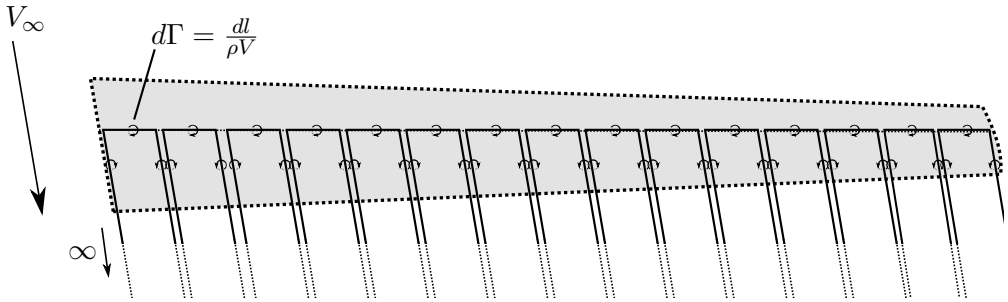

(B) LIFTING SURFACE IN INCIDENT FLOW - FULLY DEVELOPED HORSESHOE VORTICES.

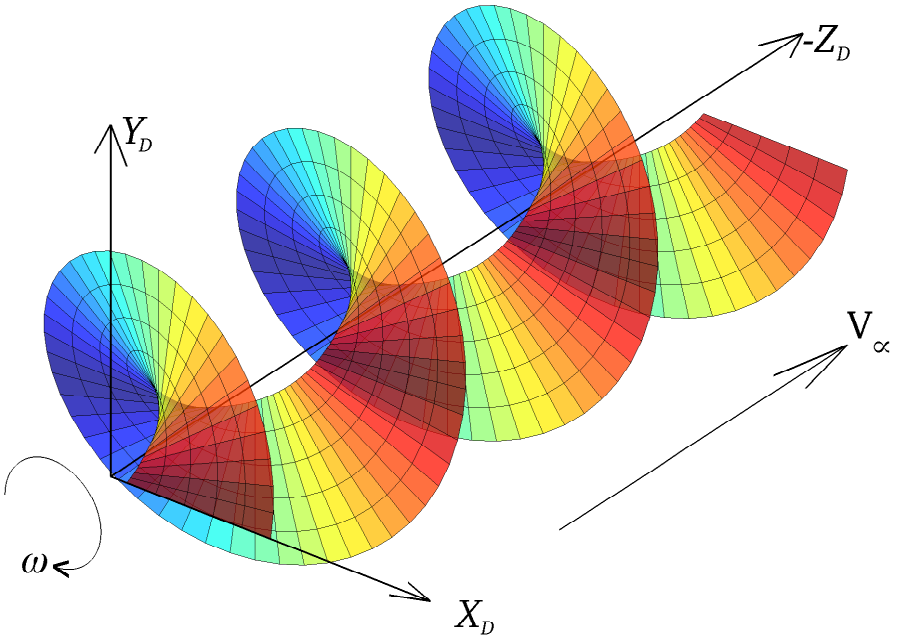

(C) HELICAL VORTEX SYSTEM FOR SINGLE BLADE OF PROPELLER AT INCIDENCE.

FIGURE 3.2: BLADE ELEMENT AND VORTEX REPRESENTATIONS

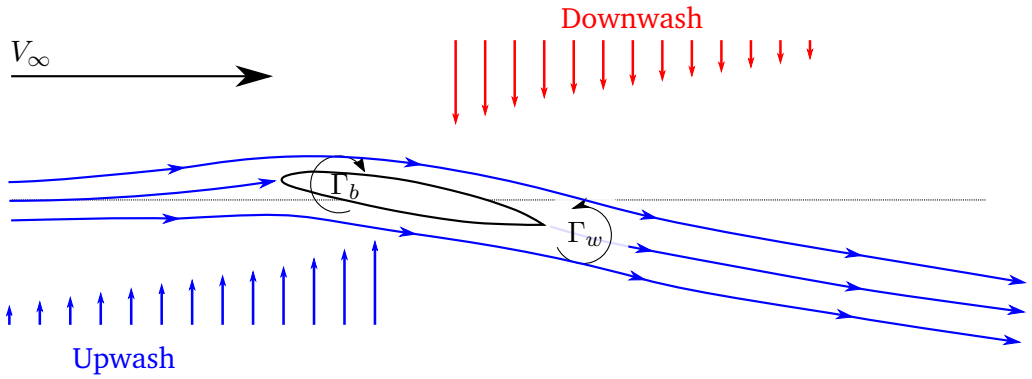

(A) TWO-DIMENSIONAL AEROFOIL IN STEADY FLOW IMPULSIVELY STARTED.

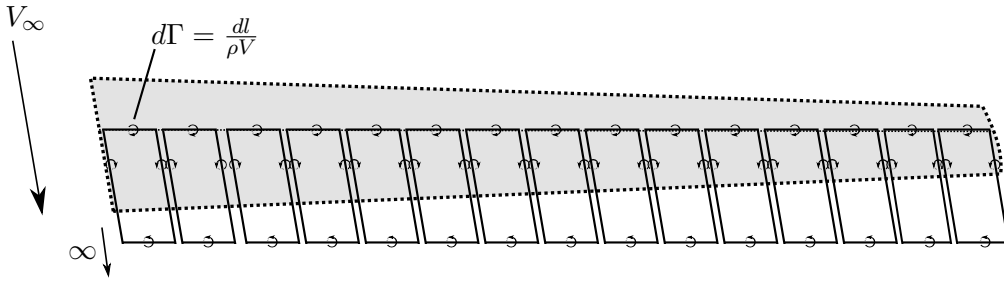

(B) BLADE ELEMENTS IN STEADY FLOW IMPULSIVELY STARTED.

FIGURE 3.3: SHED VORTEX DUE TO CHANGE IN STRENGTH OF BOUND VORTEX IN TWO AND THREE-DIMENSIONAL REPRESENTATION.

3.2 STEADY INDUCED FLOW MODELS

Momentum theory enables quick and accurate calculation of performance of a given propeller by calculation of the magnitude of the induced velocity at a propeller disc when coupled with a suitable blade-element model. In its formulation as laid out by Glauert (1943), there is no provision of an azimuthally-varying load as it is a model for axial flight. This needs to be considered in the present analysis. It makes sense physically that the azimuthal distribution of steady induced velocity at the disc is some function of the azimuthal blade loading, but there is no defined clear method to include this varying load in momentum theory. Through the literature three distributions have found use on propellers/rotors at angles of incidence - either laid out mathematically or included implicitly in analysis. These methods are:

- **Azimuthally-uniform** - the induced velocity field on a propeller at an angle of incidence is taken to be the same as a propeller at zero incidence and is hence a function of the thrust within an annulus. This approach decouples the azimuthal pressure variation with the induced velocity, and does not provide further complication to the annular momentum equations that are in common usage.
- **Skewed** - this approach has its roots in the "dynamic inflow" models of Peters et al. (1979; 1988; 1989), and finds common usage on wind turbines as laid out by Moriarty and Hansen (2005). An azimuthal variation of the induced velocity is assumed that is a function of the wake skew angle, χ. It is justified by noting that the uppermost blade ($\psi = 0$) on a propeller at a positive angle of incidence will be deeper into the wake than the lowermost blade ($\psi = \pi$) and thus experience a larger induced velocity. For a propeller at a positive angle of incidence, this gives a maximum induced velocity at the top of the disc, a minimum at the bottom and equal induced velocity at the lateral extrema loading positions.
- **Steady-state** - this approach assumes that the induced velocity *exactly* matches the pressure distribution on a propeller at an angle of incidence. It has been denoted the 'steady-state' propeller theory in the literature (Crigler and Gilman Jr, 1952; Eisenhuth, 1963), where it has been used by adapting propeller axial performance calculation methods for use in determining the thrust variation of a propeller at an angle of incidence. Such methodology implies a steady-state distribution of induced velocity over the propeller disc. Similarly, the extension of any technique that was conceived for axial flight for usage for a propeller at incidence will invoke the steady-state assumption. Thus, implementations of Lock-Goldstein or other such performance codes will be subject to the same issues that will be discussed in this chapter.

The azimuthally-uniform and the steady-state distribution may be viewed as two extremes of the supposed distribution of steady induced velocity - that is, how the velocity increment changes at the disc due to the distribution of propeller thrust. The azimuthally-uniform distribution assumes that the variation of lift with propeller position does not further affect the aerodynamic environment *i.e.,* all that matters for calculation of induced velocity is the *mean* lift. Conversely, the steady-state distribution invokes the condition that the advancing blade's higher lift causes a larger axial induced velocity, and hence an attenuation of lift asymmetry.

Cases where the three distributions of steady induced velocity have been used can be found throughout the literature, but there is a lack of a quantitative or even qualitative comparison of the methods and the assumptions within. The following paragraphs explain where different implementations of the different models/assumptions have been used. This section is not intended to provide critical review or comparison of these works at this stage.

An azimuthally-uniform distribution of induced velocity is implied in the methodology outlined by de Young (1965). The original work upon which this method was based, by Ribner (1945), stated an assumed sinusoidal distribution of 'incremental inflow'. de Young's extension of the stability derivatives removed Ribner's small angle assumption and improved the applicability of the method, in part through decoupling the solution of the advance angle and the load at the blades, which removes the load attenuation.

Skewed wake models are often used in simulating wind-turbines and have been explored in the development of this dissertation but are not presented herein. These models give a sinusoidal azimuthal distribution of induced velocity with extrema $\frac{\pi}{2}$ out of phase with the extrema loading positions. Hence the load at the advancing and retreating blades will be the same as with the azimuthally-uniform case, as they are subject to the azimuthally-mean induced velocity.

A steady-state distribution has been utilised either explicitly or implicitly through the literature. The work of Crigler and Gilman Jr (1952) makes the assertion that 'steady-state' propeller theory is adequate for determination of the forces on a propeller in yaw - equations developed for performance prediction of a non-inclined propeller by Crigler (1944) are assumed to be valid for local conditions on a propeller at an angle of incidence. The authors note that inclusion of an unsteady model (theirs was based on Theodorsen) has a tendency to attenuate the load asymmetry calculated by the steady state theory, as would be expected. Crigler and Gilman Jr validated the steady-state method to experimental results from Pendley (1945).

Gray et al. (1954) did not directly use a blade element model, but invoked a steady-state assumption implicitly. They took pressure measurements from behind the non-inclined propeller over a range of advance ratio and rotational speeds. These data were used to interpolate for the local loading conditions of the same propeller, subject to inclination. For this methodology, they utilised Equations. 2.25 and 2.26, the effective advance ratio and rotational speed introduced in the previous chapter. Their methodology implied that the local conditions meet the same equilibrium state that the propeller at zero incidence at $J = J'$, $n = n'$ would - *i.e.,* a steady-state distribution of the steady induced velocity based only on local conditions with no blade-element level unsteadiness accounted for in explicit terms.

The general momentum theory has been adapted for use on a propeller at an angle of incidence by both Eshelby (1985) and Heene (2012) using the 'steady-state' assumption. Heene showed the thrust coefficient gradient, dC'_T, at 60% radial position and found that it validated well to experiment (Gray et al., 1954). Both authors utilise a B-bladed multiplication factor from the axial momentum equations which is not used in this present work for reasons discussed in Section 3.2.1. For a propeller at an angle of incidence, rather than considering a propeller disc, or concentric annuli thereof, the General Momentum Theory may be used with a differential area formulation from the outset, allowing the induced velocity to vary with azimuthal position, directly following the load distribution. The derivation of this model is provided in Appendix A, and although it arrives at the same governing equations as Heene (2012), the derivation is slightly different:

- Rotational velocities are included in the dynamic pressure term in the Bernoulli equation from the outset. This approach is the same as in Glauert (1943) (outlined well by Lino (2010)).
- A multiplication factor of B is not included in the blade-element equations, but is instead included as a divisor in the momentum equations.

Since this steady-state momentum model may be formulated by considering a differential area of the disc, rather than the whole disc or concentric annuli, it will be referred to as **"Differential Momentum Theory" (DMT)** for the remainder of this dissertation.

It is important to note that **for azimuthally-constant load (*i.e.,* axisymmetric incident flow), DMT reduces to the well-known annular formulation of the General Momentum Theory** - widely used in engineering models for rotary aerodynamics. DMT and the 'steady-state' method may be thought of as analogous since the assumptions made therein about the distribution of induced velocity is the same in both, but the approach is different in conception. In determination of the loads on a propeller at an angle of incidence, the steady state methodo-

logy uses momentum-based performance equations which have been developed for the non-inclined propeller, whereas DMT is derived for inclined conditions. The governing equations presented for DMT below are the same as Heene's, but derived in a slightly different way. The formulation is different to Eshelby's implementation - he included a component of the axial induced velocity in the tangential direction, but the axes systems and definitions used in this dissertation mean that it is not included in this model. Differential momentum theory (DMT) has been presented in this dissertation and it reduces to the well-known annular momentum theory (AMT) for zero inclination. Alternatively, the DMT equations may be solved using the blade element forces on a propeller at an angle of incidence, averaged azimuthally, which provides AMT for a propeller at incidence[3].

The standard equations for yawing moment and in-plane force on a propeller at an angle of incidence as found in Glauert (1943) and Ribner (1945) are present in much of the work that discusses the steady state method. No comparison of steady-steady BEMT with these equations have been found, but it is shown in Chapter 6 that the momentum theories that validate well for load variation do not validate well for in-plane force without additional terms that are presented in this dissertation.

3.2.1 B-BLADED MULTIPLICATION FACTOR

In the works cited, the usage of the performance equations to determine the loads on the propeller at incidence utilise a B multiplication factor. Specifically, the coupling of blade element and momentum theory assumes that the axial or tangential force at a point on the disc due to blade element forces may be determined by taking the forces on a single blade and multiplying by the number of blades, B. This formulation allows the same BEMT equations to be used as developed for the non-inclined case, Equations 3.14 and 3.15 on page 104, but is physically counterintuitive as it **implies that the instantaneous blade element force at a point is due to all the blades passing through that point**.

This point is somewhat difficult to conceptualise, but is integral to understanding the flaws with extending methodologies derived for non-inclined propellers for use on propellers at incidence. Fundamentally, blade-element momentum theories couple the discrete forces on finite blades to the momentum flux over a continuous surface. Inherent in this methodology is the summation of blade forces to arrive at the *total force* over the propeller disc - for the case where blade forces do not vary in azimuth, it is valid to take the force on a single blade and multiply by the number of blades to arrive at the total force. To extend

[3] In actual calculation, only a single azimuthal position is calculated for AMT, which speeds up computation.

the B-bladed multiplication factor to the propeller at incidence implies

$$F_{prop}(r,\psi) = B \cdot F_{blade}(r,\psi) \tag{3.1}$$

which is erroneous.In addition, some formulations of momentum theory state that

$$T = \int_0^{2\pi} \int_{R_{Hub}}^{R} dT(r,\psi) \tag{3.2}$$

Without careful consideration, this can lead to a total thrust that is B times too large. Additionally, when integrating the momentum thrust in azimuth, a discrete operator needs to be added (*e.g., Kronecker's delta for azimuthal position*) to Eq. 3.2 as although the thrust is the integral of the pressure field, it is not the integral of the blade element forces with azimuth.

In traditional General Momentum Theory the induced velocity is assumed to be uniform azimuthally and hence coupled to the pressure difference due to *all* the blades. Blade forces are summated, which for axisymmetric incident flow is performed by multiplying a single blade force by the number of blades. For the inclined case, if using an annulus or a circular disc as the area for momentum theory, the total pressure difference is the sum of forces on all the blades which would lead to an azimuthally-uniform pressure distribution. Using a differential area provides a reason to couple the induced velocity at a point to local blade lift.

Appendix A on page 222 derives a $\frac{1}{\mathrm{B}}$ multiplication factor in the momentum equations for an assumed azimuthal variation of pressure. This derivation leads to the same final set of solution equations as Heene, but without the B multiplication factor in the blade element thrust. Although these distinctions may seem self-evident, they are provided in this dissertation to show that the coupling of the blade element and momentum equations for a propeller at an angle of incidence is not straightforward.

3.2.2 AMT VS. DMT

Figure 3.1b shows the qualitative lateral difference between the azimuthally-uniform and the steady-state distributions of the steady induced velocity on a propeller at an angle of incidence. These are taken to be the two extremes of the possible distribution of the steady induced velocity at the propeller disc. From momentum considerations, it makes sense that the local induced velocity is a function of the local pressure discontinuity - but this is a simplification of the actual flow environment and the origin of the induced velocity. DMT and AMT serve as formulations of the steady-state and azimuthally-uniform distributions, respectively. The azimuthally-uniform/AMT and steady-state/DMT distributions may both be argued to have a physical basis and/or justification for use:

- AMT does not alter the fundamental equations of momentum theory, and does not introduce any azimuthal variation of axial velocity, thus allowing a simple streamtube to be considered. It has been highlighted earlier in this dissertation that momentum theory is modelling the same phenomena as vortex theory, but from a different background. That is, the lift on the blades effects a velocity increment due to the influence of the local lift (the bound vortex) and the circulation shed into the wake (the shed vortex). Since each blade sheds a helical vortex whose influence may be felt *all over the propeller disc* (and in the entire fluid domain), it follows that azimuthal independence may not be assumed.

- DMT may be justified by considering that the advancing blade will have a stronger bound vortex and consequently shed a greater amount of vorticity locally. This will induce a larger velocity than the retreating blade. It makes sense that this induced velocity has a greater effect locally due to simple proximity considerations.

In the literature, either distribution tends to be used as part of a larger model and validity is assumed. Since both distributions have some physical basis, but aren't wholly justifiable, this dissertation proposes a distribution is some combination of the two with a physical basis. That is, that the steady induced velocity on a propeller an angle of incidence is somewhere between the steady-state and the azimuthally-uniform value. It is advantageous to develop a momentum-based method for efficiency of calculation.

Preliminary calculations[4] using AMT and DMT showed that AMT tended to *overpredict* the load variation and DMT tended to *underpredict* the load variation - with different levels of over/underprediction at different radial stations. The steady-state (DMT) distribution tended to underpredict the load variation at inboard stations, and show better predictions closer to the tip. The azimuthally-uniform (AMT) distribution tended to generally overpredict the load variation, but to a lesser degree at the inboard stations. This suggested that the steady induced velocity on a propeller at an angle of incidence is likely attenuating the load difference to a greater degree at the tip, but not to the extent of the steady-state/DMT distribution. It is impossible to decouple the steady and unsteady induced velocity experimentally, and the load attenuation is likely to be a function of both. A combination of the two momentum models, dependent on radial position, is presented in the next section - **Weighted Momentum Theory (WMT)**.

[4]Not shown in this dissertation, but the observations are present in the comparison with $\frac{dC_T}{dx}$ against Gray et al. (1954).

3.2.3 WEIGHTED MOMENTUM THEORY

Without actually using the higher-order vortex models, the geometry of the shed wake can be used to show that the actual distribution of steady induced velocity due to azimuthal load variation is likely to lie somewhere between the two extreme momentum distributions. The helical vortex system shed by a propeller at an angle of incidence has been shown in Figure 3.2c. This is a simple representation that assumes the wake is convected with the component of freestream velocity normal to the disc. Since this model is only used in a geometric discussion in this chapter, and not in actual calculation, the validity of its assumptions is not discussed.

The velocity induced by the shed wake at the propeller disc includes the effect of the trailed vorticity shed by *all blades all around the azimuth*. For a rigorous analysis, this requires knowledge of the wake geometry, and for a propeller at an angle of incidence, the geometry is highly complex and beyond the scope of this dissertation. From first principles and simple geometry considerations, however, some inferences may be made about the distribution of the induced velocity at the disc based on this simple helical geometry.

Figure 3.4 shows the assumed geometry of the trailed steady vorticity[5] shed by a two-bladed propeller at an angle of incidence - coloured to show qualitative variation of vortex strength only. The wake vorticity has a strength based on the azimuthal position from which it was shed - *i.e.,* greatest at the advancing position and least at the retreating position. Fundamental to DMT or the steady state method is the presumption that azimuthal positions on a propeller at an angle of incidence are subject to an induced velocity field of the same strength as found on a non-inclined propeller at $n = n'$ and $J = J'$. For this to be physically representative, it requires the entire propeller to be producing the same thrust, calculated differently for each azimuthal position. A corollary is that the shed wake's assumed strength is uniform but dependent on the position at which the induced velocity is to be determined. Figure 3.4a shows a *qualitative* representation of the vortex strength that is shed by the perturbational lift component - *i.e.,* a sinusoidal variation of wake strength, with extrema aligned behind the advancing and retreating blade extrema positions. Figures 3.4b and 3.4c show the strength of the wake that the steady state/DMT method assume to exist independently for the lateral load extrema positions, respectively. Clearly the wake does not change strength dependent on the disc position for which the induced velocity is required, and the actual induced velocity will be a function of the bound and shed vorticity from each blade. The induced velocity is determined by the Biot-Savart law applied to the bound vorticity at and trailed vorticity from every radial and azimuthal position. For the purely sinusoidal aerodynamic forcing of a propeller

[5]The wake shed due to the azimuthal variation of lift, with no unsteady effects.

at an angle of incidence (*i.e.,* $\alpha_R, V_R \propto \sin\psi$), the fluctuating component of the induced velocity on a propeller at an angle of incidence will follow a sinusoidal variation[6]. Hence, this gives a sine operator in evaluation of the Biot Savart law. Considering the trailed vorticity only, and assuming that it has a form that varies harmonically, $\gamma_w = \overline{\gamma_w} + \gamma_w{}' \sin\psi$, the induced velocity at a point on the disc by a single vortex filament will be of the form:

$$\vec{V} = \frac{1}{4\pi}\int_0^\infty \frac{d\vec{l}\times\vec{r}(x,\psi)}{|\vec{r}(x,\psi)|^3}\cdot\left(\overline{\gamma_w} + \gamma_w{}'\sin(\psi)\right) \tag{3.3}$$

so the mean induced velocity (*i.e.,* that induced by $\overline{\gamma_w}$) by a single filament will be:

$$\vec{V}_{mean} = \frac{\Gamma_{mean}}{4\pi}\int_0^\infty \frac{d\vec{l}\times\vec{r}}{|\vec{r}|^3} \tag{3.4}$$

and the component of velocity induced by the azimuthally-fluctuating component, $\tilde{\gamma}\sin\psi$, will be zero if

$$\vec{r}(\psi) = \text{const.} \tag{3.5}$$

where $\vec{r}$ is the vector from the point on the disc to the downstream vortex filament positions. This is because, simply, $\int_0^\infty \sin\psi = 0$. If $\vec{r}(\psi)$ is not constant then the velocity induced by the fluctuating component of the wake will also be non-zero as $\int_0^\infty(\psi)\sin\psi$ may not equal zero. The variation of $\vec{r}(\psi)$, therefore, determines the extent to which the induced velocity fluctuates.

Figures 3.5a and 3.5b represent the geometry of single vortex filaments, shed from a given radial position from both blades. The unbroken and broken lines distinguish the vortices shed from each blade, whilst l_1 and l_2 represent $|r(\psi)|$ for $\psi = \frac{\pi}{2}, \frac{3\pi}{2}$. Simple considerations of geometry show that $l_1 = l_2$ only if $x = 0$ (*i.e.,* where $l_1 = l_2$, both equal to the helix radius) and as x gets larger, $\frac{l_1}{l_2}$ gets smaller. As $\frac{l_1}{l_2}$ gets smaller, the vector $\vec{r}$ varies more with azimuth, and the magnitude of the fluctuating component of induced velocity gets larger. Though this simple representation considers only the steady induced velocity due to a single vortex filament, it shows that the fluctuating component of wake vorticity is likely to have less of an influence for positions close to the center of the disc, and more of an influence at outboard positions - and this can be extended to the fluctuating bound vorticity. What this means in effect is that positions close to the center of the disc are subject to an induced velocity field closer to the mean induced velocity field, whilst outboard positions are in an induced velocity field closer to the steady-state/DMT value (*i.e.,* mean + fluctuating component). For a rigorous analysis, the induced velocity would need to be determined via the Biot Savart law and integration over the shed vorticity from all radial positions and the bound vorticity at every radial position, from all blades from every azimuthal position. Additionally, the wake geometry will be skewed, contracting and the

[6]Neglecting, for the present discussion, aerodynamic nonlinearities.

centerbody will affect the lateral influence over the disc. Such considerations mean that a numerical study of this effect is certainly feasible, but beyond the scope of this dissertation. For this present work, the physical basis for some kind of weighting function has been discussed, and a simple means to include this in a momentum analysis will be shown.

This radial variation of steady induced velocity periodicity can be included in a momentum method. The mean induced velocity within an annulus is given by AMT, whilst the locally-induced velocity is given by DMT and these can be combined - with the ratio dependent on radius.

$$v_i = f_1 \cdot v_{AMT} + f_2 \cdot v_{DMT} \tag{3.6}$$

where f_1 and f_2 are functions to be determined. If $\frac{l_1}{l_2} = 1$ then there is no periodicity in the induced velocity (AMT), and as $\frac{l_1}{l_2}$ gets smaller, the induced velocity at a point on the disc will comprise a larger component due to the wake vorticity shed *at that azimuthal position* (closer to DMT). Since $\frac{l_1}{l_2} = 1$ *only* in the centre of the disc, and gets smaller with increasing radial position, it follows that:

$$f_1 \propto \frac{1}{x} \tag{3.7}$$

$$f_2 \propto x \tag{3.8}$$

and since the two distributions form the limits of the proposed induced velocity solution, *i.e.,*

$$f_1 + f_2 = 0 \tag{3.9}$$

The 'weighted induction factor' is introduced, a_{WMT}, and the weighting function f_2 is renamed f_{wt}:

$$a_{WMT} = (1 - f_{wt}) \cdot a_{AMT} + f_{wt} \cdot a_{DMT} \tag{3.10}$$

where f_{wt} is a to-be-determined weighting function that represents the ratio of the influence of a given azimuthal position's 'steady-state' induced velocity (DMT) to the mean induced velocity (AMT) at that radial position. From Eq. 3.8, it follows that

$$f_{wt} \propto x \tag{3.11}$$

f_{wt} could be theoretically determined for a given propeller at a certain flight condition, but for an engineering model, a simple approximation is proposed:

$$f_{wt}(x) \triangleq x \tag{3.12}$$

Using Equation 3.12, f_{wt} is smallest in the root sections, meaning that these sections are subject to an aerodynamic environment closer to that of the non-

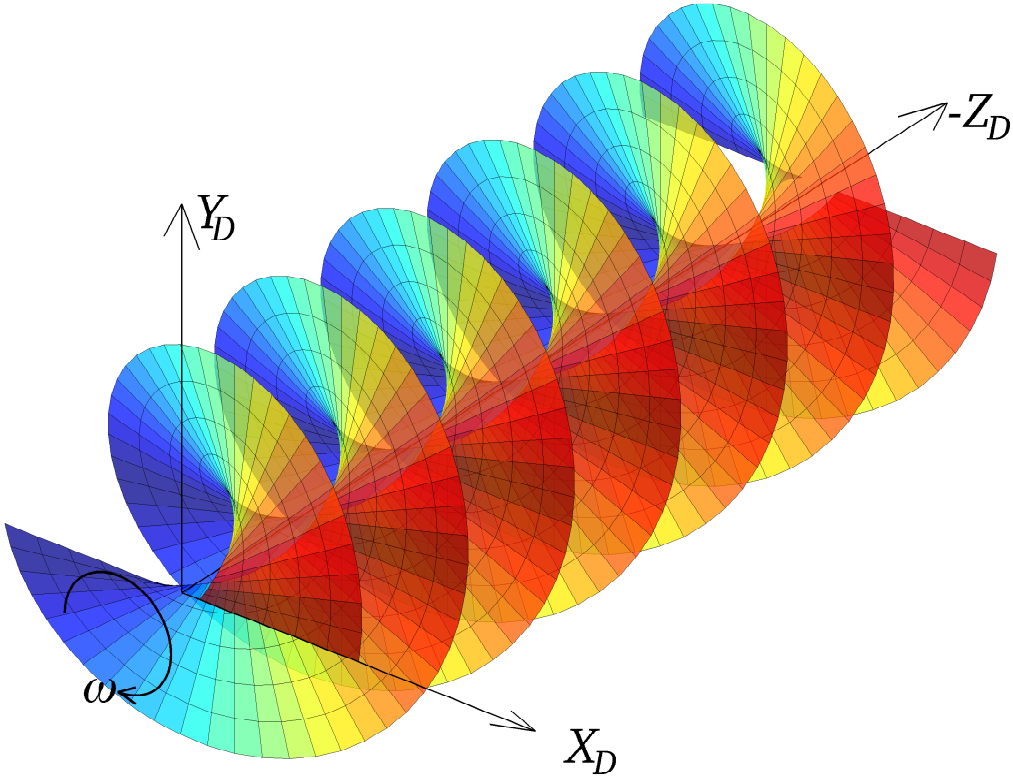

(A) SIMPLE WAKE HELIX REPRESENTATION FOR A TWO-BLADED PROPELLER AT INCIDENCE - **QUALITATIVE** WAKE VORTICITY COLOURED.

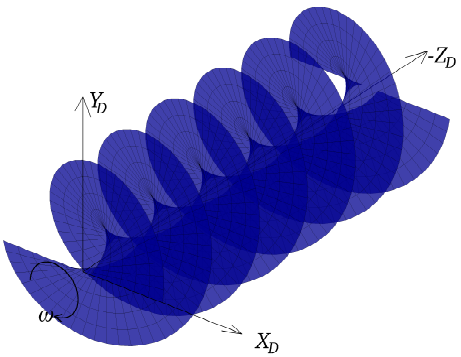

(B) STEADY STATE 'RETREATING' WAKE.

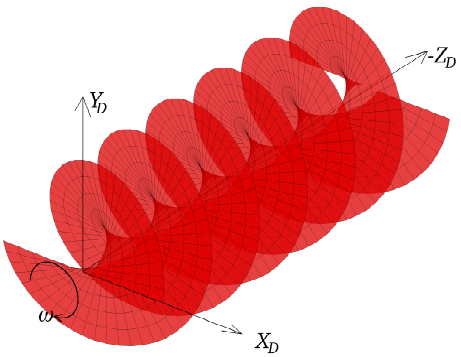

(C) STEADY STATE 'ADVANCING' WAKE.

FIGURE 3.4: HELIX GEOMETRY USED IN DISCUSSION OF WEIGHTED MOMENTUM THEORY.

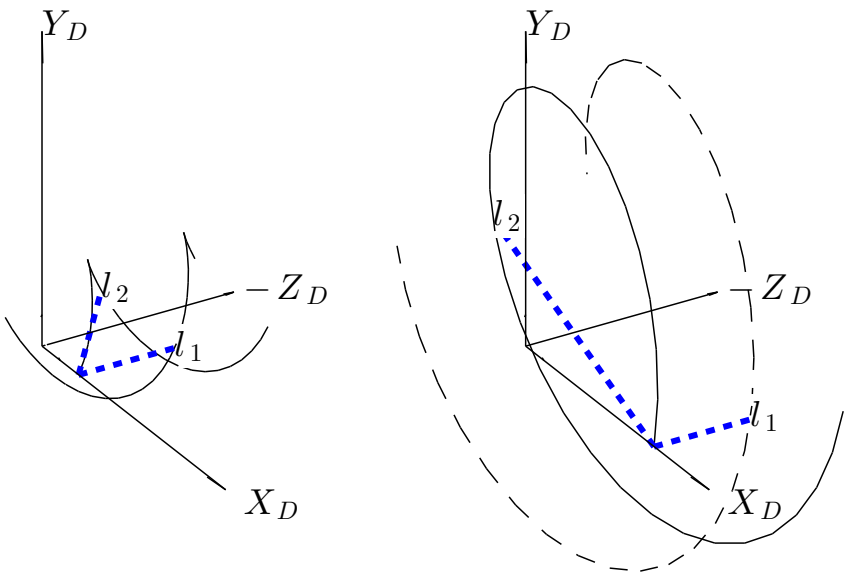

(A) DISTANCES TO WAKE EXTREMA FOR ROOT SECTIONS.

(B) DISTANCES TO WAKE EXTREMA FOR OUTBOARD SECTIONS.

FIGURE 3.5: VARIATION OF $|r|$ FOR DIFFERENT BLADE RADIAL STATIONS.

inclined propeller producing the same annular thrust (AMT), and outboard sections are subject to an aerodynamic environment closer to that of the steady-state conditions (DMT). DMT and the steady state momentum theories are a special case of Weighed Momentum Theory with $f_{wt}(x) = 1$, and traditional Annular Momentum Theory is the same with $f_{wt}(x) = 0$. All three models are calculable by the same code with a simple modification:

$$a(x,\psi)|_{WMT} = \quad (1 - f_{wt}(x)) \cdot a(x)|_{AMT} + f_{wt}(x) \cdot a(x,\psi)|_{DMT} \tag{3.13}$$

with

$f_{wt}(x) = 0$ – Annular Momentum Theory (AMT)

$f_{wt}(x) = x$ – Weighted Momentum Theory (WMT)

$f_{wt}(x) = 1$ – Differential Momentum Theory (DMT)

With this modification, blade root sections at $x \sim 0.2$ are subject to an induced velocity largely composed of the uniform induced velocity (azimuthally uniform distribution), with a small fluctuating component (steady-state distribution). The induced velocity at the tip sections will be wholly composed of the fluctuating component. This is a simplification of the aerodynamics involved, but gives a formulation that is more physically realistic than either the azimuthally-uniform distribution or the steady-state distribution - and is no more computationally intensive than the steady-state method.

Interestingly, the distribution of this effect spanwise follows the same first order variation as for the unsteady induced velocity - that is, the reduced frequency

is larger in the root sections and consequently so is the level of unsteadiness in the flow. These two induction effects, the steady and unsteady induced velocity, are both physically present and will likely have a similar distribution.

In reality, such a weighting function will be a function of the radius r, the number of blades B, the rotational velocity n, the inclination angle γ, the advance ratio J, the blade setting angle β and the actual disc loading. In addition, the weighting function will be a function of the induced velocity itself as the wake convects at different rates depending on the local induced velocity - meaning that a closed form solution to such a function is unlikely. As discussed, the centerbody will also affect the extent to which laterally opposing positions can effect an induced velocity on the opposite side of the disc, and the structure of the vortex wake will be non-axial, likely skewed and contract with increasing downstream position. This presents an opportunity for interesting theoretical and numerical investigation, but is far beyond the scope of this work.

3.2.4 SUMMARY OF MOMENTUM MODELS

The three momentum models compared in this chapter are:

- **Model 1: (General) Annular Momentum Theory (AMT)** - *The classic 'actuator disc' model of Glauert, applied in an annular formulation.*
- **Model 2: Weighted Momentum Theory (WMT)** - *Equations 3.13 and 3.12 are used to determine an induced velocity distribution by superposition of AMT (above) and DMT (below).*
- **Model 3: Differential Momentum Theory (DMT)** - *Momentum theory derived from a differential area formulation - see Appendix A.*

The governing equations for models 1-3 are the relationship between differential thrust and torque contributions and the axial and tangential induction factors, a_a and a_ω:

$$\frac{a_a}{1+a_a} = \frac{\sigma \cdot dC_{ZB}}{4\sin^2\phi} \tag{3.14}$$

$$a_\omega = \lambda_r\,(1+a_a) \cdot \frac{\sigma \cdot dC_{XB}}{2\sin^2\phi} \tag{3.15}$$

where

$$\lambda_r \triangleq \frac{V_n}{\Omega} \tag{3.16}$$

$$dC_{ZB} \triangleq [dC_l \cdot \cos\phi - dC_d \cdot \sin\phi] \tag{3.17}$$

$$dC_{XB} \triangleq [dC_l \cdot \sin\phi + dC_d \cdot \cos\phi] \tag{3.18}$$

and the relationships for the resultant velocity and advance angle at a blade element, Equations 2.11 and 2.12, are redefined to include the induction factors:

$$V_R = \sqrt{V_n^2(1+a_a)^2 + (V_w + V_p)^2(1-a_w)^2} \tag{3.19}$$

$$\phi = \tan^{-1} \frac{V_n(1+a_a)}{(V_w + V_p)(1-a_w)} \tag{3.20}$$

The derivation of Equations 3.14 through 3.18 is given in Appendix A. The solution procedure is given in Figure 3.6. As with most other formulations of BEMT (*e.g.*, Ingram, 2011), the induction factors as defined by Equations 3.14 and 3.15 are solved iteratively. Heene (2012) presented a methodology whereby 3.14 and 3.15 can be solved via Euler's method, but the calculation of the Jacobian matrix and its inverse requires calculation of $\frac{\partial C_l}{\partial a_a}$ and $\frac{\partial C_d}{\partial a_a}$ and other partial differentials. Though this methodology offers a potentially faster solution of the momentum equations, it requires changes to the lift/drag databank in use. Iterative methods are used in the models developed in this dissertation.

Prandtl's circulation distribution function has been utilised with all models in all calculations, owing to it's suitability for this work as highlighted in Section 2.6.1 on page 79.

3.3 UNSTEADY MODELS

The momentum models described in the preceding section are all steady models - and calculation of dC_l and dC_d at each position for a varying α_R and V_R implies a quasi-steady blade-element model. The reduced frequency range shown in Section 2.5.3 indicated that there is a level of unsteadiness in the flowfield for a propeller at an angle of incidence. First-order unsteady attached models have been implemented and compared with the momentum models. The models have their basis in rotorcraft theory, and are described fully in Leishman (2006), but the important details have been included in this section.

Two first-order unsteady models have been utilised: the *Theodorsen* model (Theodorsen and Mutchler, 1935) and *Loewy's* (Loewy, 1957) model. Fundamentally their formulation couples the shed vorticity from an oscillating aerofoil, and its structure in the far wake, to the induced velocity at the disc. Both models also include a non-circulatory component of lift, which is derived from potential theory. Theodorsen's method is based on thin aerofoil theory and is strictly only valid for the two-dimensional aerofoil with a wake that convects linearly downstream to infinity in the chordwise direction. Loewy's model is an extension of Theodorsen's theory with a helical wake that more accurately describes a rotor in hover - and is thus a better representation of the propeller in forward flight. Only Loewy's model is compared in this dissertation.

The shed vortex creation and the fact that the aerodynamic response of an

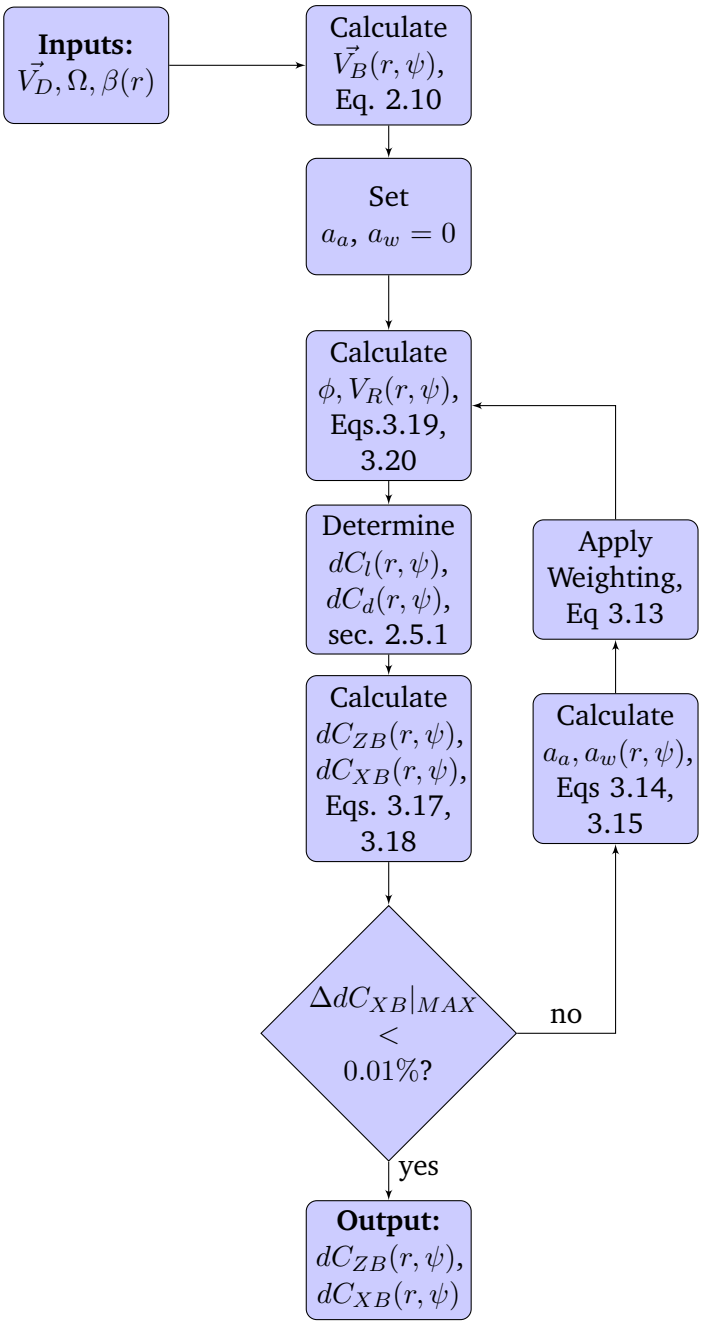

FIGURE 3.6: SOLUTION PROCEDURE FOR BLADE ELEMENT MOMENTUM THEORY MODEL

aerofoil, subject to unsteady forcing, requires the time history of unsteady forcing has been described in the introduction. Figure 3.7 shows a two-dimensional aerofoil section oscillating in angle of attack steady onset flow[7]. This gives a time-varying change in the lift of the aerofoil and hence the circulation it creates. To effect this change in circulation, the strength of the bound vortex must change, and an equal and opposite change must be shed into the wake from the trailing edge of the aerofoil and convected downstream to infinity. For an aerofoil with chordwise distribution of bound vorticity[8], γ_b, and a trailed vorticity, γ_w convecting to infinity, the chordwise distribution of downwash is given by:

$$w(x,t) = \frac{1}{2\pi}\int_0^{x_{te}} \frac{\gamma_b(x,t)}{x - x_0}dx + \frac{1}{2\pi}\int_{x_{te}}^{\infty} \frac{\gamma_w(x,t)}{x - x_0}dx \tag{3.21}$$

subject to the boundary (Kutta) condition:

$$\gamma_b(x_{te},t) = 0 \tag{3.22}$$

In order to determine the unsteady lift response, the aerodynamic environment change due to aerofoil motion must be known. Eq. 3.21 implies that this is **dependent on the entire history of aerofoil motion**. Using the unsteady Bernoulli equation and potential theory, Theodorsen and Mutchler (1935) showed that the unsteady lift could be related to the quasi-steady lift:

$$L_{US} = \frac{\displaystyle\int_{x_{te}}^{\infty} \frac{x}{\sqrt{x^2 - x_{te}^2}}\gamma_w dx}{\displaystyle\int_{x_{te}}^{\infty} \sqrt{\frac{x + x_{te}}{x - x_{te}}}\gamma_w dx} \cdot L_{QS} \tag{3.23}$$

Eq. 3.23 still requires the time history of aerofoil motion - but since for thin aerofoil theory the relationship between forcing (angle of attack change) and the output required (wake vorticity) is *linear*, Theodorsen showed that if an aerofoil is subject to harmonic forcing, the wake strength will also vary harmonically. For harmonic motion (*i.e.,* that which can be decomposed into a mean and a

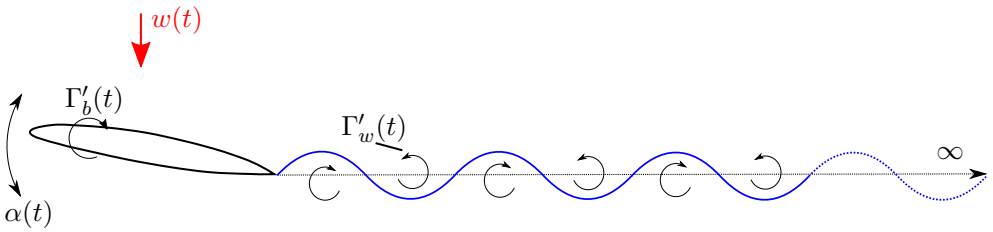

FIGURE 3.7: TWO-DIMENSIONAL AEROFOIL OSCILLATING IN ANGLE OF ATTACK - THEODORSEN'S MODEL

[7]Figures 3.7 and 3.8 adapted from Leishman (2006, pgs 431, 441)

[8]$\gamma = \frac{d\Gamma}{ds}$ where s is vortex length. Γ is used in diagrams in this discussion for simplicity and to avoid confusion with disc inclination angle.

fluctuating component):

$$\alpha_R(t) = \bar{\alpha_R} + \tilde{\alpha_R} \cdot e^{i\omega(t-\frac{x}{V})} \tag{3.24}$$

the mean component does not change the wake vorticity, only the fluctuating component. Thus:

$$\gamma_w(t) = \tilde{\gamma_w} \cdot e^{i\omega(t-\frac{x}{V})} \tag{3.25}$$

which Theodorsen used to show:

$$L_{US} = C(k)L_{QS} \tag{3.26}$$

with the Theodorsen function, $C(k)$, defined:

$$C(k) = \frac{\displaystyle\int_{x_{te}}^{\infty} \frac{x}{\sqrt{x^2 - x_{te}^2}} e^{-iks} dx}{\displaystyle\int_{x_{te}}^{\infty} \sqrt{\frac{x + x_{te}}{x - x_{te}}} e^{-iks} dx}. \tag{3.27}$$

where k is the reduced frequency. The complex-valued Theodorsen function may be calculated via Hankel functions, H:

$$C(k) = F(k) + iG(k) = \frac{H_1^{(2)}(k)}{H_1^{(2)}(k) + iH_0^{(2)}(k)} \tag{3.28}$$

where $H_v^{(2)} \triangleq J_V - iY_v$ and J_v, Y_v are Bessel functions of first and second kind. $F(k)$ and $G(k)$ may be written:

$$F(k) = \Re C(k) = \frac{J_1 (J_1 + Y_0) + Y_1 (Y_1 - J_0)}{(J_1 + Y_0)^2 + (J_0 - Y_1)^2} \tag{3.29}$$

$$G(k) = \Im C(k) = -\frac{Y_1 Y_0 + J_1 J_0}{(J_1 + Y_0)^2 + (J_0 - Y_1)^2} \tag{3.30}$$

Eq. 3.26 relates the unsteady circulatory lift to the quasi-steady lift, based on lift varying with angle of attack only, and with a wake that convects downstream to infinity. Neither of these are a fair representation of the aerodynamic environment on a propeller at an angle of incidence, and developments of Theodorsen's work for rotorcraft theory are useful in this disseration. For an aerofoil oscillating in angle of attack, additional circulatory terms arise from the chordwise change to downwash/upwash due to oscillation about the PCA[9]. The angle of attack variation may be represented as:

$$\alpha = \tilde{\alpha} e^{i\psi} \tag{3.31}$$

and the angle of attack rate:

$$\dot{\alpha} = i\omega\tilde{\alpha} e^{i\psi} \tag{3.32}$$

for which the unsteady lift coefficient is:

$$C_l\big|_{US} = 2\pi(F\,[1 + ik] + G\,[i - k])\tilde{\alpha} e^{i\psi} + \pi k \left(i - \tfrac{k}{2}\right) \tilde{\alpha} e^{i\psi} \tag{3.33}$$

[9]For a stationary aerofoil in a freestream with varying α_R, this isn't *quite* the same, though this technique finds use in well-validated rotorcraft codes and will be used herein.

The first set of terms in 3.33 are the circulatory terms - and the 2π may be replaced with the lift curve slope of the section in question. The second set of terms are flow acceleration effects and are derived from potential theory, related to the instantaneous acceleration of a mass of air by the moving aerofoil - or in this implementation, the deflection of a moving mass of air. For a further description of these terms and their derivation see Leishman (2006, ch. 8).

Eq. 3.33 on the previous page is strictly only valid for an isolated two-dimensional aerofoil with a wake that is convected downstream in the freestream direction. Loewy (1957) utilised and adapted Theodorsen's method by approximating the helical wake by a series of infinite vortex sheets extending *underneath* the rotor disc - shown in Figure 3.8. Loewy defined a modified function, based on the Theodorsen function.

Eq. 3.33 is used with Loewy's function $C'(k, \frac{\omega_f}{\omega}, h)$ in place of $C(k)$:

$$C'\left(k, \tfrac{\omega_f}{\omega}, h\right) = \frac{H_1^{(2)}(k) + 2J_1(k)W}{H_1^{(2)}(k) + iH_0^{(2)}(k) + 2\left(J_1(k) + iJ_0(k)\right)W} \tag{3.34}$$

The Loewy function similarly comprises Bessel functions but also takes the complex-valued W function as an argument:

$$W\left(\tfrac{hk}{b}, \tfrac{\omega_f}{\omega}\right) = \left(e^{kh/b}e^{i2\pi\omega_f/(B\omega)} - 1\right)^{-1} \tag{3.35}$$

ω_f is the forcing frequency, and the parameter $\frac{\omega_f}{\omega}$ determines the periodicity of shed wake fluctuations. For the periodic forcing of a propeller at an angle of incidence, $\omega_f = \omega$ and hence all the shed wake effects are in phase. The *wake spacing*, h, is a function of the number of blades, the advance angle and the average induced velocity. Defined in rotorcraft nomenclature by induced velocity ratio, blade number, semichord and rotorspeed (eq. 8.36 Leishman, 2006, pg.

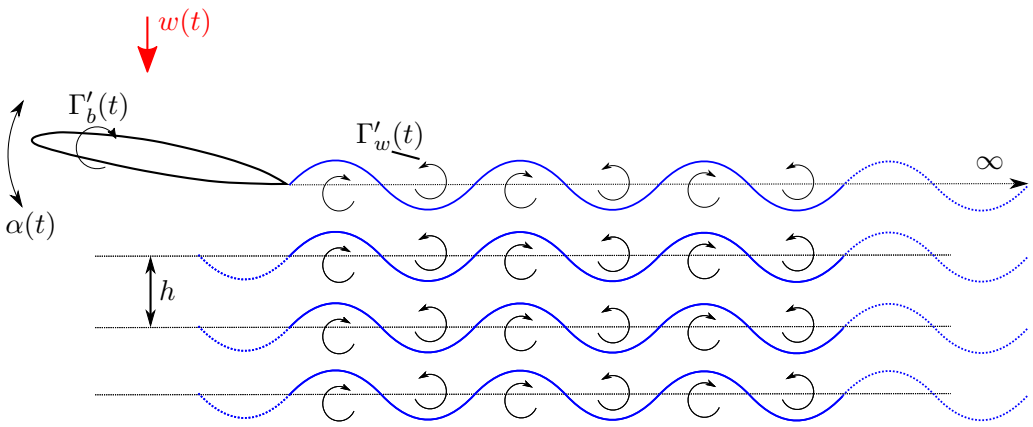

FIGURE 3.8: TWO-DIMENSIONAL AEROFOIL OSCILLATING IN ANGLE OF ATTACK - LOEWY'S MODEL

442):

$$\frac{h}{b} = \frac{\lambda \Omega R 2\pi}{\Omega N_b b} \tag{3.36}$$

it may be similarly defined in the propeller nomenclature used in this thesis, noting that the wake will be convected by the axial incident velocity in addition to the induced velocity

$$\frac{h}{b} = \frac{V_\infty \cos\gamma \, (1+a) \, 2}{\omega \sigma r} \tag{3.37}$$

COUPLING OF INDUCED FLOW MODELS AND UNSTEADY MODELS

Care needs to be taken when coupling an unsteady model and the steady induced velocity model. In the models used in this dissertation, the momentum model is run to convergence to determine the distribution of α_R and V_R using the quasi-steady loads. The angle of attack variation is then represented by a harmonic function, and the unsteady loads are calculated with Theodorsen/Loewy. The unsteady loads are coupled with the momentum model to determine the induced velocity due to the unsteady pressure difference, which is generally smaller than the quasi-steady pressure difference. This is an iterative procedure as the solution of both the induced velocity model and the unsteady model are mutually dependent. Heene (2012) used a different implementation and took the argument of the Theodorsen function to provide the phase shift, and applied this to the quasi-steady loads. His method has the benefit that it provides phase shift without another iterative loop to be solved in a calculation, but it does not take into account the unsteady shed wake, nor the impulsive lift.

3.4 DYNAMIC WAKE MODELS

The "Pitt & Peters" (Pitt and Peters, 1981), "Peters-He" (He, 1989) and "Peters-Morillo" (Morillo, 2001) models were originally suggested as a research avenue for this dissertation owing to their ability to correctly model the transient induced flow variation in response to an applied hub moment - the so-called "dynamic inflow". Though they eventually proved unsuited for this particular research project, their non-uniform discretisation of the induced flow variation at the disc was integral to understanding the importance of induced flow variation.

For a propeller/rotor disc subject to a nonuniform radial/azimuthal pressure distribution (*e.g.,* a propeller at incidence or a helicopter rotor in edgewise flight), these models determine the nonuniform distribution of steady induced velocity subject to the discretisation used in each model. Although they are colloquially called *dynamic inflow* models, they are more accurately termed *finite-state induced velocity models*, helping to clarify some confusion between 'inflow' and 'induced velocity' between propeller/rotorcraft fields. For clarification in this

discussion it should be highlighted that these models are designed to **model the unsteady behaviour of the wake and its effect at the propeller disc** (*i.e.,* transient wake dynamics), and **do not model blade-element level unsteadiness** unless coupled with a suitable model (*e.g.,* Theodorsen/Loewy).

The Pitt & Peters model has a linear variation of induced velocity in radius, with a single harmonic variation in azimuth - *i.e.,* the induced velocity distribution may be visualised as a uniform disc tilted at incidence to the propeller disc. It has often been extended for use in an annular formulation (*e.g.,* Suzuki and Hansen, 1999, sec. 2, "annular section model") - which provides good validation for wake dynamics in some wind turbine cases, but is physically unrealistic at the blade element level. Neither the original linear nor the annular formulation of the Pitt & Peters model are used in this dissertation.

The Peters-He, or the Generalised Dynamic Wake (GDW) model is more complex in formulation and relies on a truncated infinite series to describe the pressure/induced velocity distribution at the disc. This model has been implemented on propeller at incidence for this dissertation, including mass flow additions made by Makinen (2005), which were presented for axial flight.

This model was initially chosen to due to its potential extension to dynamic effects on a pitching rotor, but load predictions using the GDW showed large fluctuations in azimuth. It is more suited to a pitching propeller or one subject to a gust, as its formulation is designed to handle transient wake dynamics and the thrust hysteresis in response to aerodynamic fluctuations. It may be the subject of future work for this reason, but the azimuthal discretisation used leads to load fluctuations at the blade element level that are of significant magnitude - this is discussed in the results section.

3.5 SUMMARY OF MODELS

For greater clarity in this chapter, the six models compared are referred to by numeral and an acronym/abbreviation - summarised in Table 3.1 on the following page. Quasi-steady models utilise the local α_R and V_R and use the dC_l and dC_d from static lift/drag data. Unsteady models use Loewy's model, described above.

	Model	Description
QS Aero	1 (qsAMT)	General (Annular) Momentum Theory/$f_{wt} = 0$
	2 (qsWMT)	Weighted Momentum Theory/$f_{wt} = x$
	3 (qsDMT)	*Differential Momentum Theory/$f_{wt} = 1$*
US Aero	4 (usAMT)	AMT + Loewy
	5 (usWMT)	WMT + Loewy
	6 (usDMT)	*DMT + Loewy*

TABLE 3.1: SUMMARY OF MODELS DEVELOPED AND COMPARED - MODELS *in italics* ARE ONLY PRESENTED IN A FEW FIGURES.

3.6 VALIDATION DATA

Comparison with modern URANS-based solutions for the thrust distribution for a propeller at incidence would be in interesting exercise. Modern CFD provides valuable insight into aerodynamic problems, and is used in place of some experimental data. For a problem as complex as this, however, it would be necessary to compare with a CFD code validated very well for a propeller at incidence. Since there is no open-source analysis that has shown this adequately at the time of writing, legacy experimental data remains to be the best source of validation data - though future comparison with CFD would be an interesting exercise.

The ideal validation data for the induced velocity and load variation on a propeller at an angle of incidence would be flow visualisation and pressure measurements over a range of spanwise and azimuthal positions, covering a range of advance ratios, rotational speeds and disc inclination angles. Such measurements at first glance may be possible from measurements on a pressure-tapped blade on a rig designed to operate at different angles of incidence in a wind tunnel coupled with LDA/PIV. Pressure tappings would need to be corrected for phase-lag induced due to the latency in response of the pressure disturbance through the tube - and the centrifugal effects in columns of air in the blades themselves. In addition, even if connected to a pressure transducer capable of measuring dynamic pressure fluctuations, the response of the air inside such an array of tubing will likely preclude dynamic pressure measurements. *Ideally*, dynamic pressure transducers (*e.g.,* Kulite or Honeywell transducers) would be fitted in arrays to the blades, but this would be prohibitive in terms of expense and in the loss of structural integrity of the blades. Ultimately, such methods would afford the ability to determine the chordwise and spanwise pressure distribution at different azimuthal positions, thereby allowing the calculation of the load fluctuation in any direction. Whilst this data does not exist in the published literature, other measurements from propellers at incidence exist that prove useful:

- **Wake Survey Measurements:** through pressure probe wake traverse in the near slipstream, the pressure jump across the propeller disc may be estimated. From this, the axial force may be calculated easily.
- **Reaction Forces/Moments:** a propeller rig mounted on a force/moment balance enables determination of the axial and in-plane forces, and the yawing/pitching moment on an inclined/yawed propeller. These measurements allow no determination of spanwise force gradients, and will be intrinsically linked with body forces on the spinner/nacelle.

Wake survey measurements were taken on an inclined 3-bladed, 10ft diameter propeller with straight blades by Gray et al. (1954). Measurements were taken at $30, 45, 60, 70, 75, 80, 85, 90$ & $95\%R$ and at azimuthal positions

$75°, 105°, 150°, 255°, 285°$ and $330°$ - giving the axial force difference at these points around the azimuth. These measurements may be integrated to determine the *thrustwise bending moment*, which will be dependent on the magnitude of the blade element forces, giving reasonable confidence in a particular model's ability to predict blade bending moments due to lift and drag variation.

Measurements were taken at two disc inclination angles, $\gamma = 4.55°$ and $\gamma = 9.80°$, at $J = 1.2, 1.25$ and $RPM = 1350, 1600, 2000, 2160$ with only the smaller γ being performed at the greatest rotational speed. It should be noted that *all* data from Gray et al. presented in this thesis has been taken from digitising discrete data points on the plots presented in their paper. Effort has been taken to ensure the greatest accuracy.

Russell (1952) performed a similar set of experiments and published faired curves of radial thrust variation, with the maximum and minimum curves shown, assumed to be at the $\psi = 90°, 270°$ positions respectively. A range of blade setting angles, disc inclination angles, advance ratio and rotational speeds were performed in this set of experiments, and presented versus the normal advance ratio, defined as the advance ratio based on the velocity normal to the propeller disc:

$$\hat{J} \triangleq J \cdot \cos\gamma \tag{3.38}$$

There is little contiguous data in the paper, and only a few data points have been selected that have the same blade setting angle and disc inclination angle to compare a range of $\hat{J}$. As a range of rotational speeds have been used, results have been calculated using the lowest rotational speed and presented using coefficients to reduce the dependency on rotational speed.

Pendley (1945) measured the thrust variation using a wake survey on a two-bladed, 4ft diameter propeller at low inclination angles of 1°, 2° and 4°. The main data presented in the original paper is difficult to utilise owing to the crowded plots - comparison with Pendley is not included in this dissertation.

Yaggy and Rogallo (1960) performed a range of experiments on propellers inclined to much higher angles - up to $\gamma = 85°$, with a range of rotational speeds. There were no wake survey measurements taken, but the authors recorded both yawing moment and in-plane force due to disc inclination. These two quantities are functions of the thrust variation and tangential force variation, respectively - and it follows that adequate prediction of these two quantities with disc inclination affords confidence to a 1P prediction model. Only data for the yawing moment is shown in this chapter, as traditional means of calculating the in-plane force have proven to be insufficient. The in-plane force may be underpredicted with induced velocity models that validate *well* for yawing moment and thrust measurements, when using the traditional equations for calculation. In Chapter 6 a full discussion of the in-plane force is provided, and an additional contribution

is derived that is not modelled by more traditional methods (*e.g.,* Ribner (1945) - which is still in use in ESDU documents).

A summary of the test conditions and propeller physical parameters in the following comparisons is given in Table 3.2.

3.7 DISCUSSION OF RESULTS

Results against individual sets of data will be discussed in the relevant subsections following. It stands to state here, however, that quasi-steady weighted momentum theory consistently provides a better match to experimental data throughout the results presented. It matches the radial and azimuthal distribution of thrust over propellers at incidence better than any of the other models tested, and does so over a range of advance ratio, rotation speeds and inclination angles. In addition, the results for yawing moment show similar better matching with quasi-steady weighted momentum theory.

It *should* follow that the in-plane force due to inclination (*i.e.,* the vertical disc force on a propeller at a positive angle of incidence) would be better predicted also by quasi-steady weighted momentum theory. A na ive implementation of the theory will show that it does not, but this can be explained with a new formulation of the equations for in-plane forces. These results form a separate chapter, Chapter 6, but serve as extra validation for this chapter.

Reference	Blade No. B	J	RPM	$\gamma/^\circ$	Aerofoil	Diameter, D
Gray et al. (1954), Section 3.7.1	3	1.2-1.25	1350-2040	4.55-9.80	NACA-16	10ft/3.05m
Russell (1952), Section 3.7.2	4	$\sim$0.4-0.9	650-875	10	NACA-16	16ft/4.88m
Yaggy and Rogallo (1960), Section 3.7.4	3	$\sim$0.5-2.0	1000	15, 30, 45	NACA-16	12ft/3.65m
Rogallo et al. (1951), Section 3.8	4	$\sim$2	1250	8 (installed)	NACA-16	13.2ft/4.02m

TABLE 3.2: SUMMARY OF EXPERIMENTAL CONDITIONS COMPARED.

3.7.1 GRAY ET AL.

Figures 3.9 to 3.12 show the change to radial thrust coefficient gradient, $dC'_T \triangleq \frac{dC_T}{dx}$, at four different radii. 30, 45, 70 and 90% radius have been chosen as these show a range of performance conditions - inboard, highly-loaded and tip sections. Results from models 1, 2, 4 and 5 have been shown for all plots - results are not shown with 'steady-state' propeller theory (DMT - models 3,6) in these plots, for clarity, though calculations have been performed with all models, and the respective error in the $\pm$ thrust gradient range is shown in Figures 3.13 to 3.16 for all six models. In total, seven sets of operating conditions were run in the experiments by Gray et al., and all have been simulated with all six models, but only a few plots are shown in this thesis due to space limitations. A set of low and high rotational speeds have been shown in Figures 3.9 to 3.12 to show a range of compressibility effects. The operating conditions for each of the seven cases is given in Table 3.3.

Case	RPM	γ	J
1	1350	4.55°	1.2
2	1350	9.80°	1.2
3	1600	4.55°	1.2
4	1600	9.80°	1.2
5	2000	4.55°	1.25
6	2000	9.80°	1.25
7	2140	4.55°	1.25

TABLE 3.3: OPERATING CONDITIONS FOR CASES IN (GRAY ET AL., 1954)

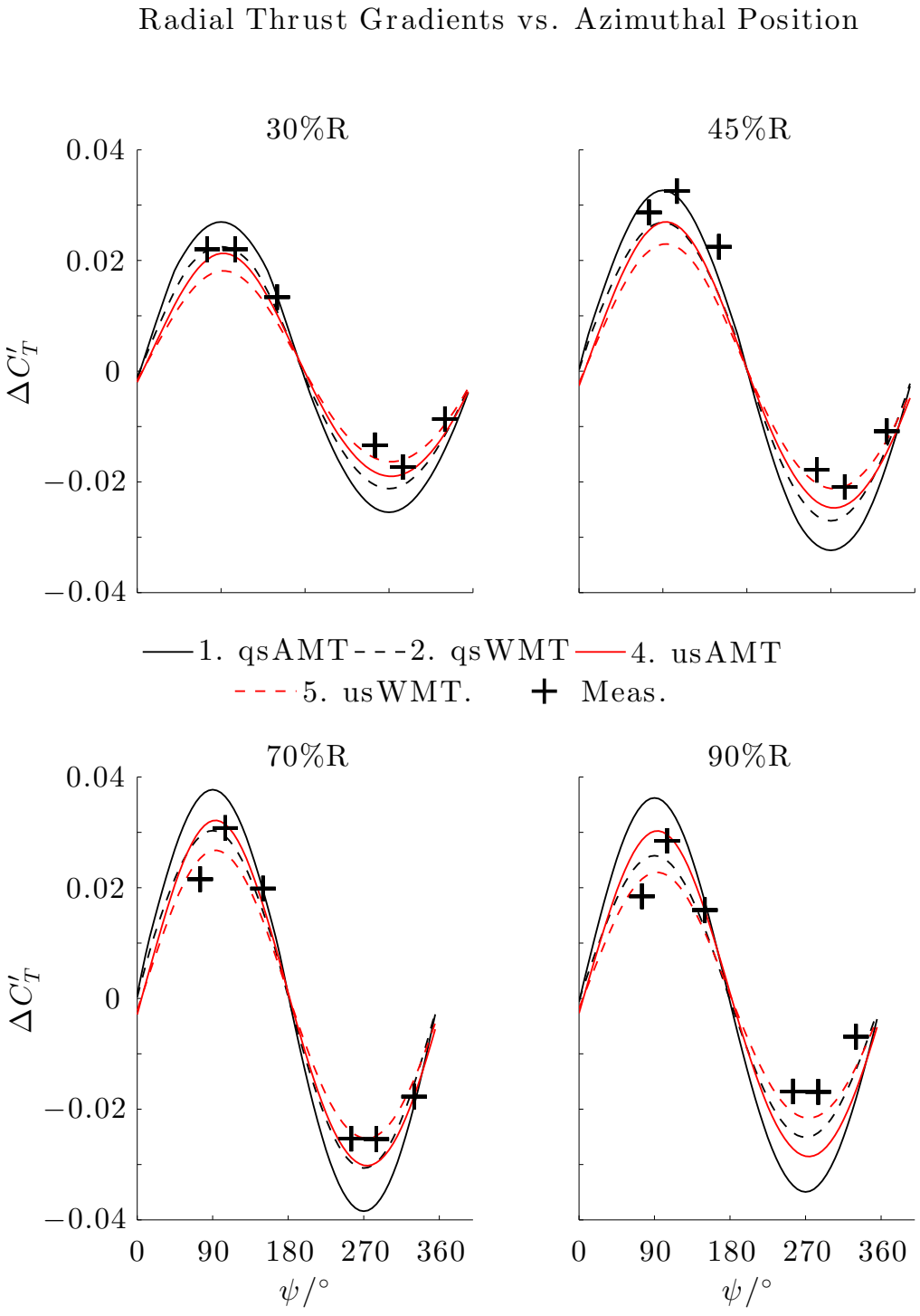

FIGURE 3.9: MODEL PREDICTIONS OF CHANGE IN RADIAL THRUST GRADIENT VS. DATA FROM GRAY ET. AL (1954). RPM = 1350, J = 1.25, $\gamma = 4.55°$.

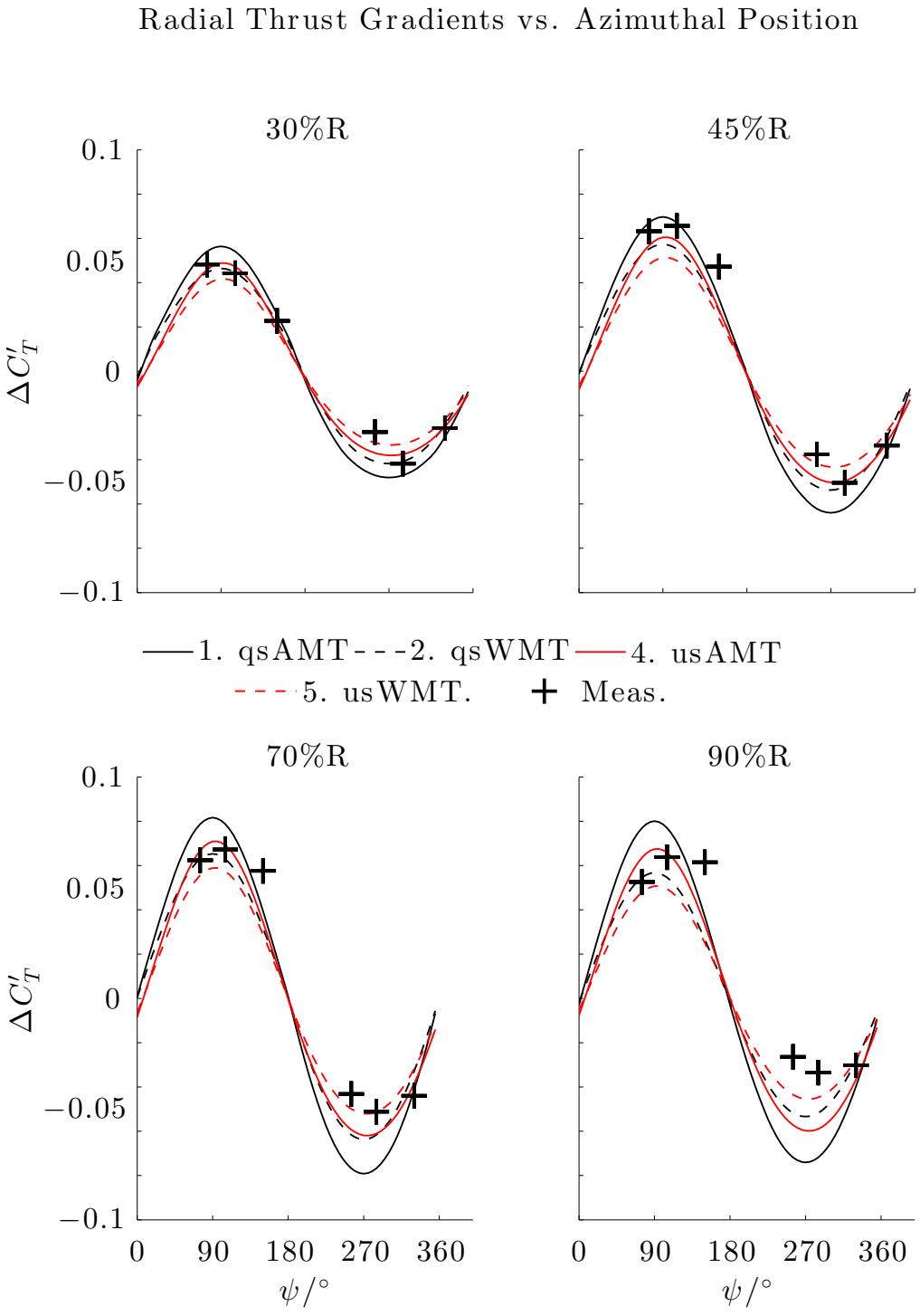

FIGURE 3.10: MODEL PREDICTIONS OF CHANGE IN RADIAL THRUST GRADIENT VS. DATA FROM GRAY ET. AL (1954). RPM = 1350, J = 1.25, $\gamma = 9.80°$.

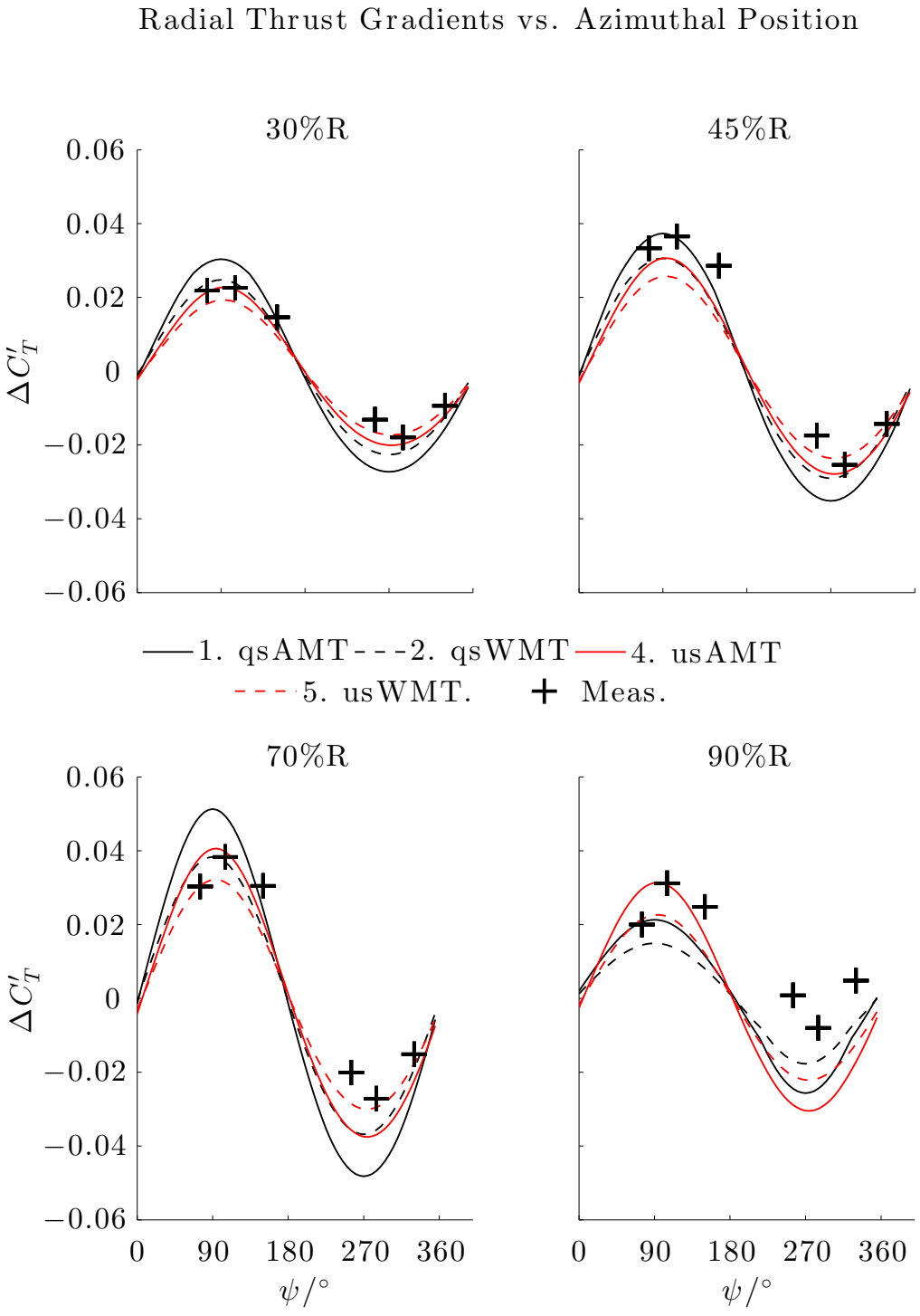

FIGURE 3.11: MODEL PREDICTIONS OF CHANGE IN RADIAL THRUST GRADIENT VS. DATA FROM GRAY ET. AL (1954). RPM = 2000, J = 1.25, $\gamma = 4.55°$.

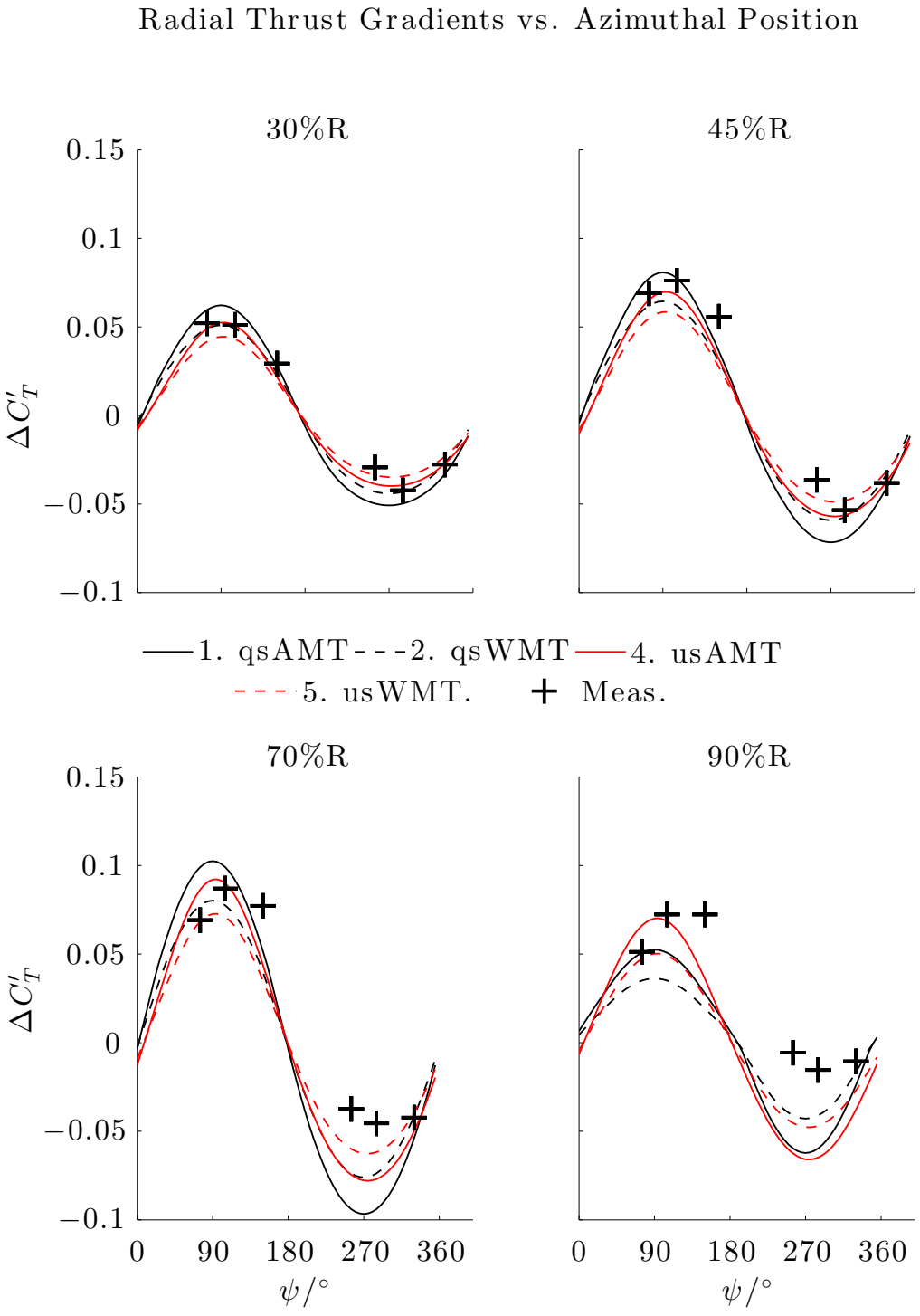

FIGURE 3.12: MODEL PREDICTIONS OF CHANGE IN RADIAL THRUST GRADIENT VS. DATA FROM GRAY ET. AL (1954). RPM = 2000, J = 1.25, $\gamma = 9.80°$.

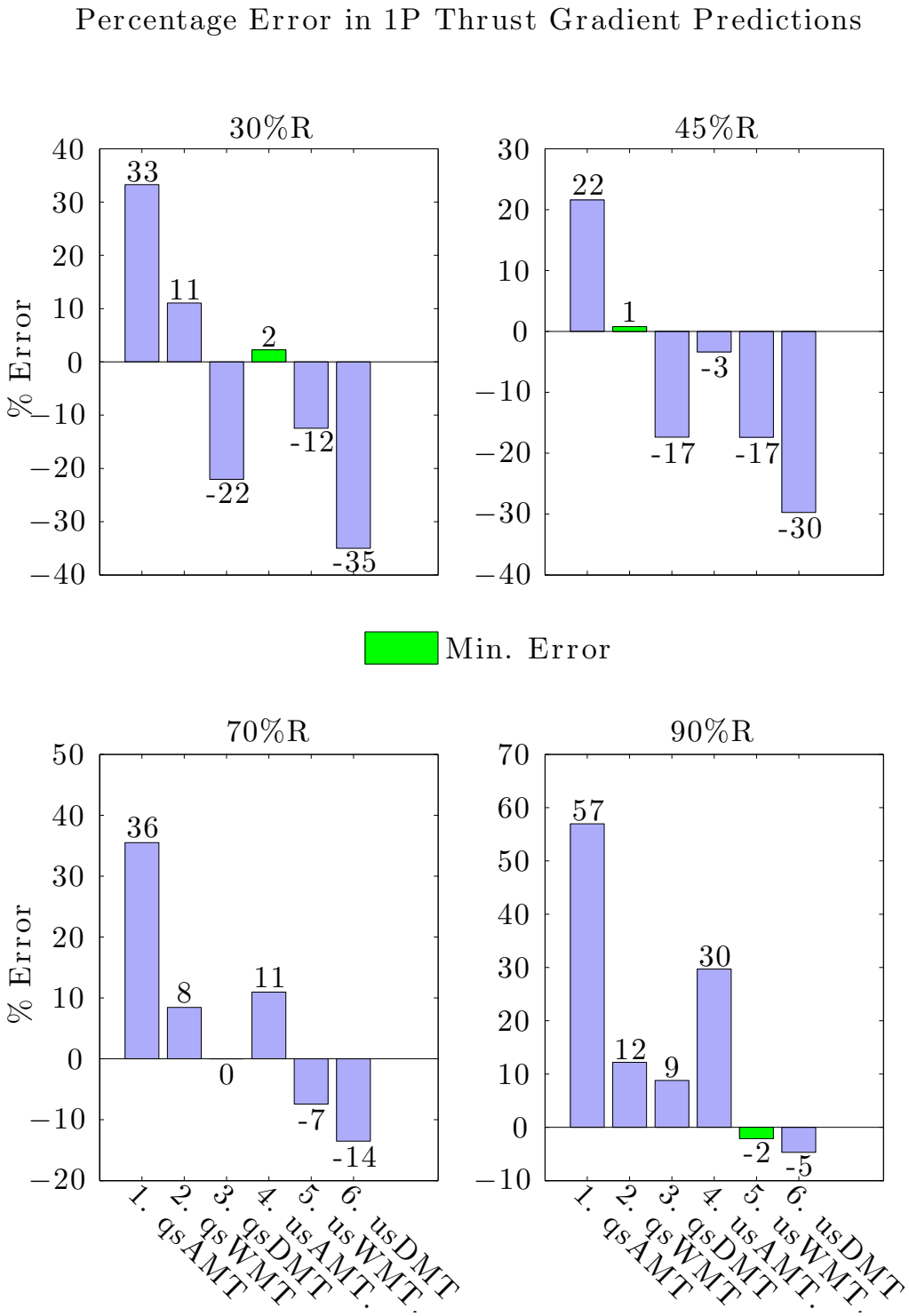

FIGURE 3.13: ERRORS IN MODEL PREDICTIONS OF 1P RADIAL THRUST GRADIENT CHANGE VS. DATA FROM GRAY ET. AL (1954). RPM = 1350, J = 1.25, $\gamma = 4.55°$.

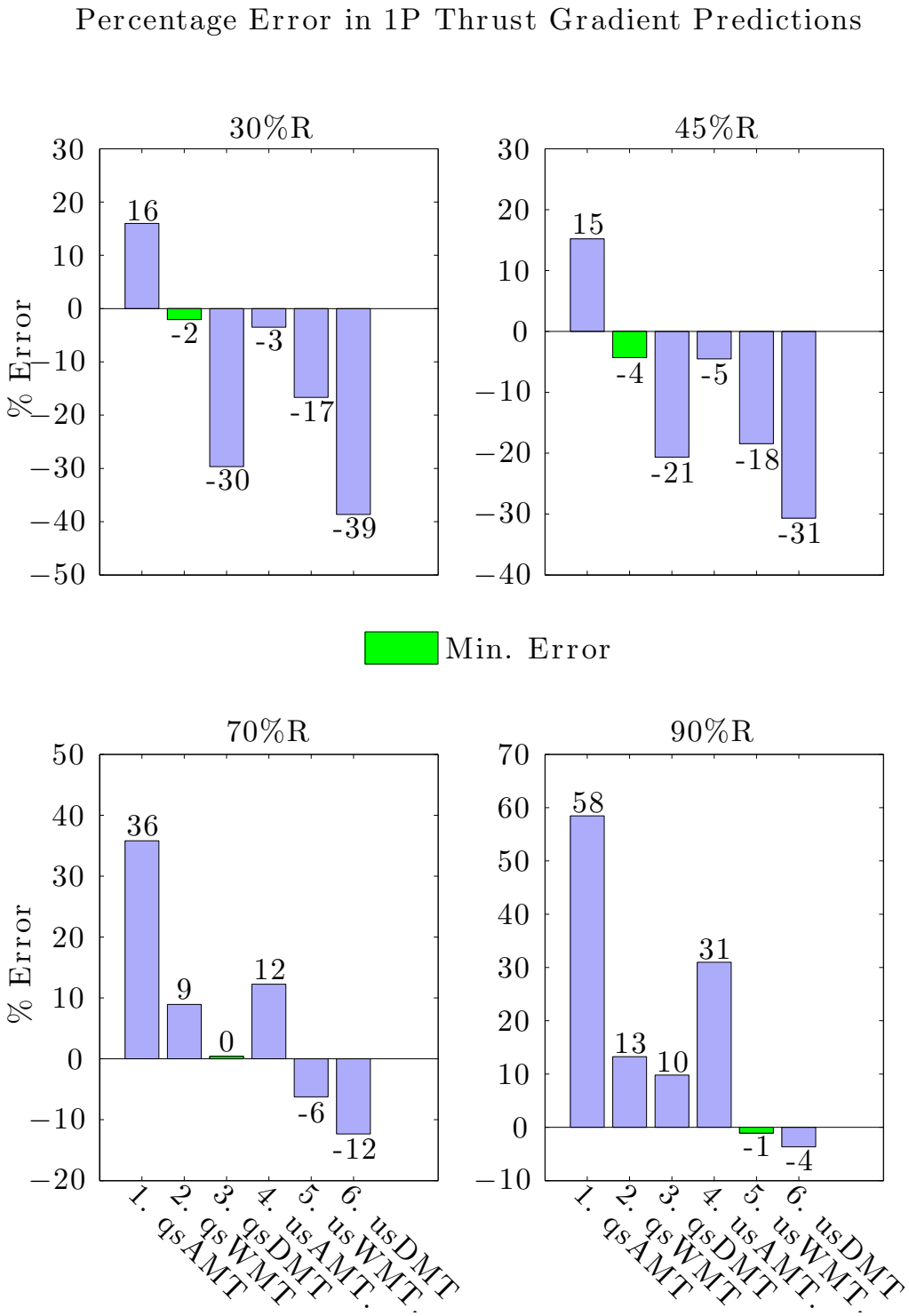

FIGURE 3.14: ERRORS IN MODEL PREDICTIONS OF 1P RADIAL THRUST GRADIENT CHANGE VS. DATA FROM GRAY ET. AL (1954). RPM = 1350, J = 1.25, $\gamma = 9.80°$.

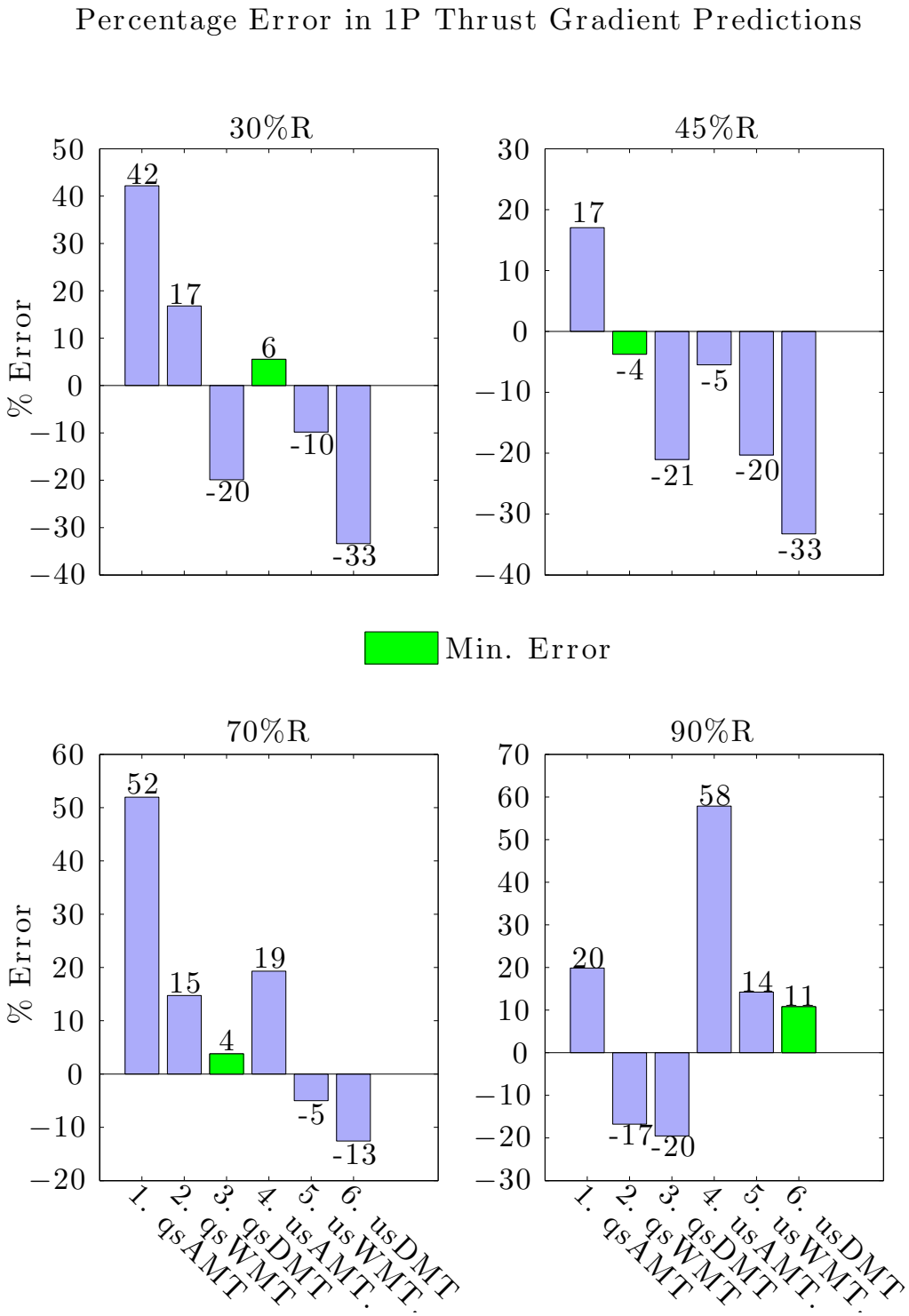

FIGURE 3.15: ERRORS IN MODEL PREDICTIONS OF 1P RADIAL THRUST GRADIENT CHANGE VS. DATA FROM GRAY ET. AL (1954). RPM = 2000, J = 1.25, $\gamma = 4.55°$.

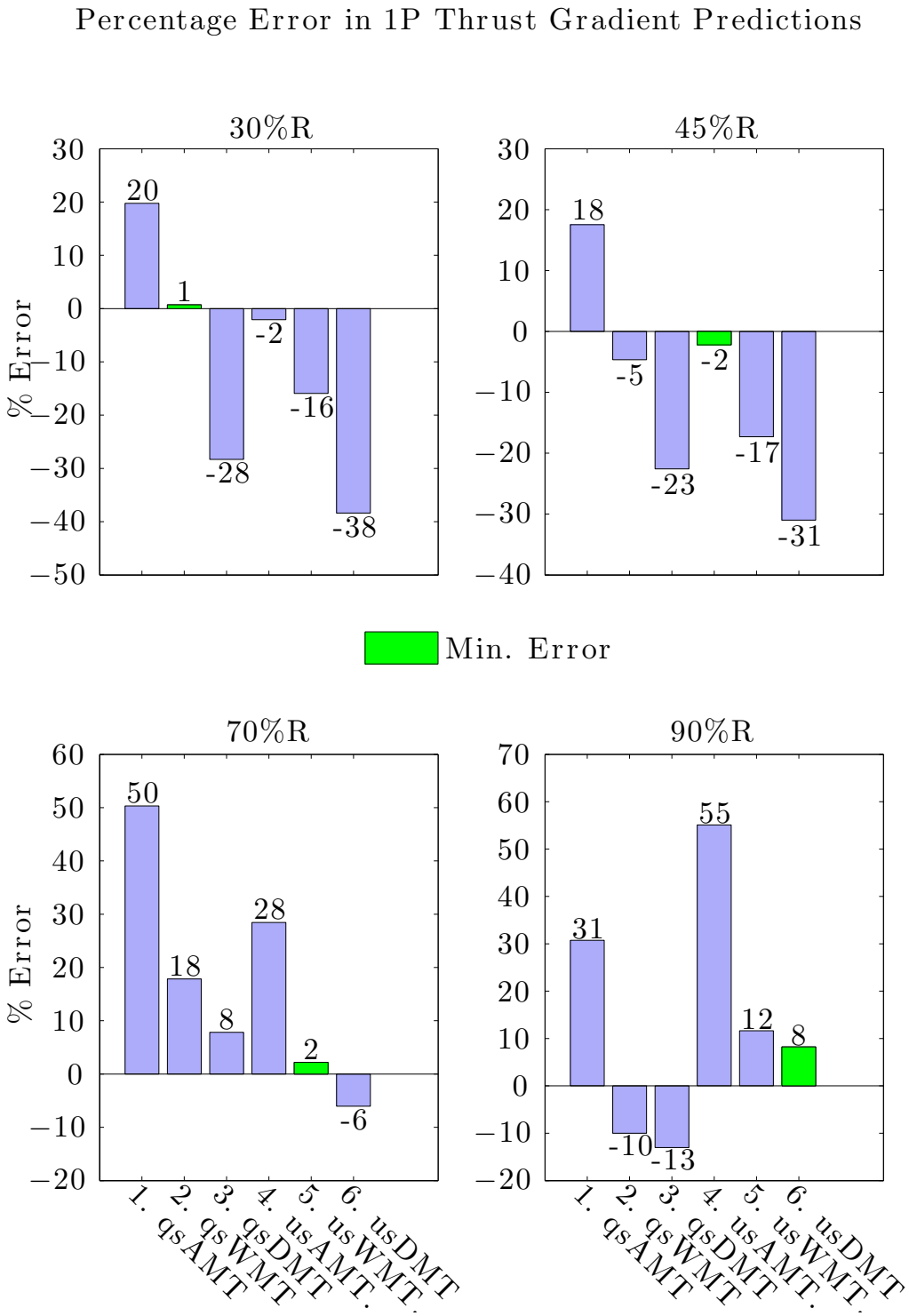

FIGURE 3.16: ERRORS IN MODEL PREDICTIONS OF 1P RADIAL THRUST GRADIENT CHANGE VS. DATA FROM GRAY ET. AL (1954). RPM = 2000, J = 1.25, $\gamma = 9.80°$.

QUASI-STEADY MODELS

Looking at the quasi-steady models first, qsAMT (Model 1) consistently over-predicts the load variation in every case, at every radial station. This confirms that the magnitude and distribution of the induced velocity over the disc is of importance for the 1P problem - as asserted in the previous chapter. It indicates that load difference is being attenuated from the AMT prediction - either through the distribution of steady induced velocity or through the unsteady induced velocity.

The respective errors in prediction of the 1P thrust gradient variation shows that qsWMT (Model 2) provides a better prediction of the peak-to-peak thrust gradient when compared with qsAMT (Model 1) at every radii. It does not always have the best overall prediction of the six models compared in the bar charts but it has the most *consistently low* error of all the models. It has a largest absolute error of 13% for the low speed and 17% for the high speed case. All other models have an absolute error of >20% for the low speed case, and > 32% for the high speed case for at least one radii. In the inboard sections, qsDMT (Model 3) underpredicts the load variation, whilst achieving good prediction in the 70% radius sections - this has been noted by Heene (2012), who showed results from the 60% radial station.

Even though prediction of the change to spanwise thrust gradient gives a good indication of how different models compare *radially*, the focus of this dissertation is on 1P bending load. Although the data in the original paper cannot be used to determine the maximum bending load on the blade, the axial forces may be integrated to give the *thrustwise bending load* - and since accurate prediction of the change to sectional lift and drag is required for both, accurate prediction of the thrustwise bending load should afford confidence in a model. To this end, the integrated load over the spanwise stations presented has been compared, defined for this experiment as:

$$\Delta C_{M,root} = \frac{1}{D} \int_{0.30R}^{0.95R} \frac{dC'_T}{dx} \cdot r \, dx \tag{3.39}$$

with the limits chosen to enable direct comparison to experimental measurements, and

$$\frac{dC_T}{dr} = \frac{dC_T}{dx} \cdot \frac{1}{R} \tag{3.40}$$

used to convert between dimensional and nondimensional radial gradients.

Figures 3.17 to 3.19 show predictions of integrated bending load vs. experimental measurements. qsWMT (Model 2) has consistently better performance than nearly all the other models. The error in prediction of integrated bending load for all seven cases are tabulated in Table 3.4 on the next page, and show that for each of the seven cases the largest error with this model is only $\sim 7\%$, and the model mean error is only $\sim 4\%$. Using the steady-state propeller method,

or qsDMT (Model 3), the root bending load is consistently underpredicted by a mean error of $\sim -7\%$. Over the range of cases compared with the data from Gray et al. (1954), **steady weighted momentum theory has the smallest error** when compared with the other two momentum models compared. Though in two cases the qsDMT (Model 2) model has the lowest absolute error, in all cases **differential momentum theory, and by extension, steady-state propeller theory underpredicts the load variation**. The analysis in this section includes the flow around the axisymmetric spinner/nacelle at incidence.

UNSTEADY MODELS

The Loewy unsteady model has a tendency to attenuate the lift difference, and hence the thrust difference for all radial stations and both inclination angles at the lower rotational speed. Though the phasing of the peak load seems to be improved *slightly*, this is higher order in terms of blade stressing purposes, and the peak load variation is predicted poorly with increasing radial position with all three momentum models when coupled with the Loewy model. At the higher rotational speed the lift difference is increased at outboard sections, likely due to the larger predicted impulsive lift.

Referring to Table 3.4, the usAMT model offers improvements in prediction from the qsAMT model, but still consistently overpredicts the load variation with an average of $\sim 14\%$ error in mean load prediction. With usDMT, the load is underpredicted by the greatest amount of all six models. usWMT lies somewhere between the two, but consistently underpredicts the load variation.

Interestingly, the unsteady models are more physically representative of the

	Percentage Error					
	Quasi-Steady Aero			**Unsteady Aero**		
Case	1. qsAMT	2. qsWMT	3. qsDMT	4. usAMT	5. usWMT	6. usDMT
1	35†	6	$-4\star$	10	-10	-17
2	35†	6	$-4\star$	12	-9	-16
3	33†	$2\star$	-8	7	-14	-21
4	29†	$0\star$	-10	6	-15	-22
5	39†	6	-6	21	$-5\star$	-13
6	38†	7	-4	25	$-1\star$	-10
7	29†	$-1\star$	-13	19	-6	-15
Mean	**34**	**4** $\star$	**-7**	**14**	**-9**	-16
Key:	Largest Error - XX†			Smallest Error - XX $\star$		

TABLE 3.4: PERCENTAGE ERROR IN ROOT THRUSTWISE BENDING AERODYNAMIC LOAD PREDICTION OF THE SIX DIFFERENT MODELS VS EXPERIMENTAL DATA (GRAY ET AL., 1954)

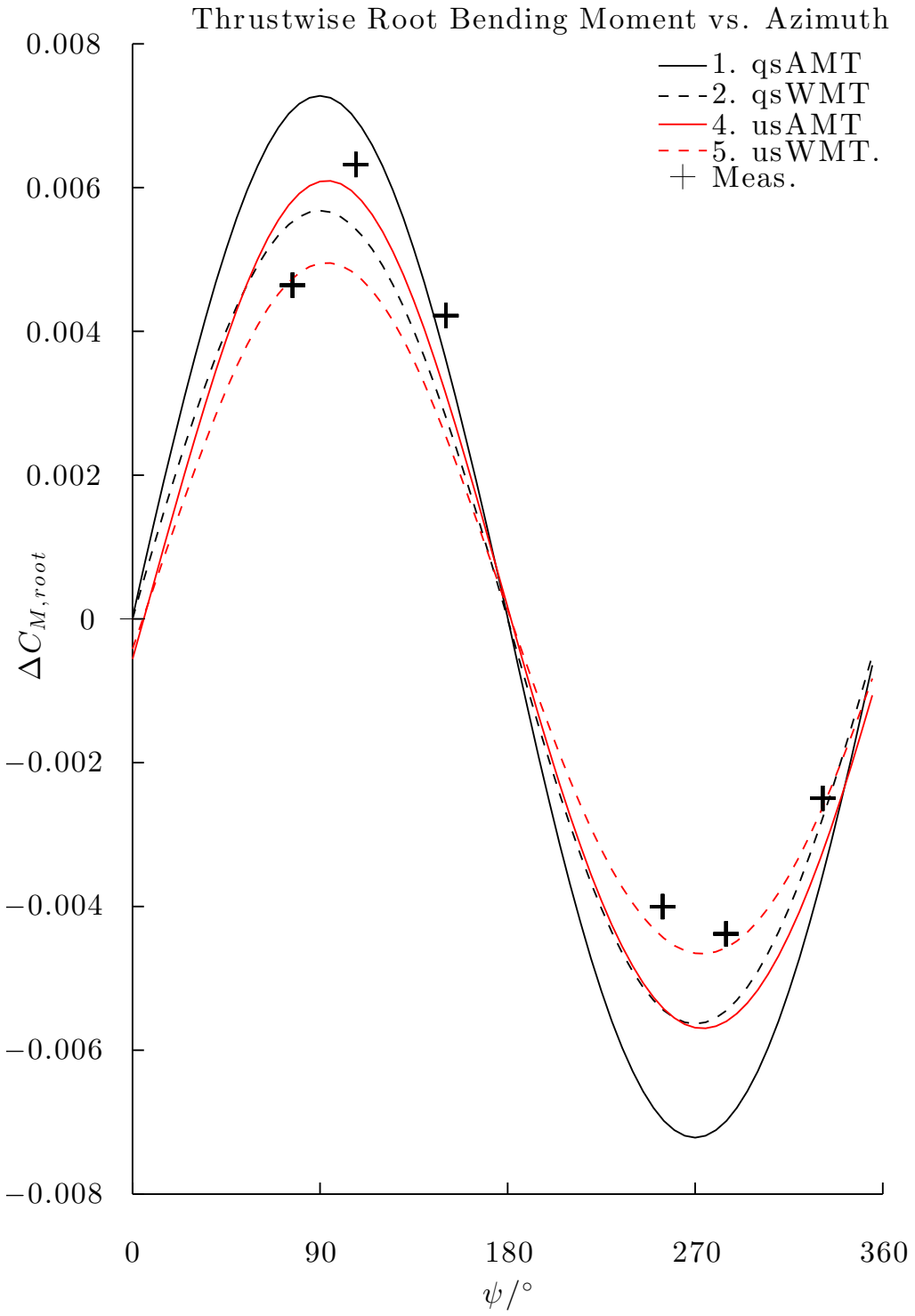

FIGURE 3.17: MODEL PREDICTION OF CHANGE IN AERODYNAMIC ROOT BENDING MOMENT DUE TO THRUST VS. AZIMUTHAL POSITION COMPARED TO DATA FROM GRAY ET. AL (1954). RPM = 1350, J = 1.25, $\gamma = 4.55°$.

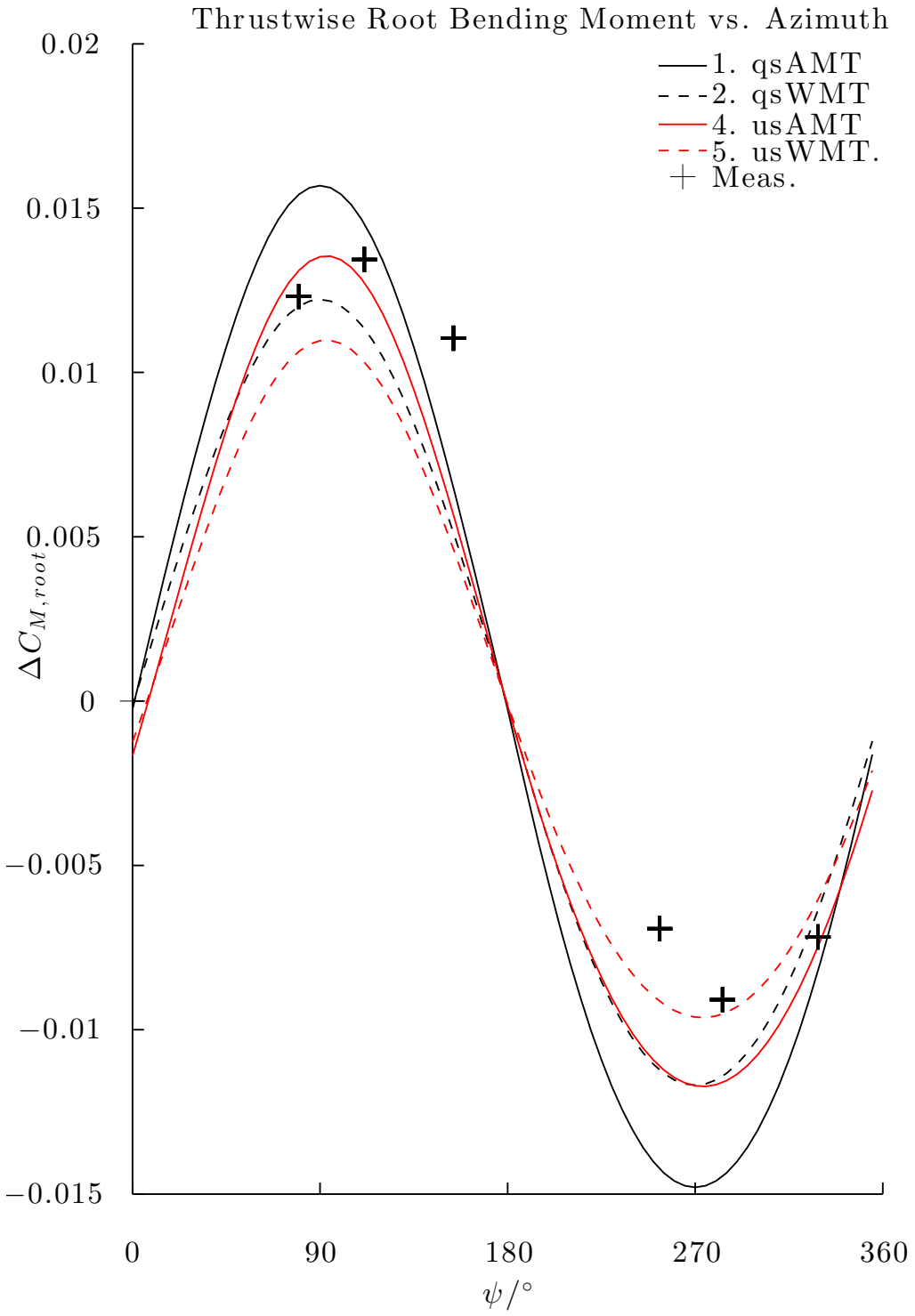

FIGURE 3.18: MODEL PREDICTION OF CHANGE IN AERODYNAMIC ROOT BENDING MOMENT DUE TO THRUST VS. AZIMUTHAL POSITION COMPARED TO DATA FROM GRAY ET. AL (1954). RPM = 1350, J = 1.25, $\gamma = 9.80^\circ$.

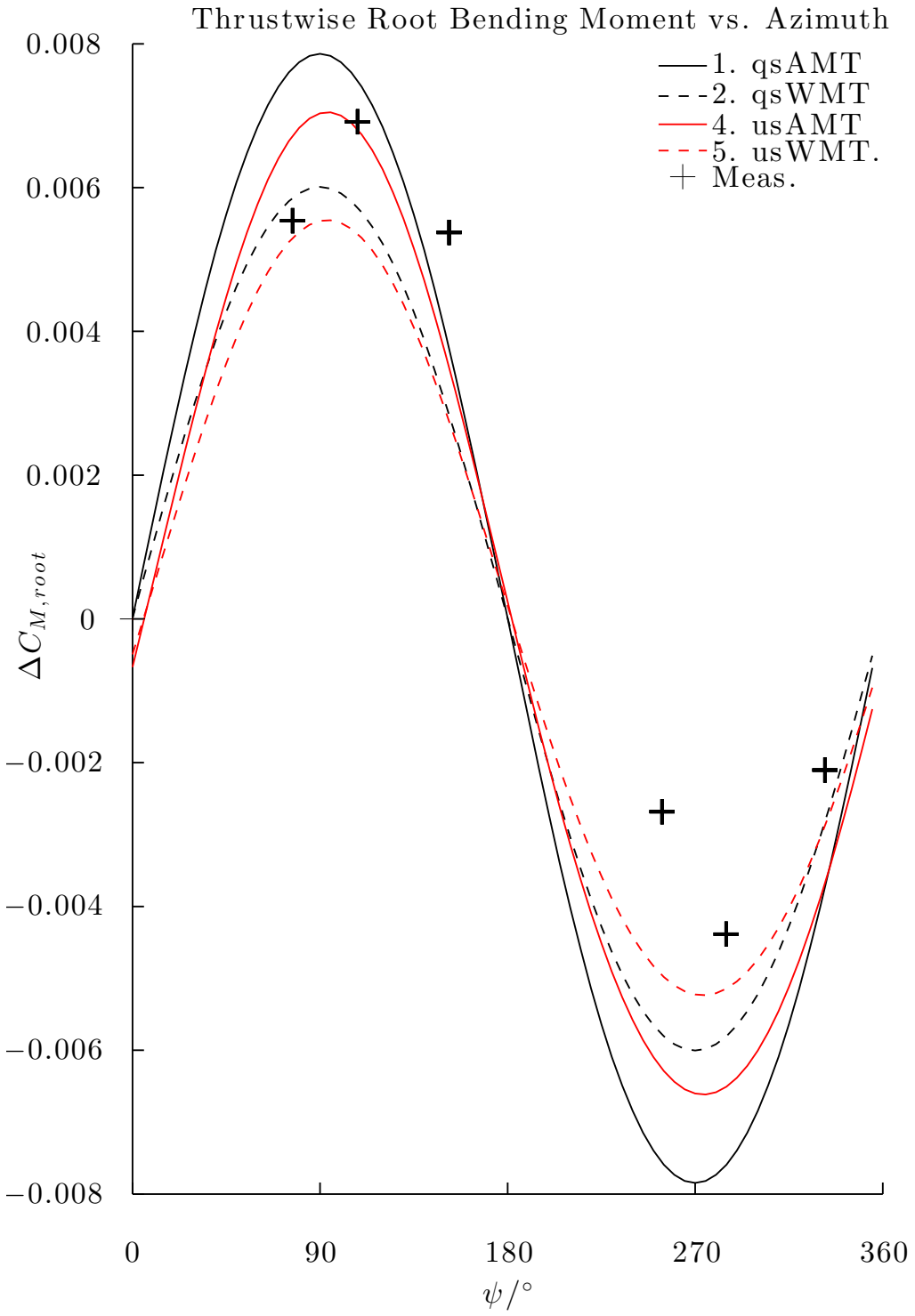

FIGURE 3.19: MODEL PREDICTION OF CHANGE IN AERODYNAMIC ROOT BENDING MOMENT DUE TO THRUST VS. AZIMUTHAL POSITION COMPARED TO DATA FROM GRAY ET. AL (1954). RPM = 2000, J = 1.25, $\gamma = 4.55°$.

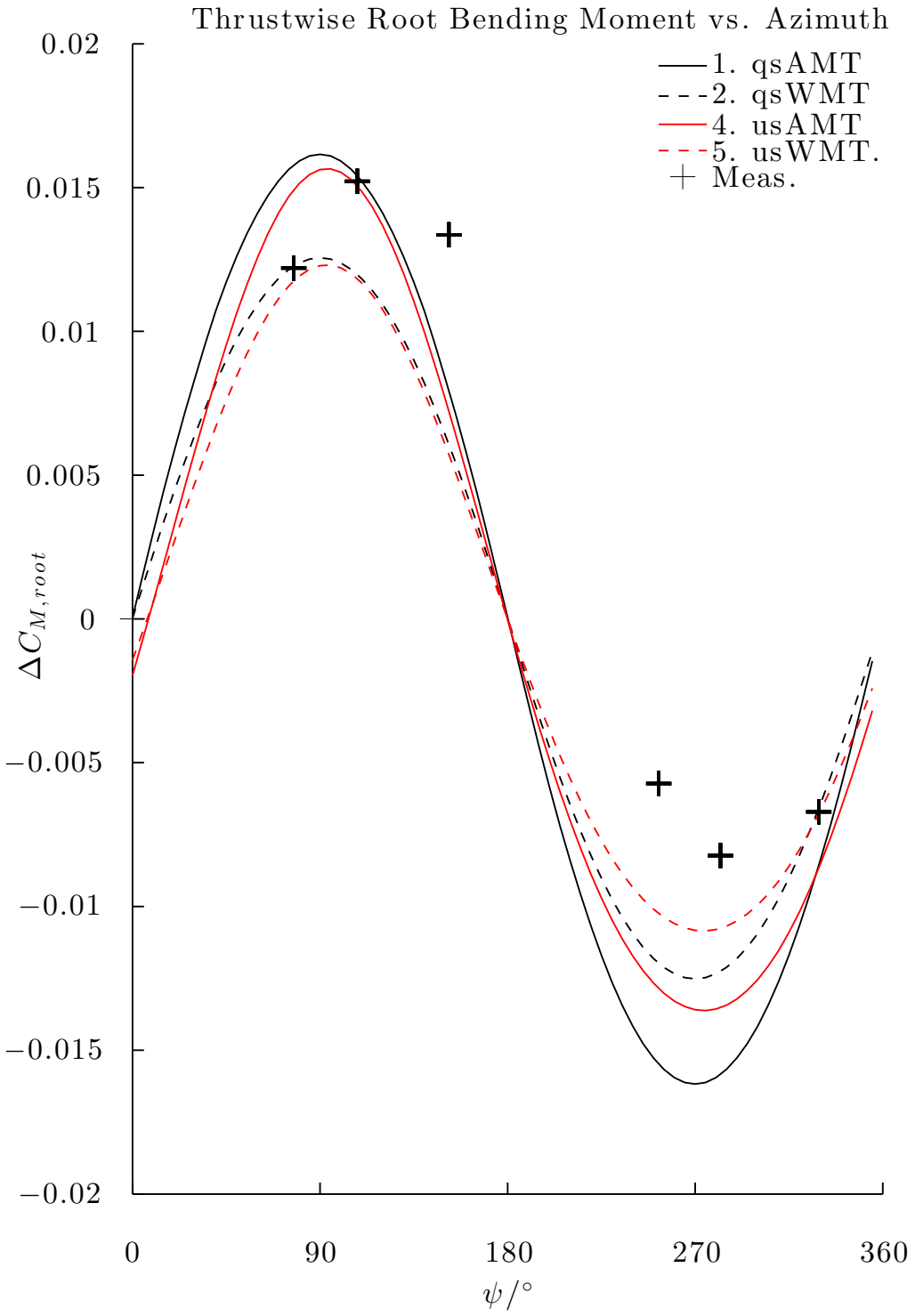

FIGURE 3.20: MODEL PREDICTION OF CHANGE IN AERODYNAMIC ROOT BENDING MOMENT DUE TO THRUST VS. AZIMUTHAL POSITION COMPARED TO DATA FROM GRAY ET. AL (1954). RPM = 2000, J = 1.25, $\gamma = 9.80°$.

blade element flowfield than the quasi-steady models, as looking at the problem from first principles, there is certainly a degree of unsteadiness in the flow, and this degree is highlighted by the reduced frequency as being significant. It should follow that the unsteady models perform better, but they do not consistently - a reason for this is suggested below.

The extra load attenuation due to unsteadiness that is predicted by the Loewy model may be captured, to some extent, by the WMT and DMT models. That is, the steady induced velocity may be closer to the AMT prediction[10], but the build up of unsteady induced velocity due to a time-varying shed wake means that the total induced velocity is closer to the WMT/DMT predictions. Without a detailed survey of the flowfield over a range of operating conditions, it is very difficult to separate these two effects (and they will always be mutually present on a propeller at an angle of incidence). From the results in this experiment, however, it is clear that the **quasi-steady weighted momentum theory performs consistently better than the two other steady momentum models, and also better than all three of the unsteady models**. Additionally, the mean error in prediction with qsWMT is not only low, but also positive - meaning that this methodology provides a close, but *conservative* estimate of load variation - which is important for an engineering-level code.

MODEL TRENDS:

Looking at the contours in Figure 3.21, a demonstration of the wider prediction of the models is given. Contours are plotted at lines of constant increments of 500Nm thrustwise root bending load, over the range of $0 \leq \gamma \leq 15^{\circ}$ and $1300\text{RPM} \leq \Omega \leq 2300\text{RPM}$. The seven known operating conditions are overlaid as discrete points, with each model's respective error in prediction of 1P change to thrustwise bending load listed next to each point, with the best/worst errors for each case highlighted with green/red rings. It should be noted that the discrete data points do not tally with the contours, but are provided to show the sparsity of data within the range tested, and where differences in respective errors lie in the range of rotational speed and inclination angle.

Notably, the contours are closely packed into the lower left-hand corner of the qsAMT plot, indicating that the **qsAMT model predicts that the root bending load will be larger for all rotational speeds and inclination angles compared to all other models** (and to measurements). A spread of the contour lines towards the top or the right of the plot indicates that a model predicts a smaller increase of blade root bending load with increasing Ω or γ, respectively, and vice versa towards the bottom/left.

What the contours highlight well is how sparse this set of data is - ideally, a

[10] Imagining that these two effects were somehow possible to decouple.

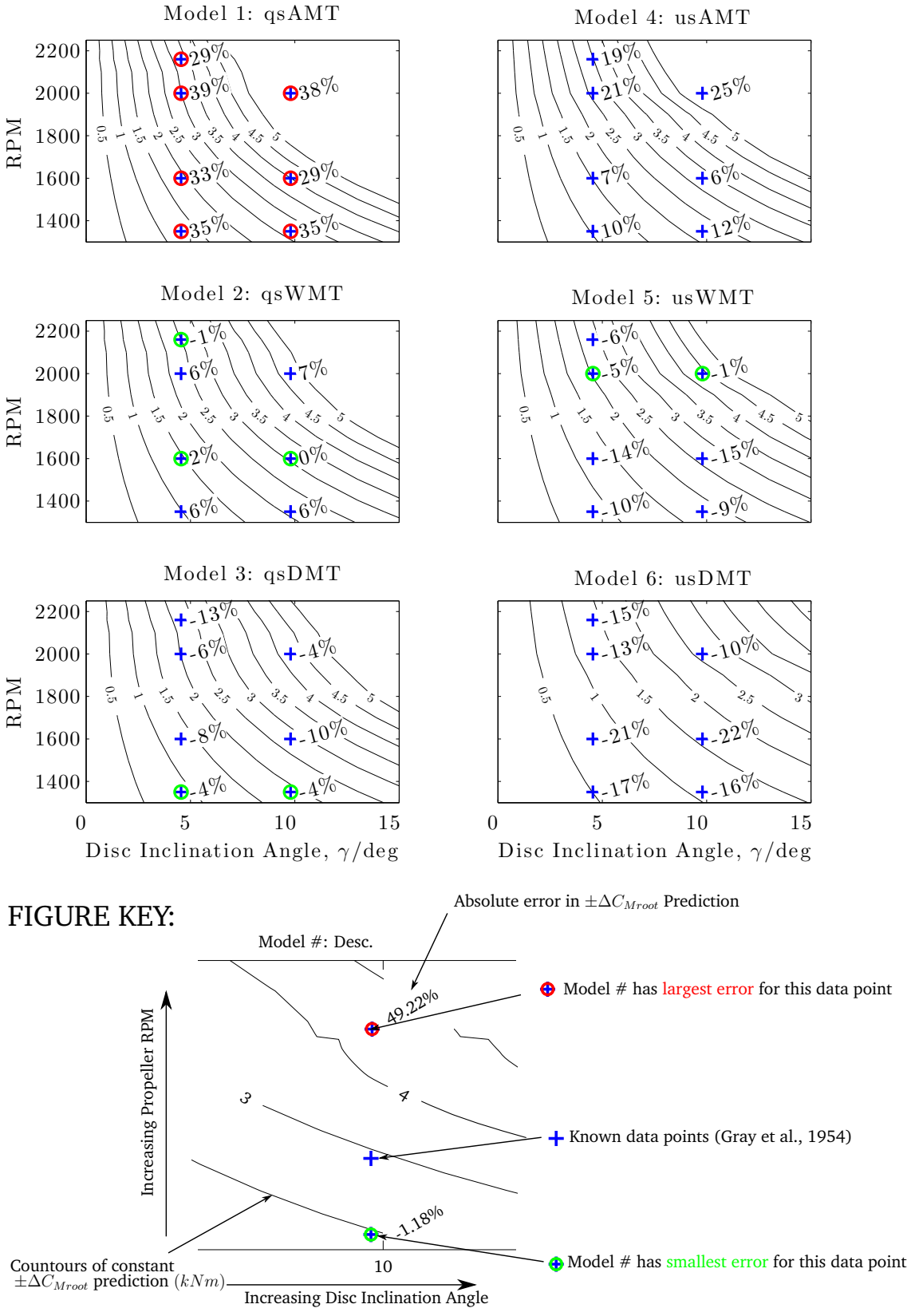

FIGURE 3.21: CONTOURS OF CONSTANT ROOT BENDING LOAD VS. DISC INCLINATION ANGLE AND RPM. DATA FROM GRAY ET AL. (1954) COMPARED WITH SIX MODELS. ALL CONTOURS AND DATA POINTS IN KNM.

set of experiments would be performed that firstly enable more data points to be filled - a greater number of inclination angles. Additionally, all the tests by Gray et al. were performed at roughly the same advance ratio, so although the in-plane component of advance ratio changes with inclination angle, the variation with actual advance ratio is not given by these tests.

Finally, these figures help to highlight the model performance with increasing rotational speed. Interestingly, the greatest compressibility effects on these data occur around 2000RPM - this may be observed as a slightly noticeable 'kink' in the contours. This comes from a discontinuity in the databank used for this dissertation, as the NACA-16 databank relies on interpolation of two-dimensional data, and a separate subsonic/transonic databank set[11]. Confidence may be afforded in the qsWMT model, however, as although its greatest error may be found in this region, it still performs reliably. The usWMT model appears to predict the $\sim$2000RPM load slightly better in terms of absolute error, but it still underpredicts the load compared to the conservative error of the qsWMT result.

It is hard to directly compare models on these contours, but it can be seen relatively clearly that qsWMT and usAMT have relatively similar behaviour at low rotational speeds - that is, the axis intercepts and spreads of the contour lines are relatively similar. With increasing rotational speed, however, the two models' performance start to diverge and the magnitude of the errors show that **quasi-steady weighted momentum theory provides the most consistent performance over the range of rotational speeds and inclination angles when compared to data from Gray et al. (1954)**.

The results presented in this section include the effect of flow around the spinner in the model.

3.7.2 RUSSELL

Since the data from Gray et al. (1954) is only for one advance ratio, but covered a range of rotational speeds and two inclination angles, the data presented by Russell (1952) was chosen to look at the variation of load prediction with advance ratio. A set of data has been chosen at a constant blade setting angle and a disc inclination of $\gamma = 10°$, with a range of advance ratios. The rotational speed changes across the set of data from 650RPM$< \Omega <$875RPM, but the change in model prediction over this 225RPM range was small compared to the variation between models, so only calculations with Ω=650RPM are shown.

The plots from the original paper have been digitised as accurately as possible for presentation in this dissertation. The curves of $dC'_T(x)$ have been integrated

[11]It should be noted that the databank used for this dissertation comes from 2D lift/drag data provided by DP, (Trchalik, 2011). This is not the same databank as presented by Korkan and Camba III (1986), as no freely-available digital version was found at the time of writing.

to give the thrustwise bending load as presented in the previous set of data. This should reduce any potential errors from the digitising process.

The variation of the peak-to-peak blade thrustwise bending load is shown with a range of normal advance ratios $0.4 \leq \hat{J} \leq 0.9$ in Figure 3.22. Over the six data points shown, qsWMT consistently performs better than any of the other models.

The usAMT model follows the qsWMT closely for the lower advance ratios - giving weight to the supposition in the previous section that the WMT/DMT distributions capture some of the unsteady induced velocity variation due to the imposed periodicity of the steady wake emulating the periodicity of the unsteady wake. The unsteady models start to diverge at higher advance ratios. The calculations have been repeated using a constant linear $a = 2\pi/\text{rad}$, to determine if the breakdown were due to a numerical error in determining $\frac{dC_l}{d\alpha}$, since due to the model formulation calculation of lift curve slope requires databank interpolation that is not utilised in the steady models, as these only need lift/drag for a given α_R, M_R. However, the results using $a = 2\pi/\text{rad}$ showed the same divergence with increasing advance ratio - the comparison of using $\frac{dC_l}{d\alpha}$ from dynamic table lookup versus using $\frac{dC_l}{d\alpha} = 2\pi$ is compared in Figure 3.23.

The formulation of the unsteady lift utilised in the unsteady models (Models 4-6) takes into account the angle of attack variation, but does not take into account the change in incident velocity *magnitude*, which will become larger with increasing advance ratio. The change to lift due to unsteadiness is effected as a change to *lift coefficient*, and the varying dynamic pressure is accounted for when the forces are dimensionalised. What is not included is the effect of the varying incident velocity on the rate at which the wake is convected. For an advancing helicopter the in-plane velocity will generally be much smaller than the tangential velocity due to blade rotation, and hence the variation of resultant velocity may be quite small as a percentage of the mean resultant velocity. For a propeller at an angle of incidence, however, this is not the case - accordingly, the at larger advance angles, the variation of this convection speed may account for some of the discrepancies with Loewy's model.

Formulations of Theodorsen's theory have been developed that include the time-varying incident velocity (*e.g.,* Greenberg, 1947), but it has been shown by Van der Wall and Leishman (1994) that the theories are more suited for the lead-lag motion of a helicopter rotor, and not that of a time-varying horizontal velocity. To include the effect of the magnitude of the time-varying velocity on the unsteady lift response requires solution of the Duhamel integral, which requires numerical methods (*e.g.,* finite-difference approximations), that preclude usage in this thesis due to complexity.

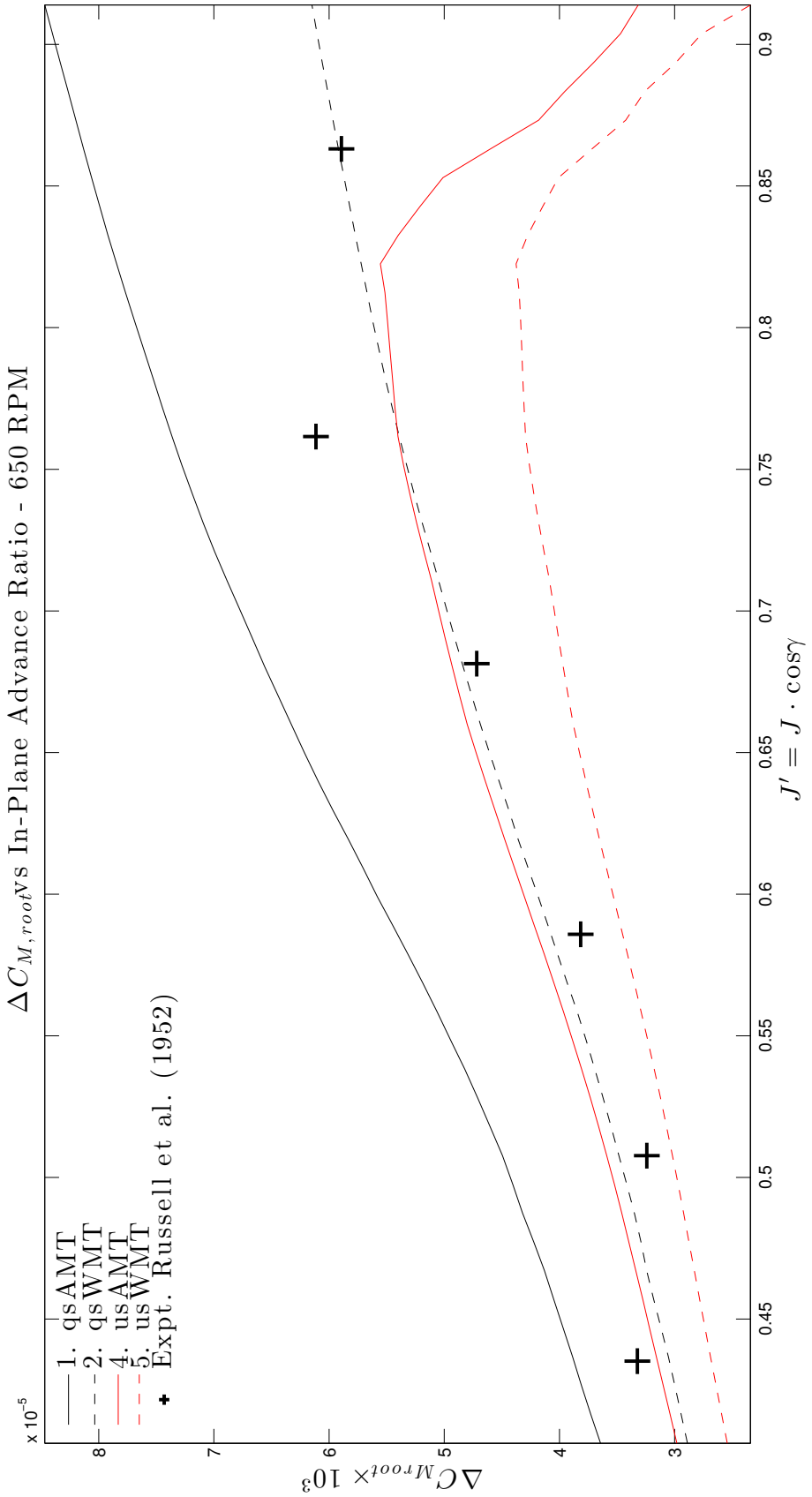

FIGURE 3.22: MODEL PREDICTION OF $\Delta C_{m,root}$ VS. DATA FROM RUSSELL (1952), $\gamma = 10°$.

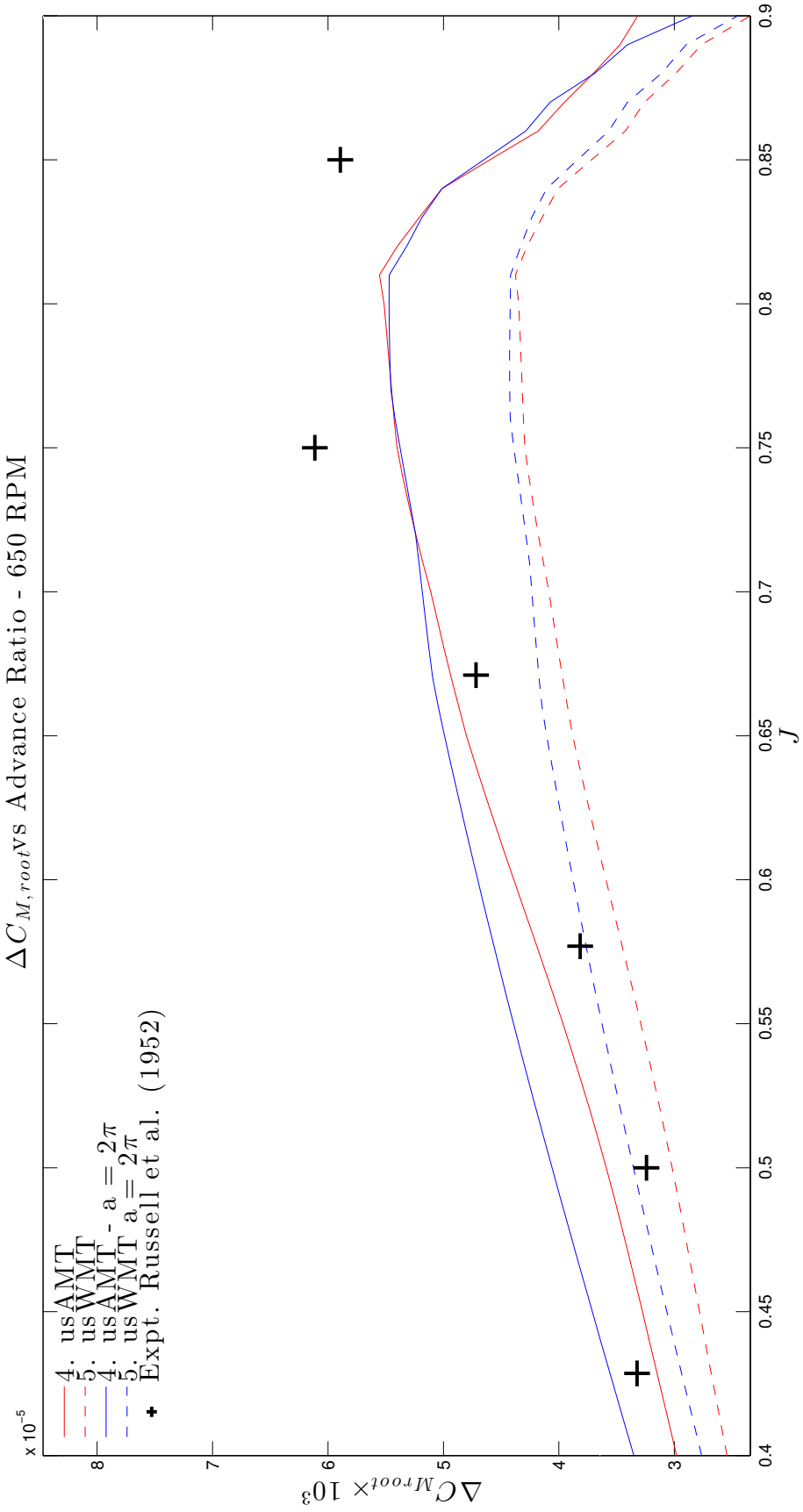

FIGURE 3.23: MODEL PREDICTION OF $\Delta C_{m,root}$ VS. DATA FROM RUSSELL (1952), $\gamma = 10°$. US MODELS COMPARED - STATIC LIFT CURVE SLOPE WITH DYNAMIC TABLE LOOKUP.

3.7.3 PENDLEY

Data are available from an earlier set of wake measurements taken from a propeller at an angle of incidence. However, the data are of such poor quality that few conclusions can be taken from them - suffice to say that all models in this chapter were compared with the data,with qsWMT tending to show a better fit to the experimental result, though the reliability of the data affords little analysis to be made. Consequently, these results are not shown in this dissertation.

3.7.4 YAGGY AND ROGALLO

The data presented in Figures 3.24 to 3.27 shows the predictions of the total yawing moment reacted at the propeller hub, at inclination angles of $\gamma = 15, 30$ and 45° from left to right in each figure, and for increasing blade setting angles (and hence disc loading) of $\beta_{.7R} = 25, 30, 35$ and 40° in successive figures. The yawing moment may be determined by considering the thrust contribution from different blades and Eq. 2.20. It is proportional to the root bending moment and its variation on a single blade, but unlike the measurements taken from wake survey, the measurement of yawing moment by Yaggy and Rogallo was performed by a calibrated balance. Although the authors took care to remove the body loads from the experiment via fairing and taring, this may not wholly decouple blade and body forces. Predictions of yawing moment coefficient are shown against the normal advance ratio, $J \cdot \cos\gamma$, covering a larger range of advance ratios than the results from the experiments based on wake survey measurements.

For each, the results from Yaggy and Rogallo are shown as a filled area including their published uncertainty due to their experimental setup. Once again, their results have been included in these plots by digitising the faired curves shown in their original publication, so the scale of the Y-axis has been kept small to avoid digitisation discontinuities showing in the results. Based on the poorer performance against the wake survey data, no unsteady models are compared with these tests. The models that are compared are qsAMT (Model 1) and qsWMT (Model 2). Also included are predictions from ESDU 89047 (Chappell, 1989) - as an indication of the 'industry standard' for these calculations. As has been mentioned earlier in this dissertation, the methodology of ESDU 89047 is based on that of de Young (1965).

Key to understanding these figures is to look at the trends of each model with both inclination angle and advance ratio. Good prediction of the gradient of $\frac{dC_M}{d\gamma}$ over a range of inclination angles shows that a model has good agreement with physical data. That is, it is imprtant to see how a model matches both the absolute Y-value but also the slope of the curves.

In all figures, qsAMT (Model 1) overpredicts the variation of the yawing mo-

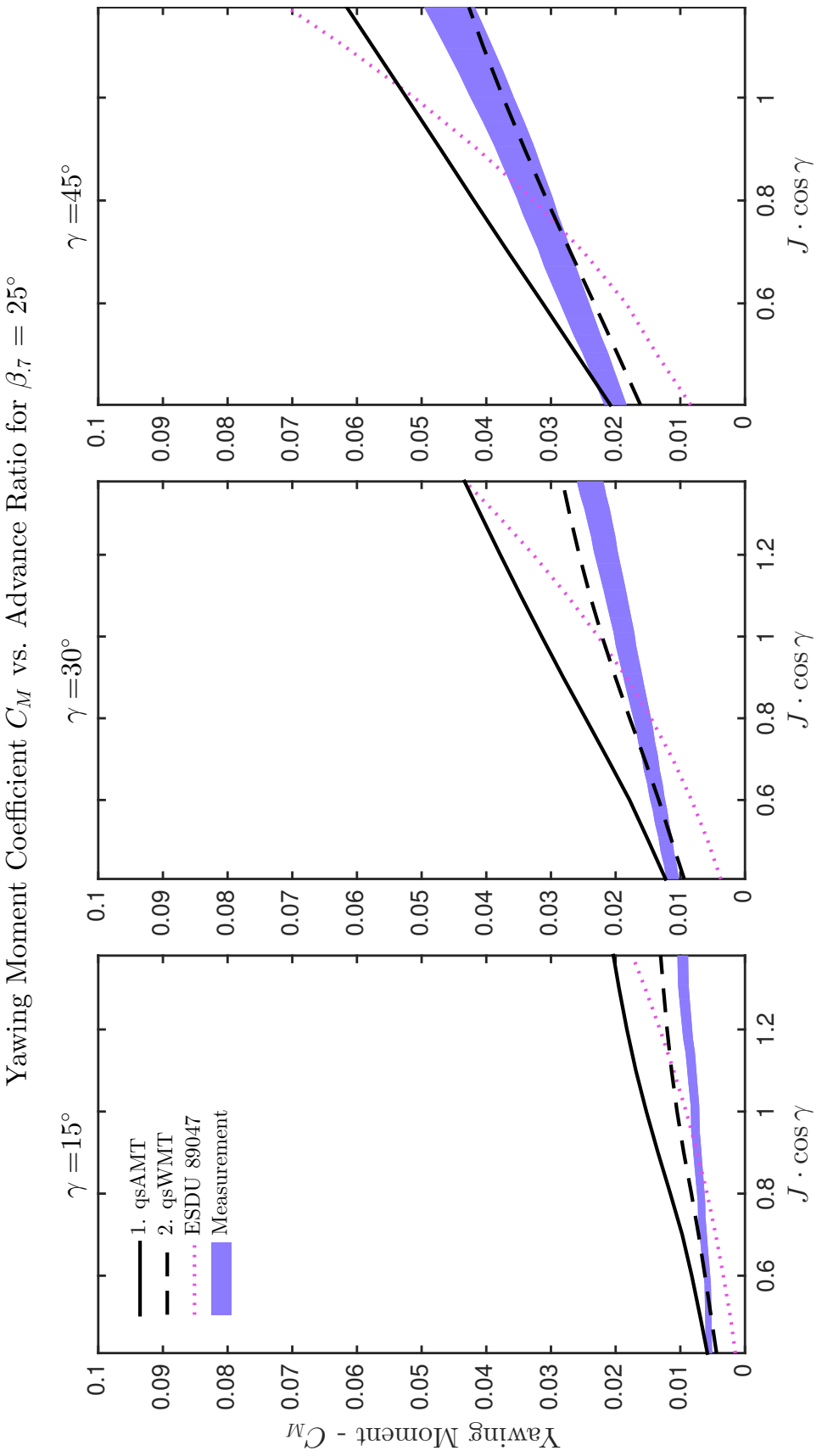

FIGURE 3.24: YAWING MOMENT COEFFICIENT VS. IN-PLANE ADVANCE RATIO FOR DIFFERENT γ. DATA FROM (YAGGY AND ROGALLO, 1960). $\beta_{.7} = 25°$.

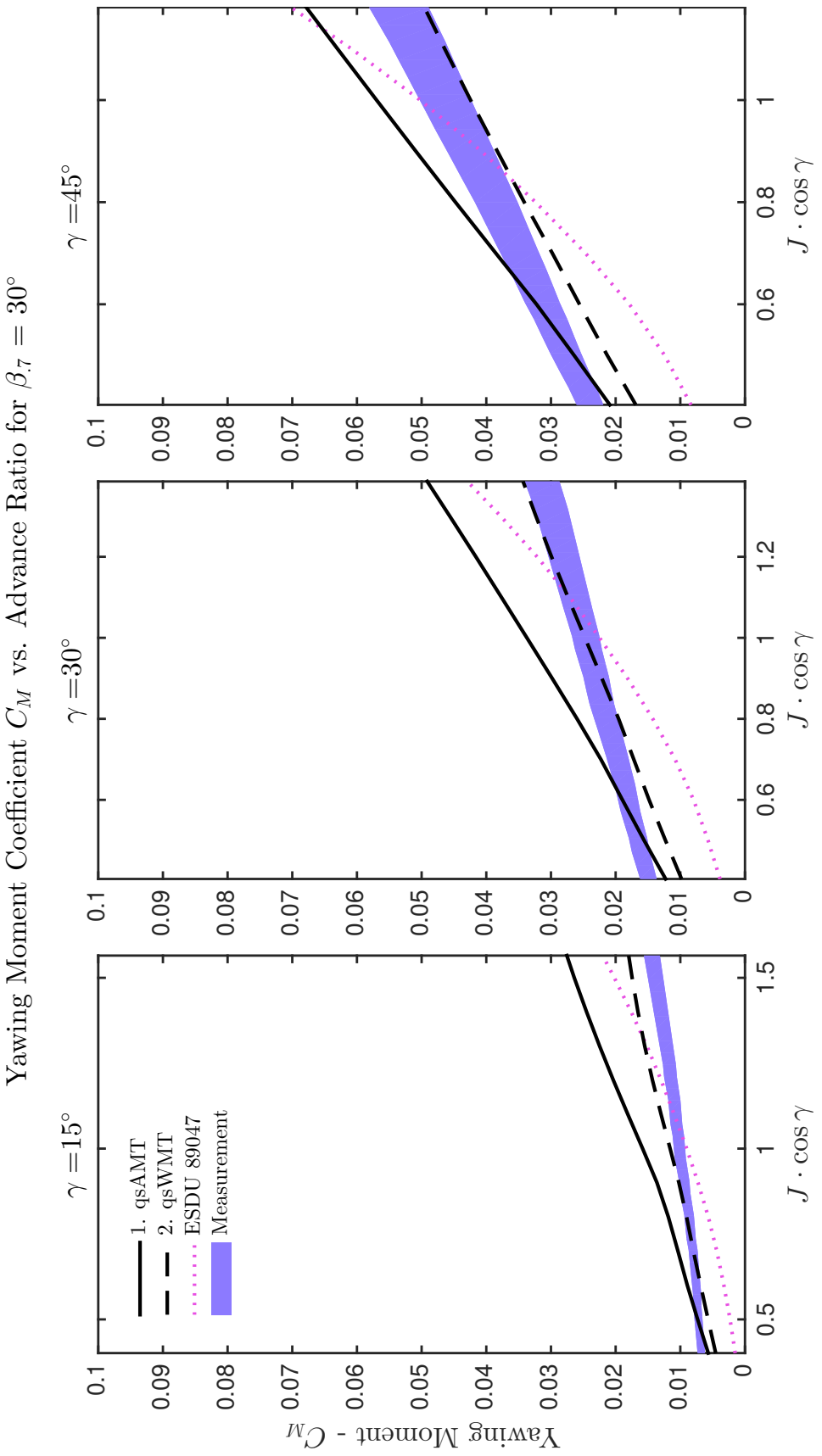

FIGURE 3.25: YAWING MOMENT COEFFICIENT VS. IN-PLANE ADVANCE RATIO FOR DIFFERENT γ. DATA FROM (YAGGY AND ROGALLO, 1960). $\beta_7 = 30°$.

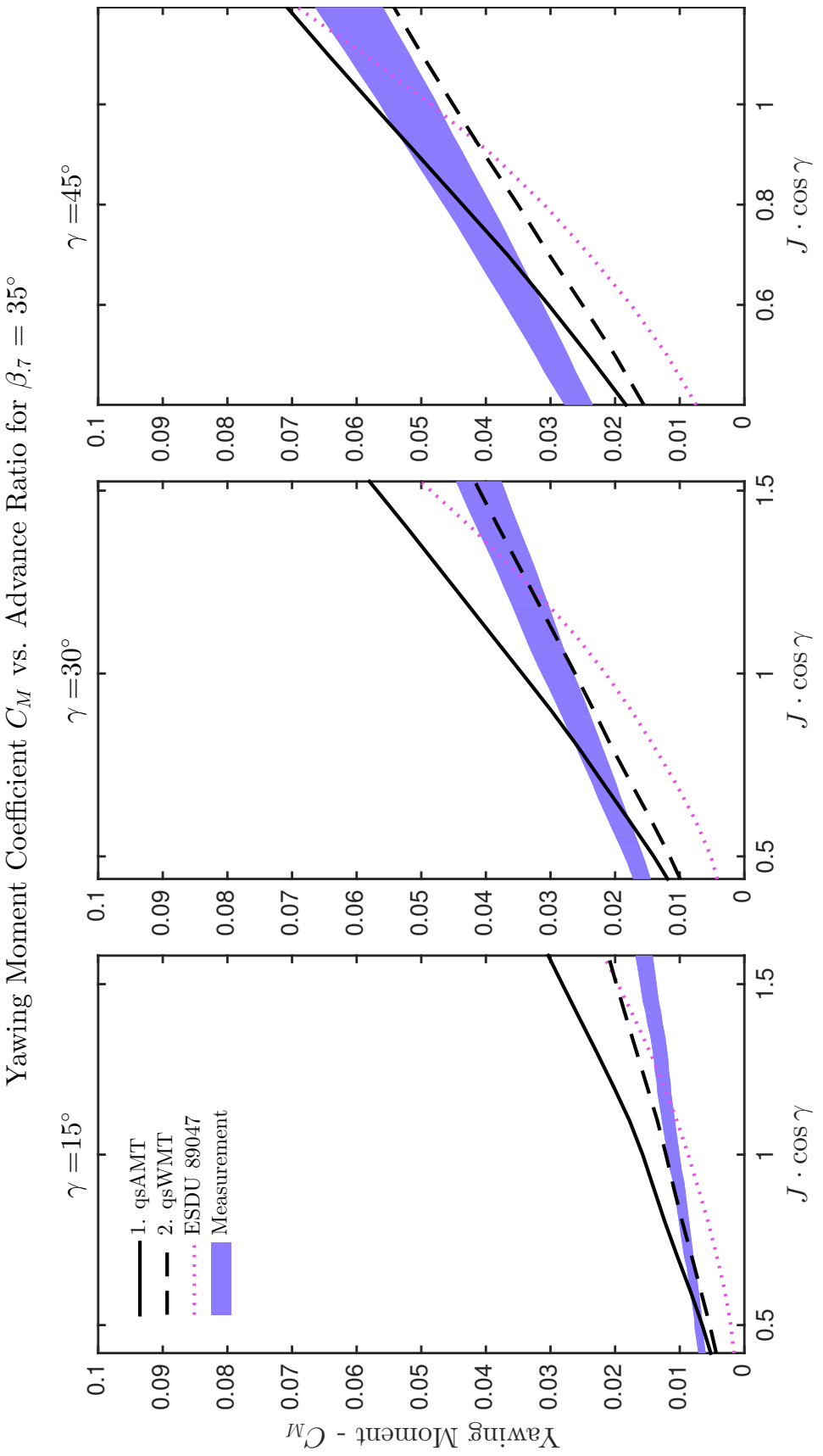

FIGURE 3.26: YAWING MOMENT COEFFICIENT VS. IN-PLANE ADVANCE RATIO FOR DIFFERENT γ. DATA FROM (YAGGY AND ROGALLO, 1960). $\beta_{.7} = 35°$.

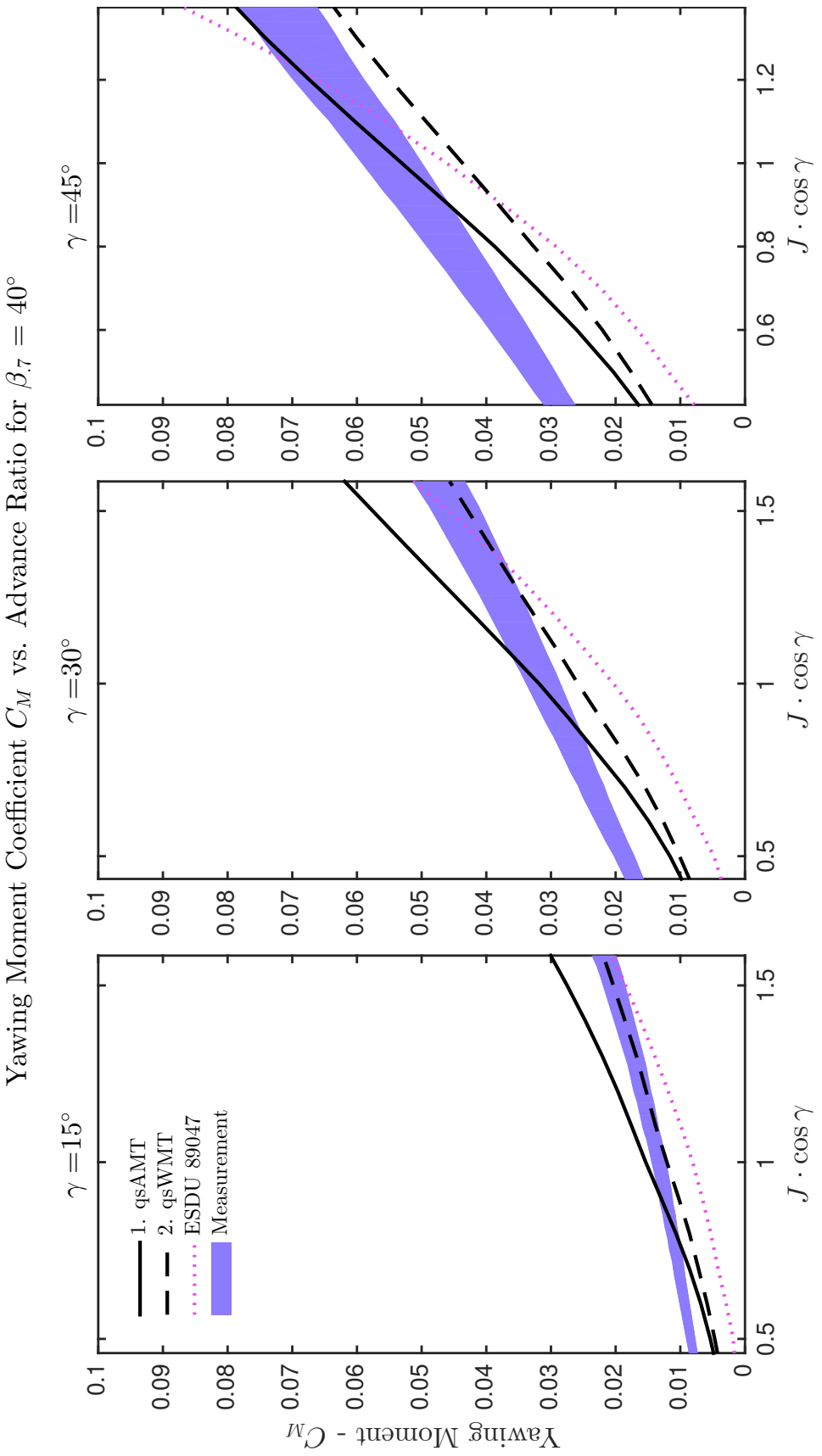

FIGURE 3.27: YAWING MOMENT COEFFICIENT VS. IN-PLANE ADVANCE RATIO FOR DIFFERENT γ. DATA FROM (YAGGY AND ROGALLO, 1960). $\beta_{.7} = 40°$.

ment with advance ratio and qsWMT (Model 2) tends to be better. qsAMT and the ESDU 89047 method tend to be quite closely aligned - certainly much closer than qsWMT and ESDU 89047. This is likely due to the implied azimuthally-uniform distribution of induced velocity in the latter.

qsWMT (Model 2) tends to slightly overpredict the gradient of $\frac{dC_{Myaw}}{dJ}$. The methodology of Yaggy and Rogallo to remove the body loads as described would adequately remove the loads exerted on the spinner/nacelle combination due to *freestream* velocity, but not due to the *slipstream* velocity - and this may have an effect on the results. Particularly, the pressure increase due to nonuniform axial induced velocity around the spinner would exert a yawing moment on the hub in the same direction as the moment due to thrust asymmetry. This effect is impossible to decouple from a test such as that performed (*i.e.,* with a shaft balance), but this effect would be largest at the highest disc loading, and at the highest axial induced velocity asymmetry - *i.e.,* at the largest blade setting angle and disc inclination angle. The predictions of qsWMT are quite good at $\beta_{.7R} = 25°$, $\gamma = 45°$ (lowest blade setting) but poorer at $\beta_{.7R} = 25°$, $\gamma = 45°$ (highest blade setting), giving weight to this assertion.

Overall, it can be seen that qsWMT (Model 2) predicts the variation of yawing moment with inclination angle (γ), advance ratio (J), and blade setting ($\beta_{.7}$) when compared to the azimuthally-uniform method and to the industry-standard ESDU 89047 for this experiment. Since this experiment covered a range of conditions, **this validation adds confidence to the usage of the quasi-steady weighted momentum theory to determine the induced velocity distribution in order to predict fluctuating blade forces**.

Data for the in-plane force were also presented by Yaggy and Rogallo (1960), but calculation of these and comparison of the two momentum models are compared in Chapter 6.

3.8 COMPARISON OF QUASI-STEADY MOMENTUM MODELS FOR INSTALLED CONDITION

The effects of installation are discussed fully in Chapter 5, and results in that chapter are presented for comparison of installation effects using qsWMT. Figure 3.28 shows the prediction of $\Delta C'_T$ with radius vs. experimental measurements of a full propeller aircraft wind tunnel model by (Rogallo et al., 1956). The results are shown here to show the potential difference between using the different momentum models. The installation model requires more refinement but validates reasonably well, and with the three momentum models shows the expected trends - that the uniform model predicts a larger load, DMT/steady-state method predicts a smaller load with weighted momentum theory somewhere in the middle, matching the data points better. At each of the six radial stations, the

azimuthal variation is shown in Figure 3.29, and the respective error in prediction of the range of $\Delta C_T'$ at each radial position is given in the legend. Notably, the errors with qsWMT have an order of magnitude of 10% or less for each radial position, whilst qsDMT has errors that have an order of magnitude twice as large, and qsAMT has errors with an order of magnitude eight times larger. Whilst installation effects will be discussed in more detail in Chapter 5, the results in this chapter add support for weighted momentum theory.

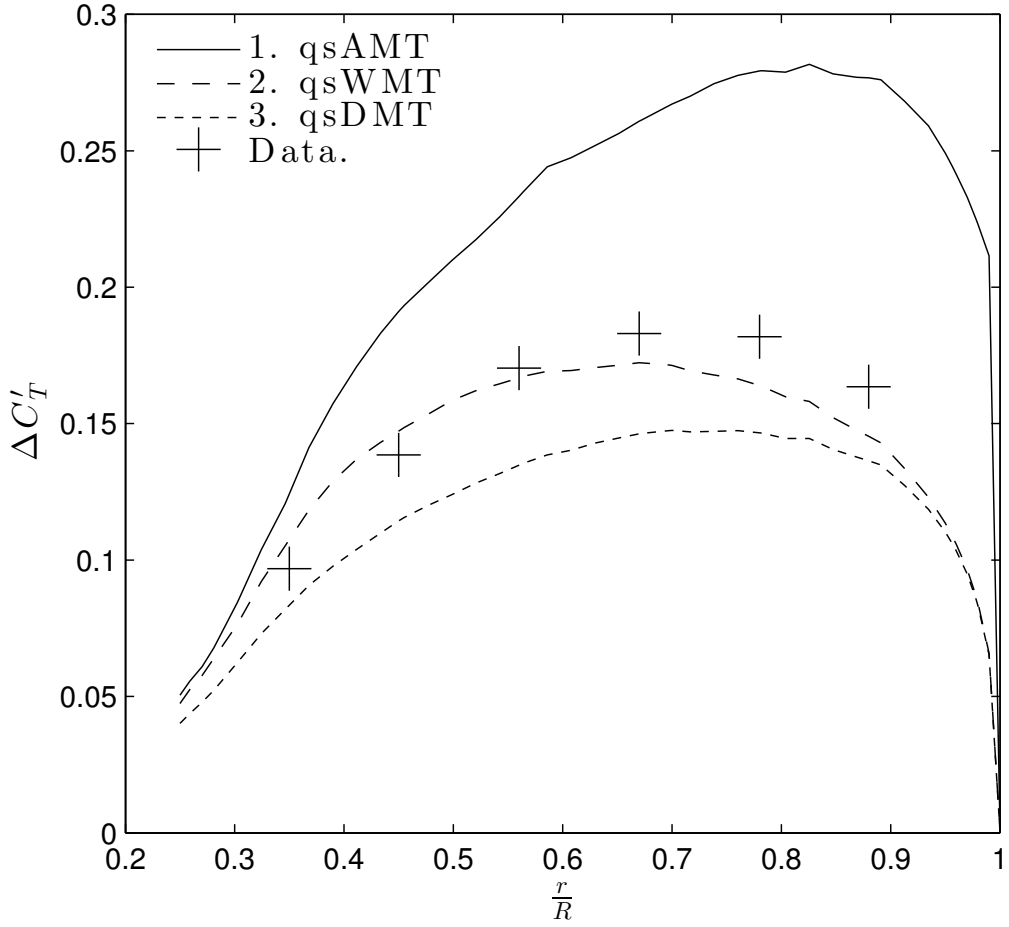

FIGURE 3.28: VARIATION OF $\Delta C_T'$ WITH RADIUS FOR $\gamma = 8^\circ$ ON INSTALLED AIRCRAFT. DATA FROM ROGALLO ET AL. (1956).

3.9 GENERALISED DYNAMIC WAKE RESULTS

The Generalised Dynamic Wake (GDW) as formulated by He (1989) was originally investigated due to its ability to model wake dynamics (*e.g.,* the transient wake behaviour and its effect at the disc due to a step change in BE conditions, akin to a ramp increase in collective pitch á la Carpenter and Fridovich (1953)). Such a model would be advantageous as it could determine an overshoot in local thrust due to dynamic propeller motions. The mathematics behind the formulation of the Generalised Dynamic Wake are complex, but it has its roots in the

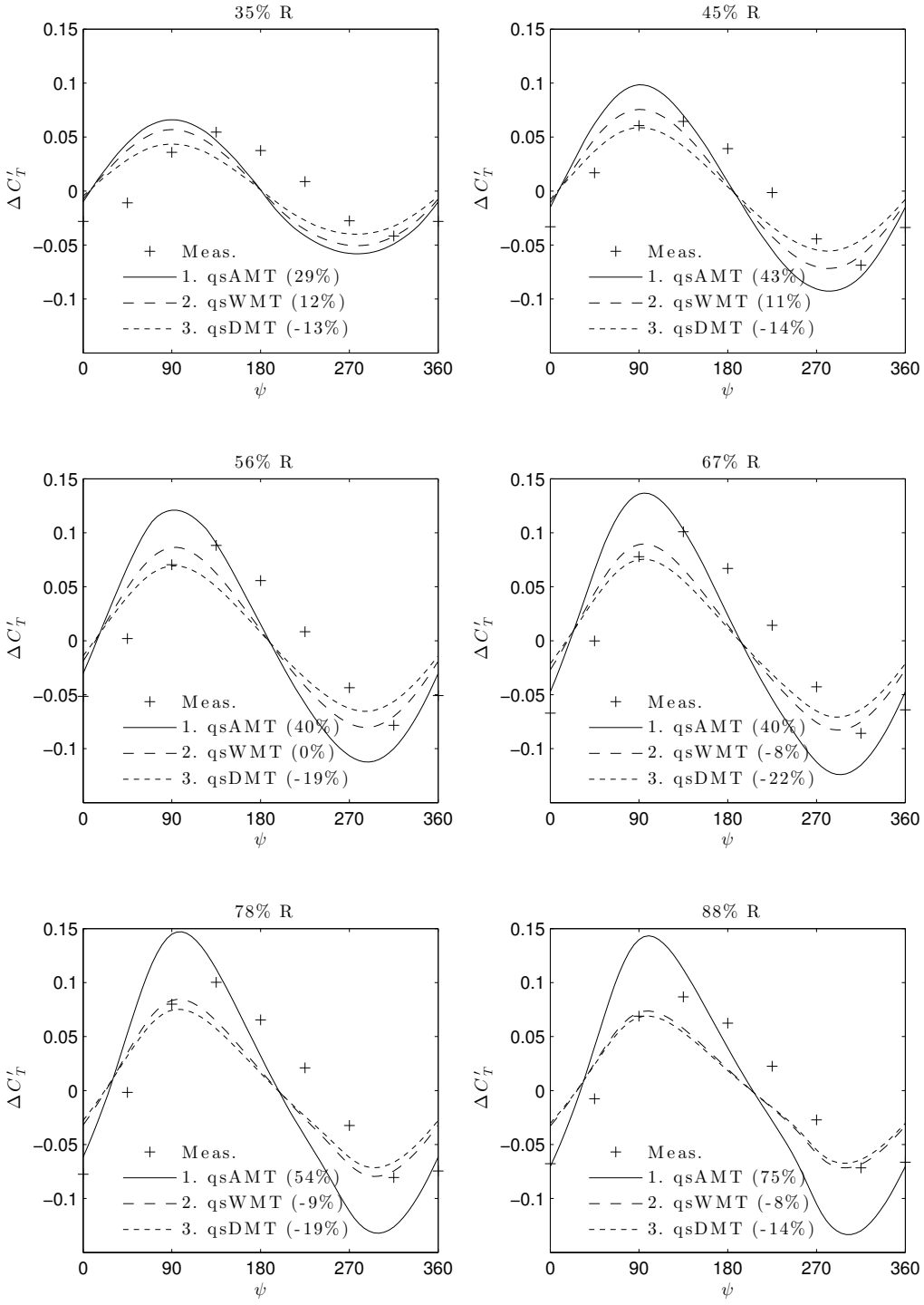

FIGURE 3.29: VARIATION OF $\Delta C_T'$ WITH AZIMUTHAL POSITION FOR $\gamma = 8°$ ON INSTALLED AIRCRAFT. DATA FROM ROGALLO ET AL. (1956). LEGEND SHOWS MODEL KEY AND BRACKETED PEAK-TO-PEAK $\Delta C_T'$ ERROR COMPARED TO EXPERIMENTAL DATA.

Pitt and Peters model and others (Peters and HaQuang, 1988; Chen, 1989; Pitt and Peters, 1981), whose family of models are described as 'Finite-State Induced Flow' models. The GDW finds good use in the literature, though its formulation is involved and complex. The best descriptions of the model and its development and application, aside from He's thesis, are provided by Murakami (2008) and Makinen and Peters (2003).

When the GDW was first implemented and compared for absolute 1P bending load (peak-to-peak) variation with the quasi-steady momentum models, it appeared to confer similar benefits to the weighted momentum theory that has been presented in this chapter (*i.e.,* it provides a result for $\Delta C_{M,root}$ somewhere between the steady-state and azimuthall uniform distributions of induced velocity). The GDW utilises a truncated infinite series comprising azimuthal harmonics and radial polynomial shape functions that *exactly* match the pressure distribution on the propeller/rotor disc. To afford solution, the azimuthal harmonics are limited to the blade number (the number of azimuthal pressure 'peaks'), and this, in conjunction with the ordering scheme defined by He that limits the radial shape functions, means that there is a smoothing of the pressure/induced velocity distribution. However, the result of this smoothing is not that the variation of blade load is smooth azimuthally, but that it adds an artificial higher-harmonic loading component - this may be seen in Figures 3.30 to 3.31 which each show the gradients of C'_T vs. azimuth for a root section and a tip section, and the integrated root bending load.

The figures show that the absolute range of $\Delta C'_T$ in the root section is predicted well (as per qsWMT), but the tip section is subject to large azimuthal 'noise', due to the azimuthal shape functions utilised - particularly at the higher rotational speed. To highlight that these harmonic oscillations are not due to poor implementation in this dissertation, Figure 3.32 is taken directly from He's thesis and shows the induced velocity variation at an outboard section, subject to 1P forcing. What can be seen is that, like the results in Figures 3.30 and 3.31, the harmonic of interest (in this case 1P) is correctly predicted, but that a higher-order harmonic is added to the induced velocity (and by extension, to the blade load). Though this effect could be filtered, it is of significant magnitude and alters the shape of the 1P load against azimuth. It also means that the model is adding a physical feature that is not present in the flow, against the aims of a physically-representative model.

The Generalised Dynamic Wake, and the models that came before and after, serve as valuable tools for rotorcraft analysis and may prove of use on the propeller problem, particularly when exploring wake dynamics with propeller-specific additional terms (*e.g.,* Makinen (by 2005)). For the problem of once-per-revolution blade loading on a propeller at an angle of incidence, the GDW is not well-suited. However, its implicit azimuthal smoothing of the 'steady-

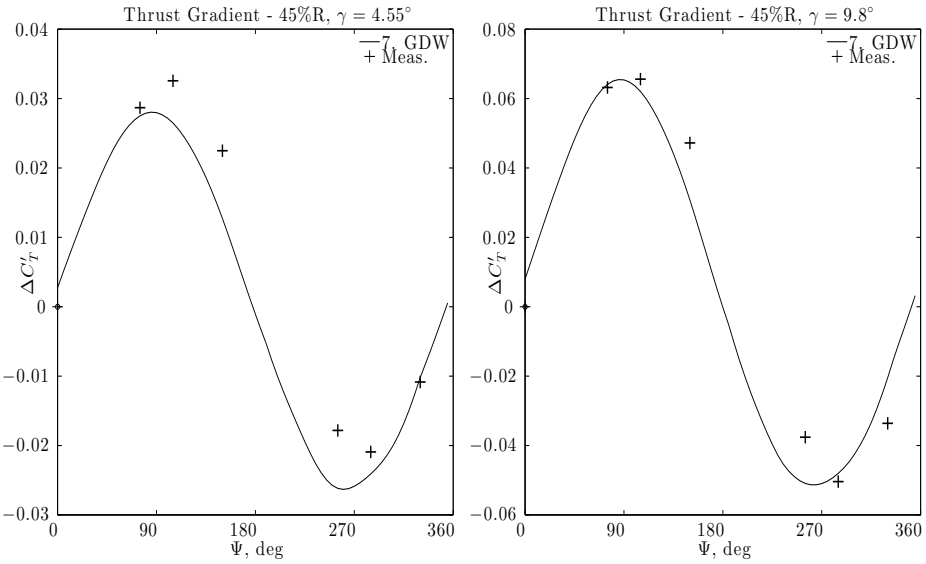

(A) ROOT SECTION THRUST GRADIENT - $45\%R$

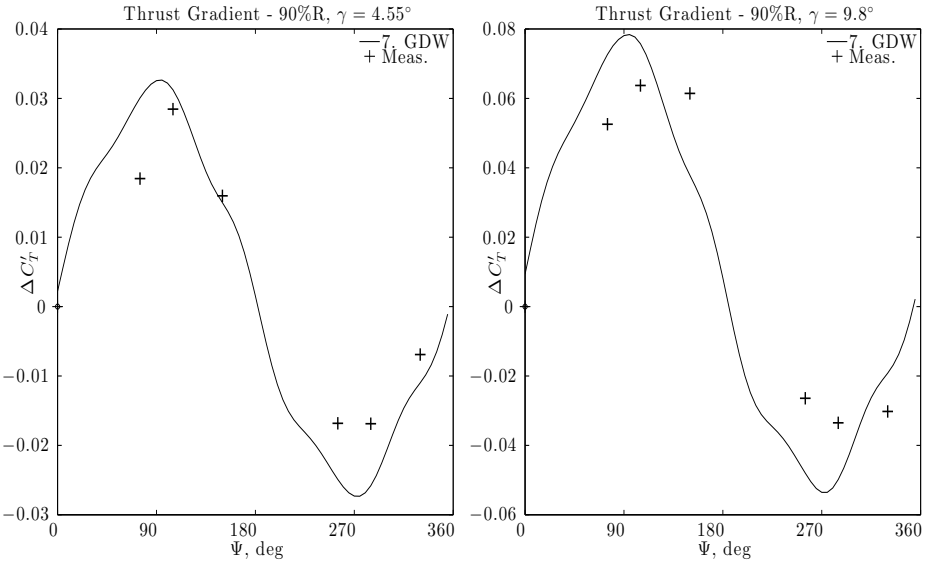

(B) TIP SECTION THRUST GRADIENT - $70\%R$

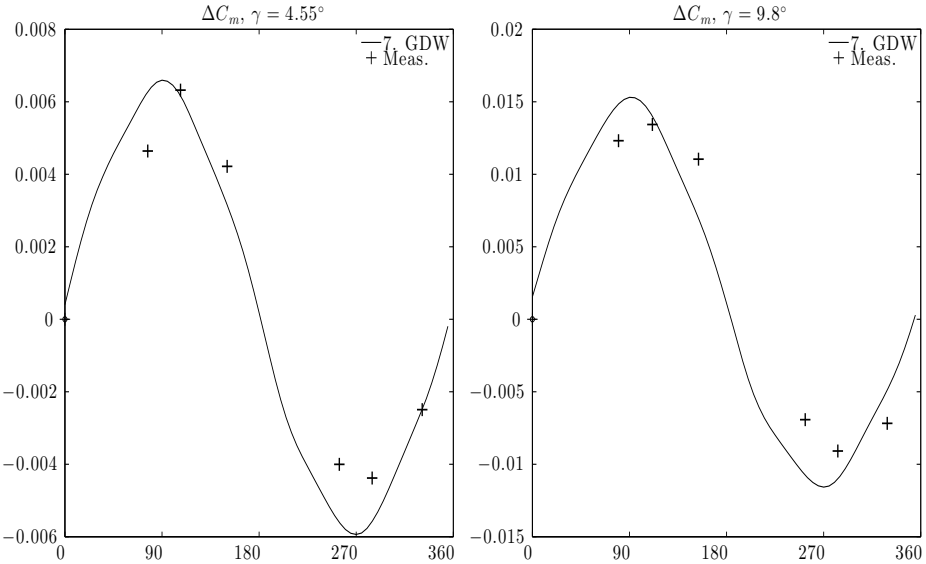

(C) INTEGRATED THRUSTWISE BENDING LOAD

FIGURE 3.30: GDW PREDICTIONS OF CHANGE IN RADIAL THRUST GRADIENT VS. DATA FROM GRAY ET. AL (1954). RPM = 1350, J = 1.2, $\gamma = 4.55°$,$9.80°$.

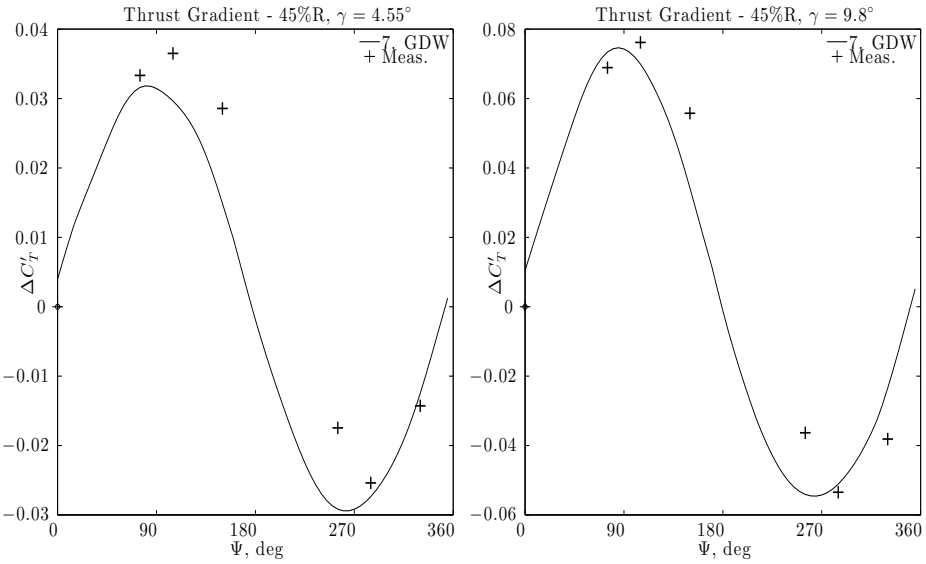

(A) ROOT SECTION THRUST GRADIENT - $45\%R$

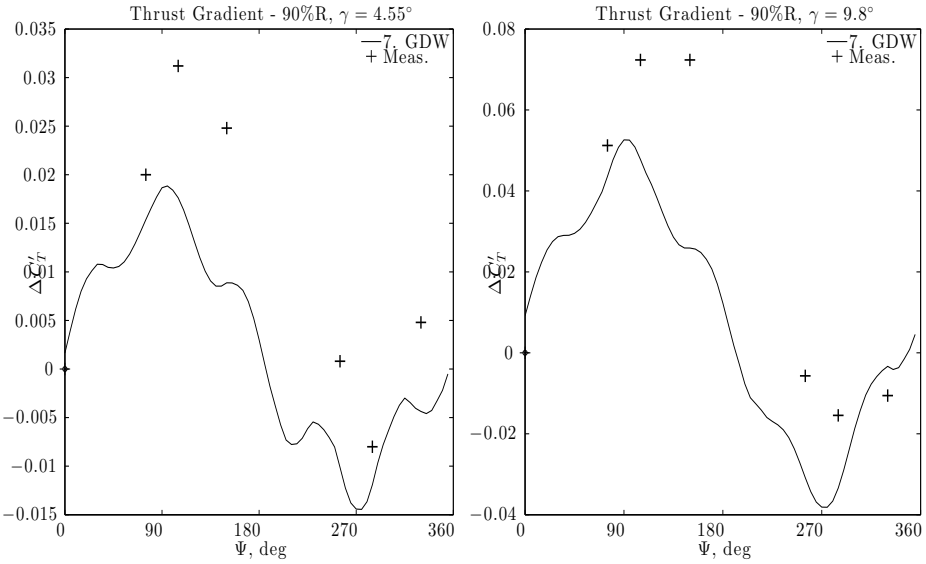

(B) TIP SECTION THRUST GRADIENT - $70\%R$

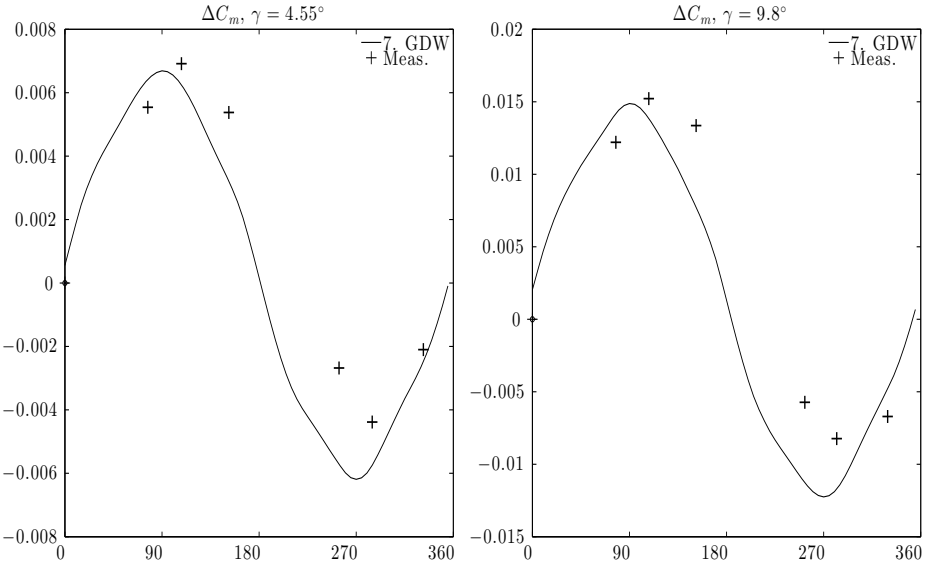

(C) INTEGRATED THRUSTWISE BENDING LOAD

FIGURE 3.31: GDW PREDICTIONS OF CHANGE IN RADIAL THRUST GRADIENT VS. DATA FROM GRAY ET. AL (1954). RPM = 2000, J = 1.25, $\gamma = 4.55°$,$9.80°$.

state'/exact induced velocity distribution (*i.e.,* qsDMT) is what led to the formulation of weighted momentum theory, and provided a wealth of background data for this thesis.

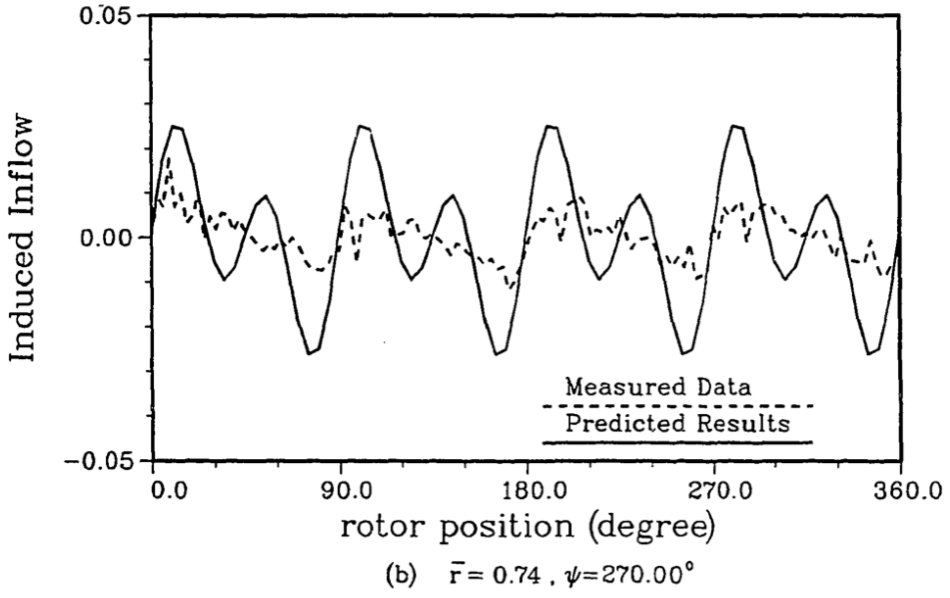

FIGURE 3.32: INDUCED FLOW ON ADVANCING 4-BLADED ROTOR AT $74\%R$, $\psi = 270^\circ$ - 1P AERODYNAMIC FORCING. (TAKEN DIRECTLY FROM HE, 1989, FIGURE 4.52, PG. 152)

3.10 CONCLUSIONS

This chapter has presented an overview of the momentum tools that find common usage for propeller aerodynamic modelling both in axial flight and at an angle of incidence. Both the azimuthally-uniform and the steady-state distributions of induced velocity have been given mathematical formulations (AMT and DMT). These models have been shown to over and underpredict the variation of 1P load, when used with both a quasi-steady (qs) and unsteady (us) blade-element model. A model that is a hybrid of the two, with a physical basis justified from first principles has been presented - weighted momentum theory.

Two first order unsteady models have been implemented to model the unsteady blade element loads - Theodorsen's theory and the returning wake additions by Loewy. Only Loewy's model has been presented in this dissertation as it is more suitable for the problem at hand, and performed better than Theodorsen over the range of results. The Loewy model showed an improvement over the qsAMT model (in the usAMT model), but *should* provide benefit to the WMT/DMT models also, which it did not (usWMT and usDMT both underpredicted the load variation consistently). It has been suggested in this dissertation that the qsWMT and qsDMT models are actually capturing some of the unsteady induced velocity due to disc inclination in its distribution of the steady induced velocity - that is, the fluctuating component of induced velocity predicted locally is larger than that which can be accounted for by the quasi-steady load variation, and that addition of an unsteady model on top of the steady induced velocity model gives a larger load attenuation than that physically present. These two contributions to the induced velocity are very difficult to decouple, but qsWMT provides better performance in most cases when compared to the other steady and unsteady formulations. There is the potential for future theoretical and experimental work for further validation of qsWMT and the magnitude of the induced velocity and its distribution across the disc, discussed in Chapter 7.

Fundamentally, of the models compared in this Chapter, qsWMT has proven to be most fit for purpose to model a propeller at incidence, subject to the caveat that it requires further investigation and validation work. It is recommended as it provides better correlation with the scant validation data, when compared to either of the momentum models that have found usage throughout the literature. The decoupling of steady/unsteady loads needs further investigation, but such work is beyond the scope of this dissertation. It is asserted that the unsteadiness in the flow is adequately captured by the model presented in this chapter and unless otherwise stated, qsWMT is used for the remainder of this dissertation.

CHAPTER 4

SWEPT BLADE ELEMENTS

Modern propeller blades exhibit a degree of sweep, and adaptation of a BEMT model for sweep may seem straightforward, but this chapter will demonstrate that it is not. The elements of a swept propeller blade are not swept in the same sense as the infinite swept wing, but displaced in three-dimensional space. Propeller blade sectional geometry is defined differently to a uniform swept wing, and the sweep is *compound* over span. Application of simple sweep corrections based on the cosine of sweep may be deleterious to propeller performance predictions, as this angle defines the construction of the blade but, may not define the orientation of blade elements with respect to incident velocity. Additionally, sweep complicates basic design factors that are common sense on a straight blade; elements may be displaced in three-dimensional space and the terms 'element' and 'radius' can be ambiguous unless rigorously defined.

Some of the concepts in this chapter pertaining to the unsuitability of simple sweep corrections for swept propeller blades have been highlighted in an internal document at Dowty Propellers.

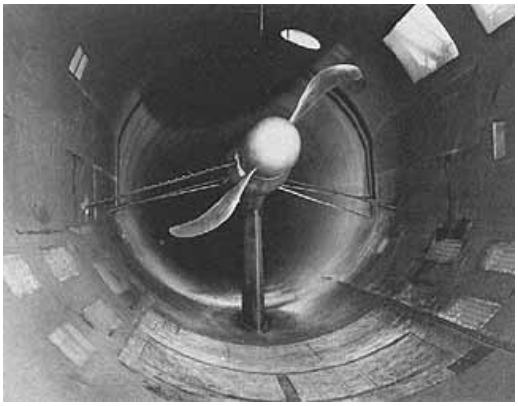

FIGURE 4.1: SWEPT PROPELLER - PROPELLER II FROM EVANS AND LINER (1951)

4.1 INTRODUCTION - HISTORY OF SWEPT BLADES

Sweepback was investigated in the 1940's by propeller researchers in the US and in Germany - with the first swept propeller blades incorporating sweepforward, a knee section and highly swept tips (Becker, 1980). Sweepback in the tip was first incorporated to delay compressibility losses in the tip sections - and this was successful, to some degree. One of the simpler views of sweep as a means to reduce compressibility losses is via an increase to the effective M_{crit} by a factor of $1/\cos\Lambda$, where Λ is the local sweep angle. A more physically-accurate explanation of the drag reduction association with sweepback is that by successfully sweeping the shockwave, the shock-induced drag is angled by the sweep angle - thus the tangential load on the blade is reduced. The propellers tested by Evans and Liner (1951) showed a delay in the onset of compressibility losses but to a smaller degree than that predicted by simple sweep theory (Becker, 1980). The conclusions of the NACA tests was actually that the added structural complexity given by incorporating sweep was large enough to negate any improvements to performance - and that simply using thinner outboard sections would result in a propeller of better performance than the early swept propellers. However, research was continued into swept propellers in the 1980s with the SR series of propellers by NASA and Hamilton Standard. The driving reason for sweepback in these propellers was aeroacoustic - destructive interference by different radial positions resulted in a quieter propeller (Rohrbach et al., 1982).

Modern-day propellers tend to exhibit a degree of sweep - and the reasons for its inclusion can be complex. Some propellers are designed with sweep for aeroacoustic reasons, for compressibility reasons, or for structural considerations. However, the procedures for designing/simulating swept propeller blades are unclear and differ between sources. An industry professional has stated '*sweep is largely added to modern propellers for marketing considerations - to make them look modern*', and not for aerodynamic benefit (Anonymous, 2014)[1]. The veracity of this assertion aside, it stands as evidence that sweep is a complex and potentially contentious topic within propeller aerodynamics.

Finally, the losses on a propeller blade will be largest close to the root - significant sweepback towards the tip will likely do little to alter the propeller performance, despite this being the original reason for inclusion of sweepback on early propellers.

4.2 THE DEFINITION OF SWEEP AND SWEPT BLADE ELEMENTS

The definition of sweep varies by source, though the angle is generally given the symbol Λ. In the early tests by NACA, blades were designed according to a con-

[1] Personal communication. Conversation August 2014.

vention laid out by Whitcomb (1948), with further discussion of blade geometry found in Whitcomb (1950). In this definition, sweep is defined as:

> "Λ - Sweep angle of a line through the midpoints of the chord lines of sections perpendicular to the radii through the midpoints, as measured from the radius of a given section in the plane through the radius and the chord line of the section for the design condition."
>
> Whitcomb (1948)

It is difficult to represent the sweep angle as defined by Whitcomb in a single diagram, owing to the three-dimensional nature of the blade. The sweep angle is as defined in the quotation, but it is only clear through supplementary diagrams and later definitions that sweep refers to the *projection of the semi-chord line in the disc plane*. That is, sweep in this sense refers to the in-plane gradient of the semi-chord line. *Dihedral*, κ, refers to the out-of-plane gradient and is defined the same as sweep, but referring to the projection of the semi-chord line in the plane formed by the blade PCA and the rotation axis. These two angles are very difficult to represent in a single diagram[2], and it is easiest to represent the resultant of both angles, shown in Figure 4.2. Figure 4.2 is a simplification showing the curved semi-chord line in three-dimensional axes, whilst the sweep and dihedral angles are defined in the $X_B - Y_B$ and $Y_B - Z_B$ planes, respectively. What is shown as the sweep angle on this diagram gives an indication of the physical significance of the angle with respect to a section, but is not a true representation of the geometry.

Other definitions of the sweep angle exist in papers produced by NASA looking at advanced turbofans, where the sweep angle is defined as the angle between the semichord line, and the straight blade axis (the PCA) (see Fertis and Maser, 1988, fig 2(a)).

[2] see fig. 3 in Whitcomb (1950, pg. 25) for a representation of both angles in a complex diagram.

The different definitions of sweep arise from the complexity of defining the geometry of a three-dimensional propeller blade comprising two-dimensional sections. For an unswept blade, a designer needs only to supply the following parameters to fully define a blade in two-dimensional sections. Each of these needs to be defined at a number of points along the blade span.

- Element radial/spanwise locations (the Y_B position).
- Element profile characteristics (*e.g.,* $\left[\frac{t}{c}, C_{L_D}, c\right]$ for NACA-16 sections, $\left[K1, \frac{t}{c}, c\right]$ for ARA-D sections).
- Element local twist (β).
- Element Y axis location with respect to blade PCA/(along X_B, Z_B) - defining how sections are joined together.

In construction of a blade element model, a straight blade is attractive as sectional geometry is defined with the element chordwise plane being normal to the blade pitch change axis for every element. Thus, the defined camber and thickness properties are defined in a plane coincident with the local tangential velocity. A change to in-plane rotation (twist) at a given radial location due to a change in root setting is easy to determine. For a change of $\delta\beta$ at the root, this is simply added to the local setting at every radial station.

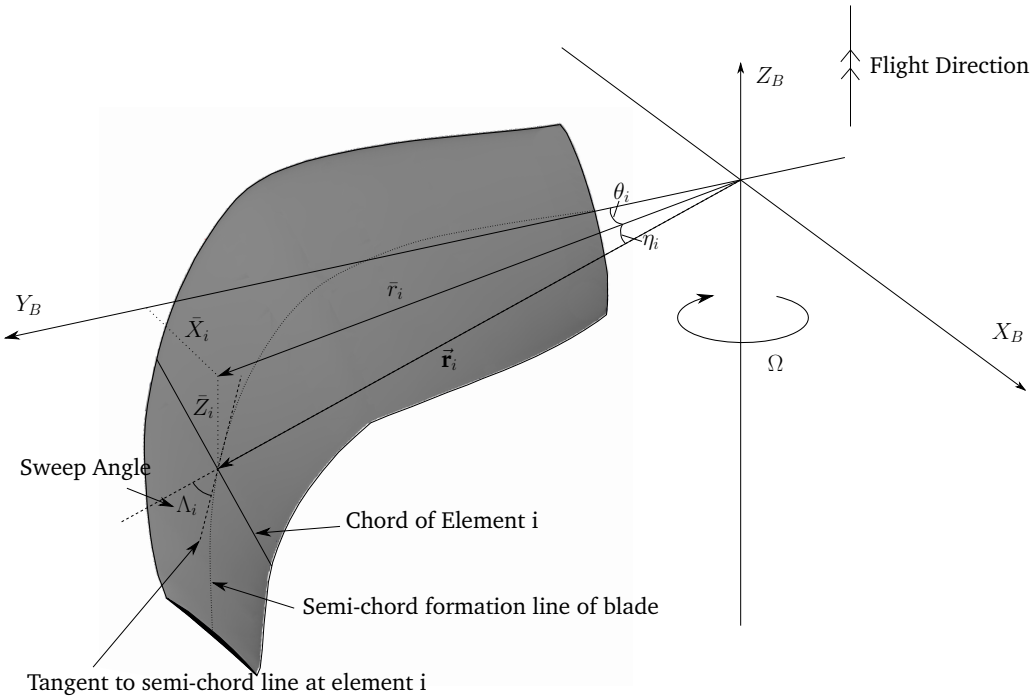

FIGURE 4.2: DISPLACEMENT OF SWEPT BE SEMI-CHORD POSITION FROM BLADE AXES. *Note: This is a simplified diagram.*

Note 4.2.3
Key Observations for **straight blades**:

- The blade and blade element Y-axis will always be collinear, irrespective of blade setting angle.
- The tangent to the rotational velocity will always be normal to the Y-axes, at any setting angle.
- Notwithstanding three-dimensional effects, for any blade setting angle in axial flight the incident velocity can resolved fully into the two-dimensional blade element axes.

For a swept blade, however, a designer must also supply more data to define element orientations in three-dimensional space. There are at least two defintions[3] for how to define blade elements and where they lie with respect to the blade axis. The names given to these conventions below are defined in this chapter, and not from wider literature. Generally, blade element definitions are only supplied implicitly in the literature.

- **Parallel-Sections:** Blade elements are defined like the straight-bladed elements; in a plane normal to the pitch change axis.
- **Radial-Sections:** Blade elements are defined in a plane normal to a radial line drawn from the center of rotation to a reference point on the chord ($\frac{1}{2}c$ in Whitcomb (1948)).

A simple comparison between parallel and radial elements may be seen in Figures 4.3a and 4.3b. The blade planform in the Figures is taken from Evans and Liner (1951) with the twist and dihedral set to zero.

With section properties defined using parallel elements, a benefit is simplicity. Existing techniques suitable for analysis on straight bladed propellers are easily adapted for swept propellers, and the geometry is easy to understand and recreate. The translation between blade and blade element co-ordinate systems involves a simple offset with no rotation. A change to root setting angle is effected equally at each blade element, as per the straight blade. The drawback is that the section displacement in Y_B/PCA, which is often considered the radius, is not the same as the actual radius to the quarter-chord of the blade element. Since a section may be displaced from the PCA, its actual radial distance to the rotational axis will be larger than the distance along the PCA, and a function of blade setting. Shown in Figure 4.3b, the projection of the radius in the disc plane,

[3]Two *well-referenced* definitions, see Section 4.2 for an example of another definition.

i.e., the element distance to the rotation axis is:

$$\bar{r_i} = \sqrt{X_{Bi}^2 + Y_{Bi}^2} \tag{4.1}$$

this radius is the value that should be multiplied by ω to determine the tangential velocity. When using parallel elements, the component of the tangential velocity in the chordwise direction is:

$$V_\omega = \omega \cdot \bar{r_i} \cdot \cos\theta_i \tag{4.2}$$

$$= \omega \cdot r_i \tag{4.3}$$

So the distance along the pitch change axis is valid to use as the radius for determination of the tangential velocity in the chordwise plane of a parallel element, but this velocity will always be smaller than the maximum tangential velocity, which

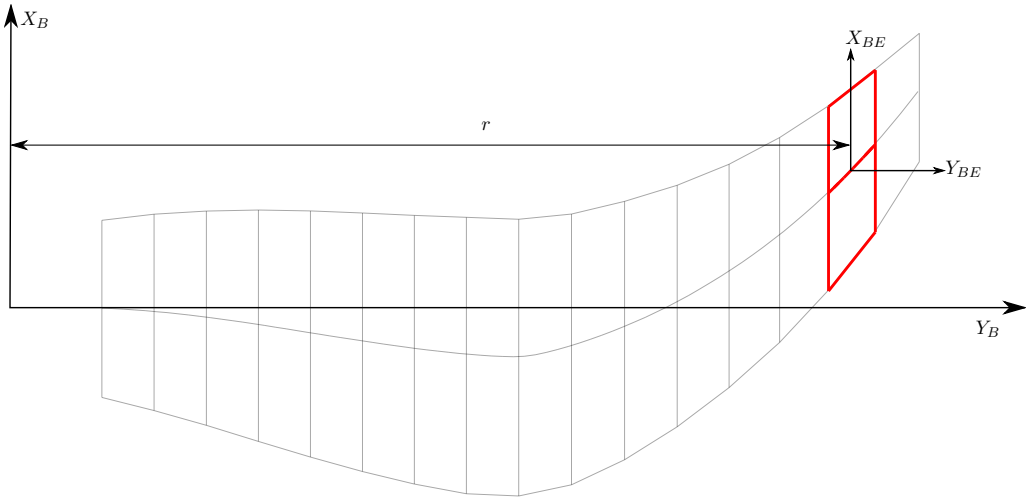

(A) SWEPT BLADE - "PARALLEL ELEMENTS"

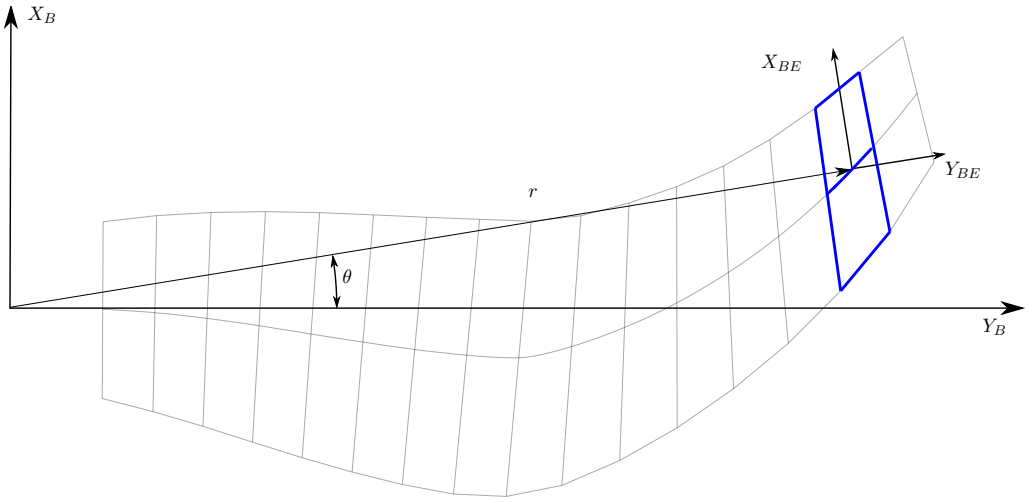

(B) SWEPT BLADE - "RADIAL ELEMENTS"

FIGURE 4.3: COMPARISON OF BE PARALLEL/RADIAL CO-ORDINATE SYSTEMS OVERLAID ON PROPELLER I OF EVANS AND LINER (1951)

is in the plane in which radial elements are defined.

The orientation of a blade element in the disc plane determines which components of inflow are resolved into the blade element two-dimensional axes. The disc inflow is a three-dimensional velocity field, and by resolution into a two-dimensional axis system, a velocity component has to be lost. For a straight blade, both the tangential velocity and axial inflow will always be fully resolved into the blade element axes and since there is no spanwise flow, no flow information is lost. This is not the case for swept blades, and the orientation of blade elements determine if the tangential or the axial velocity is wholly resolved into the blade element axes. Figure 4.4 shows the projection of the curved rotational streamline in the disc plane at a single radius with the blade set at $\beta = 0$ (fully unfeathered). The tangent to this line is the tangential velocity, $V_\omega = \omega \cdot r$. Parallel and radial elements are overlaid on the blade planform close to the tip, and magnified. Figure 4.5 shows the path of the normal velocity, V_n, with the blade set at $\beta = 90^\circ$ (fully feathered).

In Figure 4.4, the tangential velocity vector passes through the plane of the radial sections, but crosses the plane of the parallel sections. A transform into parallel sections reduces the tangential velocity component in blade-element axes. Conversely, in Figure 4.5, the axial inflow vector passes through the plane of the parallel element but crosses the plane of the radial element. A transform into radial sections reduces the disc-normal velocity in blade-element axes. Whilst these diagrams show the unfeathered and fully-feathered blade, respectively, the vector resolution of V_n and V_ω into blade element axes will be subject to this effect for any blade setting. The components $V_n \cdot \sin\beta_i$ and $V_\omega \cdot \cos\beta_i$ are resolved into blade axes and each is subject to the same effect.

This is obviously a simplification of the actual flowfield. Any blade element model explicitly disregards three-dimensional effects. With a swept propeller blade, three-dimensional effects are not necessarily any more influential or likely to occur, but the three-dimensional nature of the geometry means that representation as a set of two-dimensional elements is problematic, and that a local representation of the flowfield is liable to miss a velocity component.

Referring back to Note 4.2.4 - the key observations made for straight blades, the contrast with swept blades is due to the shape of the geometry in three-dimensional space. The observations made for straight blades are not valid for swept blades and there is a compromise to be made with geometry definitions. *Parallel elements* by definition, set the Y_{BE} as collinear with Y_B. Thus the projection of the axial inflow in the blade element axis will be wholly captured by such an element. The projection of the tangential velocity in the blade element axis will include a spanwise component, however, which is disregarded in a blade element model. *Radial elements*, by definition set X_{BE} normal to the blade tangential velocity, *at the design condition (setting)*. Thus the projection of the

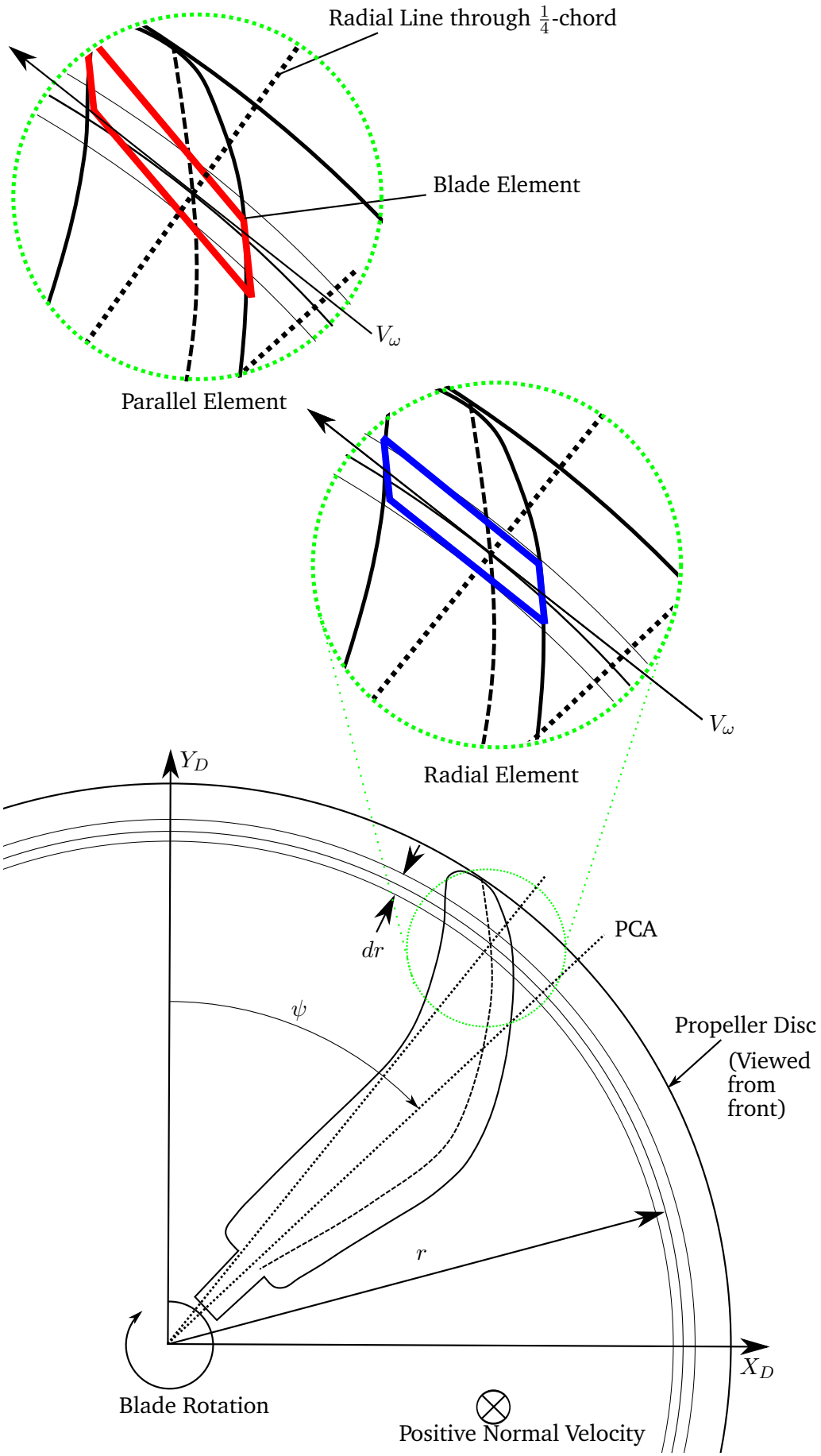

FIGURE 4.4: TANGENTIAL VELOCITY VECTOR PATH - PARALLEL AND RADIAL ELEMENTS COMPARED.

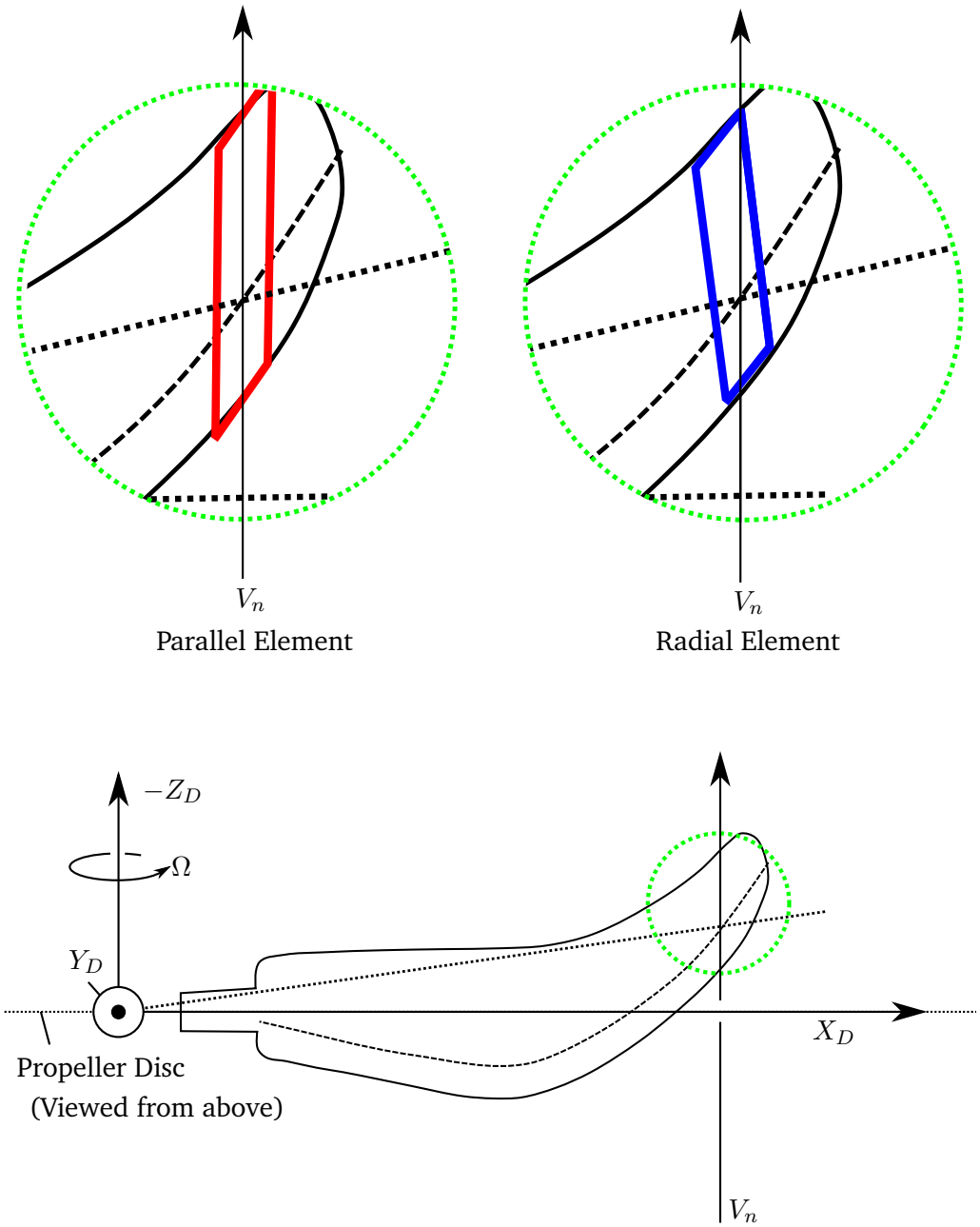

FIGURE 4.5: AXIAL VELOCITY VECTOR PATH - PARALLEL AND RADIAL ELEMENTS COMPARED.

tangential velocity in the blade element axis will be wholly captured by such an element. The projection of the axial inflow in the blade element axes will include a spanwise component.

To make a blade element model for an existing propeller blade, it makes sense to use the blade element definition with which the propeller was defined. In Section 4.6, a comparison of radial and parallel elements is made to the performance data of a set of swept propeller blades. The blades were defined with radial elements, but an axis transform into parallel elements has been made, though using the same two-dimensional sectional properties, simply oriented differently. Since

both definitions are somehow failing to capture an element of the flow, it would be advantageous to define a set of blade elements for which this is not an issue. In blade element analysis, the magnitude and direction of the incident flow vector[4], $\vec{\mathbf{V}}_R$, is easily calculable. It would make more physical sense to define blade element geometry/properties in the plane formed by the projection of *this vector* in blade axes. However, this would require a redefinition of blade sectional geometry for each change to aerodynamic conditions (*i.e.,* advance ratio, rotational speed and even perturbations in induced velocity within a single model implementation) - and the shape of sections in such an axis system will likely be removed from standard aerofoil families. Whilst this approach would prove an interesting avenue of future research, it would require further experimental work or higher-fidelity simulation which is beyond the scope of this dissertation.

One might follow logically from the discussion of swept blade element definitions and suppose that straight blade elements (and also swept elements) should actually be defined along a *circumferential* path. Whilst this reasoning is sound, preliminary calculations showed that the actual difference to results from using a chord based on an arc length was negligible.

OTHER ELEMENT DEFINITIONS

With the extra parameter of blade element orientation with respect to the blade PCA, a designer has a near-infinite choice of co-ordinate system in which to define blade elements and hence design the blades. A test of swept propellers designed before the definitions of Whitcomb (1948) was published by Gray (1948). The blades comprise NACA 16 series sections, and the elements are defined in an axis system *perpendicular* to the blade semi-chord line. Without the definition of the centreline of the blade, *i.e.,* the *formation line* in Whitcomb's definition, the geometry of these blades is impossible to reconstruct. This definition of sectional geometry would be interesting to explore, though, as the orientation of blade elements mean that a component of both tangential and axial velocity will be lost. The work by Gray (1948) notes that the blades are defined fully in an earlier reference (ref. 4 of Gray (1948)), which is an industrial report by the Curtiss-Wright Corp., and unavailable. Whilst it would be ideal to validate to another set of blade element definitions, with the literature that is available this is currently not possible. What this highlights is the complexity of the geometry definition of the swept propeller blade, and the need in the literature for a discussion of swept blade element definitions.

[4]Usually used in a scalar context as V_R at incident angle α_R to BE zero-lift line

4.3 AN EULER TRANSFORM FOR SWEPT BLADES

To accommodate for the blade element displacement in the blade axis, an a Euler transformation can be made that resolves blade element forces into blade forces, through a sequence of four rotations; *local twist* β_{tw} (rotation about X_E), *lagwise displacement* (rotation about Z_B) θ_i, *flapwise displacement* (rotation about X_B) η_i and *blade setting* (rotation about Y_B) A_0. Angles θ_i and η_i are shown in Figure 4.2.

$$\vec{R}_{BE} = [T]_{A_0} \cdot [T]_{\eta_i} \cdot [T]_{\theta_i} \cdot [T]_{\beta_i} \cdot \vec{R_B} \tag{4.4}$$

$$\vec{R}_{BE} = [T]_{tot} \cdot \vec{R_B} \tag{4.5}$$

The construction of Eq. 4.5 and closed form solutions of $[T]_{tot}$ and its inverse are provided in Appendix B. The Euler transform is used to:

- Resolve disc velocities $\vec{V}_D$ into the blade element axes for calculation of α_R, V_R and hence determine dC_l, dC_d in blade element axes.
- Transform blade element forces, Eqs. 3.17 and 3.18, into blade axes for coupling with the disc-level momentum model and to obtain thrust/torque.

With two different means of defining blade elements and hence sectional properties, both are formulated in the model in a similar way - using the full Euler transformation when calculating with radial elements, whilst using the Euler transformation with $\theta_i = \eta_i = 0$ when using parallel elements. Although this method is a complex means of calculating using the parallel elements, it means the same model may be used for both which makes for a fair comparison. With the added step of the Euler transformation, the solution procedure of Figure 3.6 from Chapter 3 is adapted to Figure 4.6 with the additional steps highlighted in red.

This methodology is different to that presented by Whitcomb. He provided a set of successive calculations to be made to determine local sweep and setting for changes to root setting angle, which is easier to perform by hand, but is much more time-consuming than using the Euler transform on a computer.

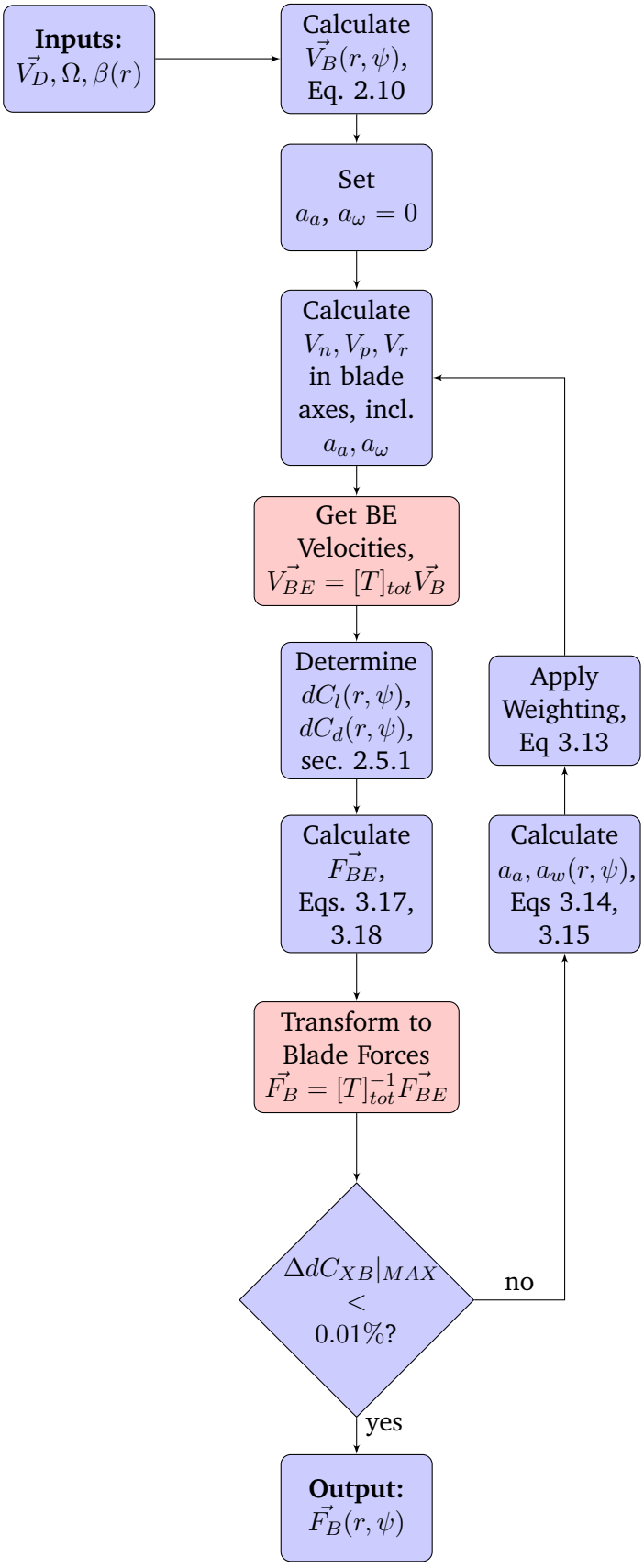

FIGURE 4.6: SOLUTION PROCEDURE FOR SWEPT BLADE ELEMENT MOMENTUM THEORY MODEL INCLUDING EULER TRANSFORM

4.4 AERODYNAMIC SWEEP CORRECTIONS

Blade element/strip theory has at its roots the concept that individual blade elements behave independently, as sections of infinite, uniform, straight wings. It is easy to assume that for the elements of a swept propeller blade, fixed-wing sweep corrections may be similarly applied. This methodology is common in the literature when dealing with blade element models for swept propeller blades and corrections such as:

$$\left.\begin{bmatrix} M_R \\ V_R \end{bmatrix}\right|_{swept} = \cos\Lambda \cdot \left.\begin{bmatrix} M_R \\ V_R \end{bmatrix}\right|_{straight} \tag{4.6}$$

$$\left.\begin{bmatrix} \alpha_R \\ K1, C_{L_D} \\ \frac{t}{c} \end{bmatrix}\right|_{swept} = \frac{1}{\cos\Lambda} \cdot \left.\begin{bmatrix} \alpha_R \\ K1, C_{L_D} \\ \frac{t}{c} \end{bmatrix}\right|_{straight} \tag{4.7}$$

$$C_L|_{swept} = \cos^2\Lambda \cdot C_L|_{straight} \tag{4.8}$$

$$C_D|_{swept} = \cos^3\Lambda \cdot C_D|_{straight} \tag{4.9}$$

or some variation thereof used with little discussion of their physical basis. Equations 4.6 to 4.9 are representative of the corrections used in industrial codes (*e.g.*, Bielawa et al., 1983; Morrison and Bocci, 1985; Yamane, 1992)[5], and in discussion of swept propeller blades in the literature. Note that the correction should be applied to V_R in calculation of dynamic pressure, OR to C_L by multiplying by $\cos^2\Lambda$, but not both. The correction is applied to M_R and used to determine the compressibility-related lift and drag properties.

> "Assuming that each section operates as a portion of an infinite-span surface [...] **the actual lift coefficients for each of the sections will be reduced below the design values by a factor equal to approximately the reciprocal of the cosine of the sweep angle**."
>
> Whitcomb (1950, pg. 9, '*Corrections for Sweep*')

To understand the effect of using these simple sweep corrections, and to show why they are not well-suited for swept propeller blades, the following section briefly highlights from where they originate.

[5] Bielawa et al. (1983) does not specifically mention sweep corrections in discussion of a larger model, but the sectional velocities are resolved into an axis through angle Λ, making an effective correction to dynamic pressure.

4.4.1 INFINITE WING SWEEP CORRECTIONS

The corrections for an infinite wing in steady flow at some angle, Λ, with respect to a line normal to the wing leading edge, may be found in any good basic aerodynamic textbook (*e.g.*, Houghton et al., 2012; Gulcat, 2010). There is some confusion about the origin of the various cosine terms that appear in the corrections, and a naïve interpretation of the equations may lead to the conclusion that there is an erroneous extra cosine factor. A discussion of why this is not the case, and a derivation of the sweep corrections using a potential flow method has been presented by Rosen and Rand (1985).

A section of an infinite wing in sideslip is shown in Figure 4.7. Chord, thickness and camber are all defined in the direction normal to the leading edge and are constant with spanwise position. The onset flow may be decomposed into components normal to the leading edge and parallel to the leading edge, $V \cdot \cos\Lambda$ and $V \cdot \sin\Lambda$, respectively. Betz (1937) showed the sweep corrections for this case, noting from the outset that the spanwise component of velocity is 'undeflected by the wing' and since the generation of lift requires creation of circulation, this component of velocity produces none. Only the component of velocity normal to the leading edge is considered, giving a factor of $\cos^2\Lambda$ in the dynamic pressure. Other cosine factors appear in the vector translation of the angle of attack into the defined chordwise direction, and in the *effective chord*, $c' = c \cdot \cos\Lambda$.

On a propeller blade the camber, thickness and chord are all defined in the direction of the blade element definition. It is erroneous, therefore, to apply sweep corrections to the geometric characteristics. Additionally, the velocity component of interest is already resolved into this plane and no correction should be applied to V_R. The angle of attack is defined in the plane of the blade element and needs

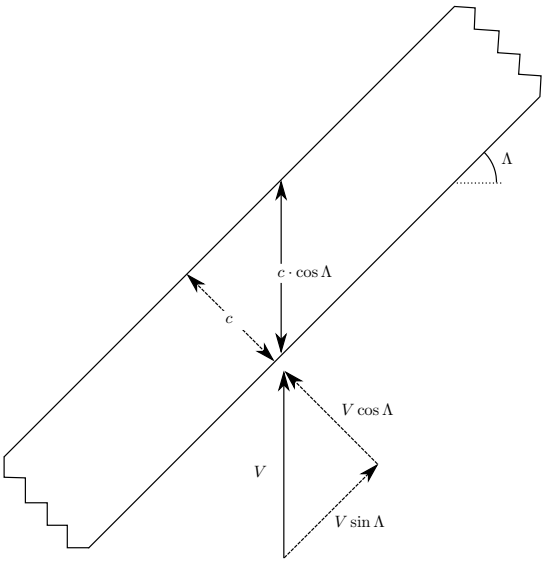

FIGURE 4.7: INFINITE WING IN STEADY FLOW AT SWEEP ANGLE Λ.

no resolution through Λ. Though the leading edge of such a section is indeed 'swept' at an angle with respect to the incident flow vector (and also the trailing edge, potentially at a *different* angle), the flow is turned through an angle based on the camber of the section and the local incidence. Though there may be a reduction in drag due to an oblique shock only being able to form when $M \cdot \cos\Lambda = M_{crit}$, this will only affect the wave component of drag and will not be considered in this section. A correction to the wave drag has been included in the methodology of some industrial documents reviewed (commercially sensitive), and is possible owing to the lift and drag databank available for ARA-D/A blades, but not in the databank for NACA 16 sections.

Another counter to the use of the simple sweep corrections for swept propeller blades is a consideration of a tapered, unswept wing. Like the sections of a swept propeller blade, in steady flight at zero angle of attack/sideslip, the tapered unswept wing has a leading and trailing edge that is at some angle to the incident flow. Sectional aerodynamic properties are defined in chordwise direction, which lies in the streamwise plane. In a two-dimensional strip/lifting line model, no correction based on the cosine of the leading edge angle would be included, and aside from the potential inclusion in the wave drag neither should one for a propeller blade element model. It should also be noted that for fixed wing aircraft, though a reasonable estimate of the critical Mach number of a wing may be gained using the simple sweep corrections, higher-fidelity models will generally be used for determination of spanwise lift. Many large aircraft have a degree of sweep in their main lifting surface - much of the reason for the inclusion of sweep is to sweep the wing shockwave rearward and reduced the shock-induced losses, but it is also included for structural reasons. Rearward sweep increases the divergence speed, thus reducing static aeroelastic problems, so it is often included for structural safety considerations. Again - this serves to highlight that the addition of sweep to an aerodynamic problem is far from simple.

Despite the 'simple' sweep corrections having less physical applicability to swept propeller blades, they find common usage in the literature and in engineering-level codes. Accordingly, they will be compared in terms of their performance predictions in this chapter.

4.4.2 INTEGRATED FORCES AND MOMENTS

Determination of the forces and moments on a straight-bladed propeller is relatively simple. Once the aerodynamic environment of the propeller blade elements (*i.e.,* $\alpha_R(r,\psi)$ and $V_R(r,\psi)$) is determined, a lift/drag databank will return the aerodynamic lift and drag coefficients, dC_l and dC_d. These are multiplied by chord and dynamic pressure to give the dimensional lift and drag per unit length, dl and dd, and resolved into the axial direction to give elemental thrust per unit

length, dT. This is integrated along the blade span to give total thrust, T, and moment. Thus for a straight blade, the thrustwise force and root bending moment is given by:

$$T = \int_{root}^{R} [dC_l \cos\phi - dC_d \sin\phi] \cdot c \cdot q \cdot dr \tag{4.10}$$

$$M_{XB} = \int_{root}^{R} [dC_l \cos\phi - dC_d \sin\phi] \cdot (r - r_{root}) \cdot c \cdot q \cdot dr \tag{4.11}$$

The variable of integration in equations 4.10 and 4.11 has to be the radius pertinent to the type of blade elements in use. It has to be perpendicular to the definition of the chord, such that $\int c\,dr = dA$ is equal for both definitions. This means that for parallel elements, the radius is defined as the distance along the blade pitch change axis - also the case for straight elements. For radial elements, the variable of integration is the magnitude of the vector defining a blade element position. So at any point on the three-dimensional vector, $\vec{\mathbf{r}}$, defining the blade semi-chord line, the two radii are as follows. For element position i the variable of integration for parallel and radial elements are r_p and r_i, respectively:

$$\vec{\mathbf{r}}_i = \begin{bmatrix} X_{Bi} \\ Y_{Bi} \\ Z_{Bi} \end{bmatrix} \tag{4.12}$$

$$r_{p,i} = Y_{Bi} \tag{4.13}$$

$$r_{r,i} = \sqrt{X_{Bi}^2 + Y_{Bi}^2 + Z_{Bi}^2} \tag{4.14}$$

This may seem self-explanatory, but it is necessary to highlight the distinction in this dissertation. The blade semi-chord line is a curved line in three-dimensional space, and it may seem more sensible to perform the integrals as line integrals of the force vector field over the vector path describing the formation line. This would only be valid, however, if the chord of elements is defined normal to the semi-chord line[6]. With parallel elements, the variable of integration is the same variable used as the radius for determination of tangential velocity. With radial elements, the variable of integration is *not* the same variable, as the determination of the tangential velocity requires the distance to the rotational axis, Eq. 4.1. For radial sections, this value changes with blade setting, whereas the integral operator (Eq. 4.14) does not.

An alternative to integration is to determine the area of each element, recognising that the area is defined by a quadrilateral and thus easily calculable, $\int c\,dr = dA$. This turns the integration into a summation which has the potential to reduce computation time - although since integrations are only needed at the end of the iterative cycle, the potential for computational savings is not that

[6] As per the definition in Gray (1948).

large. Equations 4.10 and 4.11 can be replaced by:

$$F_{ZBn} = \sum_{i=1}^{n} [dC_l \cos\phi - dC_d \sin\phi] \cdot dA \cdot q \tag{4.15}$$

$$M_{XBn} = \sum_{i=1}^{n} [dC_l \cos\phi - dC_d \sin\phi] \cdot (r - r_i) \cdot dA \cdot q \tag{4.16}$$

Equations 4.15 and 4.16 have been used to determine the performance of a straight and swept propeller and give identical results to equations 4.10 and 4.11, which proves the validity of using different variables of integration with each definition.

4.4.3 PHASING OF INFLOW FOR SWEEP

The models described up to this point determine how blade element calculations are performed, and how elemental forces are summated to provide total force either for a whole blade, or portion thereof. Sweep provides another complication to the propeller model that requires a modification of the blade velocities, $\vec{V_B}$, and their resolution from disc velocities. For a straight blade, Eq. 2.10 determines the velocity due to inflow in blade axes as shown in Chapter 2.

$$\vec{\mathbf{V_B}}(r,\psi) = \begin{bmatrix} V_p \\ V_r \\ -V_n \end{bmatrix} = \begin{bmatrix} U_D(r,\psi) \cdot \cos\psi + V_D(r,\psi) \cdot \sin\psi \\ U_D(r,\psi) \cdot \sin\psi + V_D(r,\psi) \cdot \cos\psi \\ W_D(r,\psi) \end{bmatrix} \tag{2.10}$$

Eq. 2.10 assumes that the blade quarter-chord line lies along the pitch change axis. This is not strictly true for straight blades as it will be by definition a quarter-chord ahead of the semichord, but the effect of this is quite small. For swept blades, however, the curved formation line has a projection in the disc axis - and the projection of a radial line drawn to a blade element position is defined as $\bar{r}$, which will be displaced in azimuth from the pitch change axis. This is shown in Figure 4.8. The effective azimuthal angle, ψ' is defined, and the angular displacement between the pitch change axis and blade element quarter chord is $\delta\psi \triangleq \psi - \psi'$. This is effectively a phase lag in azimuthal position for each blade element, and will be dependent on setting angle.

For a swept blade, element quarter chord positions lie at some displacement, $\delta\psi$, from the pitch change axis. Eq. 2.10 is modified to:

$$\vec{\mathbf{V_B}}(r,\psi) = \begin{bmatrix} U_D(r,\psi+\delta\psi(r)) \cdot \cos\psi + V_D(r,\psi+\delta\psi(r)) \cdot \sin\psi \\ U_D(r,\psi+\delta\psi(r)) \cdot \sin\psi + V_D(r,\psi+\delta\psi(r)) \cdot \cos\psi \\ W_D(r,\psi+\delta\psi(r)) \end{bmatrix} \tag{4.17}$$

Noting that the azimuthal angle in the trigonometric terms are not modified by

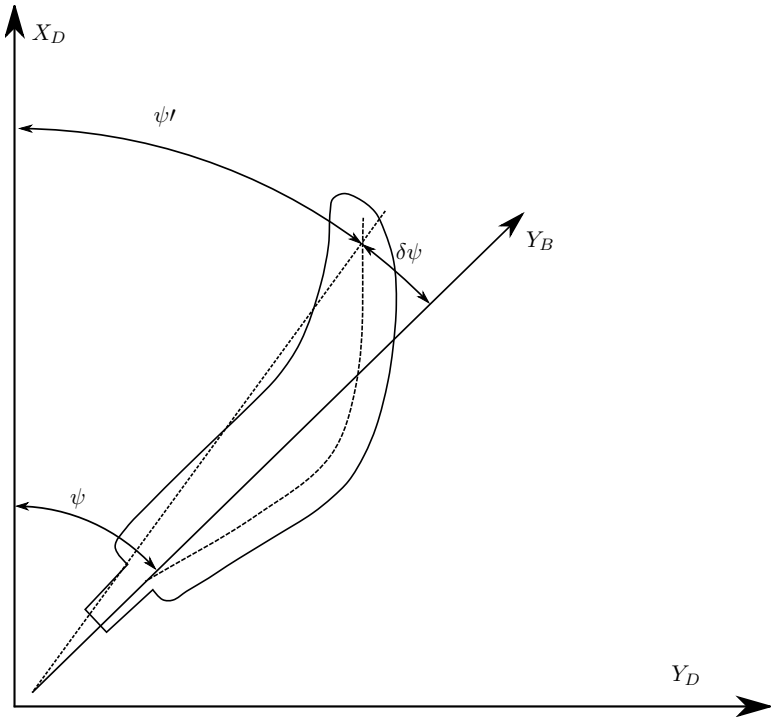

FIGURE 4.8: EFFECTIVE AZIMUTHAL ANGLE.

$\delta\psi$, as these angles are determined by orientation of Y_B, and resolution from this angle into blade element axes is performed via the Euler transform. In actual calculation, disc velocities are calculated at positions around the azimuth determined by the azimuthal step size. Accordingly, values of $\vec{V_D}$ are interpolated for the effective azimuthal positions ψ'. This interpolation only needs to be performed once, so it is not a large computational cost. For uniform incident flow and pure disc inclination it also has no effect as $\vec{\mathbf{V_B}}$ is constant over the disc, but needs to be considered for nonuniform incident velocity.

4.4.4 PARALLEL/RADIAL ELEMENTS 1P LOAD

The two means of defining swept blade elements have been presented in the preceding sections, and they will be compared in axial flight in Section 4.5. This dissertation aims to determine the best means of predicting load variation on a propeller at incidence, and the effect of in-plane velocity needs to be determined.

For a propeller at an angle of incidence with straight blades, the in-plane velocity in disc axes is transformed to blade axes by Eq. 2.10. For a swept propeller blade with elements defined using parallel sections, the radial velocity in blade axes is disregarded as per the straight bladed propeller as Y_B and Y_{BE} are parallel. The local angle of attack and incident flow magnitude are determined just as for straight blades - except a phase shift noted in the previous section. If elements are defined using the radial definition, however, the blade radial velocity needs to be taken into account via the Euler transform, as Y_B and Y_{BE} are not parallel.

With both element defintiions, this is taken into account in the Euler transform. For uniform incident velocity and disc inclination, with parallel elements the extrema of α_R and V_R will appear at the same azimuthal position for every radial element - the peak advancing and retreating blades, just as for straight blades. For radial elements, however, the extrema of different radial elements will not be in phase. For pure disc inclination in uniform incident velocity, a propeller model using radial elements is likely to predict a lower integrated bending load than one using parallel elements, due to the different radial elements producing load variation of the same magnitude but different phasing.

Without validation data, it is not possible to determine which methodology is the most accurate for load variation, but some predictions may be made and this will be compared in Section 4.7.

4.5 SWEEP MODEL VALIDATION

In the literature that is available, it is difficult to obtain both performance measurements *and* blade geometry of swept propeller blades. The NACA SR-series of propellers have plenty of published data, but details of both their two-dimensional (sectional) and three-dimensional (formation line) geometry is not in the public domain.

At the time of writing there is no data available, to this author's knowledge, on swept propeller blades at an angle of incidence to the freestream and no wake survey data with accompanying blade geometry. As such, there is no data available on 1P load of swept propeller blades or the radial variation of axial performance, so this cannot be validated directly. To this end, the validation criteria for the swept propeller model will be that as in Note 2.4.2, Criterion 1 - *accurate prediction of propeller performance over a range of advance ratio and rotational speed.* So the aim of this validation is to determine the best means of predicting $\frac{dC_T}{dJ}$ and $\frac{dC_P}{dJ}$ over different rotational speeds.

The ideal data is a set of experiments performed on both straight and swept propeller blades. This means that the sweep additions can be isolated on a model validated for straight blades. The report by Evans and Liner (1951) is ideal as the authors tested two straight propellers and a swept propeller in axial flight. There appears to be only one other case published in the literature where a blade element model has been successfully used for performance predictions against this set of data (or any other swept propeller) - the swept propeller model used by Gur and Rosen (2008). In their sweep model, they note that for swept blades, the following considerations need to be taken into account (Gur and Rosen, 2008, pg. 691):

- "The velocity components should be projected in a proper manner onto the cross-sectional plane that, in general, is not normal to the local radius."
- "The contributions [...] to thrust and torque are calculated using an appropriate transformation [...] to the direction of the propeller axis."

Through discussion with the the authors of the paper, it has been highlighted that they also use an Euler transform (Gur and Rosen, 2014), but that they use parallel elements[7]. They also highlighted that they had the same problem finding geometry parameters for the Evans and Liner propeller as encountered in the work for this dissertation, and had to resort to the same method described in the paragraph below.

The geometry definitions used by Whitcomb are described fully in his 1948 report, and in Appendix B. This present work uses a different set of nomenclature, but still uses Whitcomb's definition for building up the formation line of the blade. The three-dimensional vector defining the formation line requires the local sweep angle, but also the *dihedral angle*, κ, at each position. The blade geometry defined by Evans and Liner never included the dihedral angle of the blade, and the blade is not referenced elsewhere. Since it was constructed according to the definitions of Whitcomb, in a similar era, the best methodology was to use the dihedral angle defined in Whitcomb's (1950) publication for a similar planform propeller. This is the same method that Gur and Rosen used in their comparison with Evans and Liner.

Whilst this section is comparing the parallel vs. radial blade element definition on the propeller of Liner and Evans, it is not a true comparison. The blade was designed and constructed using the definition of Whitcomb, and thus the chord, thickness and camber are defined in the plane of the radial blade element. With the formation line, twist angle and chord, the blade three-dimensional geometry may be easily constructed. Once the blade semi-chord line, leading edge and trailing edge are defined, the quarter-chord line may be determined. With

[7]But it is unclear whether they redefine chord and thickness. They also describe the process of building a swept blade element model 'complex' and 'tricky'!

the quarter-chord point of each radial element determined, a parallel element may be defined by drawing a plane of constant Y_B at each quarter chord point, and finding the intercepts with the leading edge and trailing edge. The new parallel chord sections are the distances between the intercepts, and the thickness/chord ratios may be redefined. The change to the camber through this rotation into parallel sections is not easy to determine, however, and it is taken to be the same as defined for the radial elements. With these new elements defined, the transformation matrices for each can be determined.

4.6 AXIAL VALIDATION RESULTS

All the data in this section comes from prediction of the data from Propeller I of Evans and Liner (1951) - the planform of these blades is shown in Figure 4.3. The model has already shown good prediction of the performance of Propeller II, the straight bladed propeller - this is the propeller used in the performance plots of Chapter 3.

4.6.1 UNSUITABILITY OF SIMPLE SWEEP CORRECTIONS

Before looking at the comparison of radial and parallel blade elements over a range of flight conditions, a comparison of sweep corrections at the lowest rotational speed is shown in Figure 4.9. Shown in this figure is the model using radial elements with no legacy sweep corrections (*i.e.,* exactly as described in the preceding sections), and the broken line is the same model with the legacy sweep corrections of Equations 4.6-4.9 from page 163 included.

The predictions using legacy sweep corrections are generally poorer than the predictions without. The slope of $\frac{dC_T}{dJ}$ is incorrect at all advance ratios, and the model generally predicts a lower thrust than the measurements. In the model using legacy sweep corrections, it appears that low advance ratio stall appears at a higher advance ratio than experimental results - and when compared to the models using no legacy corrections. Using the simple sweep corrections, the dynamic pressure at each blade element is reduced by a factor of $\cos^2\Lambda$, which is a factor of about a half at the 70% radius station. Additionally, the angle of attack is increased at each element by the reciprocal of $\cos\Lambda$ such that the sections encounter stall at a lower actual α_R than the "uncorrected" model. The prediction of the power coefficient appears to be slightly better with the sweep corrections than the prediction of the thrust coefficient, but it is difficult to tell over the ranges shown here and in the plots not included in this dissertation. It would interesting to explore the effect of the prediction of drag on the performance characteristics, but without extra experimental data this is beyond the scope of this dissertation.

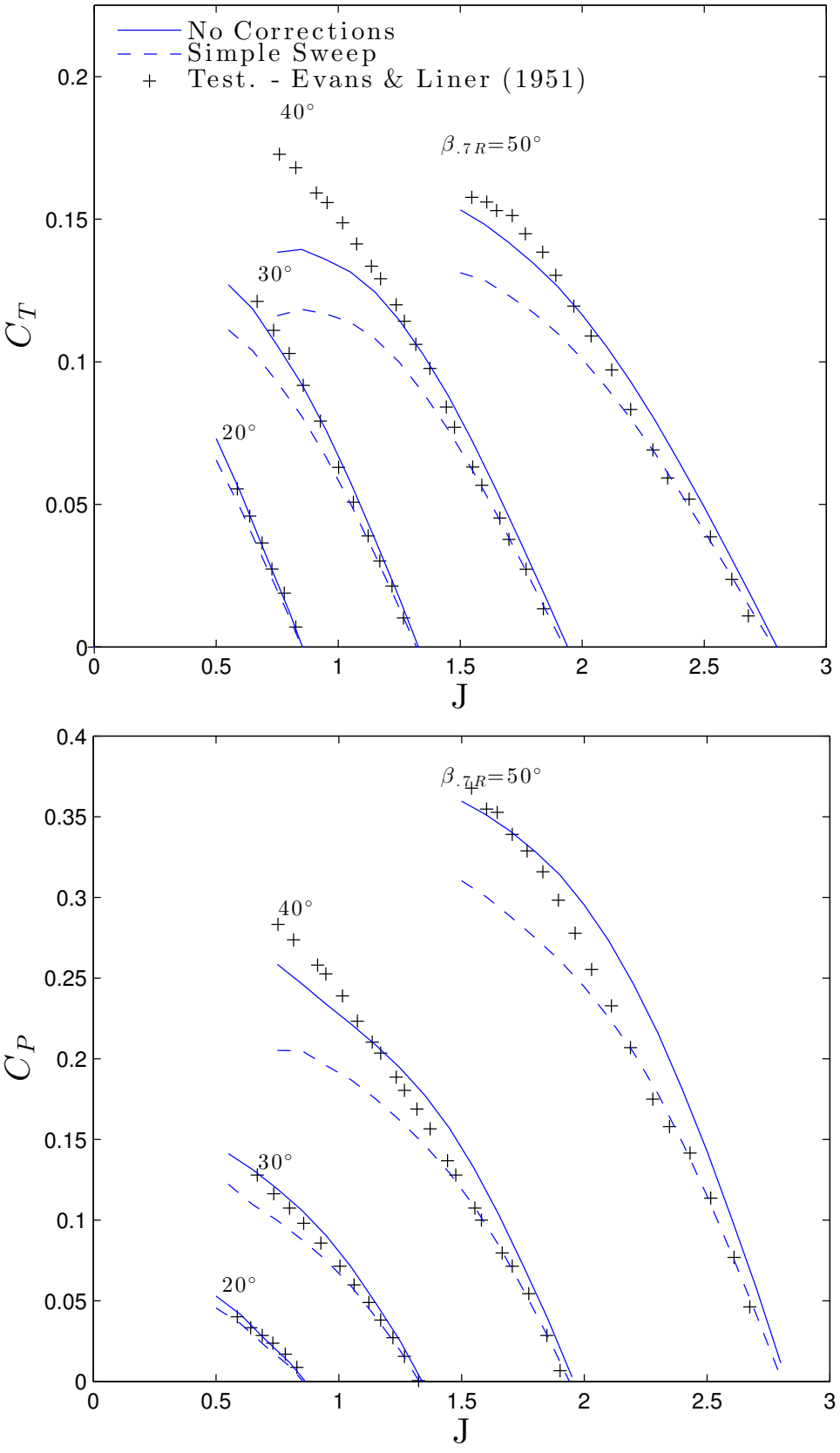

FIGURE 4.9: PERFORMANCE WITH/WITHOUT SIMPLE SWEEP CORRECTIONS VS. TEST DATA FROM EVANS AND LINER (1951) - 1350RPM - BOTH MODELS USING RADIAL ELEMENTS

$\beta_{70\%}$	D/m
20°	3.08
30°	3.07
40°	3.05
50°	3.03

TABLE 4.1: VALUES OF THE DIAMETER, D USED IN DETERMINATION OF PERFORMANCE COEFFICIENTS.

Owing to the poor performance predictions of the simple sweep corrections, and the demonstration that they are ill-suited for swept propeller blades, no further exploration of their performance qualities is included in this dissertation.

4.6.2 PARALLEL AND RADIAL ELEMENT COMPARISON

Compared in Figures 4.10 to 4.12 are the predictions of C_T and C_P vs. J at different blade setting angles over three rotational speeds using parallel and radial blade element definitions. It should be noted that in determination of the non-dimensional performance coefficients, the diameter used is that calculated as per the radial element definition (*i.e.,* it changes with setting angle). This is the definition used by Evans and Liner (1951), and the calculations of the diameter in the formation of the blade geometry match the listed values in their paper. For a fair comparison of the two models, the same value of D is used for both models.

GENERAL OBSERVATIONS: MODEL TRENDS

Firstly, it should be noted that the performance of the models using parallel and radial elements is very similar - particularly at higher advance ratios on each curve. The performance curves of both models move to the right of the experimental data with increasing blade setting angle (*i.e.,* an offset), and far more at the higher rotational speeds. There are two potential reasons for this. The blade setting is difficult to measure in the definition of Whitcomb, as it is defined in the plane of the radial element at $70\%R$. The root setting angle is easy to determine with the Euler transform, but it would be difficult to measure and set the blades in this plane, so the blade setting described in the report may not be wholly accurate. The apparent offset with increasing blade setting/advance ratio is more marked at higher rotational speeds - this highlights that it is potentially due to an aeroelastic untwisting of the blade due to centrifugal forces. Gur and Rosen (2014) investigated this effect, and found that it could account for part of the difference, but could not fully explain it. It is possible, therefore, that a combination of the two effects mentioned is contributing to the noted behaviour. As aeroelasticity was ruled out as contributory to 1P loading, it will not be explored

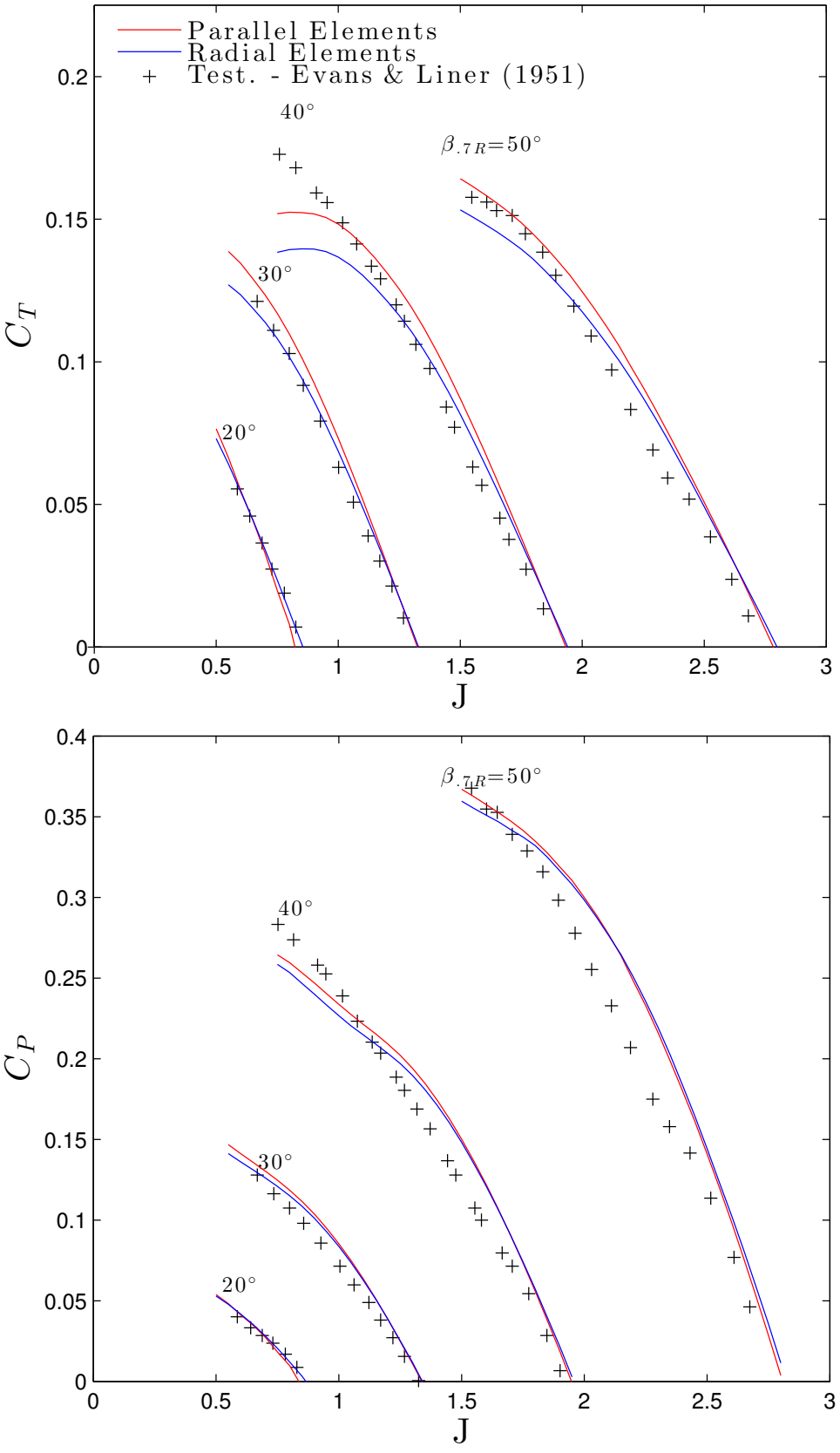

FIGURE 4.10: PERFORMANCE PREDICTIONS WITH PARALLEL ELEMENTS VS. RADIAL ELEMENTS VS. TEST DATA FROM EVANS AND LINER (1951) - 1140RPM - NO SWEEP CORRECTIONS

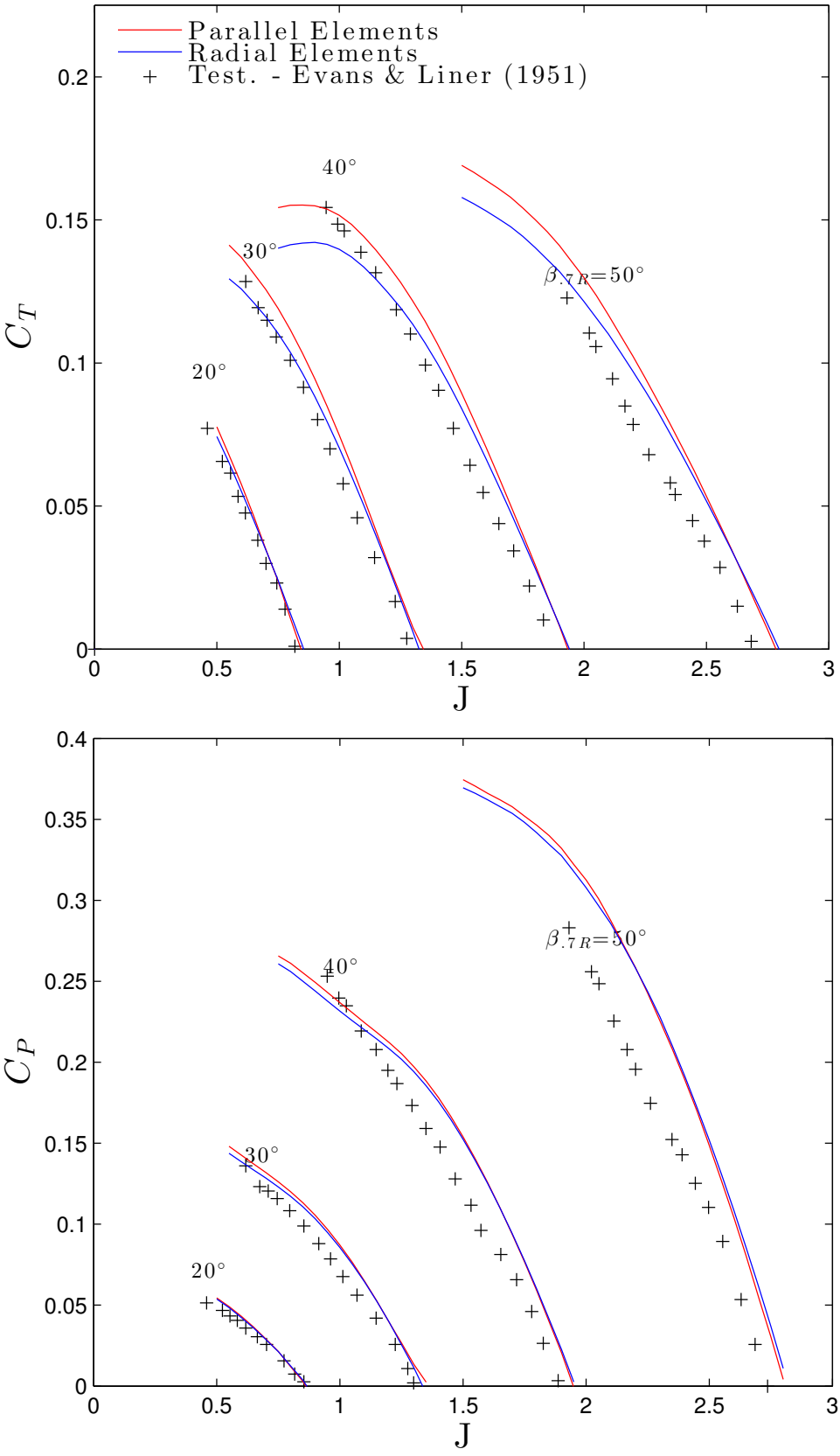

FIGURE 4.11: PERFORMANCE PREDICTIONS WITH PARALLEL ELEMENTS VS. RADIAL ELEMENTS VS. TEST DATA FROM EVANS AND LINER (1951) - 1350RPM - NO SWEEP CORRECTIONS

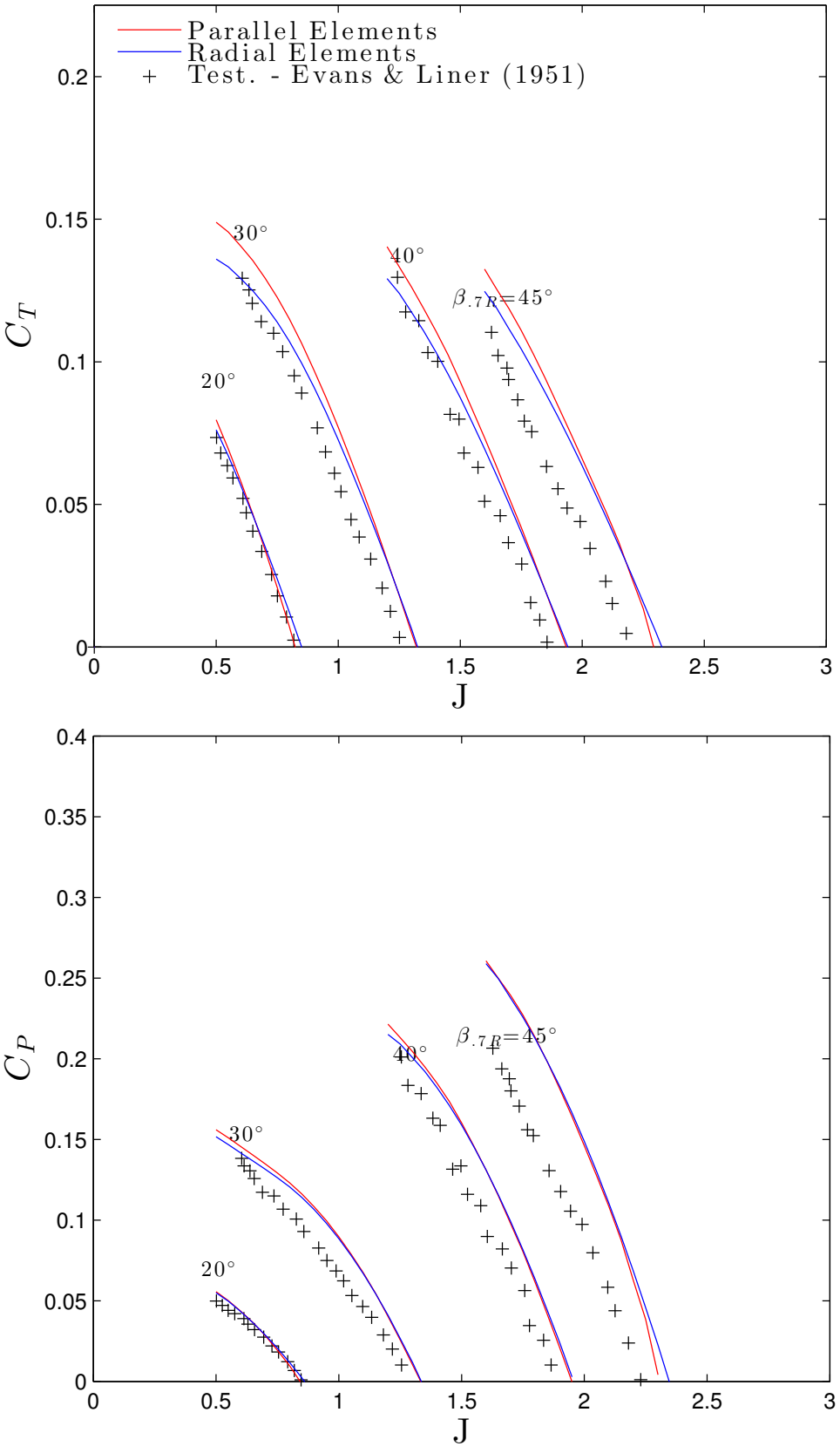

FIGURE 4.12: PERFORMANCE PREDICTIONS WITH PARALLEL ELEMENTS VS. RADIAL ELEMENTS VS. TEST DATA FROM EVANS AND LINER (1951) - 1600RPM - NO SWEEP CORRECTIONS

further. Additionally, Evans and Liner mention that the aerodynamic moment along the pitch change axis was very large for the swept blades, and that special precautions had to be taken to ensure that the blades did not change their own setting by slipping in the root clamps - but it does not say whether this was wholly successful.

Looking at the thrust coefficient predictions, the radial and parallel elements curves tend to have an intersection at $C_T > 0$ and before aerodynamic nonlinearities dominate the curve shape. This is easiest to see in the $\beta = 20°$ and $50°$ at 1140RPM and 20 and $45°$ at 1600RPM. This means that the two models are predicting a different $\frac{dC_T}{dJ}$ over the portion of roughly linear $\frac{dC_T}{dJ}$ in the data. By fitting a linear curve through the data from Liner and Evans in the portion before low advance ratio stall becomes obvious, the ability of the two models to predict the gradient can be determined.

Over the linear portion, the respective error in prediction of $\frac{dC_T}{dJ}$ with the two blade element types can be compared - summarised in Table 4.2, where the percentage errors have been rounded to integer values. For each set of operating conditions, the blade element type with the lowest absolute error has been highlighted in blue. Of the twelve sets of data, the radial elements has the smallest error in nine cases. When the errors are averaged over blade setting angle, the models using radial elements have the smallest error in all cases.

It is difficult to draw firm conclusions from this limited set of data, but it should be noted that the radial elements method always has an error of $< 10\%$, whilst the parallel elements has a maximum error of 34%. The largest errors occur in all models at the lowest blade setting angle, which is also the lowest advance ratio. Whilst this is the smallest curve on the plots, it is also fairly linear. Low advance ratio, by definition, has a greater proportion of tangential velocity in V_R than at high advance ratio. The tangential velocity is poorly resolved by parallel sections, and these show the poorest performance at low advance ratio. At the higher blade setting/advance ratios, the parallel elements seem to perform better than at low setting. This may be due the axial inflow being correctly projected into the blade element plane. In terms of absolute error, however, the two models perform about equally well at the higher setting angles.

With this small data set it is difficult to draw firm conclusions. What is clear is that the two models are performing differently, and this is likely due to the reasons suggested in the preceding sections. Any blade element model is an attempt to represent the three-dimensional blade aerodynamics by superposition of two-dimensional elemental aerodynamics, and this is fairly simple for straight blades, but much more involved on a propeller blade that has sweep and dihedral. The orientation of the blade element clearly has an effect on the prediction of local aerodynamics and by extension the whole propeller performance. The next step is to determine their differences in prediction of once-per-revolution loading.

	Parallel Elements			Radial Elements		
	Rot. Speed/RPM			Rot. Speed/RPM		
$\beta_{70\%}$	**1140**	**1350**	**1600**	**1140**	**1350**	**1600**
20°	34%	13%	17%	**9%**	**4%**	**3%**
30°	13%	1%	5%	**4%**	**-1%**	**-3%**
40°	**1%**	5%	**-2%**	-8%	**-4%**	-9%
45/50°	**2%**	8%	10%	-6%	**0%**	**-1%**
Mean	12%	7%	8%	**$\sim$ 0%**	**$\sim$ 0%**	**-2%**

TABLE 4.2: PERCENTAGE ERROR IN PREDICTION OF LINEAR $\frac{dC_T}{dJ}$ WITH PARALLEL AND RADIAL BLADE ELEMENTS. SMALLEST ERROR FOR SINGLE CASE HIGHLIGHTED IN BLUE.

4.7 1P PREDICTIONS OF A SWEPT PROPELLER

The simple sweep corrections have been used with both types of blade elements modelling a swept propeller at an angle of incidence. In all cases the force gradient variation from the mid-span outboard was reduced by a factor proportional to the local sweep angle. The integrated root bending loads were reduced between 75-90% depending on operating conditions, and the mid and 75% span bending loads were reduced further. Results for the 1P force variation or integrated bending load are not included in this dissertation as without validation data, the figures add little to the discussion and the corrections have been highlighted as ill-suited for this problem.

It has been suggested in Section 4.4.4 that the orientation of blade elements will introduce a phasing component to the once-per-revolution load. For a model formulated using radial elements, if the fluctuating load is modelled for pure disc inclination in axial incident velocity, the position of 1P load extrema will *not* necessarily be 90° and 270°, as they would be on a straight bladed propeller. Additionally, the integrated bending load will likely be lower with any given azimuthal position due to the out-of-phase forcing along the radius.

For Propeller I of Liner and Evans (1951), the $\pm$ thrustwise bending moment has been compared over a range of rotational speeds and disc inclination angles. In Figures 4.13 and 4.14 the root and semi-span thrustwise bending moments are shown as contours of constant bending moment over the range of operating conditions. The plots show the variation at low advance ratio with $\beta_{.7} = 20^\circ$ and $J = 0.7$, and at high advance ratio $\beta_{.7} = 50^\circ$ and $J = 2.25$. What is evident is that the parallel sections, as expected, predict a larger bending moment in these conditions. This is evidenced by red contours being shifted towards the lower left of the plots.

The effect is more pronounced in the semi-span bending load, with the parallel and radial sections showing a greater difference in their predictions. This is to be expected as the semi-span bending loads are composed mainly of the bending fluctuation due to the highly swept sections, and these are the portions for which the parallel and radial elements will show the greatest differences due to the considerations highlighted earlier in this chapter.

With no validation data to compare to, it is difficult to make any strong conclusions on performance or prediction of 1P load. Suffice to say, for pure disc inclination, a model formulated using radial elements will always predict a lower integrated root 1P bending load than one using parallel elements, due to the out-of-phase forcing at different radial stations. In addition, the larger component of tangential velocity resolved into the radial blade elements means that the fractional increase in tangential velocity due to disc in-plane velocity is slightly smaller than for the parallel elements - it is difficult to draw firm conclusions

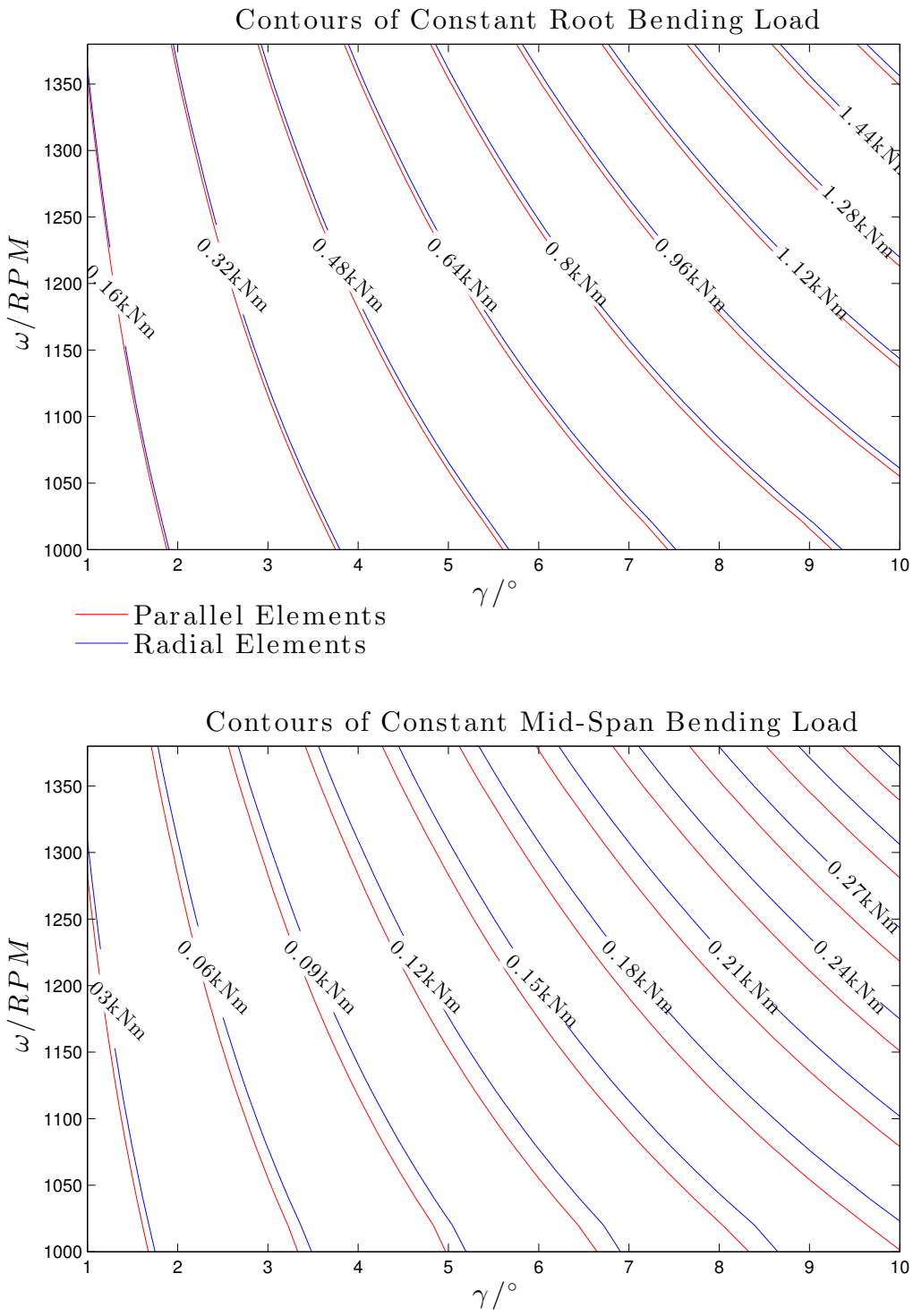

FIGURE 4.13: CONTOURS OF 1P THRUSTWISE BENDING LOAD AT ROOT AND MID-SPAN WITH PARALLEL AND RADIAL ELEMENTS. $J=0.7$, $\beta_{.7} = 20°$

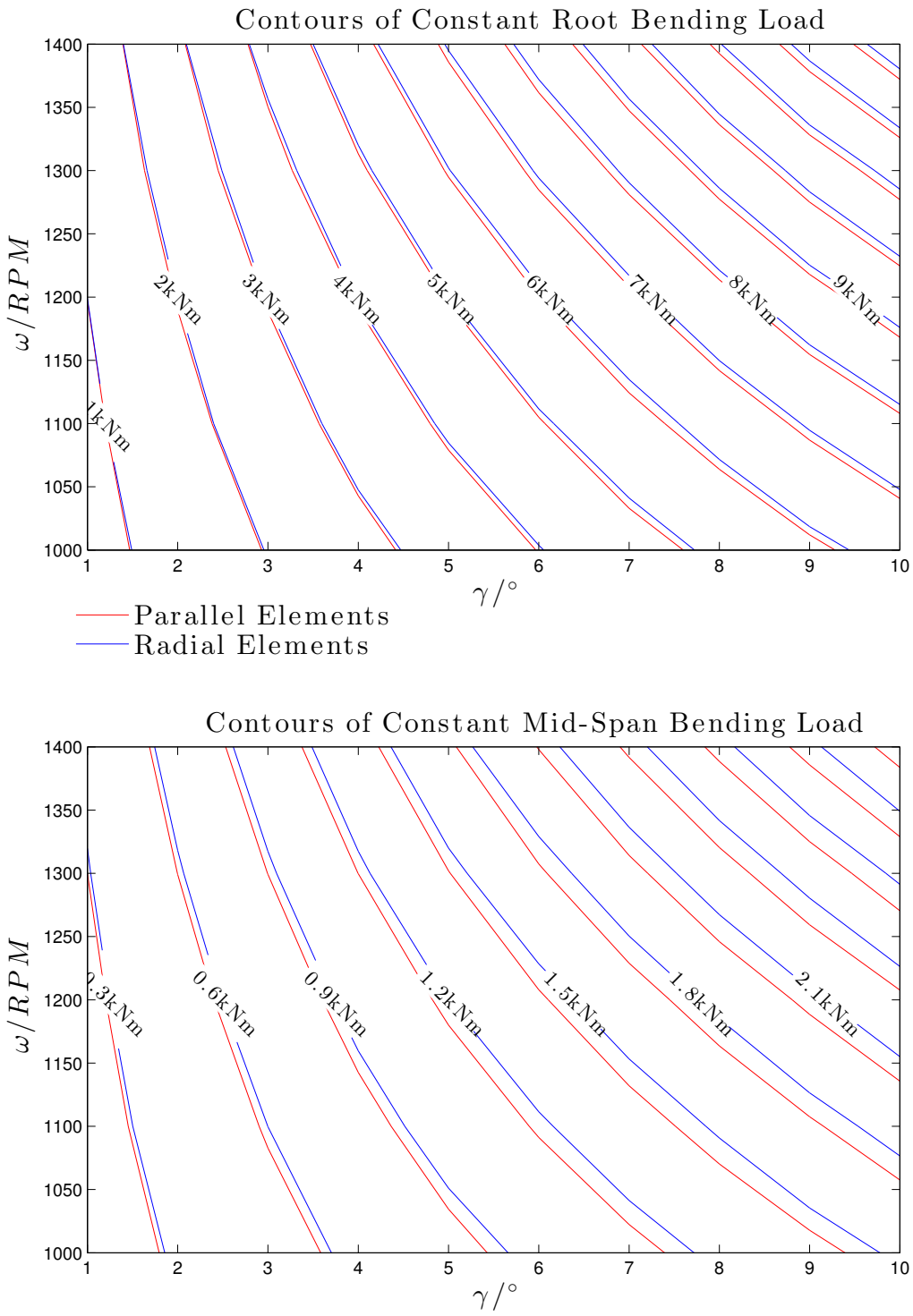

FIGURE 4.14: CONTOURS OF 1P THRUSTWISE BENDING LOAD AT ROOT AND MID-SPAN WITH PARALLEL AND RADIAL ELEMENTS. $J=2.25$, $\beta_{.7} = 50°$

from this limited data set. Suffice to say that there *is* a difference between the two blade element definitions, and this highlights the computational complexity added due to blade sweep..

4.8 FUTURE WORK/FURTHER VALIDATION

Using the two different blade element definitions to model a propeller with swept blades has highlighted the importance of the orientation of blade elements in determination of both the performance characteristics, and the load fluctuation on a propeller at an angle of incidence. Whilst the two models have shown the potential for a variation in load prediction, without a suitable set of data to validate against, it is not currently possible to determine which model is accurately modelling the physical situation. Rather than one or the other being more suitable, it is likely that some combination of both may need to be used to accurately represent the flowfield. Since the radial elements predict a phase shift in the position of the peak load, and the parallel elements do not, an experiment to determine the position of the peak load should be performed.

For proposed future work, a set of blades representative of a modern turboprop should be manufactured, complete with unsteady pressure transducer in the blades. Dynamic PSP (Pressure Sensitive Paint) could be advantageous, but since the flow phenomenon of interest is the azimuthal phasing, the added latency of paint sensitivity would make analysis an order of magnitude more complex. Ideally, a range of blades with increasing levels of sweep will be created. Such blades can be mounted on a propeller rig in a wind tunnel and operated at a range of J, γ, β and n. PIV or LDA measurements of the flowfield will afford determination of the inflow field at the propeller disc plane, and this will provide insight into the position of maximum load when compared with straight blades.

The pressure tappings on the propeller blades will allow determination of the chordwise and spanwise pressure distribution, to a degree. An issue with this method is that the pressure tappings have to be oriented in either the parallel or radial chordwise direction, and this will impact the results. Ideally, both orientations would be compared. Pressure-sensitive paint (PSP) has the potential to determine the whole surface pressure distribution, but the latency in response of PSP systems will complicate the determination of load phasing. A combination of pressure-tapping and PSP would help with post-processing of data, but makes an experimental setup very complex.

4.9 CONCLUSIONS

The addition of sweep and dihedral[8] complicates propeller geometry and aerodynamics. Though it may seem simple to extend an existing model for straight propeller blades to model swept propeller blades, the nature of the problem means that factors taken for granted on a straight blade may not be assumed for a swept one - particularly the coincidence of the pitch change axis and the radius, which determines the extent to which rotational or normal velocities may be resolved into the blade element axis system.

The addition of simple sweep 'corrections' has been argued to be incorrect for a blade element model of a swept propeller blade. Although the addition of sweep to a propeller will change the aerodynamic behaviour, particularly relating to drag properties, a better first order model is to resolve velocities into the blade element axis and apply no sweep corrections at all. For a truly representative blade element model, a rigorous study of the effect of sweep on the two-dimensional behaviour of blade elements needs to be carried out. Until such an experiment/study is performed, it is advised that simple sweep corrections not be used in an engineering-level model.

The effect of sweep on once-per-revolution loading remains to be determined. The orientation of blade elements presents a potential phasing of the position of load extrema, but this effect is only present depending on the definition of blade elements and their respective orientation. Any blade element model is an attempt to represent a three-dimensional flowfield via superposition of two-dimensional flows, and this has been demonstrated to be less suitable for swept blades from geometric considerations. However, the fundamental flow physics of 1P loading on a propeller at an angle of incidence are not likely to be wildly altered by the addition of sweep. That is, the in-plane velocity ($V_\infty \cdot \sin\gamma$) will produce a resultant angle of attack and incident velocity that has extrema *somewhere* on the propeller disc, that may be shifted in azimuth from the 90° and 270° positions due to the addition of sweep/dihedral. Since radial independence is already assumed in a blade element model, a radially-dependent phase shift should not alter the response of the blades in a two-dimensional model. The assumptions made in Chapter 4 regarding induced velocity and unsteadiness should be applicable to swept propeller blades.

For a given axial inflow and rotational speed, the effective velocity at each blade element will pass through a plane somewhere between the radial and parallel element definition. The results using parallel and radial elements may then be thought of as the bounds of the propeller aerodynamic behaviour - but further investigation is required for firm conclusions.

[8]Noting that a designer cannot add sweep without also adding dihedral, except for a single blade setting angle.

CHAPTER 5

INSTALLATION EFFECTS AND MODEL PREDICTIONS

The model that has been formulated and presented in this dissertation has been written from the outset to determine the load variation due to arbitrary incident flow. Whilst there is little validation data for determination of the incident flowfield at the propeller plane of an *installed* propeller, this chapter outlines the effect of different approaches on prediction of once-per-revolution loading.

5.1 INTRODUCTION

The incident flowfield at the disc plane of an installed aircraft propeller can be determined from a variety of methods with a range of complexities. Full RANS CFD calculation has been performed by (Ruiz-Calavera and Perdones-Diaz, 2012), but it too computationally intensive for present usage. A method by Yaggy (1951) utilises a lifting-line model for the wing, and models the flow around the spinner/nacelle and fuselage by axisymmetric potential theory, using centre-line sources. This methodology forms the basis for the methodology currently promoted in ESDU 90020 (Chappell, 2009). Yaggy (1951) and Chappell (2009) highlight the importance of the upwash field induced at the propeller plane by the wing, fuselage and nacelle - as for an installed propeller at an angle of incidence, the installation flowfield can increase the effective angle of incidence in disc axes. ESDU 90020 defines the upwash at the disc plane as:

$$\epsilon \triangleq \tan^{-1} \left. \frac{V_D}{-W_D} \right|_{induced} \tag{5.1}$$

and provides a means of calculating this value at the horizontal centreline of the propeller disc. For determination of propeller normal force (discussed in Chapter 6), yawing moment, and for blade vibration purposes, the data sheet advocates taking the value of upwash at the 70% radial station and using this

value as an effective disc inclination angle.

$$\gamma_e = \gamma_g + \epsilon_{.7R} \tag{5.2}$$

The data sheet states that the horizontal distribution of ϵ will likely be asymmetric and it suggests taking the mean value of advancing and retreating blades:

$$\gamma_e = \gamma_g + \frac{\epsilon|_{\pi/2} + \epsilon|_{3\pi/2}}{2} \tag{5.3}$$

> "One simple means of allowing for this [*incident flow asymmetry*] in determining γ_e might be to use the average of the values of $\epsilon_{0.7}$ at $\psi = 90°$ and $270°$."
>
> Chappell (2009) - ESDU 90020: Airframe-induced upwash at subsonic speeds.

The data sheet notes that this hypothesis is untested for a propeller at an angle of incidence and that suitable test data are unavailable, so the potential difference between using a nonuniform incident flowfield and an equivalent uniform one (*i.e.,* γ_e in uniform V_∞) will be explored in this chapter.

5.2 INSTALLATION MODELS

The model of Yaggy (1951) has been extended to include the axial velocity increment and to determine the entire three-dimensional flow around the spinner/nacelle, fuselage and wing. Validation of this model for prediction of the upwash at the propeller plane is presented in Appendix C. In coupling this model with the propeller model presented in the preceding chapters, three methods are compared:

1. Disregard installation effects and use $\gamma = \alpha_{a/c}$ in Eq. 2.9 to determine velocity in blade-fixed axes - uniform freestream incident velocity.

2. Determine the equivalent upwash angle, Eq. 5.3, and model the isolated propeller at incidence $\gamma = \bar{\epsilon}_{0.7}$ using Eq. 2.9 to determine velocity in blade-fixed axes - equivalent uniform incident velocity.

3. Determine the velocity field $\vec{\mathbf{V}}_{\mathbf{D}}(r, \psi)$ and use Eq. 2.10 to determine velocity in blade-fixed axes - fully nonuniform incident velocity.

For utilisation of the propeller at incidence model developed in this dissertation, a suitable means of determining the flowfield at the propeller disc plane is recommended - incorporating viscous effects and compressibility if necessary. The

potential model developed for this chapter is adequate to determine the upwash at the horizontal centerline of the spinner and, by extension, *should* accurately determine the incident flowfield, but it is only validated for the upwash at the horizontal centerline. The discussion in this chapter is a comparison of the potential effect of using a uniform vs. nonuniform incident velocity field on blade once-per-revolution loading. Prediction of the three-dimensional flowfield at the propeller disc plane using the combined potential/vortex lattice model described in Appendix C validates well for determination of the upwash angle at the fuselage centerline - calculated via Eq. C.7. Without further validation data the comparison in this chapter is included as a hypothetical comparison of the potential effect of uniform vs. nonuniform incident flow on a propeller at an angle of incidence.

Looking at the results for the upwash effect, in Figure C.5, on page 245, it is apparent that the spinner/nacelle provides the largest flow disturbance at the propeller disc plane, when compared to the fuselage and wing effects. Clearly a higher-order spinner model should be utilised in an industrial code, such as a surface panel model. The purpose of this chapter is to **explore the effect of modelling the incident flow field as uniform vs. nonuniform** - as industrial 'best practice' as suggested in EDSU 90020 is to use a uniform incident flow approximation, though this approach is questionable since *it is known that the incident flowfield at an installed aircraft propeller at incidence is far from uniform.*

5.3 DISCUSSION OF RESULTS

Figure 5.3 shows the predictions of radial thrust gradient at different radial positions using the three methods of determining the velocity at the disc from the previous page[1]. The data points are taken from (Yaggy, 1951), and the respective error in prediction of $\pm\Delta C'_T$ is given in the legend of each plot. The first two methods both predict lower variations of thrust at every radial station. This is true of the 'mean upwash' method at $67\%R$, where there is an error over twice as large as that of the 'fully nonuniform' method, despite γ_e being based on data taken from $70\%R$. The flow around the combined spinner/nacelle, wing and fuselage is asymmetric with the upwash due to the nacelle decreasing with wing spanwise distance. Since the propeller in these results rotates inboard-down[2], the downgoing blade is the 'advancing' blade, and experiences a greater $\Delta\alpha_R$ and ΔV_R than the upgoing, 'retreating' blade. The methodology of ESDU 90020 disregards this difference and effectively applies the mean angle of attack and resultant velocity at both azimuthal stations, hence the underprediction.

Figures 5.2 and 5.3 show the integrated bending load over the measured sta-

[1] Results using the third methodology (the entire incident flowfield) have been presented in Chapter 3, to compare the effect of different momentum models.

[2] CCW when viewed from front, positioned on the port wing.

tions (from $34\%R$ to $85\%R$) and the spanwise variation of the thrust gradient change, respectively. Using the full nonuniform flowfield shows the smallest error in prediction of ΔC_M with an order of magnitude of error less than 10%. The method of ESDU 90020 has an error twice as large, and using the geometric angle of attack alone predicts a change in root bending moment half that of the measurements. The respective radial predictions of the three modelling approaches is shown in Figure 5.3, where the methodology utilising the fully nonuniform distribution of incident flow shows not only the most accurate prediction compared to the data, but also the largest prediction of $\Delta C'_T$.

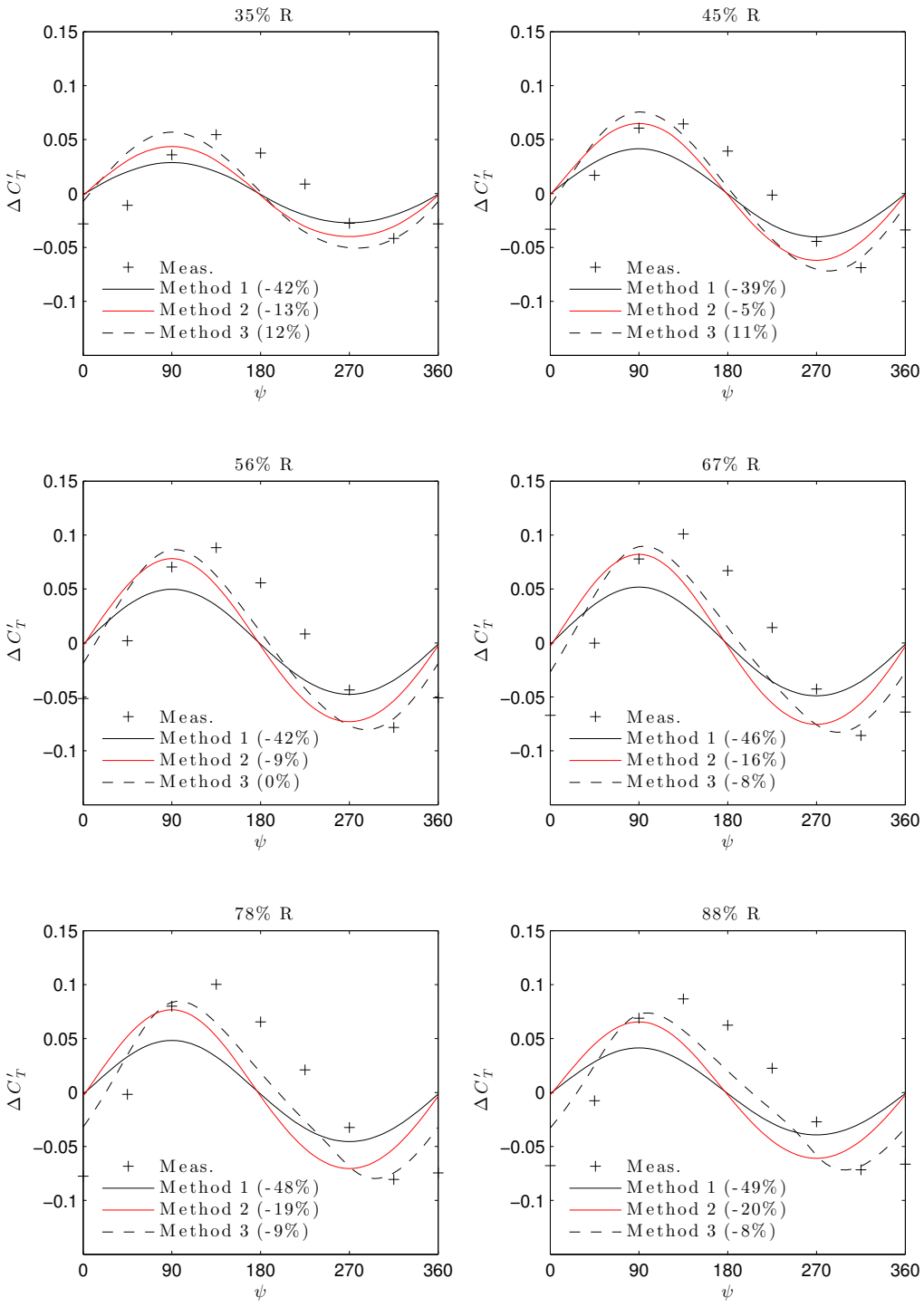

FIGURE 5.1: THREE METHODS OF DETERMINING VELOCITY IN BLADE AXES DUE TO NONUNIFORM INCIDENT FLOWFIELD COMPARED IN PREDICTIONS OF C_T' VS. ψ. ERRORS IN PREDICTION OF $\Delta C_T'$ SHOWN.
METHOD 1: NO INSTALLATION.
METHOD 2: EQUIVALENT INCLINATION DUE TO UPWASH.
METHOD 3: FULLY NON-UNIFORM FLOWFIELD.

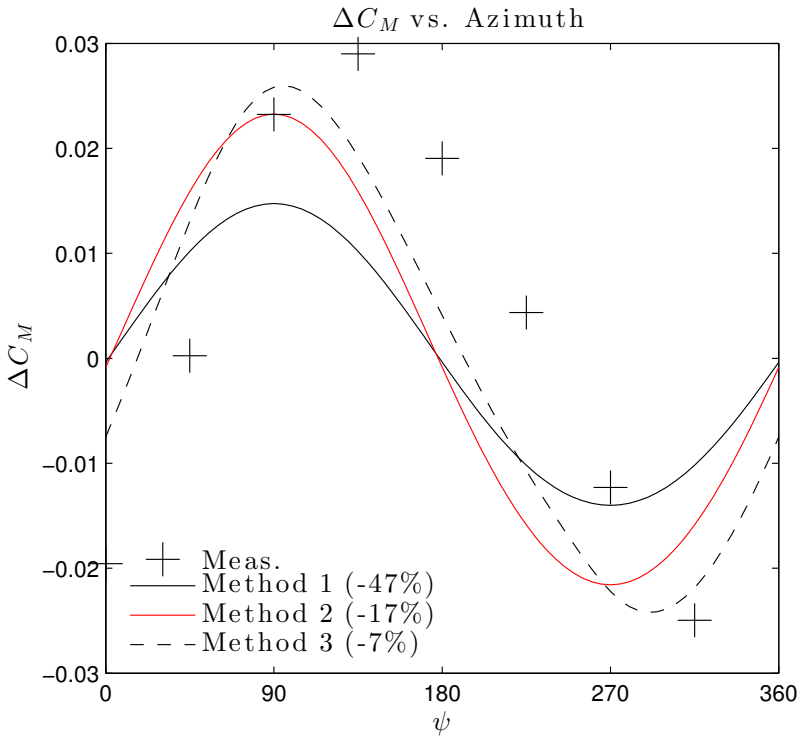

FIGURE 5.2: PREDICTIONS OF C_M VS. ψ. ERRORS IN PREDICTION OF ΔC_M SHOWN.

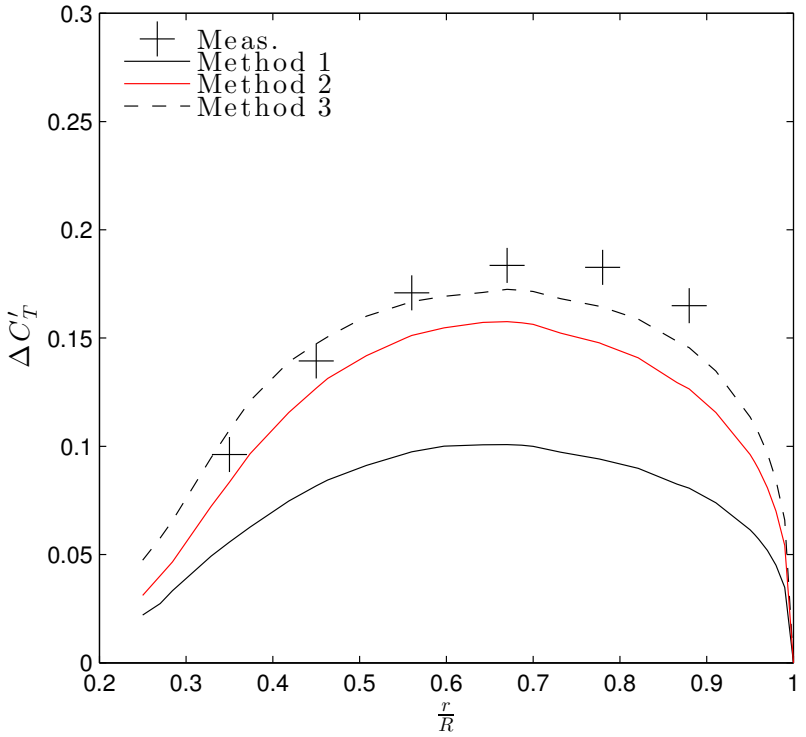

FIGURE 5.3: PREDICTIONS OF $\Delta C'_T$ VS. x.
METHOD 1: NO INSTALLATION.
METHOD 2: EQUIVALENT INCLINATION DUE TO UPWASH.
METHOD 3: FULLY NON-UNIFORM FLOWFIELD.

5.4 MODEL PREDICTIONS

With the model developed for installation showing reasonable validation to the data available, it can be used to show potential differences with other loading conditions. An aircraft at an angle of attack, $\alpha_{\text{a/c}}$, and sideslip, $\beta_{\text{a/c}}$ will produce an incident flowfield at the propeller disc that has loading extrema dependent on both angles. Whilst the methodology of ESDU 90020 is for angle of attack only, in that it determines the equivalent upwash at the horizontal propeller plane, it may be extended by considering the *sidewash*, τ at the vertical propeller plane, defined as

$$\tau \triangleq \tan^{-1} \left. \frac{U_D}{-W_D} \right|_{induced} \tag{5.4}$$

With the equivalent upwash and sidewash angles, an installed propeller can be converted into two equivalent inclination angles, $\gamma_1 = \bar{\epsilon}_{0.7}$ about X_D and $\gamma_2 = \bar{\tau}_{0.7}$. With these two angles, a propeller can be pitched and yawed with respect to the freestream through γ_1 and γ_2 respectively, to provide an equivalent freestream loading condition for combined aircraft angle of attack and sideslip.

Over the range $0 \leq \alpha_{\text{a/c}} \leq 5^\circ$ and $0 \leq \beta_{\text{a/c}} \leq 5^\circ$, predictions using the second and third methods have been compared - the equivalent inclination method and the fully nonuniform incident velocity field method, respectively. The root bending load with each has been calculated, and Figure 5.4 shows the ratio of predicted root bending load using the fully nonuniform method over the equivalent method - showing contours of constant ratio versus $\alpha_{\text{a/c}}$ and $\beta_{\text{a/c}}$. What is clear is that the fully nonuniform method *always* predicts a larger load than using the method of equivalent inclination angle/angles, and the effect is more marked at lower aircraft AoA/SS.

5.5 CONCLUSIONS AND FUTURE WORK

The analysis in this chapter indicates that installation effects have the potential to significantly increase blade once-per-revolution loading. Though this has been known and stated in the literature, a comparison of lower order modelling techniques has not been performed - probably due to lack of suitable validation data. The installation model used in this chapter is a good research tool, but will need more validation and refinement for use in actual industrial design. What the model has served to show is that if installation effects predict changes in aerodynamic environment with azimuth and radius, these should be correctly resolved into disc axes and utilised in a blade element model. The model presented in this dissertation for a propeller at an angle of incidence has been formulated to accept such a flowfield, and this work has shown that it works to a reasonable degree of accuracy.

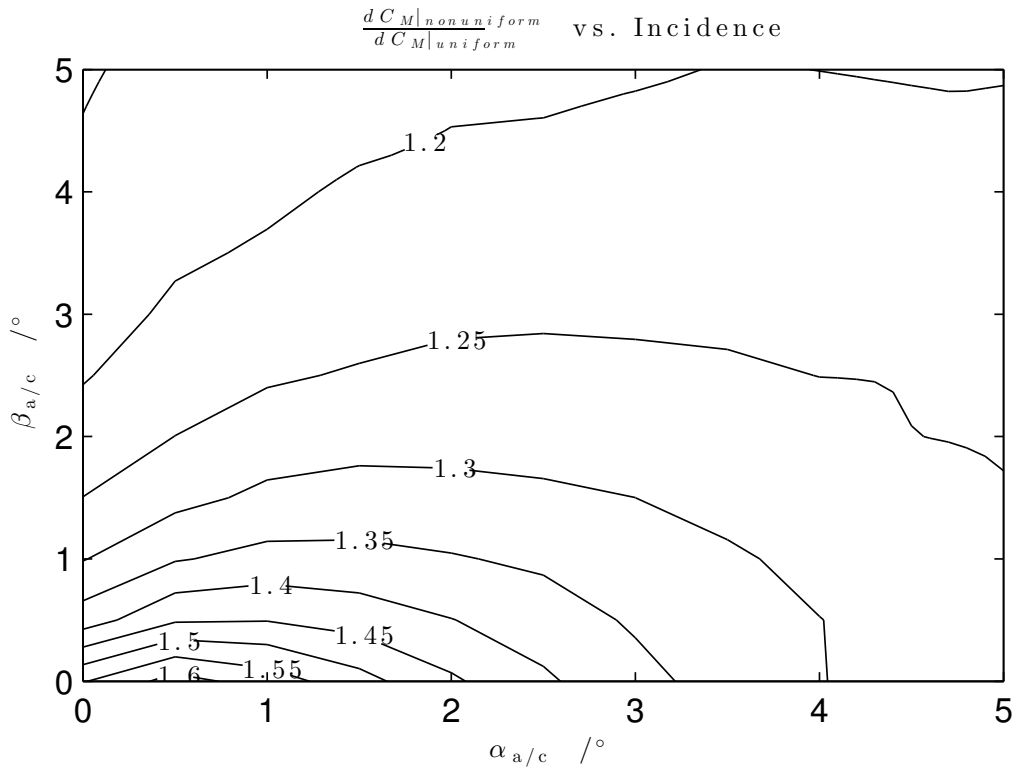

FIGURE 5.4: CONTOURS OF THE RATIO OF PREDICTED ROOT BENDING MOMENT BETWEEN NONUNIFORM INCIDENT VELOCITY AND UNIFORM INCIDENT VELOCITY. VALUES > 1 INDICATE A LARGER PREDICTION WITH NONUNIFORM VELOCITY.

A wind tunnel test with flowfield measurements of the incident velocity field at the propeller would provide invaluable insight and validation data. It has been shown the the slipstream due to a tractor propeller affects the lift distribution on an aircraft wing (Lino, 2010), but the variation of this effect with high wing loading and sideslip has not been explored. A combined experimental and numerical study to determine the salient flow phenomena would be advantageous, but is far beyond the scope of this dissertation.

CHAPTER 6

IN-PLANE FORCES

With a model for blade 1P loading validated for azimuthal variation of blade forces, it *should* model related phenomena. Particularly, the in-plane force reacted at the propeller shaft by the blades of a propeller at incidence. A naïve application of a blade element model, using sWMT to determine the in-plane forces and using standard Equations, leads to a curious conclusion - sWMT actually *underpredicts* the in-plane force, and a uniform induced flow (sAMT) actually predicts the in-plane force *better* (though still not that *well*!).

The in-plane force arises due to the same periodic load fluctuation, but due to the increase in *tangential load* rather than *thrust load*. The means of calculating in-plane force in a blade element model is well-documented, by Glauert (1943, 1926b), de Young (1965) and Chappell (1989). Section 6.1, below, outlines the traditional means of determining in-plane load due to a disc inclination angle.

6.1 THE TRADITIONAL DETERMINATION OF IN-PLANE FORCES

On a propeller at an angle of incidence, γ, the fluctuating sectional velocities have been outlined in Chapter 2. Since advance angle will be a function of azimuthal position it may be denoted as the sum of a mean $\overline{()}$ and a fluctuating $()'$ component:

$$\phi = \overline{\phi} + \phi' \sin\psi \tag{6.1}$$

and hence so may angle of attack, lift and drag:

$$\alpha_R = \overline{\alpha_R} + \alpha' \sin\psi \tag{6.2}$$

$$dC_l = \overline{dC_l} + dC_l' \sin\psi \tag{6.3}$$

$$dC_d = \overline{dC_d} + dC_d' \sin\psi \tag{6.4}$$

and contributions to blade axial and tangential force:

$$dF_{ZB} = \overline{dF_{ZB}} + dF'_{ZB} \sin\psi \tag{6.5}$$

$$dF_{XB} = \overline{dF_{XB}} + dF'_{XB} \sin\psi \tag{6.6}$$

These fluctuating components are what cause the 1P load - and it has been shown in Chapter 3 that for the models compared and the data available, sWMT is the best means of predicting these load variations when compared to wake survey measurements and yawing moment measurements on inclined isolated propellers.

These elemental forces may be integrated and resolved into disc axes to get the total forces experienced at the hub due to a single blade:

$$F_{ZD} = \int_0^R dF_{ZB}\, dr = F_{ZB} \tag{6.7}$$

$$F_{YD} = \int_0^R dF_{XB}\, dr \cdot \sin\psi = F_{XB} \cdot \sin\psi \tag{6.8}$$

$$F_{XD} = \int_0^R dF_{XB}\, dr \cdot \cos\psi = F_{XB} \cdot \cos\psi \tag{6.9}$$

Summating over blades gives the total forces effected at the hub, and inserting the expressions for the fluctuating force due to incidence:

$$\begin{aligned} F_{ZD} &= \sum_{b=1}^{B} F_{ZB} \\ &= \sum_{b=1}^{B} \overline{F_{ZB}} + F'_{ZB} \sin\psi_b \end{aligned} \tag{6.10}$$

$$\begin{aligned} F_{YD} &= \sum_{b=1}^{B} F_{YB} \cdot \sin\psi \\ &= \sum_{b=1}^{B} \left(\overline{F_{YB}} + F'_{YB} \sin\psi_b\right) \cdot \sin\psi_b \end{aligned} \tag{6.11}$$

$$\begin{aligned} F_{XD} &= \sum_{b=1}^{B} F_{YB} \cdot \cos\psi \\ &= \sum_{b=1}^{B} \left(\overline{F_{YB}} + F'_{YB} \sin\psi_b\right) \cdot \cos\psi_b \end{aligned} \tag{6.12}$$

$\psi_b = \psi + \frac{2\pi}{B} \cdot (b-1)$ with ψ being the azimuthal position of blade one. A single-bladed propeller would experience an oscillatory thrust due to the blade oscillatory thrust[1] and a two-bladed propeller would experience a cyclic yawing

[1] Obviously, also a *massive* eccentric problem.

moment, but for $B > 2$, the following trigonometric identities are useful:

$$\sum_{b=1}^{B} \sin\psi_b = \sum_{b=1}^{B} \cos\psi_b = \sum_{b=1}^{B} \sin\psi_b \cdot \cos\psi_b = 0 \tag{6.13}$$

$$\sum_{b=1}^{B} \sin^2\psi_b = \sum_{b=1}^{B} \cos^2\psi_b = \tfrac{B}{2} \tag{6.14}$$

which, when inserted into Equations 6.10-6.12 give:

$$F_{ZD} = B \cdot \overline{F_{ZB}} \tag{6.15}$$

$$F_{YD} = \frac{B}{2} \cdot F'_{YB} \tag{6.16}$$

$$F_{XD} = 0 \tag{6.17}$$

So, a propeller at an angle of incidence produces a steady thrust equal to the *mean blade thrust* multiplied by B, and a constant in-plane vertical force equal to *half the magnitude of the fluctuating tangential force component* multiplied by B. Clearly, both forces are linearly proportional to the number of blades.

The total yawing moment due to disc inclination may also be determined. The moment about the Y-axis will be:

$$M = \sum_{b=1}^{B} \int_0^R dF_{ZB} \cdot r \sin\psi \, dr \tag{6.18}$$

$$= \sum_{b=1}^{B} \int_0^R \left(\overline{dF_{ZB}} + dF'_{ZB} \sin\psi_b \right) \cdot r \sin\psi \, dr \tag{6.19}$$

$$= \frac{B}{2} \int_0^R dF'_{ZB} \cdot r \, dr \tag{6.20}$$

These Equations to determine the in-plane forces and yawing moments may be applied, and compared to measurements from experiments (Yaggy and Rogallo, 1960). Figures 3.24 to 3.27 on pages 139 to 142 have been presented for validation of the induced flow model, and show the prediction of total yawing moment vs. in-plane advance ratio over a range of blade setting angles. The experimental data is plotted as an area covering the upper and lower measurement bounds based on the uncertainty published in the paper. Compared in the figures are the predictions of yawing moment using Equation 6.20 with results from both sAMT and sWMT. Also compared is the methodology from ESDU 89047 (Chappell, 1989). What is apparent is that sWMT is better at predicting the yawing moment in all cases - which has already been shown as part of the validation in Chapter 3.

The improved performance with sWMT makes sense logically as the yawing moment is, from first principles, directly proportional to the fluctuating blade

thrust - and sWMT predicts this the best when compared to wake survey measurements. It can be logically expected that sWMT would also predict the in-plane force with greater accuracy than AMT and also ESDU 89047. Figures 6.1 to 6.4 on pages 196 to 199 show the respective predictions of in-plane force coefficient using sAMT, sWMT and the Equations presented above. Also compared is the methodology from ESDU 89047.

For all disc inclination angles, the in-plane force is underpredicted by sWMT, whilst for the lowest disc inclination angle, sAMT seems to match well with the methodology from ESDU 89047 and predict the results slightly better. Either the steady weighted momentum theory induced flow model isn't predicting the blade tangential force correctly, or the methodology used to predict the in-plane force is incomplete somehow. Through a consideration of the aerodynamic environment of the inclined propeller, it can be shown that Equations 6.11 and 6.12 do not account for a significant contribution to in-plane force.

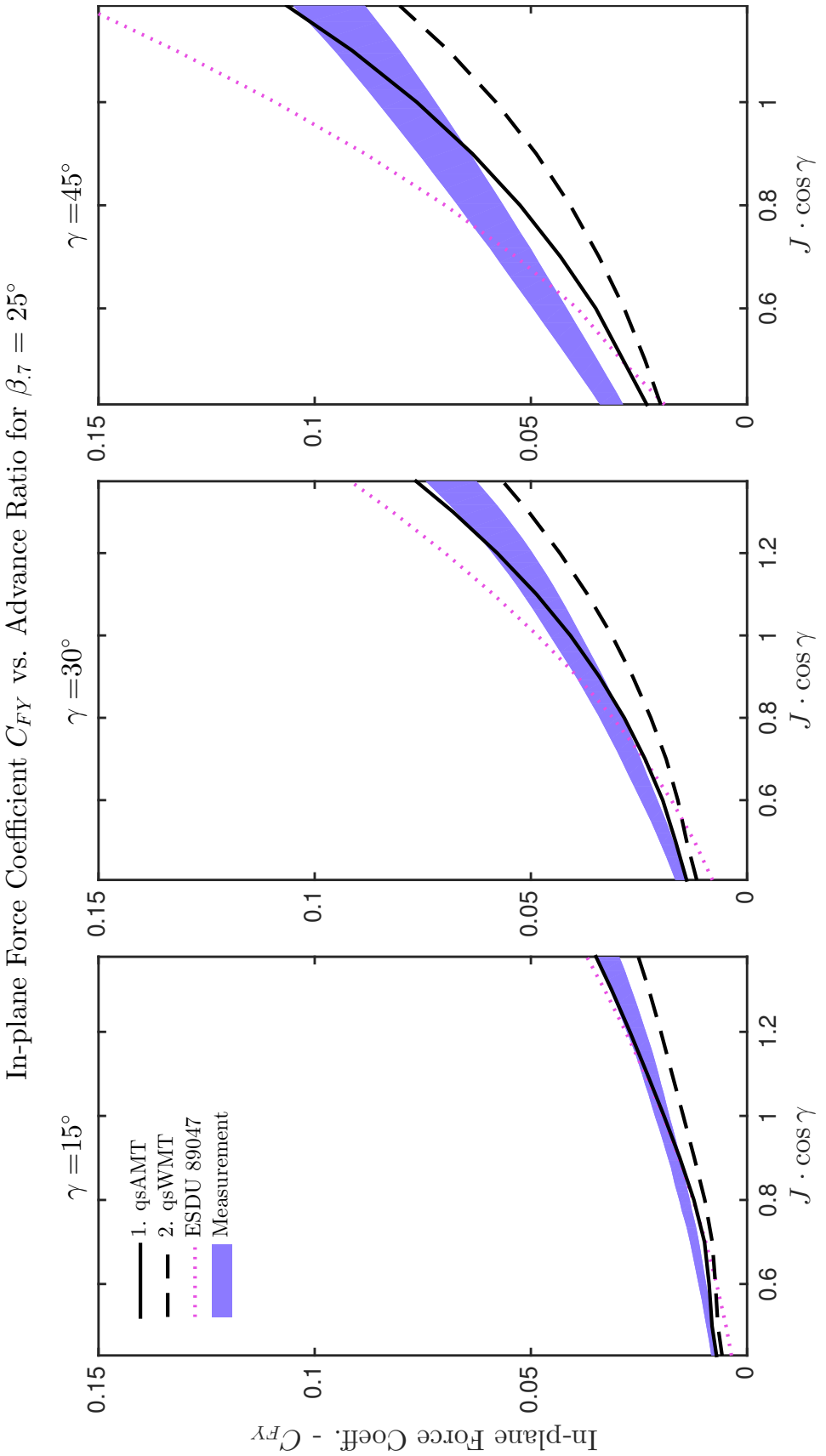

FIGURE 6.1: TOTAL PROPELLER IN-PLANE FORCE COEFFICIENT VS. IN-PLANE ADVANCE RATIO FOR DIFFERENT INCLINATION ANGLES. DATA FROM (YAGGY AND ROGALLO, 1960). $\beta_{.7} = 25°$.

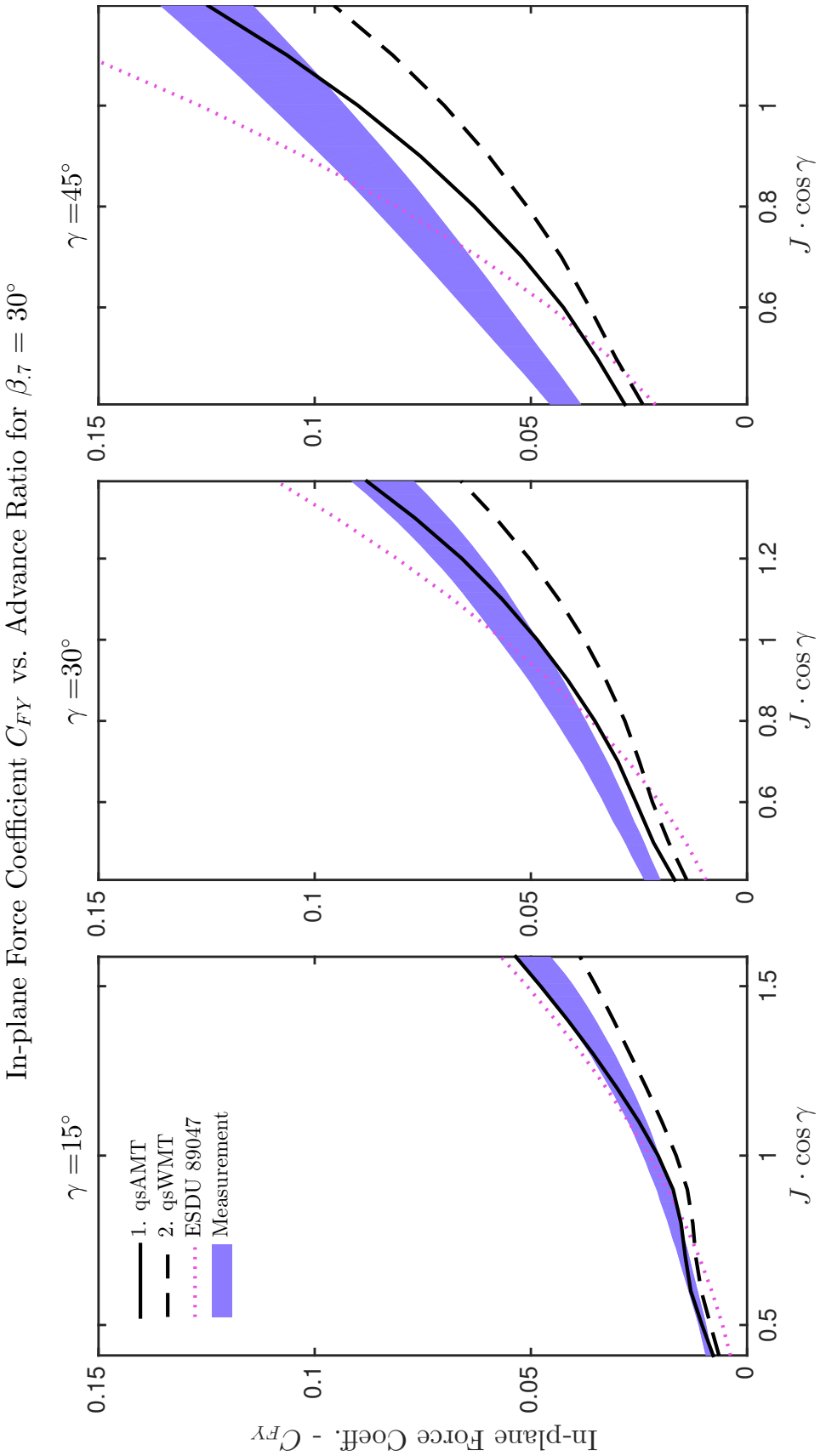

FIGURE 6.2: TOTAL PROPELLER IN-PLANE FORCE COEFFICIENT VS. IN-PLANE ADVANCE RATIO FOR DIFFERENT INCLINATION ANGLES. DATA FROM (YAGGY AND ROGALLO, 1960). $\beta_{.7} = 30°$.

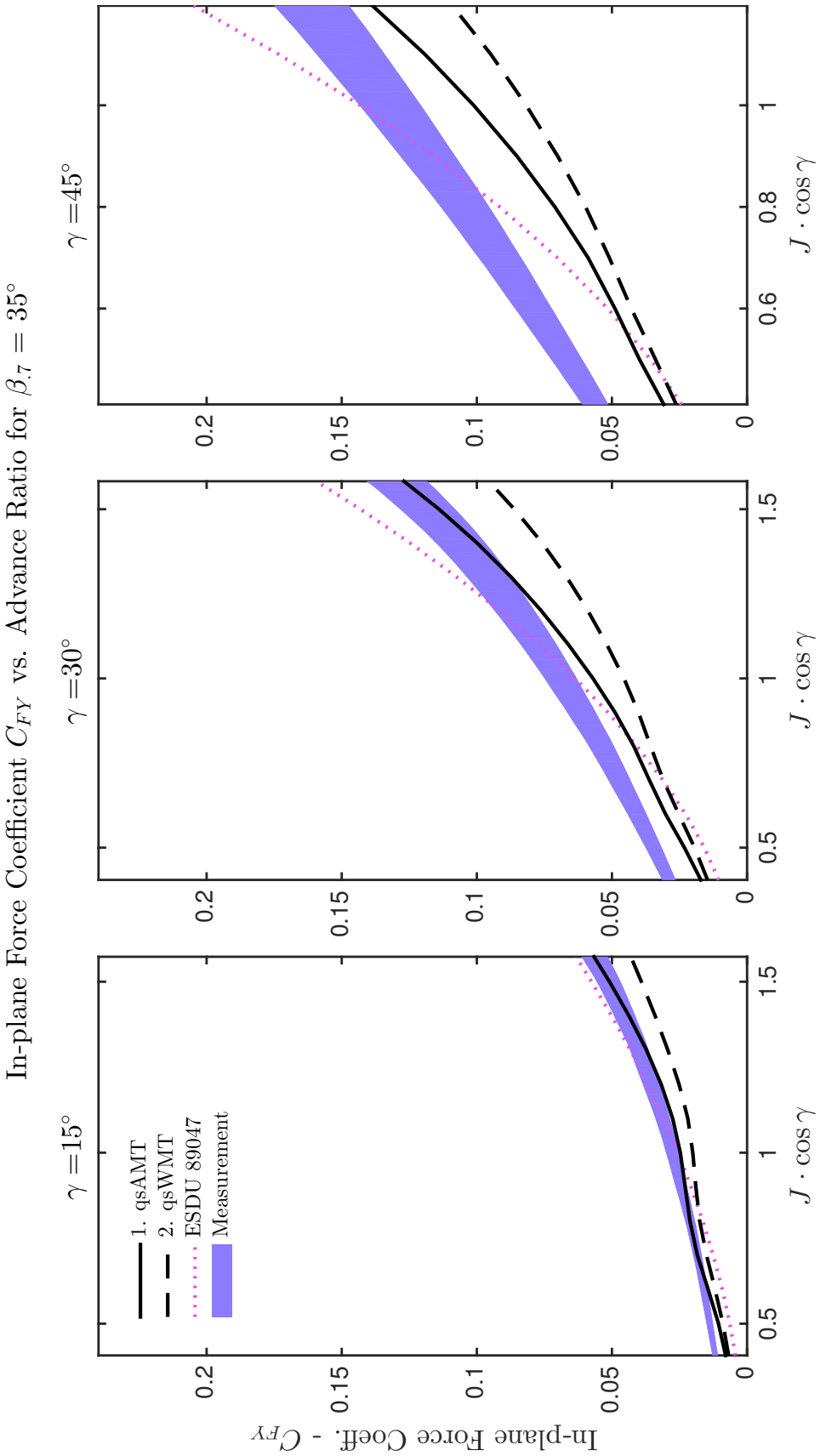

FIGURE 6.3: TOTAL PROPELLER IN-PLANE FORCE COEFFICIENT VS. IN-PLANE ADVANCE RATIO FOR DIFFERENT INCLINATION ANGLES. DATA FROM YAGGY AND ROGALLO (1960). $\beta_{.7} = 35°$.

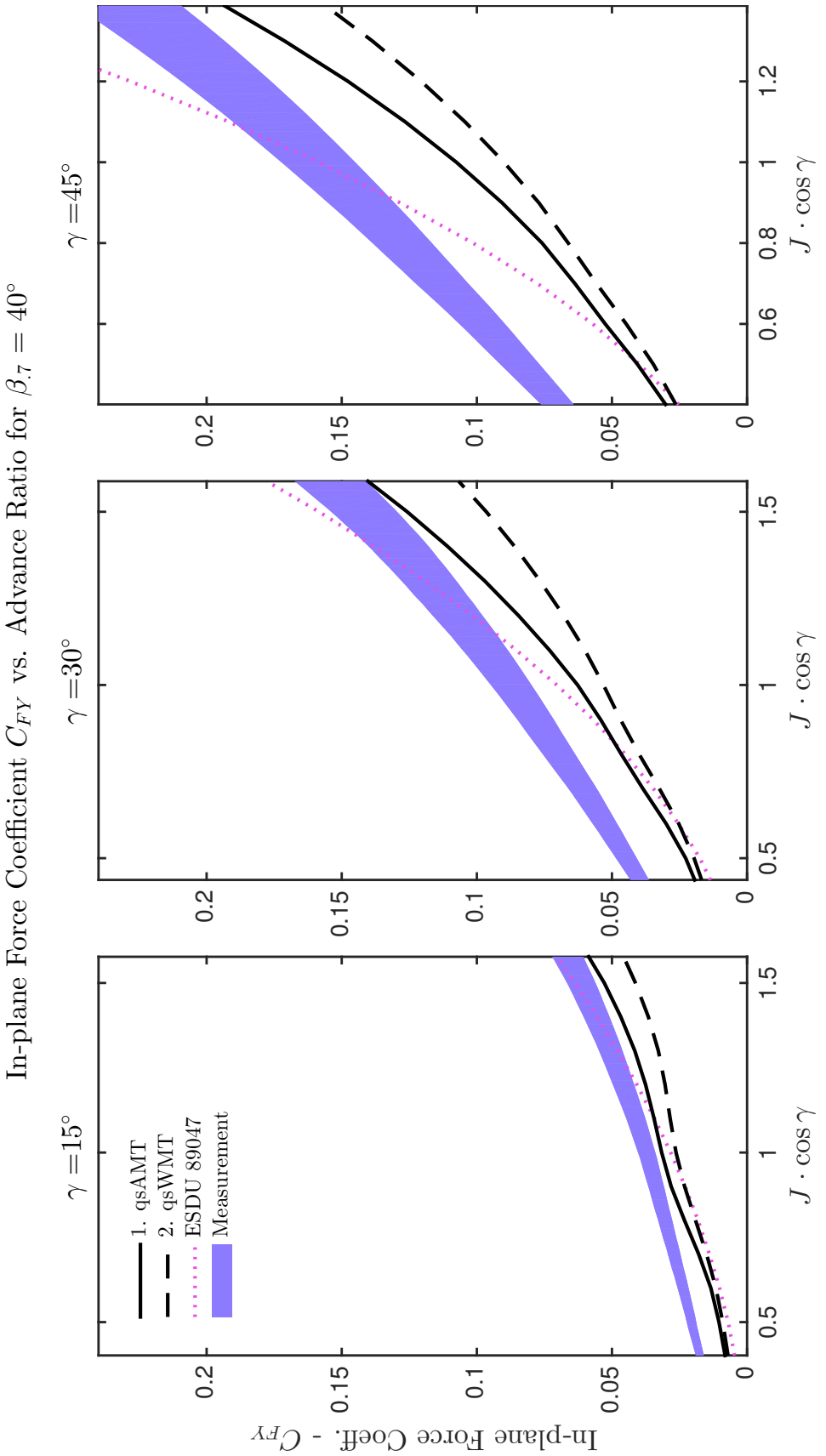

FIGURE 6.4: TOTAL PROPELLER IN-PLANE FORCE COEFFICIENT VS. IN-PLANE ADVANCE RATIO FOR DIFFERENT INCLINATION ANGLES. DATA FROM (YAGGY AND ROGALLO, 1960). $\beta_{.7} = 40°$.

6.2 A VERTICAL CONTRIBUTION TO IN-PLANE FORCE

When coupled with a blade element model, the methodology outlined in the previous section disregards spanwise velocity, as it provides no circulation directly, and does not alter the two-dimensional section aerodynamics. Hence, only the components of velocity normal to the leading edge of the blade are taken into account. For a blade element model of a propeller at an angle of incidence, this is effectively applying infinite wing sweep corrections for the blade section - as clearly the blades at the bottom and top of an inclined disc will have the disc in-plane velocity, $V_D = V_\infty \sin\gamma$, along the blade axis. Figure 6.5 is repeated from Chapter 4 - showing a wing with a constant chord and aerofoil section, sweep angle Λ and onset velocity V.

To accommodate for sweep, sectional velocities are resolved in the direction normal to the leading edge, and hence:

$$V' = V\cos\Lambda \tag{6.21}$$

and the chord is modified:

$$c' = \frac{c}{\cos\Lambda} \tag{6.22}$$

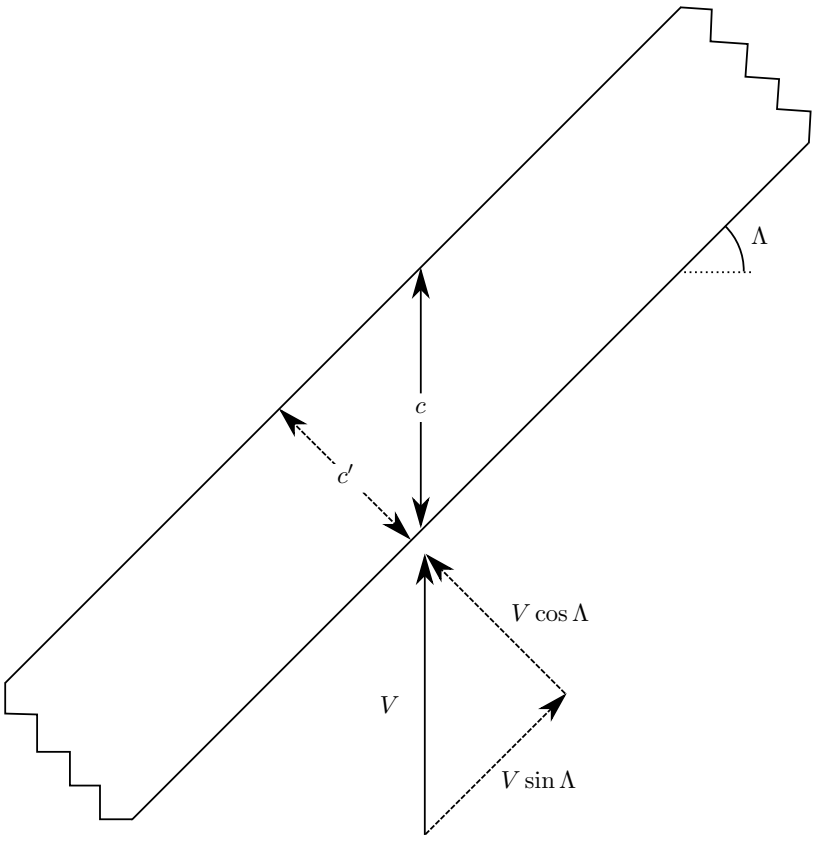

FIGURE 6.5: INFINITE SWEPT WING

The blade at the topmost position of the propeller will have an in-plane onset flow that is the resultant of $\omega \cdot r$ and U_D at some *effective sweep angle*, ζ. In the blade-element model as formulated, the velocity V_{YB} is already resolved into the plane normal to the leading edge, and the chord of the propeller blade section is defined in this plane, so no modification is necessary. Additionally, the change to angle of attack due to this effective sweep is also included implicitly, as the in-plane velocity due to disc inclination is not included in its calculation. The angle ζ may be calculated from the geometry.

$$\begin{aligned}\sin\zeta &= \frac{V_{YD}\cos\psi}{\sqrt{(V_\omega + V_{YD}\cdot\sin\psi)^2 + (V_{YD}\cos\psi)^2}} \\ &= \frac{V_{YD}\cos\psi}{\sqrt{V_\omega^2 + 2\cdot V_\omega \cdot V_{YD}\cdot\sin\psi + V_{YD}^2}}\end{aligned} \tag{6.23}$$

$$\begin{aligned}\cos\zeta &= \frac{V_\omega + V_{YD}\sin\psi}{\sqrt{(V_\omega + V_{YD}\cdot\sin\psi)^2 + (V_{YD}\cos\psi)^2}} \\ &= \frac{V_\omega + V_{YD}\sin\psi}{\sqrt{V_\omega^2 + 2\cdot V_\omega \cdot V_{YD}\cdot\sin\psi + V_{YD}^2}}\end{aligned} \tag{6.24}$$

What isn't taken into account in the blade element model as presented, however, is the change in orientation of the lift and drag vectors, which will be normal to and parallel to the incident flow vector by definition, which makes angle ζ with the chord line - shown in Figure 6.6 for an untwisted blade. Whilst the change to the drag cannot easily be predicted without knowledge of the geometry through this effective chord line (similar to the discussion of parallel vs. radial elements in Chapter 4), a first approximation for the effect this change in orientation has on the tangential force may be used instead.

The calculated value for the blade tangential force from the blade element method is denoted dF_T, but is assumed to act in the direction parallel with the incident flow vector. It has components in blade axes:

$$dF_{XB} = dF_T\cos\zeta \qquad \text{(Tangential Direction)} \tag{6.25}$$

$$dF_{YB} = dF_T\sin\zeta \qquad \text{(Radial Direction)} \tag{6.26}$$

Which gives a new component to add to the disc Y-force (eq. 6.8):

$$dF_{YD} = dF_{XB}\sin\psi + dF_{YB}\cos\psi \tag{6.27}$$

$$F_{YD} = \sum_{b=1}^{B}\int_0^R dF_{XB}\sin\psi + dF_{YB}\cos\psi\, dr \tag{6.28}$$

which may be separated into:

$$F_{YD} = [F_{YD}]_T + [F_{YD}]_R \tag{6.29}$$

and calculated separately, to avoid confusion. First the contribution to in-plane

force from the blade tangential force:

$$
\begin{aligned}
[F_{YD}]_T &= \sum_{b=1}^{B} \int_0^R dF_{XB} \sin\psi \, dr \\
&= \sum_{b=1}^{B} \int_0^R dF_T \cos\zeta \sin\psi \, dr \\
&= \sum_{b=1}^{B} \int_0^R \left[\overline{dF_T} + dF'_T \sin\psi\right] \cos\zeta \sin\psi \, dr \\
&= \sum_{b=1}^{B} \int_0^R \left[\overline{dF_T} + dF'_T \sin\psi\right] \frac{V_\omega + V_{YD}\sin\psi}{\sqrt{V_\omega^2 + 2 \cdot V_\omega \cdot V_{YD} \cdot \sin\psi + V_{YD}^2}} \sin\psi \, dr
\end{aligned}
\tag{6.30}
$$

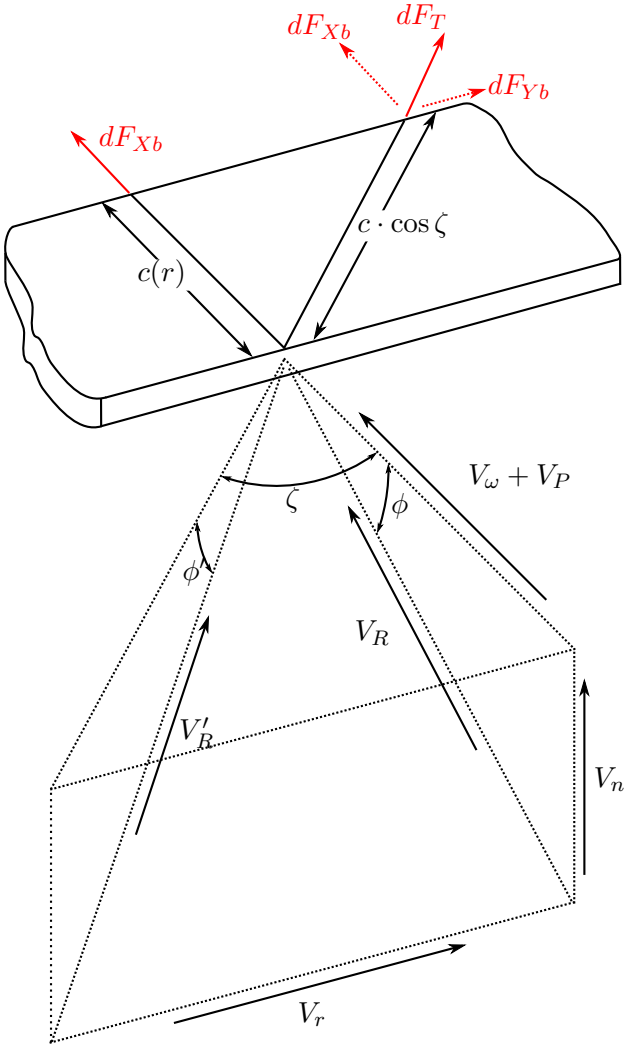

FIGURE 6.6: UNTWISTED BLADE SECTIONAL VELOCITIES, SHOWING EFFECTIVE SWEEP, ζ.

and the contribution due to blade radial force:

$$\begin{aligned}
[F_{YD}]_R &= \sum_{b=1}^{B} \int_0^R dF_{XB} \cos\psi \, dr \\
&= \sum_{b=1}^{B} \int_0^R dF_T \sin\zeta \cos\psi \, dr \\
&= \sum_{b=1}^{B} \int_0^R \left[\overline{dF_T} + dF'_T \sin\psi\right] \sin\zeta \cos\psi \, dr \\
&= \sum_{b=1}^{B} \int_0^R \left[\overline{dF_T} + dF'_T \sin\psi\right] \frac{V_{YD}\cos\psi}{\sqrt{V_\omega^2 + 2 \cdot V_\omega \cdot V_{YD} \cdot \sin\psi + V_{YD}^2}} \cos\psi \, dr
\end{aligned} \tag{6.31}$$

Since the denominators of both Equations 6.30 and 6.31 both contain a $\sin\psi$ term, it is not easy to evaluate the sum analytically, but may instead be performed numerically. Alternatively, considering only the peak loading positions - that is, $\psi = 0, 180°$ for the radial load, and $\psi = 90, 270°$ for the tangential load - and recalling the trigonometric summation identities, Equations 6.30 and 6.31 reduce to:

$$\begin{aligned}
[F_{YD}]_T &= \int_0^R dF'_T \cdot \frac{B}{2} \, dr \\
&= F'_{ZB} \cdot \frac{B}{2}
\end{aligned} \tag{6.32}$$

$$[F_{YD}]_R = \int_0^R \overline{dF_T} \cdot \frac{B}{2} \cdot \frac{V_{YD}}{\sqrt{V_\omega^2 + V_{YD}^2}} \, dr \tag{6.33}$$

Hence, as an approximation, since Equation 6.32 is the same as Equation 6.16, Equation 6.33 can be used as an additional contribution to in-plane force that isn't captured by a traditional blade element methodology using the well-documented Equations for in-plane force. This gives a new formulation for the in-plane force Equation:

$$F_{YD} = \frac{B}{2} \cdot F'_{ZB} + \int_0^R \overline{dF_T} \cdot \frac{B}{2} \cdot \frac{V_{YD}}{\sqrt{V_\omega^2 + V_{YD}^2}} \, dr \tag{6.34}$$

It must be noted that the methodology above is an approximation to this physical effect, and that the three-dimensional aerodynamics of the propeller at an angle of incidence are not modelled by this approach. The recognition of the orientation of the tangential force vector through ζ is more physically realistic than the existing approach, however, and the results will be compared in the next section.

6.3 RESULTS

Using the new formulation in both the numerical and approximate form, Equations 6.30-6.31 and Equation 6.34 respectively, the new predictions of the in-plane force using sWMT are presented vs. the data from Yaggy and Rogallo (1960) in Figures 6.7 to 6.10. It can be seen that both the numerical and the approximate forms have very similar behaviour, and that both models show a better prediction of the in-plane force coefficient than the sWMT and existing Equations, and the ESDU 89047 methodology. The gradient of $\frac{dC_N}{dJ'}$ still appears to be well-predicted when using the new formulation, and the results are displaced vertically in the figures, falling within the range of predictions for $\gamma = 15, 20°$.

The performance at the $\gamma = 45°$ is still a slight underprediction of the measured in-plane force coefficient, and moreso at higher disc loadings. This was also seen in the yawing moment coefficient, and was discussed as potentially being due to the slipstream imparting a larger load on the body at high disc loading.

Results have also been compared with the earlier tests by McLemore and Cannon (1954). The quality of the results printed in this report is much lower than that in the result of Yaggy et al., and it is difficult to reproduce the data in this dissertation without making assumptions. The plots for which values could be reliably extracted in the report by McLemore and Cannon were at very high disc loading and inclination angles, where aerodynamic nonlinearities started to dominate the behaviour of the model. For the lower inclination and setting angles, the model performed well, but differences between the models compared in this chapter were small compared to the measurement and digitisation uncertainty.

6.4 CONCLUSIONS

A re-evaluation of the equations for the in-plane force on a propeller at incidence has been presented that includes a significant component of force that was not present in many previously published sources. The methodology has been presented in both an approximate and numerical form, and may be included easily in a blade element calculation. The results using this method have been compared to a set of experimental data shown earlier in this report, and validates well.

Since the component of in-plane force arises from a radial component of blade force, this provides another component of blade cyclic loading that is not currently modelled. The spanwise force produced will have extrema $\frac{\pi}{2}$ out of phase with the axial/tangential force extrema on a propeller at an angle of incidence, and for a straight bladed propeller this amounts to a force in and out of the hub along the blade Y_B axis. For a propeller with swept blades, however, the displacement of blade elements in the disc plane means that this radial forcing may

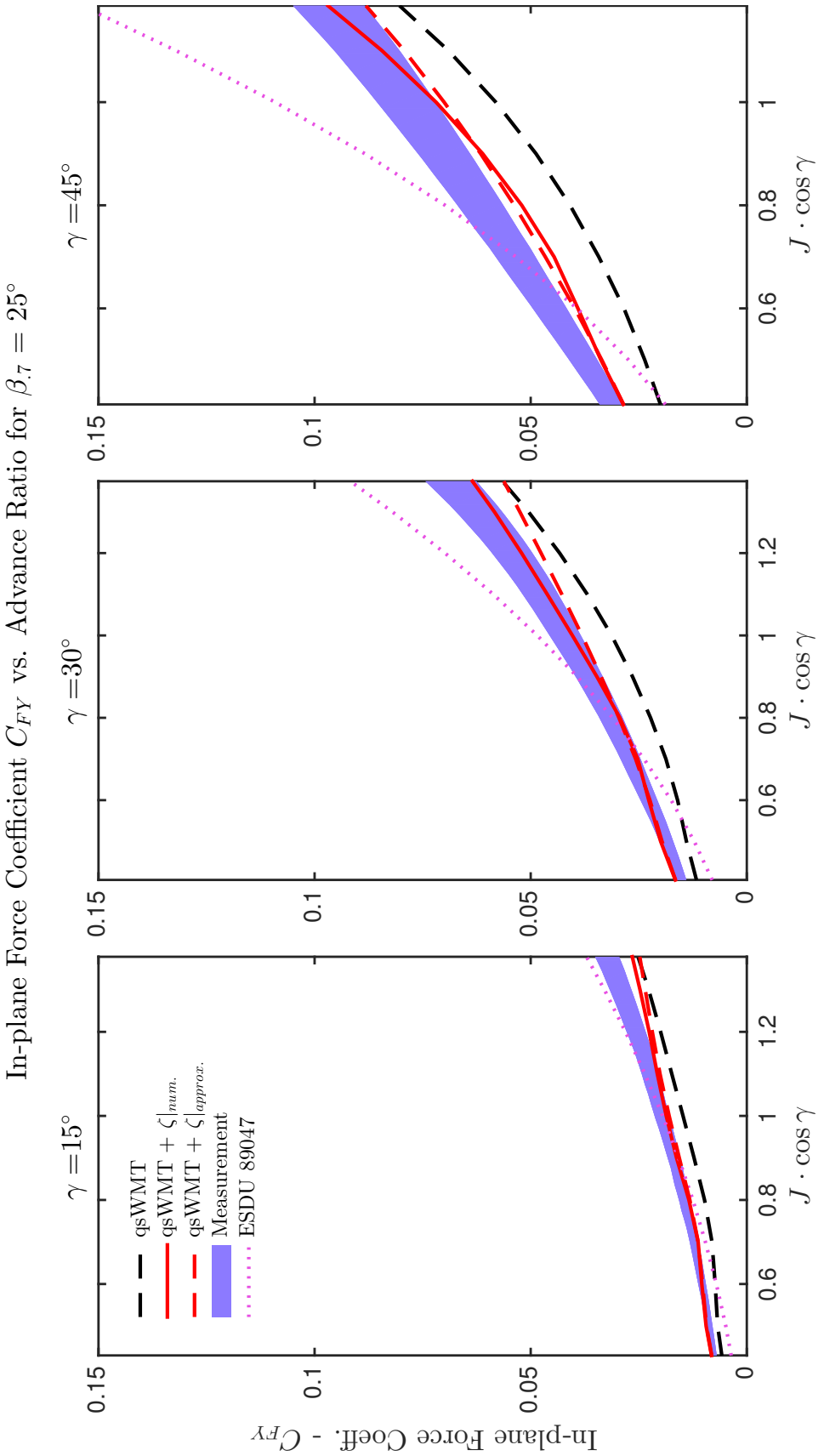

FIGURE 6.7: TOTAL PROPELLER IN-PLANE FORCE COEFFICIENT VS. IN-PLANE ADVANCE RATIO FOR DIFFERENT INCLINATION ANGLES. DATA FROM (YAGGY AND ROGALLO, 1960). $\beta_{.7} = 25°$.

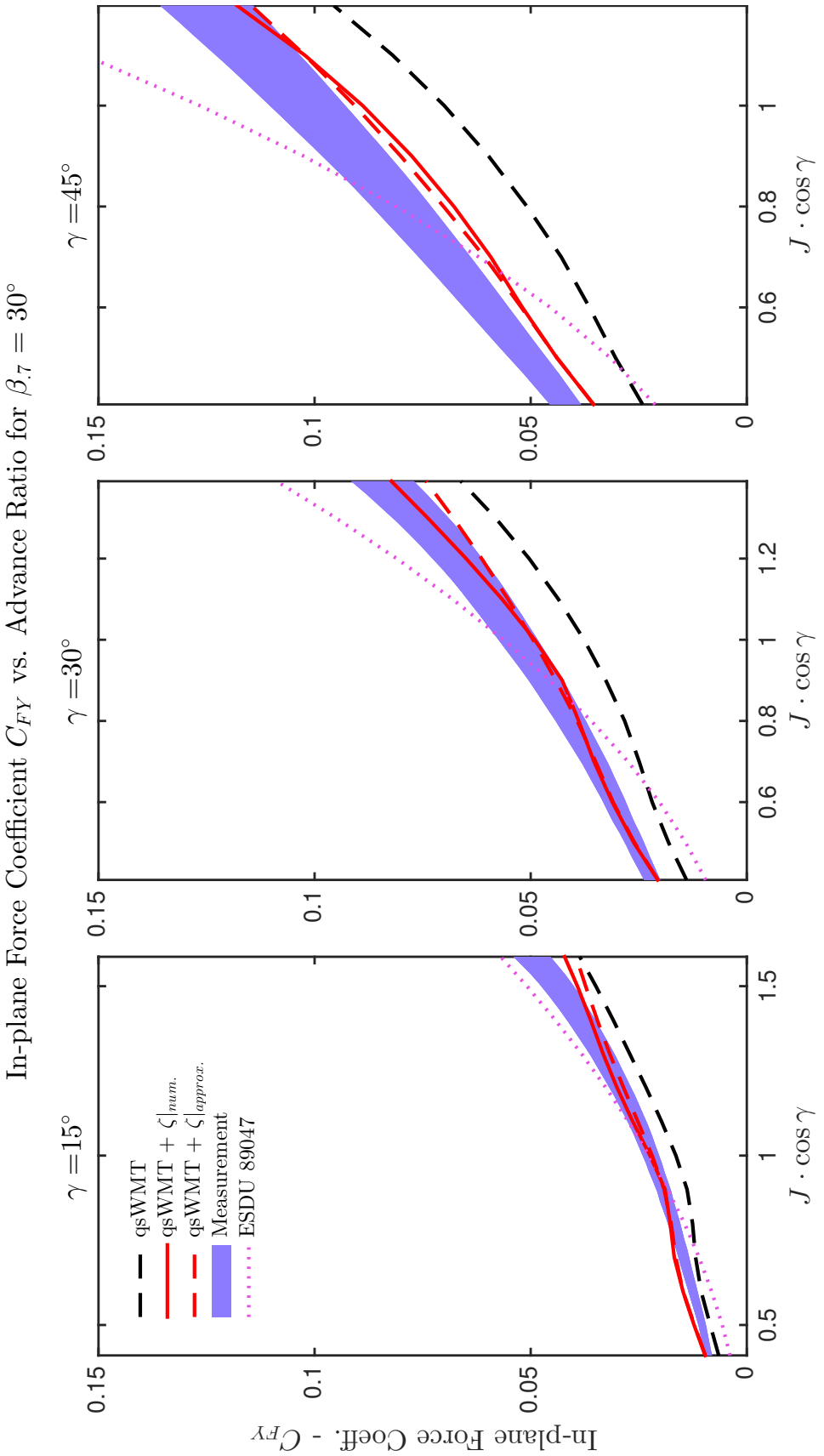

FIGURE 6.8: TOTAL PROPELLER IN-PLANE FORCE COEFFICIENT VS. IN-PLANE ADVANCE RATIO FOR DIFFERENT INCLINATION ANGLES. DATA FROM (YAGGY AND ROGALLO, 1960). $\beta_{.7} = 30°$.

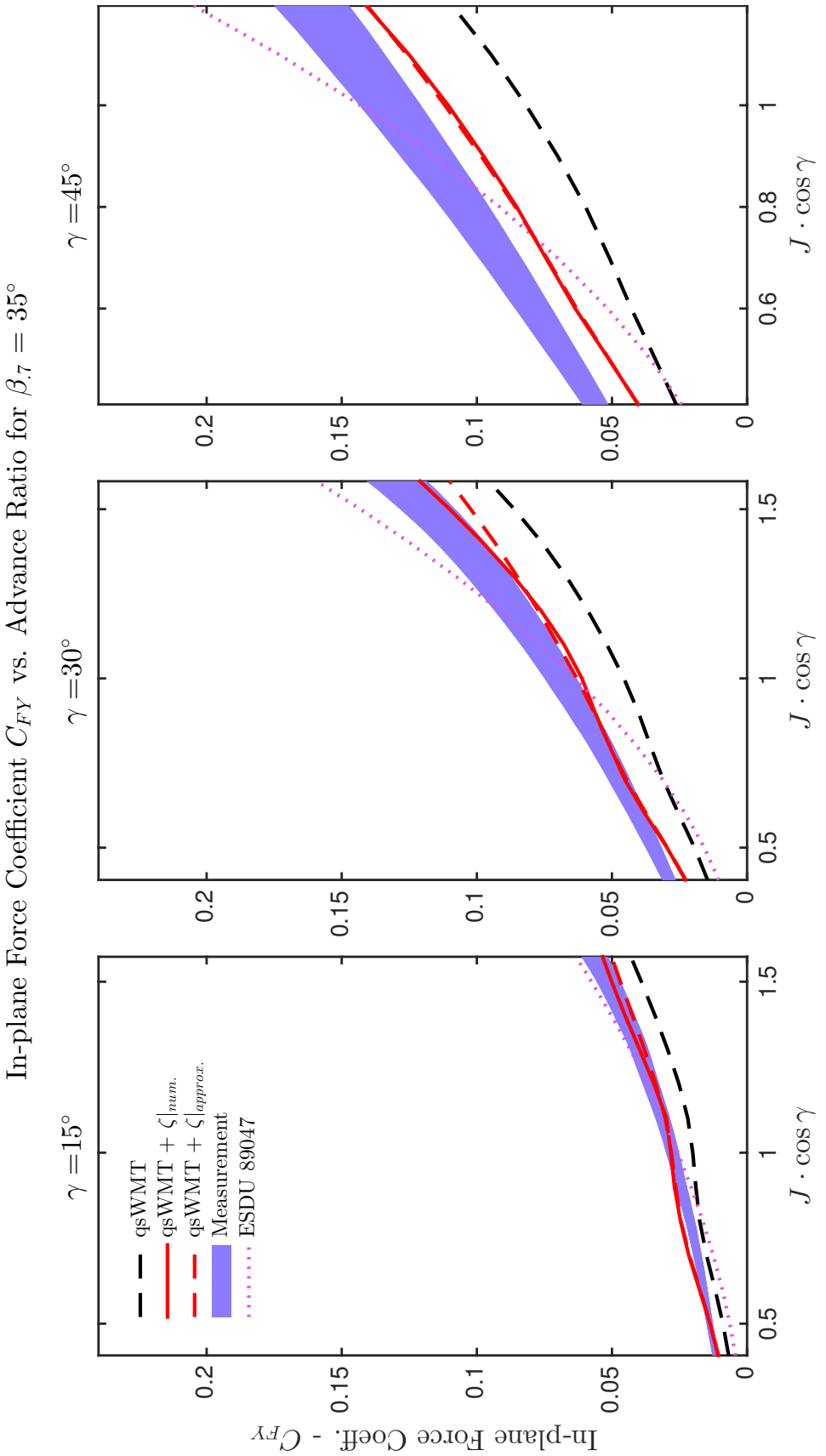

FIGURE 6.9: TOTAL PROPELLER IN-PLANE FORCE COEFFICIENT VS. IN-PLANE ADVANCE RATIO FOR DIFFERENT INCLINATION ANGLES. DATA FROM (YAGGY AND ROGALLO, 1960). $\beta_{.7} = 35°$.

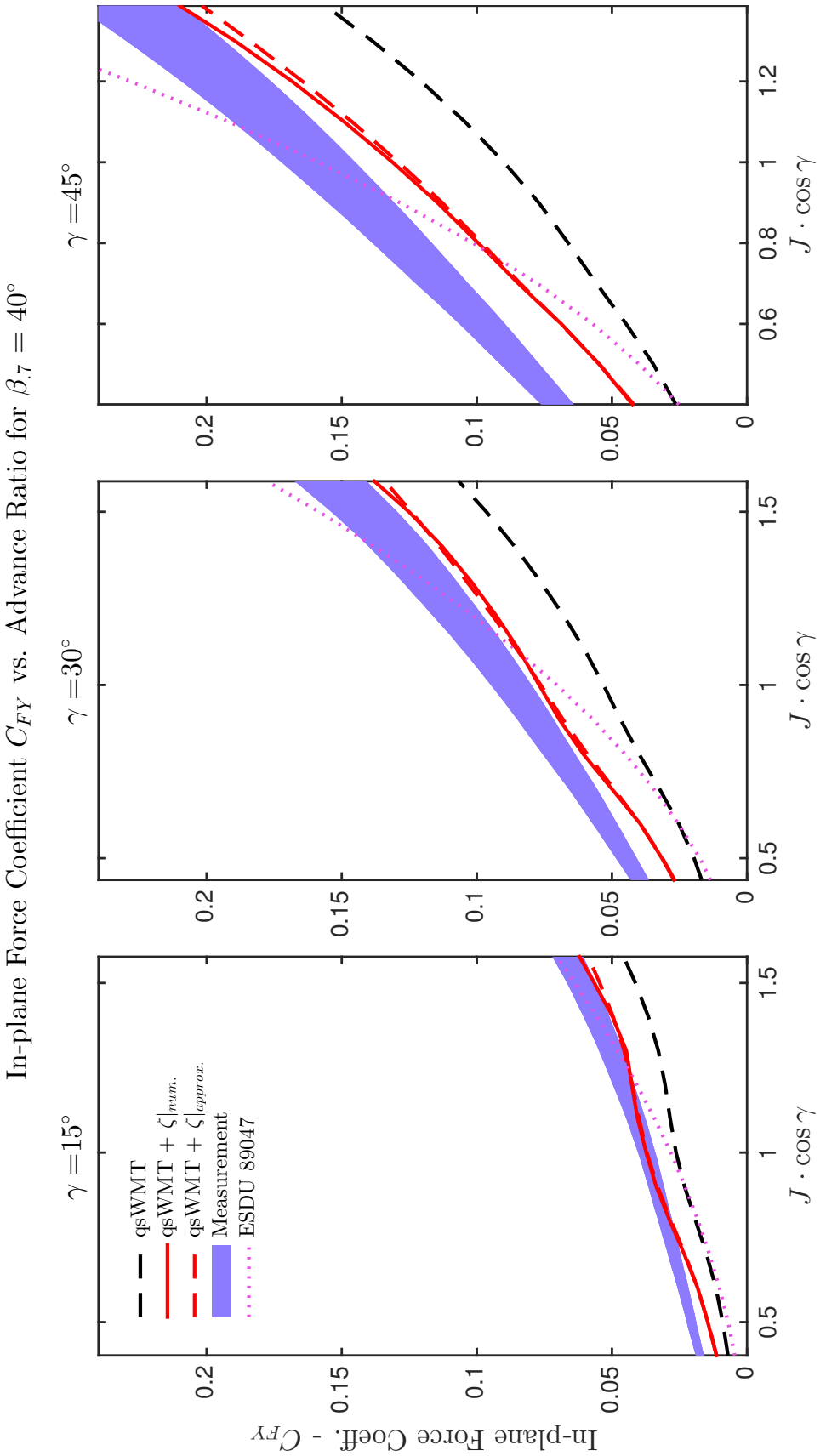

FIGURE 6.10: TOTAL PROPELLER IN-PLANE FORCE COEFFICIENT VS. IN-PLANE ADVANCE RATIO FOR DIFFERENT INCLINATION ANGLES. DATA FROM (YAGGY AND ROGALLO, 1960). $\beta_{.7} = 40°$.

contribute to stresses at the propeller root. The methodology given in this dissertation allows this force to be added to the vector of blade element forces over the disc, $\vec{F_{BE}}(r, \psi)$, which can be utilised for determination of stresses and the blade structural response.

If more experimental data becomes available, the reliability of this methodology vs. rotational speed and number of blades should be compared.

CHAPTER 7

CONCLUSIONS AND FUTURE WORK

In this dissertation the problem of aircraft propellers at an angle of incidence to the freestream has been thoroughly reviewed and investigated. In order to build an engineering-level model for prediction of once-per-revolution loading, an order of magnitude analysis has identified the areas that need to be modelled in greater detail.

7.1 MODEL FORMULATION

- A blade element model for a propeller subject to arbitrary incident velocity, for any operating condition has been presented.
- An ordering scheme to compare and contrast the effect of different order modelling techniques has been presented - the first order angle of attack is defined as the change in sectional angle of attack due to disc inclination based on geometry effects only. The relative changes in sectional angle of attack provided by different flow features/modelling effects have been compared to the first order angle of attack, and it has been shown that:
  - Induced flow and its variation over the propeller disc can have a significant effect.
  - Blade structural deflection is unlikely to alter 1P loading significantly as out-of-plane blade bending (flapwise) can only serve to damp the 1P variation, and twisting of the blade is largely determined by centrifugal affects and only affected in a minor way by the azimuthal load variation.
  - The flowfield at the blade elements can be quite unsteady in terms of reduced frequency, and this needs to be taken into consideration in a suitable model.

7.2 INDUCED FLOW

- A new methodology for determining the induced flow distribution over a propeller disc at incidence has been presented - **weighted momentum theory**. This model validates better to any momentum model in common usage.
- The Prandtl function and the Goldstein or Lock-Goldstein functions have been shown to behave only *slightly* differently in terms of the difference in sectional angle of attack between peak advancing and retreating sides of the propeller disc. Since both the Prandtl and the Goldstein functions behave similarly, both changing the AoA in the same direction, predictions made with Prandtl in this dissertation should be extensible to Goldstein and Lock-Goldstein.
- The reduced frequency indicates that unsteadiness is significant for a propeller at incidence. First-order unsteady models have been used in conjunction with different momentum models, and all formulations with unsteady effects have proven to be less consistently accurate than the quasi-steady formulation of weighted momentum theory.
- **Weighted momentum theory is likely capturing some of the unsteadiness present in the wake**, but the degree to which this effect is separate from the induced flow due to the pressure difference across the actuator disc is indeterminable from the data available at present.
- More numerical work needs to be performed to determine a more physically-realistic weighting function based on the number of blades, wake convection/contraction effects, advance ratio, inclination angle and rotational speed.
- Fundamentally, **the steady-state assumption has been shown to be invalid**. That is, azimuthal independence cannot be justified in a model for a propeller at an angle of incidence, and *all* models implicitly invoking the steady-state assumption are unlikely be correctly predicting the load variation.
- A set of experiments that would assist in determination of the magnitude of the induced flow has been suggested, and it is hoped that such an experiment may be performed to further refine the presented model.

7.3 SWEPT PROPELLER BLADES

- A complete discussion of the aerodynamic effect of sweep on propeller blades has been presented from a blade element model basis.
- Blade element representation of swept blades has been demonstrated to be

inherently flawed, and further work to define a new set of blade elements has been discussed.

- An Euler transform to couple a BEMT model has been presented, and validates reasonably compared to the data available.
- The orientation of blade elements has an associated effect on the phasing of predicted once-per-revolution aerodynamic loading, and the physical reality of this effect needs to be determined. The experimental procedure required to determine this effect has been presented in this dissertation.
- 'Simple sweep' corrections in a blade element model have been shown to be theoretically inapplicable and demonstrated as deleterious to propeller performance predictions.
- More work is required for determination of the aerodynamic effect of sweep on propeller blades, but until such work is performed, **the findings of this dissertation are that sweep corrections based on the cosine of the local sweep angle will hinder calculation accuracy.**

7.4 INSTALLATION

- The model presented in Chapters 2 and 3 has shown good validation of load variation of an installed aircraft propeller.
- An extension of the industry-standard ESDU 90020 (Chappell, 2009) shows that 'averaging' of the incident flow field in terms of an equivalent incidence angle will likely under-predict the load variation for a given 1P loading condition.
- Due to lack of suitable validation data, the model used has not been further validated. **It is recommended that for determination of the once-per-revolution loading on an installed aircraft propeller in any given loading condition, a suitable means of providing the incident flowfield is determined.** The methodology presented in Chapter 5 and Appendix C is an extension of a well-validated existing technique with a new application, but requires further work to prove its reliability.

7.5 IN-PLANE FORCES

- Existing methods used for calculation of in-plane force from blade element forces miss a component due to tilting of the tangential force vector.
- A procedure for including this effect based on simple geometric considerations has been presented, including a closed-form approximate method. This gives an additional term to be used in conjunction with the existing procedure.

- Both numerical and approximate forms of this extra term validate well and raise the predictions of in-plane force using the steady weighted momentum theory to better correlation with measurements.

Overall, this dissertation has provided a mathematical model that is robust and allows determination of the variation of force on the blades of a propeller at an angle of incidence as they rotate. Different modelling techniques have been compared and contrasted, and the ones most fit for simulating propellers at incidence have been utilised in this dissertation. Insight has been provided into the nature of fluctuating loads due to in-plane velocity on a propeller, and a means of predicting them with engineering-level models has been provided, showing good validation and interesting predictions based on sweep and installation that provide avenues for future research.

REFERENCES

Becker, J. V. (1980). The High-speed Frontier. Case Histories of Four NACA Programs, 1920 - 1950. NASA Scientific and Technical Information Branch, Washington.

Beddoes, T. S. (1984). Practical Computation of Unsteady Lift. *Vertica*, 8(1):55–71.

Betz, A. (1937). Aerodynamic Theory: a General Review of Progress Under a Grant of the Guggenheim Fund for the Promotion of Aeronautics. California Institute of Technology.

Bielawa, R. L., Johnson, S. A., Chi, R. M., and Gangwani, S. T. (1983). Aeroelastic Analysis for Propellers. Technical Report NASA Contractor Report 3729, NASA Lewis Research Center.

Bocci, A. J. (1977). A New Series of Aerofoil Sections Suitable for Aircraft Propellers. *Aeronautical Quarterly*, pages 59–73.

Bocci, A. J. and Morrison, J. I. (1988). A Review of ARA Research Into Propeller Aerodynamic Prediction Methods. In *AGARD Aerodynamics and Acoustics of Propellers*, pages 1–22.

Bramwell, A. R. S., Done, G., and Balmford, D. (2001). *Helicopter Dynamics*. Butterworth-Heinemann Ltd, second edition.

Carpenter, P. J. and Fridovich, B. (1953). Effect of a Rapid Blade-pitch Increase on the Thrust and Induced-velocity Response of a Full-scale Helicopter Rotor. Technical Report Technical Note 3044, Washington.

Chappell, P. D. (1989). in-plane forces and moments on installed inclined propellers at low forward speed . Technical Report ESDU 89047.

Chappell, P. D. (2009). Airframe-induced upwash at subsonic speeds. Technical Report ESDU 90020.

Chen, R. T. N. (1989). A survey of nonuniform inflow models for rotorcraft flight dynamics and control applications. Technical Report 102219, Ames Research Center, Moffett Field, California.

Chinoy, C. B. (1992). ESDU 96027: Estimation of the unsteady lift coefficient of subsonic propeller blades in non-axial inflow. Technical Report ESDU 96027.

Clorius, C. O. (2001). *Fatigue in Wood: An investigation in tension perpendicular to the grain*. PhD thesis, Danmarks Tekniske Universitet, Lyngby.

Crigler, J. L. (1944). Comparison of Calculated and Experimental Propeller Characteristics for Four-, Six-, and Eight-Blade Single-Rotation Propellers. Technical Report ACR 4B04, NACA, Springfield.

Crigler, J. L. and Gilman Jr, J. (1952). Calculation of Aerodynamic Forces on a Propeller in Pitch or Yaw. Technical Report TN 2585, NACA, Washington.

de Young, J. (1965). Propellers at High Incidence. *Journal of Aircraft*, 2:241–250.

Denton, J. D. (2002). The effects of lean and sweep on transonic fan performance: a computational study. *Task Quarterly*.

Drzewiecki, S. (1900). Des Helices Propulsives. In *Congres d'Architecture et de Constructions Navales*, Paris.

Drzewiecki, S. (1901). Du Choix Des Elements Determinant Les Helices Propulsives Permettant Leur Facile Comparaison Entre Elles. *Bulletin de lAssociation Technique Maritime*.

Dunn, M. H. and Farassat, F. (1992). High-Speed Propeller Noise Prediction - a Multidisciplinary Approach. *AIAA journal*, 30(7):1716–1723.

Eisenhuth, J. (1963). Propellers with Distorted Inflow. Technical Report TM 5.2410-20, The Pennsylvania State University, Pennsylvania.

ESDU (1978). **A Framework Relating the Drag-Rise Characteristics of a Finite Wing/Body Combination to Those of Its Basic Aerofoil** . Technical report.

Eshelby, M. E. (1985). On the Aerodynamics of Installed Propellers. In *AGARD Aerodynamics and Acoustics of Propellers*, pages 8–1 to 8–14, Toronto.

Evans, A. J. and Liner, G. (1951). A Wind-Tunnel Investigation of the Aerodynamic Characteristics of a Full-Scale Sweptback Propeller and Two Related Straight Propellers. Technical Report NACA RM L50J05, Washington.

Fertis, D. G. and Maser, J. G. (1988). Parametric studies of advanced turboprops. In *29th Structures, Structural Dynamics and Materials Conference cosponsored by the AIAA,ASME, ASCE, AHS, and ACS*, Williamsburgh, Virginia.

Glauert, H. (1926a). A General Theory of the Autogyro. Technical Report Reports and Memoranda No. 1111., Scientific Research Air Ministry.

Glauert, H. (1926b). *The Elements of Aerofoil and Airscrew Theory*. Cambridge University Press.

Glauert, H. (1943). *Aerodynamic Theory: A General Review of Progress*. Div. L - Airplane Propellers. California Institute of Technology.

Goldstein, S. (1929). On the vortex theory of screw propellers. In *Proceedings of the Royal Society of London*, pages 440–465.

Gray, W. H. (1948). Wind-Tunnel Tests of a Swept-Blade Propeller and Related Straight Blades Having Thickness Ratios of 5 and 6 Percent. Technical Report RM L8H19, Washington.

Gray, W. H., Hallissy, J. M., and Heath, A. R. (1954). A Wind-tunnel Investigation of the Effects of Thrust-axis Inclination on Propeller First-order Vibration. Technical Report R 1205.

Greenberg, J. (1947). Airfoil in Sinusoidal Motion in a Pulsating Stream. Technical Report TN 1326, NACA.

Gulcat, U. (2010). *Fundamentals of Modern Unsteady Aerodynamics*. Springer, Heidelberg.

Gur, O. and Rosen, A. (2008). Comparison between blade-element models of propellers. *Aeronautical Journal*, 112(1138):689–704.

Gur, O. and Rosen, A. (2014). Personal Communication: Discussion of Swept Blades in Evans and Liner (1951).

HaiLong, Y. and PinQi, X. (2009). A wake bending unsteady dynamic inflow model of tiltrotor in conversion flight of tiltrotor aircraft. *Science in China Series E-Technological Sciences*, 52(11):3188–3197.

Hansen, M. H., Gaunaa, M., and Madsen, H. A. (2004). A Beddoes-Leishman Type Dynamic Stall Model in State-Space and Indicial Formulations. Technical Report Riso-R-1354 (EN), Riso National Laboratory, Roskilde, Denmark.

He, C. (1989). *Development and Application of a Generalized Dynamic Wake Theory for Lifting Rotors*. PhD thesis, Georgia Institute of Technology.

Heene, M. (2012). Aerodynamic Propeller Model for Load Analysis. Master's thesis, Stockholm.

Houghton, E. L., Carpenter, P. W., Collicott, S., and Valentine, D. (2012). *Aerodynamics for Engineering Students*. Elsevier, Oxford.

Ingram, G. (2011). Wind Turbine Blade Analysis using the Blade Element Momentum Method. Master's thesis.

Jayne, N. (2002). Blade Natural Frequencies and Campbell Diagram. Technical Report TI503 Att A, Dowty Aerospace Propellers, Gloucester.

Katz, J. and Plotkin, A. (2001). *Low-Speed Aerodynamics*. Cambridge University Press.

Korkan, K. and Camba III, J. (1986). Aerodynamic data banks for Clark-Y, Naca 4-digit, and Naca 16-series airfoil families. Technical Report Contract NAS 3-272, Texas A&M University.

Korkan, K. D., Gregorek, G. M., and Mikkelson, D. C. (1980). A Theoretical and Experimental Investigation of Propeller Performance Methodologies. In *AIAA/SAE/ASME 16th Joint Propulsion Conference*, Hartford, Conneticut.

Kosmatka, J. B. (1986). *Structural Dynamic Modeling of Advanced Composite Propellers by the Finite Element Method*. PhD thesis, University of California.

Kosmatka, J. B. and Friedmann, P. P. (1987). Structural Dynamic Modeling of Advanced Composite Propellers by the Finite Element Method. In *28th Structures, Structural Dynamics and Materials Conference*, pages 1–14, Monterrey, CA.

Kurkov, A. P. (1988). Optical measurement of propeller blade deflections. Technical Report NASA-TP-284, NASA Lewis Research Center, Cleveland.

Leishman, J. G. (2006). *Principles of Helicopter Aerodynamics*. Cambridge, second edition.

Lindsey, W. F., Stevenson, D. B., and Daley, B. N. (1948). Aerodynamic Characteristics of Naca 16-Series Airfoils at Mach Numbers Between 0.3 and 0.8. Technical Report Technical Note No. 1546, National Advisory Committee for Aeronautics.

Lino, M. (2010). Numerical Investigation of Propeller-Wing Interaction Effects for a Large Military Transport Aircraft. Master's thesis, TU Delft, Brussels, Belgium.

Lock, C. N. H. (1932). Application of Goldstein's Airscrew Theory to Design.

Lock, C. N. H., Pankhurst, R. C., and Conn, J. F. C. (1945). Strip Theory Method of Calculation for Airscrews on High-Speed Aeroplanes. Technical Report R&M No. 2035 (5078, 5233, 5939, 6512 and 8962).

Loewy, R. G. (1957). A two-dimensional approximation to the unsteady aerodynamics of rotary wings. *J Aeronautical Sciences*, 24:96.

Makinen, S. (2005). *Applying dynamic wake models to large swirl velocities for optimal propellers*. PhD thesis, Washington University Sever Institute of Technology Department of Mechanical Engineering.

Makinen, S. and Peters, D. A. (2003). Propeller Solutions with Dynamic Wake Models. In *Tenth Internation Workshop on Aeroelasticity of Rotor Systems*, Atlanta.

McLemore, H. C. and Cannon, M. D. (1954). *Aerodynamic Investigation of a Four-Blade Propeller Operating Through an Angle-of-Attack Range From 0° to 180°*. NACA, Washington.

Methven, P. (1998). 1P PREDICTION FACTORS FOR THE R408 PROPELLER ON THE DASH 8-400 AIRCRAFT. Technical Report POR2315, Gloucester.

Moriarty, P. J. and Hansen, A. C. (2005). AeroDyn Theory Manual. Technical Report NREL/TP-500-36881.

Morillo, J. (2001). *A Fully Three-Dimensional Unsteady Rotor Inflow Model from a Galerkin Approach*. PhD thesis, PhD. Thesis, Saint Louis, Missouri.

Morrison, J. I. and Bocci, A. J. (1985). A Numerical Treatment of the Vortex Screw Theory of Propellers. Technical Report Mode Test Note E26/2, ARA, Bedford.

Murakami, Y. (2008). *A New Appreciation of Inflow for Autorotative Rotors*. PhD thesis, University of Glasgow Dept. of Aerospace Engineering.

Ortun, B., Boisard, R., and Gonzalez Martino, I. (2011). Assessment of propeller 1P loads predictions. In *46th Symposium of Applied Aerodynamics Polytech'Orléans*, pages 36–46, Orléans. ONERA, Applied Aerodynamics Department, Inderscience.

Pendley, R. E. (1945). Effect of Propeller-Axis Angle of Attack on Thrust Distribution Over the Disk in Relation to Wake-Survey Measurement of Thrust. Technical Report ARR L5J02b, NACA.

Peters, D. A., Boyd, D. D., and He, C. J. (1989). Finite-State Induced-Flow Model for Rotors in Hover and Forward Flight. *Journal of the American Helicopter Society*, 34(4):5–17.

Peters, D. A. and Gaonkar, G. H. (1979). Theoretical Flap-Lag Damping with Various Dynamic Inflow Models. In *35th Annual Forum of the American Helicopter Society*, Washington DC.

Peters, D. A. and HaQuang, N. (1988). Dynamic Inflow for Practical Applications. *Journal of the American Helicopter Society*, 33.

Peters, D. A. and He, C. J. (1995). Finite State Induced Flow Models Part II: Three-Dimensional Rotor Disk. *Journal of Aircraft*, 32:1–11.

Peters, D. A., Kurunamoorthy, S., and Cao, W. M. (1995). Finite State Induced Flow Models Part I: Two-Dimensional Thin Airfoil. *Journal of Aircraft*, 33.

Pitt, D. M. and Peters, D. A. (1981). Theoretical Prediction of Dynamic-Inflow Derivatives. *Vertica*, 5(1):21–34.

Prandtl, L. and Betz, A. (1927). Schraubenpropeller mit Gerinstem Energieverlust, Göttinger Nachrichten, Göttinggen. *Vier Abhandlungen uber Hydro- und Aerodynamik*, pages 193–197.

Prouty, R. (2009). *Helicopter Aerodynamics Volume II*. Eagle Eye Solutions (eBook).

Prouty, R. W. (2002). *Helicopter Performance, Stability, and Control*. Krieger Publishing Company, Malabar, third edition.

Rankine, W. J. M. and Rankine, W. J. M. (1865). *On the mechanical principles of the action of propellers*. Transactions of the Institute of Naval Architects.

Ribner, H. S. (1945). Formulas for propellers in yaw and charts of the side-force derivative. Technical Report Report No. 819.

Ribner, H. S. and Ribner, H. S. (1945). Propellers in Yaw. Technical Report ARR No. 3L09, Washington.

Roberts, J. C. and Yaggy, P. F. (1950). A Survey of the Flow at the Plane of the Propeller of a Twin-Engine Airplane. Technical Report TN-2192, NACA Ames Aeronautical Laboratory.

Rogallo, V. L., McCloud, J. L., Yaggy, P. F., McCloud III, J. L., and Aeronautics, U. S. N. A. C. f. (1956). An analysis of once-per-revolution oscillating aerodynamic thrust loads on single-rotation propellers on tractor airplanes at zero yaw. Technical Report Report 1295, NACA.

Rogallo, V. L., Roberts, J. C., and Oldaker, M. R. (1951). Vibratory Stresses in Propellers Operating in the Flow Field of a Wing-Nacelle-Fuselage Combination. Technical Report TN 2308, NACA.

Rohrbach, C., Rohrbach, C., Metzger, F. B., Metzger, F. B., Black, D. M., Black, D. M., Ladden, R. M., and Ladden, R. M. (1982). Evaluation of wind tunnel performance testings of an advanced 45° swept eight-bladed propeller at Mach numbers from 0.45 to 0.85. Technical Report NASA Contracter Report 3505.

Rosen, A. and Gur, O. (2005). Propeller performance at low advance ratio. *Journal of Aircraft*, 42(2):435–441.

Rosen, A. and Rand, O. (1985). The aerodynamic behavior of infinite swept wings - Another point of view. *electronicsandbooks.com*, 22(1):83–85.

Ruiz-Calavera, L. and Perdones-Diaz, D. (2012). CFD Based Aeroelastic Calculation of Propeller Loads. In *28th International Congress of the Aeronautical Sciences (ICAS 2012)*, page 11. Airbus Military, Spain.

Russell, J. G. (1952). Wake Survey and Strain-Gauge Measurements on an Inclined Propeller in the R.A.E. 24-ft Tunnel. Technical Report CP No. 117, Ministry of Supply - Aeronautical Research Council, Gloucester.

Silva, C. T. and Donadon, M. V. (2013). Unsteady Blade Element-Momentum Method Including Returning Wake Effects. . . . , 5:27–42.

Snel, H., Houwink, R., and Bosschers, J. (1994). Sectional Prediction of Lift Coefficients on Rotating Wind Turbine Blades in Stall. Technical Report ECN-C–93-052, ECN Renewable Energy.

stack, j. (1940). Tests of Airfoils Designed to Delay the Compressibility Burble. Technical Report NACA R. 763, NACA.

Suzuki, A. and Hansen, A. C. (1999). Dynamic Inflow Models with Nonlinear Induced Velocity Distribution for YAWDYN/AERODYN Codes. In *Windpower 1999*, pages 1–10, Burlington. Department of Mechanical Engineering, University of Utah.

TH. Von Karman and Sears, W. R. (1938). Airfoil Theory for Non-Uniform Motion. *Journal of the Aeronautical Sciences (Institute of the Aeronautical Sciences)*, 5(10):379–390.

Theodorsen, T. (1944a). The Theory of Propellers I: Determination of the Circulation Function and the Mass Coefficient for Dual-rotating Propellers. Technical Report Report No. 775, NACA.

Theodorsen, T. (1944b). The Theory of Propellers II: Method for Calculating the Axial Interference. Technical Report Report No. 776, NACA.

Theodorsen, T. (1944c). The Theory of Propellers III: The Slipstream Contraction with Numerical Values for Two-blade and Four-blade Propellers. Technical Report Report No. 777, NACA.

Theodorsen, T. (1944d). The Theory of Propellers IV: Thrust, Energy, and Efficiency Formulas for Single and Dual Rotating Propellers with Ideal Circulation Distribution. Technical Report Report No. 778, NACA.

Theodorsen, T. (1948). *Theory of propellers*. McGraw-Hill Book Company.

Theodorsen, T. and Mutchler, W. H. (1935). General theory of aerodynamic instability and the mechanism of flutter. Technical Report Report No. 496, NACA.

Tibery, C. L. and Wrench, Jr, J. W. (1964). Tables of the Goldstein factor. Technical Report Report 1534, Department of the Navy - Applied Mathematics Laboratory.

Tomblin, J. S. and Seneviratne, W. P. (2011). Determining the fatigue life of composite aircraft structures using life and load-enhancement factors. Technical Report DOT/FAA/AR-10/6, U.S. Department of Transportation Federal Aviation Administration.

Trchalik, J. (2011). NACA 16 Lift and Drag Experimental Databanks - Without Report.

Van der Wall, B. G. and Leishman, J. G. (1994). On the Influence of Time-Varying Flow Velocity on Unsteady Aerodynamics. *Journal of the American Helicopter Society*, 39:25–36.

Veldhuis, L. L. M. (2004). Review of Propeller-Wing Aerodynamic Interference. In *th International Congress of the Aeronautical Sciences*, pages 1–21, Yokohama.

Veldhuis, L. L. M. and Veldhuis, L. L. M. (2005). *Propeller Wing Aerodynamic Interference*. PhD thesis.

Von Kármán, T. (1930). Calculation of Pressure Distribution on Airship Hulls. Technical Report TM-574, NACA, Washington.

Wald, Q. R. (2006). The aerodynamics of propellers. *Progress in Aerospace Sciences*, 42(2):85–128.

Whitcomb, R. T. (1948). Method for Stress Analysis of a Swept Propeller. Technical Report RM L8F11, NACA Langley Aeronautical Laboratory.

Whitcomb, R. T. (1950). A Description of the Design of Highly Swept Propeller Blades. Technical report, NACA Langley Aeronautical Laboratory.

Yadykin, Y., Ognev, V., and Rosen, A. (2006). Aeroelastic Analysis of Propellers. Technical Report TAE No. 966, Faculty of Aerospace Engineering: Technion - Israel Institute of Technology.

Yaggy, P. F. (1951). A Method for Predicting the Upwash Angles Induced at the Propeller Plane of a Combination of Bodies with an Unswept Wing. Technical Report TN-2528, NACA Ames Aeronautical Laboratory, Washington.

Yaggy, P. F. and Rogallo, V. L. (1960). A wind-tunnel investigation of three propellers through an angle-of-attack range from 0 degree to 85 degrees. Technical Report NACA TN D-318, NACA Ames Research Center, Washington.

Yamane, T. (1992). Aeroelastic tailoring analysis for advanced turbo propellers with composite blades. *Computers & Fluids*.

Young, W. C. and Budynas, R. G. (2002). *Roark's Formulas for Stress and Strain*. McGraw Hill Book Company, seventh edition.

APPENDIX A

DERIVATION OF MOMENTUM THEORIES

This Appendix derives the governing equations for Differential Momentum Theory (DMT), which may be reduced to Annular Momentum Theory (AMT) and Momentum Theory (MT) by removing the dependencies on azimuthal position and radius, respectively.

The theory in this thesis is based on the General Momentum Theory, which is an extension of the axial momentum theory of (Rankine and Rankine, 1865) by R.E. Froude by including the rotational velocity.

Figure A.1a shows the assumed bounding streamtube around the propeller disc. It is assumed to be a differential streamtube comprised of streamlines that pass through a radial and azimuthal position at the propeller disc - hence the velocity may depend on radial and azimuthal position.

Assumptions:

- The propeller is replaced by an actuator disc of equal radius to the propeller disc, and of infinitesimal thickness.
- There is a nonuniform pressure discontinuity Δp at the disc, that is dependent on axial and radial position. The pressure in front of the disc is p_f and the pressure behind is p_r.
- The actuator disc imparts an axial and circumferential momentum jump to the flow - but there is no axial velocity discontinuity.
- This momentum injection leads to a pressure discontinuity across the disc.
- The flow is assumed to be inviscid and incompressible.

In the far upstream position (1), the flow has the freestream velocity V_∞ and ambient freestream pressure p_∞. The flow is accelerated and passes through the

actuator disc (2) with velocity V_2 and continues to accelerate to its ultimate value V_3 in the far downstream position (3). In this analysis, uppercase velocities refer to absolute values whereas lowercase velocities refer to the velocity perturbations from freestream values. That is:

$$V_1 = V_\infty \tag{A.1}$$

$$V_2 = V_1 + v_2 \tag{A.2}$$

$$V_3 = V_1 + v_3 \tag{A.3}$$

v_a, v_r, v_t refer to axial, radial and tangential velocities, respectively - and V without a subscript refers to axial velocity for simplicity. The subscripts $()_f$ and $()_r$ refer to the 'front' and 'rear' sides of the propeller, respectively, viewed from upstream.

Because of the third assumption above, Bernoulli's equation is valid everywhere except for the pressure discontinuity across the disc. So it may be applied separately upstream and downstream. Upstream:

$$p_1 + \tfrac{1}{2}\rho V_{a1}^2 = p_f + \tfrac{1}{2}\rho\left[V_{a2}^2 + V_{r2}^2\right] \tag{A.4}$$

$$p_f = p_1 + \frac{1}{2}\rho\left[V_{a1}^2 - V_{a2}^2 - V_{r2}^2\right] \tag{A.5}$$

and downstream

$$p_r + \tfrac{1}{2}\rho\left[V_{a2}^2 + V_{r2}^2 + V_{t2}^2\right] = p_3 + \tfrac{1}{2}\rho\left[V_{a3}^2 + V_{r3}^2 + V_{t3}^2\right] \tag{A.6}$$

since the slipstream is fully contracted in the far wake, $V_{r3} = 0$

$$p_r = p_3 + \frac{1}{2}\rho\left[V_{a3}^2 + V_{t3}^2 - V_{a2}^2 - V_{r2}^2 - V_{t2}^2\right] \tag{A.7}$$

it follows that

$$\Delta p = p_r - p_f \tag{A.8}$$

$$= p_3 - p_1 + \frac{1}{2}\rho\left[\left(V_{a3}^2 - V_{a1}^2\right) + \left(V_{t3}^2 - V_{t2}^2\right)\right] \tag{A.9}$$

it is assumed that the difference between the angular velocity in the wake is smaller than the axial velocity change over the whole slipstream - or

$$V_{t3}^2 - V_{t2}^2 \ll V_{a3}^2 - V_{a1}^2 \tag{A.10}$$

which has been shown (see Gur and Rosen, 2008, *'Simplified Momentum Model'*) to produce near identical results to the full general momentum model. And by definition, the pressure far downstream and upstream is equal to the ambient pressure $p_1 = p_3 = p_a$

$$\Delta p = \frac{1}{2}\rho\left(V_{a3}^2 - V_{a1}^2\right) \tag{A.11}$$

and the elemental axial force on a differential area of the disc is simply the pressure difference multiplied by elemental area

$$dF|_{_{pressure}} = dp \cdot dA \tag{A.12}$$

$$= \tfrac{1}{2}\rho\left(V_3^2 - V_1^2\right) \cdot dA \tag{A.13}$$

Hence the axial force is equal to the dynamic pressure rise between the far upstream and downstream positions. Axial force may also be determined from Newton's second law applied through the streamtube using mass flow determined at the disc

$$dF|_{momentum} = dm \cdot \dot{V} \tag{A.14}$$
$$= d\dot{m} \cdot \Delta V \tag{A.15}$$
$$= dA\rho V_2 \left(V_3 - V_1\right) \tag{A.16}$$

equating A.13 and A.16

$$\tfrac{1}{2}\rho\left(V_3^2 - V_1^2\right) \cdot dA = dA\rho V_2 \left(V_3 - V_1\right) \tag{A.17}$$
$$\frac{1}{2}(V_3 - V_1)(V_3 + V_1) = V_2(V_3 - V_1) \tag{A.18}$$
$$\rightarrow V_2 = \frac{V_1 + V_3}{2} \tag{A.19}$$

hence the axial velocity increase at the disc is equal to half the total axial velocity increase. The axial induction factor, a_a, is introduced

$$a_a \triangleq \frac{V_2 - V_1}{V_1} \tag{A.20}$$
$$\therefore V_2 = V_1(1 + a_a) \tag{A.21}$$
$$\therefore V_3 = V_1(1 + 2a_a) \tag{A.22}$$

which gives the expression for momentum thrust

$$dT|_m = 2\rho V_1^2 \left(1 + a_a\right) a_a dA \tag{A.23}$$

A similar analysis may be performed for the rotation in the slipstream. The formulation of the elemental torque contribution varies in derivation between sources, and is not always rigorous. The following is taken from Glauert (1943). For constant angular momentum between (2) and (3):

$$V_{t2} r_2 = V_{t3} r_3 \tag{A.24}$$
$$\omega_2 r_2^2 = \omega_3 r_3^2 \tag{A.25}$$

The torque contribution is the rate of change of angular momentum in the streamtube:

$$dQ = \omega_3 r_3^2 d\dot{m} \tag{A.26}$$

r_3 is unknown, but due to A.25 it may be written as

$$= \omega_2 r_2^2 d\dot{m} \tag{A.27}$$
$$= \rho v_2 \omega_2 r_2^2 dA \tag{A.28}$$

recognising that the angular momentum contribution is the tangential velocity (v_ω) divided by radial distance

$$= \rho V_2 V_{t2} r_2 dA \tag{A.29}$$

and introducing the tangential induction factor, nondimensionalised with rotor speed Ω:

$$a_\omega \triangleq \frac{V_t}{\Omega r} \quad \left(= \frac{\omega}{\Omega}\right) \tag{A.30}$$

hence the momentum torque contribution may be written as

$$dQ|_m = \rho V_2 \, a_\omega \, \Omega \, r_2^2 \, dA \tag{A.31}$$

$$= \rho V_1 (1 + a_a) \, a_\omega \, \Omega \, r_2^2 \, dA \tag{A.32}$$

Both the expressions for momentum thrust and torque contain the term for differential area, dA. For a circular disc or annulus, this is evaluated as:

$$dA = \int_0^{2\pi} \int_{R1}^{R2} r \cdot dr d\psi \tag{A.33}$$

$$= \pi R^2 \qquad \text{(Circular disc)} \tag{A.34}$$

$$= \pi \left(R_2^2 - R_1^2 \right) \qquad \text{(Annulus)} \tag{A.35}$$

In a traditional blade element momentum model, the axial and tangential forces on a single blade element are summated to give the total forces in either the disc or an annulus. For axial cases, this gives a B multiplication factor:

$$dT|_m = B \cdot dT|_{BE} \tag{A.36}$$

$$dQ|_m = B \cdot dQ|_{BE} \tag{A.37}$$

For the case where blade forces vary with azimuth, as on the inclined propeller, the B multiplication factor cannot be included from the same reasoning. Both Heene (2012) and Eshelby (1985) utilise a differential form of momentum theory for different performances, and they both include this B multiplication factor in the blade element equations, though it is without physical justification. The following shows that it exists as a denominator in the momentum equations so is physically correct, but should not be derived within the blade element equations in a rigorous analysis.

For the purposes of this implementation of DMT, it will be assumed that:

- Each blade travels within a field of its own induced velocity that changes according to its own lift.
- The differential area in which this induced velocity is held to be true is, for a blade element at position (r, ψ), from $\left[r - \frac{\Delta r}{2}\right]$ to $\left[r + \frac{\Delta r}{2}\right]$, $\left[\psi - \frac{2\pi}{2B}\right]$ to $\left[\psi + \frac{2\pi}{2B}\right]$.

The second assumption is clearly an abstraction of the physical situation as it leads to an azimuthal discontinuity in the pressure. However, for the purposes of this analysis, it will be used. It is also possible to assume a distribution that matches the form of the loading with azimuth, but since this implementation is only used to determine the flow at the centre of the area (*i.e.,* at ψ), it makes no difference and simply adds complexity.

With these new limits, the differential area, dA becomes:

$$dA = \int_{\psi-\frac{\pi}{B}}^{\psi+\frac{\pi}{B}} \int_{R1}^{R2} r \cdot dr d\psi \tag{A.38}$$

$$= \int_{R1}^{R2} \frac{2\pi r}{B}\, dr \tag{A.39}$$

$$= \frac{2\pi r \delta r}{B} \tag{A.40}$$

The expressions for axial force and torque contribution are given in 2.15 and 2.16. These give the dimensional blade element forces:

$$dT = \sum F_{ZB} = dl \cdot \cos\phi - dd \cdot \sin\phi \tag{2.15}$$

$$\tfrac{dQ}{r} = \sum F_{XB} = dl \cdot \sin\phi + dd \cdot \cos\phi \tag{2.16}$$

using the definitions of two-dimensional lift and drag coefficients

$$dC_l \triangleq \frac{dl}{\frac{1}{2}\rho V_R^2 \cdot c} \tag{A.41}$$

$$dC_d \triangleq \frac{dd}{\frac{1}{2}\rho V_R^2 \cdot c} \tag{A.42}$$

dT and $\frac{dQ}{r}$ may be written

$$dT = c \cdot \tfrac{1}{2}\rho V_R^2 \left[dC_l \cdot \cos\phi - dC_d \cdot \sin\phi\right] \tag{A.43}$$

$$\tfrac{dQ}{r} = c \cdot \tfrac{1}{2}\rho V_R^2 \left[dC_l \cdot \sin\phi + dC_d \cdot \cos\phi\right] \tag{A.44}$$

and hence the blade element thrust and torque contributions, per elemental radius

$$dT|_{BE} = c \cdot \tfrac{1}{2}\rho V_R^2 \left[dC_l \cdot \cos\phi - dC_d \cdot \sin\phi\right] \cdot \delta r \tag{A.45}$$

$$\left.\tfrac{dQ}{r}\right|_{BE} = c \cdot \tfrac{1}{2}\rho V_R^2 \left[dC_l \cdot \sin\phi + dC_d \cdot \cos\phi\right] \cdot \delta r \tag{A.46}$$

Equations A.23 and A.45 may be equated and A.39 inserted. Similarly for A.32 and A.46. Firstly for thrust

$$2\rho v_\infty^2 \left(1 + a_a\right) a_a dA = c \cdot \tfrac{1}{2}\rho V_R^2 \left[dC_l \cdot \cos\phi - dC_d \cdot \sin\phi\right] \cdot \delta r \tag{A.47}$$

$$2\rho v_\infty^2 \left(1 + a_a\right) a_a \tfrac{2\pi r}{B} \delta r = c \cdot \tfrac{1}{2}\rho V_R^2 \left[dC_{ZB}\right] \cdot \delta r \tag{A.48}$$

introducing axial and tangential force coefficients

$$dC_{ZB} \triangleq \left[dC_l \cdot \cos\phi - dC_d \cdot \sin\phi\right] \tag{A.49}$$

$$dC_{XB} \triangleq \left[dC_l \cdot \sin\phi + dC_d \cdot \cos\phi\right] \tag{A.50}$$

which refer to the axial and tangential force coefficient in disc axes, due to blade element forces

$$4v_\infty^2 \left(1 + a_a\right) a_a \delta r = \frac{Bc}{2\pi r} \cdot V_R^2 \cdot \left[dC_{ZB}\right] \delta r \tag{A.51}$$

V_1 is V_n using the blade element nomenclature (refer to Figure A.2) and it can be

seen from the geometry that

$$\sin\phi = \frac{V_n\left(1+a_a\right)}{V_R} = \frac{V_1\left(1+a_a\right)}{V_R} \tag{A.52}$$

hence

$$4v_\infty^2\left(1+a_a\right)a_a\delta r = \frac{Bc}{2\pi r}\cdot\frac{v_\infty^2\left(1+a_a\right)^2}{\sin^2\phi}\cdot\left[dC_{ZB}\right]\delta r \tag{A.53}$$

substituting the local solidity $\sigma(x) \triangleq \frac{Bc}{2\pi r}$, the final relationship between axial forces and axial induced velocity may be written

$$\frac{a_a}{1+a_a} = \frac{\sigma\cdot dC_{ZB}}{4\sin^2\phi} \tag{A.54}$$

Similarly in the tangential direction, equations A.32 and A.46 give

$$\frac{a_\omega}{1+a_a}\cdot\frac{\Omega}{v_\infty} = \frac{\sigma\cdot dC_{XB}}{2\sin^2\phi} \tag{A.55}$$

$$a_\omega = \lambda_r\left(1+a_a\right)\cdot\frac{\sigma\cdot dC_{XB}}{2\sin^2\phi} \tag{A.56}$$

where

$$\lambda_r \triangleq \frac{v_\infty}{\Omega} \tag{A.57}$$

Equations A.54 through A.57 provide the formulation for a nonuniform induced flow model from momentum considerations, utilising a differential area and thus negating any erroneous blade multiplication of the blade-element forces.

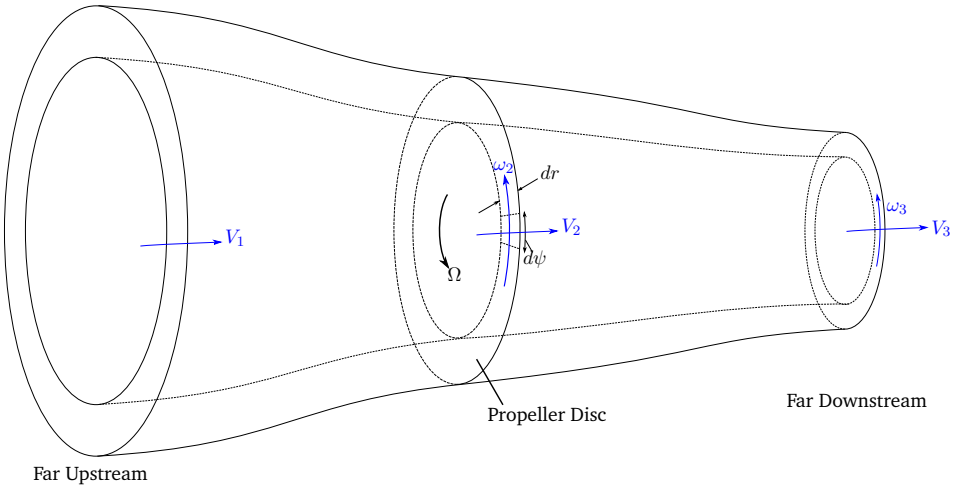

(A) 3D BOUNDING STREAMTUBE SHOWING DIFFERENTIAL AREA AT PROPELLER DISC

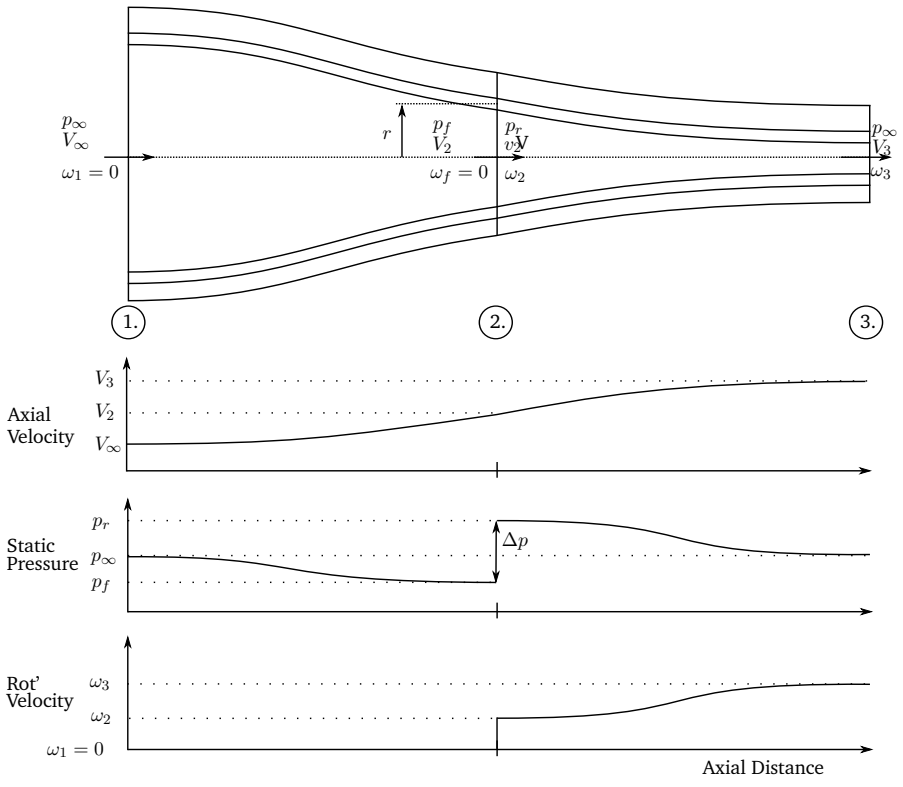

(B) VELOCITY/PRESSURE PROFILES

FIGURE A.1: SIDE VIEW AND PLOTS OF VELOCITIES AND PRESSURE WITH AXIAL DISTANCE

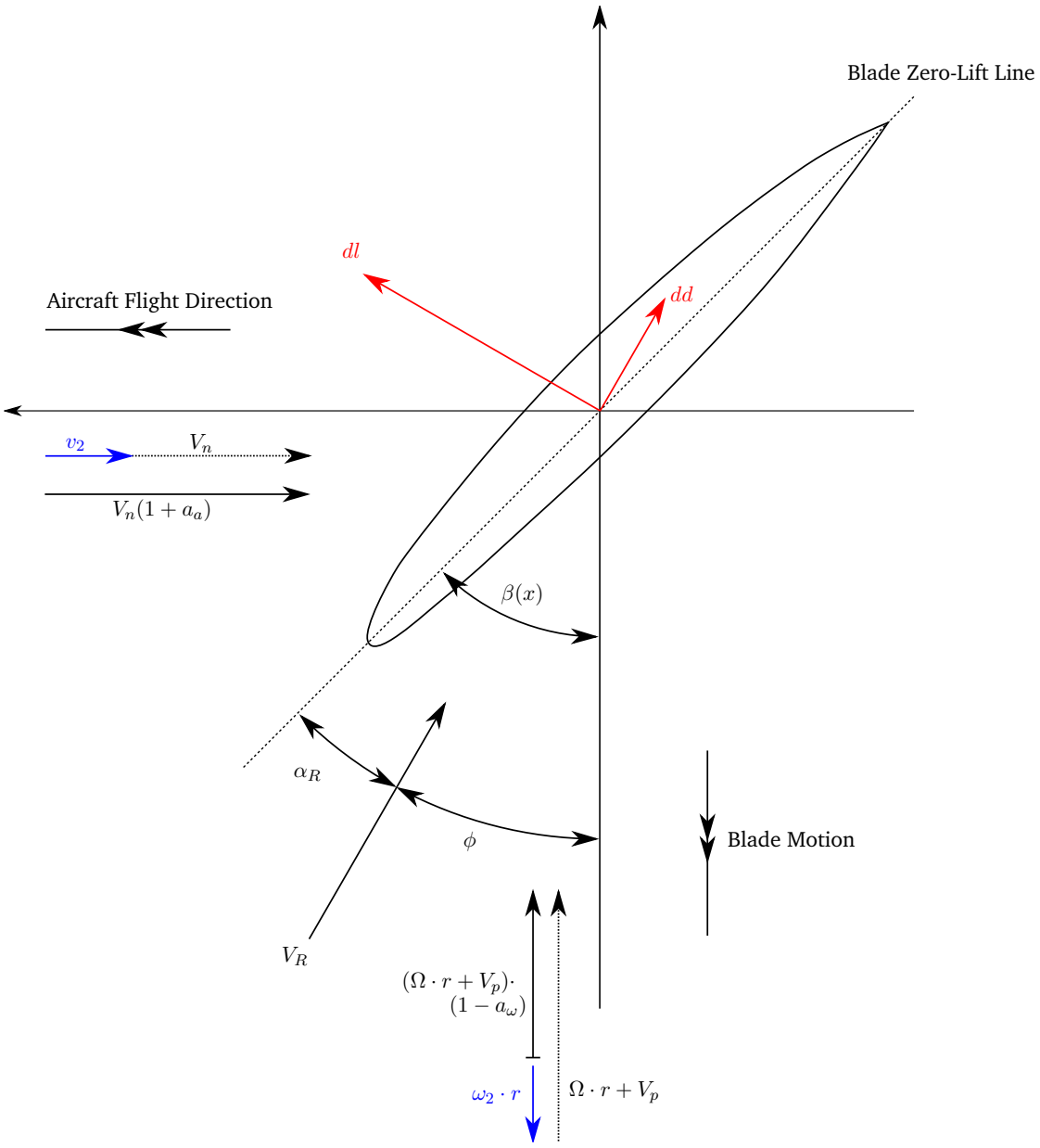

FIGURE A.2: BLADE ELEMENT AXES, VELOCITIES AND ELEMENTAL FORCES. Y_B IS $+ive$ OUT OF PAGE. VALID FOR STRAIGHT BLADES ONLY.

APPENDIX B

SWEPT BLADE CO-ORDINATE TRANSFORM

This section describes the axes systems in use in the swept blade model presented in Chapter 4. In this mode, three distinct axes systems are used and the model converts between all three with an Euler transform that converts disc velocities into blade element velocities in the swept BE axes, in which the BE forces are determined. These forces are then converted back into the disc axes, the reference frame in which the momentum model solves for the induced flow velocities at the disc. This transform is achieved via a single transformation matrix for each blade element, and is a function of dihedral, $\kappa(r)$, azimuthal shift, $\delta\psi(r)$, built-in structural twist, $\theta(r)$, and blade setting (feather) angle, $\beta_{.7}$, which is defined at the 70% radius but converted back to the blade root[1] and applied to the whole blade.

The transform converts from Disc $\rightarrow$ (Unswept) Blade Axes $\rightarrow$ (Swept) Blade Element Axes, and it should be noted that for a straight-bladed propeller, the first transform is used to get $[V_R, V_P, V_N]$, which along with the structural twist and setting may determine the sectional effective velocity, V_R, and angle of attack, α_R.

B.1 DISC AXES

This is a simple cartesian axis system that describes the three inflow components at the propeller disc, see Figure B.1. For simple pure disc inclination (aircraft

[1] This is not a linear transform based on twist at the 70% radius, as it would be for a straight blade.

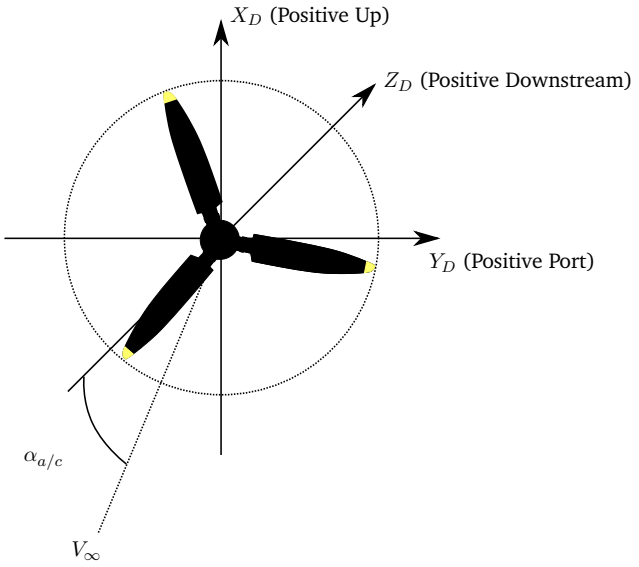

FIGURE B.1: DISC AXES - STRAIGHT-BLADED PROPELLER INCLUDED FOR ILLUSTRATION.

angle of attack), they are:

$$\vec{\mathbf{V_D}} = \begin{bmatrix} V_1 \\ V_2 \\ V_3 \end{bmatrix} = \begin{bmatrix} V_{XD} \\ V_{YD} \\ V_{ZD} \end{bmatrix} = \begin{matrix} V_\infty \cdot \sin\alpha_{a/c} \\ 0 \\ V_\infty \cdot \cos\alpha_{a/c} \end{matrix} \tag{B.1}$$

Whereas for a continuous, non-uniform distribution, all three are a function of radial and azimuthal position; $\vec{V_D} = f(r, \psi)$.

B.2 STRAIGHT, UNTWISTED BLADE AXES

For efficient calculation, these velocities are converted into the vector components normal to and parallel to the *straight*-bladed propeller chordline, which are dependent on azimuthal position. The radial component is not of use for the straight-bladed propeller, as spanwise-flow is assumed to have no contribution to sectional lift/drag. For the swept-bladed propeller, however, the radial component along the blade axis will have a component normal to the leading edge of the swept blade element. $\vec{V_B}$ is determined from transformation through the azimuthal position, ψ. With ψ defined as clockwise from the X-axis, at zero azimuth, the blade Y-axis is coincident with the Disc X-axis, whilst the blade X-axis is co-linear with the Disc Y-axis, but in the opposite direction. The transformation is independent of radial position, and a new angle $\zeta \triangleq \psi - \frac{\pi}{2}$ is defined.

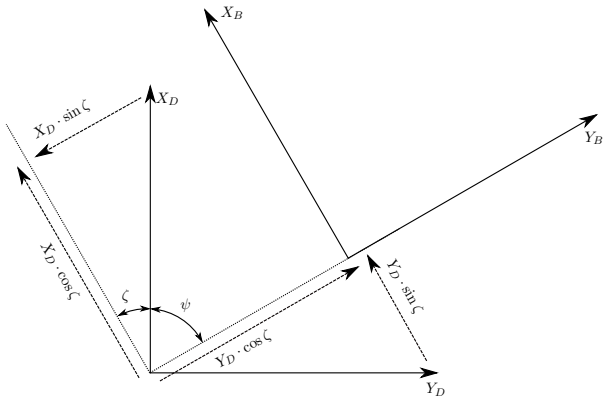

FIGURE B.2: DISC AXES TO BLADE AXES THROUGH ANGLE ψ.

$$\vec{R_B} = \begin{bmatrix} X_B \\ Y_B \\ Z_B \end{bmatrix} = \begin{bmatrix} \cos\zeta & \sin\zeta & 0 \\ -\sin\zeta & \cos\zeta & 0 \\ 0 & 0 & 1 \end{bmatrix} \cdot \begin{bmatrix} X_D \\ Y_D \\ Z_D \end{bmatrix} \tag{B.2}$$

And hence

$$\begin{aligned} \vec{V_B} &= \begin{bmatrix} V_{XB} \\ V_{YB} \\ V_{ZB} \end{bmatrix} \\ &= \begin{bmatrix} \cos\zeta & \sin\zeta & 0 \\ -\sin\zeta & \cos\zeta & 0 \\ 0 & 0 & 1 \end{bmatrix} \cdot \begin{bmatrix} V_{XD} \\ V_{YD} \\ V_{ZD} \end{bmatrix} \\ &= \begin{bmatrix} \sin\psi & -\cos\psi & 0 \\ \cos\psi & \sin\psi & 0 \\ 0 & 0 & 1 \end{bmatrix} \cdot \begin{bmatrix} V_{XD} \\ V_{YD} \\ V_{ZD} \end{bmatrix} \end{aligned}$$

For a straight blade, these velocities are enough to determine the sectional velocities from:

$$\begin{aligned} \phi &= \tan^{-1}\frac{V_N}{V_P} \\ V_R &= \sqrt{{V_N}^2 + {V_P}^2} \\ \alpha_R &= \beta(r) - \phi \end{aligned}$$

Which way then be used to determine $\frac{dC_l}{dr}$ and $\frac{dC_d}{dr}$ from either empirical formulae or from table lookup from experimental data (Korkan and Camba III, 1986).

B.3 SWEPT, UNTWISTED BLADE AXES

The first step that is taken before any axis transformation is made is to apply an azimuthal shift to the $\vec{V_B}$ matrices, based on the *effective azimuthal angle,* $\psi\prime$. When the blade is at azimuthal position ψ_i, based on the unswept blade axes, sections along the radius lie at different azimuthal positions. The difference, $\delta\psi$ is calculated, and a vector of azimuthal positions may be determined from $\psi\prime = \psi + \delta\psi$. The matrices $\vec{V}(r, \psi)$ may then be interpolated using a suitable interpolation scheme to find the velocities at each effective azimuthal position $\vec{V\prime} = \vec{V}(r, \psi\prime)$.

The new matrices of total velocity at the disc, $\vec{V\prime}$ are then used in each calculation and ensures that when the blade is at any azimuthal position, the correct velocities at any radial station are used.

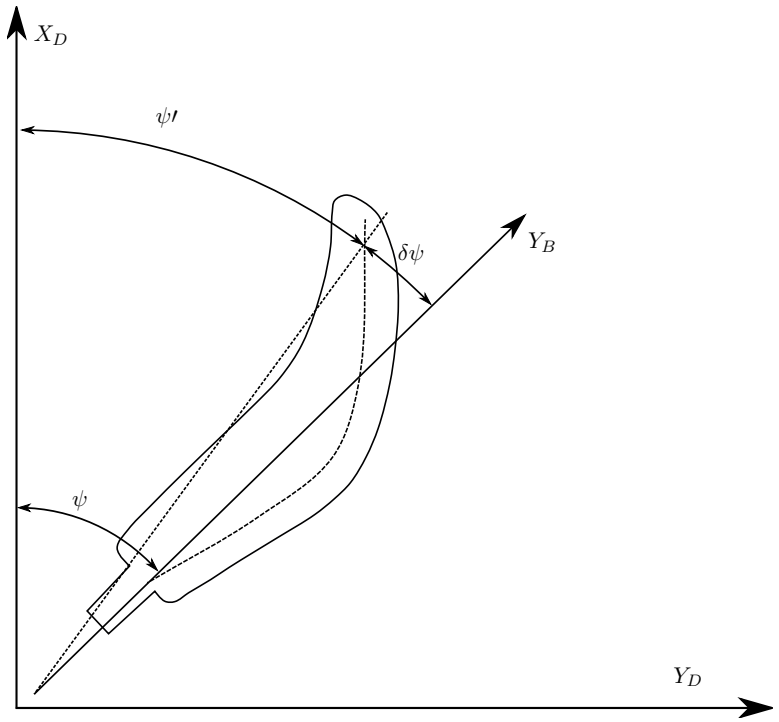

FIGURE B.3: EFFECTIVE AZIMUTHAL ANGLE - BLADE PLANFORM TAKEN FROM PROPELLER II FROM EVANS AND LINER (1951).

B.4 SWEPT, TWISTED BLADE ELEMENT AXES

The transformation matrices in this section are based on the definition of sweep and the conventions as laid out by Whitcomb (1948), which describes the construction of the curved formation line of a swept propeller blade based on sweep, Λ, and dihedral, κ, angles. Note that the nomenclature here differs from that used by Whitcomb to avoid confusion with other sections of this work.

The formation line lies along the centres of chords of blade sections, and its

geometry is based on incremental values of $\bar{z}$, parallel to the rotation axis, $\bar{x}$, in the lead/lag direction and θ, the angle between the radii to two points.

A new angle, μ, is defined as the angle between the chord of a section (which is defined as being normal to the radial line of a section), and a line through the midpoints of *all* the mid chord points, for the design condition angle.

$$\mu \triangleq \tan^{-1} \frac{\tan \kappa}{\tan \Lambda} \tag{B.3}$$

The incremental functions are defined:

$$\Delta \bar{z} = -\Delta r \frac{\tan \Lambda \sin(\beta - \mu)}{\cos \kappa} \tag{B.4}$$

$$\Delta \theta = \frac{\Delta \bar{x}}{r} = -\frac{\Delta r}{r} \frac{\tan \Lambda \cos(\beta - \mu)}{\cos \kappa} \tag{B.5}$$

The total displacement of a blade section is determined by summating the incremental values inboard of that section. Figure 4.2 shows the displacement of the semi-chord of a swept blade element section from the straight blade axes - note that the relationships used in the aerodynamic model are taken with respect to the quarter-chord, but the semi-chord is easier to display in this diagram.

With the total displacements for each section determined, the angular displacements of each blade element axis may be calculated:

$$\eta = \tan^{-1} \left(\frac{\bar{z}}{r} \right)$$

These angles, along with the local twist, $\beta_{tw}(r)$, are used to define an Euler transformation matrix from the unrotated, unswept blade axes to the swept blade element axes, and the sequence of rotations used is *root setting*, *out-of-plane rotation/flap*, *in-plane rotation or lead/lag*, *twist* - [A_0, η_i, θ_i, β_{twi}]. The angle θ_i defines the change to azimuthal position, $\delta\psi$ used to determine the azimuthal phase shift effected in the inflow matrices, discussed in section B.3.

The individual rotation matrices are:

$$[T]_{A_0} = \begin{bmatrix} \cos A_0 & 0 & \sin A_0 \\ 0 & 1 & 0 \\ -\sin A_0 & 0 & \cos A_0 \end{bmatrix}$$

$$[T]_{\eta_i} = \begin{bmatrix} 1 & 0 & 0 \\ 0 & \cos\eta & -\sin\eta \\ 0 & \sin\eta & \cos\eta \end{bmatrix}$$

$$[T]_{\theta_i} = \begin{bmatrix} \cos\theta & -\sin\eta & 0 \\ \sin\eta & \cos\eta & 0 \\ 0 & 0 & 1 \end{bmatrix}$$

$$[T]_{\beta_{twi}} = \begin{bmatrix} \cos\beta_{twi} & 0 & \sin\beta_{twi} \\ 0 & 1 & 0 \\ -\sin\beta_{twi} & 0 & \cos\beta_{twi} \end{bmatrix}$$

and total transformation matrices:

$$\vec{R}_{BE} = [T]_{A_0} \cdot [T]_{\eta_i} \cdot [T]_{\theta_i} \cdot [T]_{\beta_i} \cdot \vec{R_{BU}}$$

$$\vec{R}_{BE} = [T]_{tot} \cdot \vec{R_{BU}}$$

$$[T]_{tot} = \begin{bmatrix} T_t^{11} & T_t^{12} & T_t^{13} \\ T_t^{12} & T_t^{22} & T_t^{23} \\ T_t^{13} & T_t^{32} & T_t^{33} \end{bmatrix}$$

$$[T]_{tot}^{-1} = \begin{bmatrix} T_i^{11} & T_i^{12} & T_i^{13} \\ T_i^{12} & T_i^{22} & T_i^{23} \\ T_i^{13} & T_i^{32} & T_i^{33} \end{bmatrix}$$

where $[T]_{tot}$ components are:

$$T_t^{11} = \cos\beta_i(\cos A_0 \cos\theta_i + \sin A_0 \sin\eta_i \sin\theta_i) - \cos\eta_i \sin A_0 \sin\beta_i$$
$$T_t^{12} = \cos\theta_i \sin A_0 \sin\eta_i - \cos A_0 \sin\theta_i$$
$$T_t^{13} = \sin\beta_i(\cos A_0 \cos\theta_i + \sin A_0 \sin\eta_i \sin\theta_i) + \cos\eta_i \cos\beta_i \sin A_0$$

$$T_t^{21} = \sin\eta_i \sin\beta_i + \cos\eta_i \cos\beta_i \sin\theta_i$$
$$T_t^{22} = \cos\eta_i \cos\theta_i$$
$$T_t^{23} = \cos\eta_i \sin\beta_i \sin\theta_i - \cos\beta_i \sin\eta_i$$

$$T_t^{31} = -\cos\beta_i(\cos\theta_i \sin A_0 - \cos A_0 \sin\eta_i \sin\theta_i) - \cos A_0 \cos\eta_i \sin\beta_i$$
$$T_t^{32} = \sin A_0 \sin\theta_i + \cos A_0 \cos\theta_i \sin\eta_i$$
$$T_t^{33} = \cos A_0 \cos\eta_i \cos\beta_i - \sin\beta_i(\cos\theta_i \sin A_0 - \cos A_0 \sin\eta_i \sin\theta_i)$$

and $[T]_{tot}^{-1}$ components are:

$$
\begin{aligned}
T_i^{11} = {} & (\cos A_0 \cos\beta_i \cos\eta_i^2 \cos\theta_i - \sin A_0 \sin\beta_i \cos\eta_i \cos\theta_i^2 \cdots \\
& - \sin A_0 \sin\beta_i \cos\eta_i \sin\theta_i^2 + \cos A_0 \cos\beta_i \cos\theta_i \sin\eta_i^2 + \cos\beta_i \sin A_0 \sin\eta_i \sin\theta_i)/\cdots \\
& (\cos A_0^2 \cos\eta_i^2 \cos\beta_i^2 \cos\theta_i^2 + \cos A_0^2 \cos\eta_i^2 \cos\beta_i^2 \sin\theta_i^2 + \cos A_0^2 \cos\eta_i^2 \cos\theta_i^2 \sin\beta_i^2 + \cdots \\
& \cos A_0^2 \cos\eta_i^2 \sin\beta_i^2 \sin\theta_i^2 + \cos A_0^2 \cos\beta_i^2 \cos\theta_i^2 \sin\eta_i^2 + \cos A_0^2 \cos\beta_i^2 \sin\eta_i^2 \sin\theta_i^2 + \cdots \\
& \cos A_0^2 \cos\theta_i^2 \sin\eta_i^2 \sin\beta_i^2 + \cos A_0^2 \sin\eta_i^2 \sin\beta_i^2 \sin\theta_i^2 + \cos\eta_i^2 \cos\beta_i^2 \cos\theta_i^2 \sin A_0^2 + \cdots \\
& \cos\eta_i^2 \cos\beta_i^2 \sin A_0^2 \sin\theta_i^2 + \cos\eta_i^2 \cos\theta_i^2 \sin A_0^2 \sin\beta_i^2 + \cos\eta_i^2 \sin A_0^2 \sin\beta_i^2 \sin\theta_i^2 + \cdots \\
& \cos\beta_i^2 \cos\theta_i^2 \sin A_0^2 \sin\eta_i^2 + \cos\beta_i^2 \sin A_0^2 \sin\eta_i^2 \sin\theta_i^2 + \cos\theta_i^2 \sin A_0^2 \sin\eta_i^2 \sin\beta_i^2 + \cdots \\
& \sin A_0^2 \sin\eta_i^2 \sin\beta_i^2 \sin\theta_i^2) \\
T_i^{12} = {} & (\sin\eta_i \sin\beta_i \cos\theta_i^2 + \sin\eta_i \sin\beta_i \sin\theta_i^2 + \cos\eta_i \cos\beta_i \sin\theta_i)/\cdots \\
& (\cos\eta_i^2 \cos\beta_i^2 \cos\theta_i^2 + \cos\eta_i^2 \cos\beta_i^2 \sin\theta_i^2 + \cos\eta_i^2 \cos\theta_i^2 \sin\beta_i^2 + \cdots \\
& \cos\eta_i^2 \sin\beta_i^2 \sin\theta_i^2 + \cos\beta_i^2 \cos\theta_i^2 \sin\eta_i^2 + \cos\beta_i^2 \sin\eta_i^2 \sin\theta_i^2 + \cdots \\
& \cos\theta_i^2 \sin\eta_i^2 \sin\beta_i^2 + \sin\eta_i^2 \sin\beta_i^2 \sin\theta_i^2) \\
T_i^{13} = {} & -(\cos\beta_i \sin A_0 \cos\eta_i^2 \cos\theta_i + \cos A_0 \sin\beta_i \cos\eta_i \cos\theta_i^2 + \cdots \\
& \cos A_0 \sin\beta_i \cos\eta_i \sin\theta_i^2 + \cos\beta_i \sin A_0 \cos\theta_i \sin\eta_i^2 - \cos A_0 \cos\beta_i \sin\eta_i \sin\theta_i)/\cdots \\
& (\cos A_0^2 \cos\eta_i^2 \cos\beta_i^2 \cos\theta_i^2 + \cos A_0^2 \cos\eta_i^2 \cos\beta_i^2 \sin\theta_i^2 + \cos A_0^2 \cos\eta_i^2 \cos\theta_i^2 \sin\beta_i^2 + \cdots \\
& \cos A_0^2 \cos\eta_i^2 \sin\beta_i^2 \sin\theta_i^2 + \cos A_0^2 \cos\beta_i^2 \cos\theta_i^2 \sin\eta_i^2 + \cos A_0^2 \cos\beta_i^2 \sin\eta_i^2 \sin\theta_i^2 + \cdots \\
& \cos A_0^2 \cos\theta_i^2 \sin\eta_i^2 \sin\beta_i^2 + \cos A_0^2 \sin\eta_i^2 \sin\beta_i^2 \sin\theta_i^2 + \cos\eta_i^2 \cos\beta_i^2 \cos\theta_i^2 \sin A_0^2 + \cdots \\
& \cos\eta_i^2 \cos\beta_i^2 \sin A_0^2 \sin\theta_i^2 + \cos\eta_i^2 \cos\theta_i^2 \sin A_0^2 \sin\beta_i^2 + \cos\eta_i^2 \sin A_0^2 \sin\beta_i^2 \sin\theta_i^2 + \cdots \\
& \cos\beta_i^2 \cos\theta_i^2 \sin A_0^2 \sin\eta_i^2 + \cos\beta_i^2 \sin A_0^2 \sin\eta_i^2 \sin\theta_i^2 + \cos\theta_i^2 \sin A_0^2 \sin\eta_i^2 \sin\beta_i^2 + \cdots \\
& \sin A_0^2 \sin\eta_i^2 \sin\beta_i^2 \sin\theta_i^2)
\end{aligned}
$$

$$
\begin{aligned}
T_i^{21} = {} & -(\cos A_0 \sin\theta_i \cos\eta_i^2 + \cos A_0 \sin\theta_i \sin\eta_i^2 - \cos\theta_i \sin A_0 \sin\eta_i)/\cdots \\
& (\cos A_0^2 \cos\eta_i^2 \cos\theta_i^2 + \cos A_0^2 \cos\eta_i^2 \sin\theta_i^2 + \cos A_0^2 \cos\theta_i^2 \sin\eta_i^2 + \cdots \\
& \cos A_0^2 \sin\eta_i^2 \sin\theta_i^2 + \cos\eta_i^2 \cos\theta_i^2 \sin A_0^2 + \cos\eta_i^2 \sin A_0^2 \sin\theta_i^2 + \cdots \\
& \cos\theta_i^2 \sin A_0^2 \sin\eta_i^2 + \sin A_0^2 \sin\eta_i^2 \sin\theta_i^2) \\
T_i^{22} = {} & (\cos\eta_i \cos\theta_i)/(\cos\eta_i^2 \cos\theta_i^2 + \cos\eta_i^2 \sin\theta_i^2 + \cos\theta_i^2 \sin\eta_i^2 + \sin\eta_i^2 \sin\theta_i^2) \\
T_i^{23} = {} & (\sin A_0 \sin\theta_i \cos\eta_i^2 + \sin A_0 \sin\theta_i \sin\eta_i^2 + \cos A_0 \cos\theta_i \sin\eta_i)/\cdots \\
& (\cos A_0^2 \cos\eta_i^2 \cos\theta_i^2 + \cos A_0^2 \cos\eta_i^2 \sin\theta_i^2 + \cos A_0^2 \cos\theta_i^2 \sin\eta_i^2 + \cdots \\
& \cos A_0^2 \sin\eta_i^2 \sin\theta_i^2 + \cos\eta_i^2 \cos\theta_i^2 \sin A_0^2 + \cos\eta_i^2 \sin A_0^2 \sin\theta_i^2 + \cdots \\
& \cos\theta_i^2 \sin A_0^2 \sin\eta_i^2 + \sin A_0^2 \sin\eta_i^2 \sin\theta_i^2)
\end{aligned}
$$

$$
\begin{aligned}
T_i^{31} = {} & (\cos A_0 \sin \beta_i \cos \eta_i^2 \cos \theta_i + \cos \beta_i \sin A_0 \cos \eta_i \cos \theta_i^2 + \cos \beta_i \sin A_0 \cos \eta_i \sin \theta_i^2 + \cdots \\
& \cos A_0 \sin \beta_i \cos \theta_i \sin \eta_i^2 + \sin A_0 \sin \beta_i \sin \eta_i \sin \theta_i) / \cdots \\
& (\cos A_0^2 \cos \eta_i^2 \cos \beta_i^2 \cos \theta_i^2 + \cos A_0^2 \cos \eta_i^2 \cos \beta_i^2 \sin \theta_i^2 + \cos A_0^2 \cos \eta_i^2 \cos \theta_i^2 \sin \beta_i^2 + \cdots \\
& \cos A_0^2 \cos \eta_i^2 \sin \beta_i^2 \sin \theta_i^2 + \cos A_0^2 \cos \beta_i^2 \cos \theta_i^2 \sin \eta_i^2 + \cos A_0^2 \cos \beta_i^2 \sin \eta_i^2 \sin \theta_i^2 + \cdots \\
& \cos A_0^2 \cos \theta_i^2 \sin \eta_i^2 \sin \beta_i^2 + \cos A_0^2 \sin \eta_i^2 \sin \beta_i^2 \sin \theta_i^2 + \cos \eta_i^2 \cos \beta_i^2 \cos \theta_i^2 \sin A_0^2 + \cdots \\
& \cos \eta_i^2 \cos \beta_i^2 \sin A_0^2 \sin \theta_i^2 + \cos \eta_i^2 \cos \theta_i^2 \sin A_0^2 \sin \beta_i^2 + \cos \eta_i^2 \sin A_0^2 \sin \beta_i^2 \sin \theta_i^2 + \cdots \\
& \cos \beta_i^2 \cos \theta_i^2 \sin A_0^2 \sin \eta_i^2 + \cos \beta_i^2 \sin A_0^2 \sin \eta_i^2 \sin \theta_i^2 + \cos \theta_i^2 \sin A_0^2 \sin \eta_i^2 \sin \beta_i^2 + \cdots \\
& \sin A_0^2 \sin \eta_i^2 \sin \beta_i^2 \sin \theta_i^2) \\
T_i^{32} = {} & -(\cos \beta_i \sin \eta_i \cos \theta_i^2 + \cos \beta_i \sin \eta_i \sin \theta_i^2 - \cos \eta_i \sin \beta_i \sin \theta_i) / \cdots \\
& (\cos \eta_i^2 \cos \beta_i^2 \cos \theta_i^2 + \cos \eta_i^2 \cos \beta_i^2 \sin \theta_i^2 + \cos \eta_i^2 \cos \theta_i^2 \sin \beta_i^2 + \cdots \\
& \cos \eta_i^2 \sin \beta_i^2 \sin \theta_i^2 + \cos \beta_i^2 \cos \theta_i^2 \sin \eta_i^2 + \cos \beta_i^2 \sin \eta_i^2 \sin \theta_i^2 + \cdots \\
& \cos \theta_i^2 \sin \eta_i^2 \sin \beta_i^2 + \sin \eta_i^2 \sin \beta_i^2 \sin \theta_i^2) \\
T_i^{33} = {} & (-\sin A_0 \sin \beta_i \cos \eta_i^2 \cos \theta_i + \cos A_0 \cos \beta_i \cos \eta_i \cos \theta_i^2 + \cos A_0 \cos \beta_i \cos \eta_i \sin \theta_i^2 - \cdots \\
& \sin A_0 \sin \beta_i \cos \theta_i \sin \eta_i^2 + \cos A_0 \sin \beta_i \sin \eta_i \sin \theta_i) / (\cos A_0^2 \cos \eta_i^2 \cos \beta_i^2 \cos \theta_i^2 + \cdots \\
& \cos A_0^2 \cos \eta_i^2 \cos \beta_i^2 \sin \theta_i^2 + \cos A_0^2 \cos \eta_i^2 \cos \theta_i^2 \sin \beta_i^2 + \cos A_0^2 \cos \eta_i^2 \sin \beta_i^2 \sin \theta_i^2 + \cdots \\
& \cos A_0^2 \cos \beta_i^2 \cos \theta_i^2 \sin \eta_i^2 + \cos A_0^2 \cos \beta_i^2 \sin \eta_i^2 \sin \theta_i^2 + \cos A_0^2 \cos \theta_i^2 \sin \eta_i^2 \sin \beta_i^2 + \cdots \\
& \cos A_0^2 \sin \eta_i^2 \sin \beta_i^2 \sin \theta_i^2 + \cos \eta_i^2 \cos \beta_i^2 \cos \theta_i^2 \sin A_0^2 + \cos \eta_i^2 \cos \beta_i^2 \sin A_0^2 \sin \theta_i^2 + \cdots \\
& \cos \eta_i^2 \cos \theta_i^2 \sin A_0^2 \sin \beta_i^2 + \cos \eta_i^2 \sin A_0^2 \sin \beta_i^2 \sin \theta_i^2 + \cos \beta_i^2 \cos \theta_i^2 \sin A_0^2 \sin \eta_i^2 + \cdots \\
& \cos \beta_i^2 \sin A_0^2 \sin \eta_i^2 \sin \theta_i^2 + \cos \theta_i^2 \sin A_0^2 \sin \eta_i^2 \sin \beta_i^2 + \sin A_0^2 \sin \eta_i^2 \sin \beta_i^2 \sin \theta_i^2)
\end{aligned}
$$

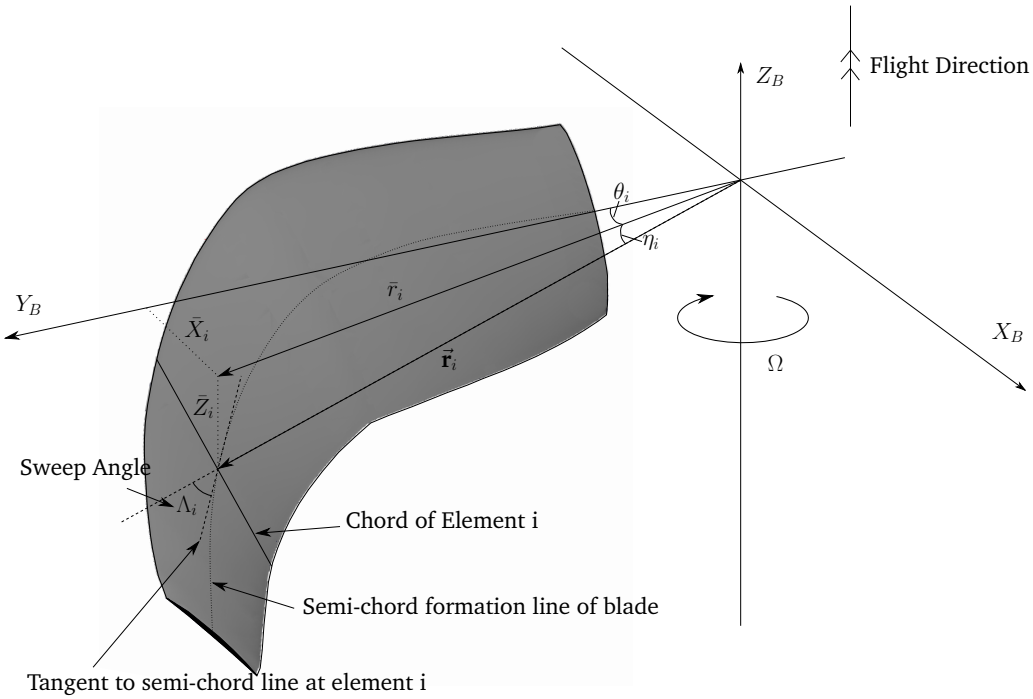

FIGURE B.4: DISPLACEMENT OF SWEPT BE SEMI-CHORD POSITION FROM BLADE AXES. *Note: This is a simplified diagram and does not show dihedral, κ.*

APPENDIX C

INSTALLATION MODEL

To determine the three-dimensional flowfield at the propeller disc plane, the model for determination of disc-plane upwash presented by Yaggy (1951)[1] has been extended to include the axial perturbation to incident flow. This component is determined by an axisymmetric potential method as shown in Katz and Plotkin (2001).

A vortex-lattice model (VLM) based on Katz and Plotkin (2001) is used for determination of the wing upwash, with a single spanwise row of horseshoe vortices at the wing quarter chord. Prediction of the incident flowfield at the propeller disc plane is by superposition of the contributions of the nacelle, fuselage and wing. The work of Roberts and Yaggy (1950) has been used to validate the potential model in isolation and the combined effect of nacelle, fuselage and wing. The geometry of the model is shown in Figure C.2, and the origin of the axes system is with X_I on the fuselage centreline, Y_I positive starboard at the position of the wing lead edge and Z_I positive upwards.

C.1 AXISYMMETRIC BODIES AT INCIDENCE

The flow around the spinner/nacelle and fuselage is based on superposition of the axial and transverse velocity solutions. The body is represented by a distribution of sources along the centerline, whose strength is determined the boundary condition of zero normal velocity at the body surface. Full derivation is provided by Katz and Plotkin (2001), but the final equations are given here. An axisymmetric body in a uniform freestream at an angle of incidence, γ, is shown in Figure C.1.

At position r, z, θ, the velocity components in the axial, radial and tangential

[1] Based on work of Von Kármán (1930), utilised in ESDU 90020 (Chappell, 2009).

direction, induced by the equivalent sources to the axisymmetric body are:

$$v_z(r,z) = \frac{V_Z}{4\pi}\int_0^l \frac{S'(Z)\cdot(z-Z)}{[(z-Z)^2+r^2]^{3/2}}\cdot dZ \tag{C.1}$$

$$v_r(r,z) = \frac{V_Z}{4\pi}\int_0^l \frac{S'(Z)\cdot r}{[(z-Z)^2+r^2]^{3/2}}\cdot dZ \tag{C.2}$$

$$v_\theta = \frac{V_X\cdot\sin\theta}{2r^2}\int_{\kappa_{Z=0}}^{\kappa_{Z=l}} R(Z)^2\sin\kappa d\kappa \tag{C.3}$$

where

$$S(Z) = \pi\cdot R^2(Z) \tag{C.4}$$

$$S'(Z) = 2\cdot\pi\cdot R(Z)\frac{dR(Z)}{dZ} \tag{C.5}$$

$$\kappa = \tan^{-1}\frac{r}{Z} \tag{C.6}$$

For the spinner/nacelle, conversion of v_r and v_θ involves a simple offset in ψ, whilst for the fuselage, disc points have to be given co-ordinates with respect to the centerline of the fuselage. For nacelle inclination angle, γ, Yaggy (1951) presented the upwash at the centreline of the propeller plane, defined as:

$$\epsilon \triangleq \tan^{-1}\frac{V_X + v_x}{V_Z} - \gamma \tag{C.7}$$

for a defined nacelle with a range of different spinners over $\gamma = 4, 8, 12, 16°$. Differences between different spinner geometries were minimal, and only results for the conical and conical faired spinner are presented in this dissertation as the hub geometry of the basic nacelle is unknown and without knowledge, determination of the in-plane velocity is guesswork. Figures C.3 and C.4 show the calculated upwash (eq C.7) at the centreline of the propeller disc (X_D in disc axes) vs measurements from Yaggy (1951). The 'nacelle model' results calculate the velocity

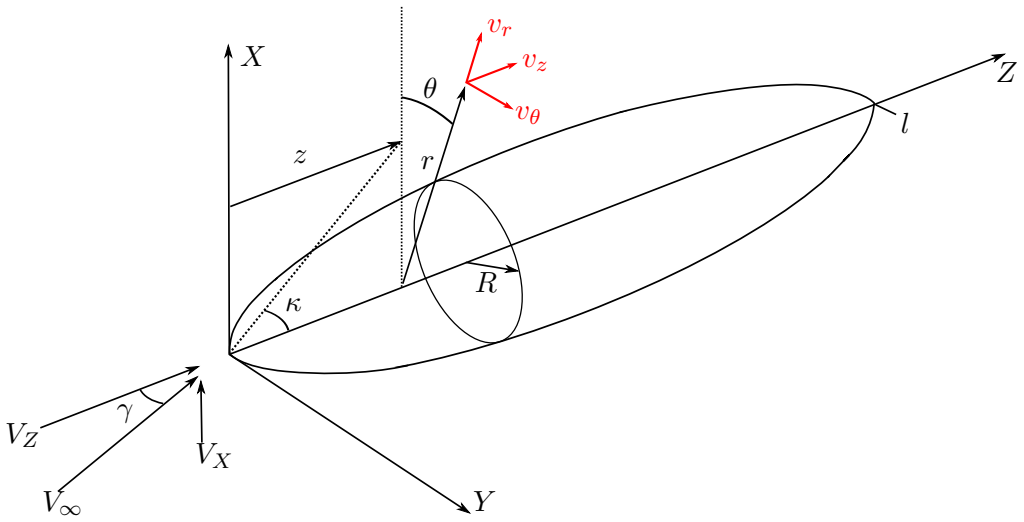

FIGURE C.1: CO-ORDINATE SYSTEM FOR AXISYMMETRIC BODY AT ANGLE OF INCIDENCE IN FREESTREAM.

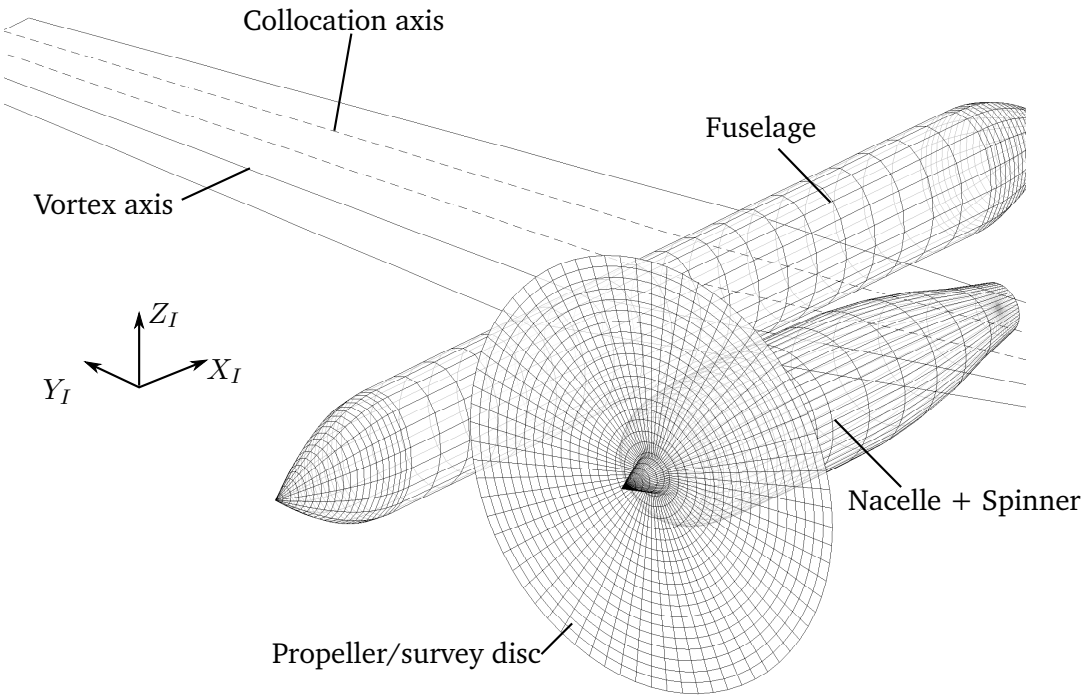

FIGURE C.2: INSTALLATION MODEL REPRESENTATION OF FIGHTER-TYPE AIRCRAFT FROM YAGGY (1951). *Note, origin of axis system is on fuselage centreline at* $X_O = X_{L.E.}$.

increment along the nacelle longitudinal axis, whilst Yaggy's method does not. Generally, good correlation is afforded over the range of inclination angles, with the inclusion of v_z in V_Z generally making for a better prediction - the increase to the upwash at the disc with Δv_z can be explained as the nacelle longitudinal axis is inclined by -2° with respect to the thrust axis, and part of v_z is in the disc plane. The difference between the two models is only small.

C.2 VALIDATION

The VLM model has shown excellent validation to experimental data in other sources, and will not be included here. Validation of the prediction of the upwash angle due to the entire aircraft via superposition of the potential and VLM model is shown in Figure C.5. Prediction of the upwash angle across the propeller disc is generally good, although slightly overestimated at close to the spinner. Since this model is used for determination of the possible effect of using an equivalent inclination angle vs. using a full incident flow field, the good first-order correlation is acceptable for this dissertation.

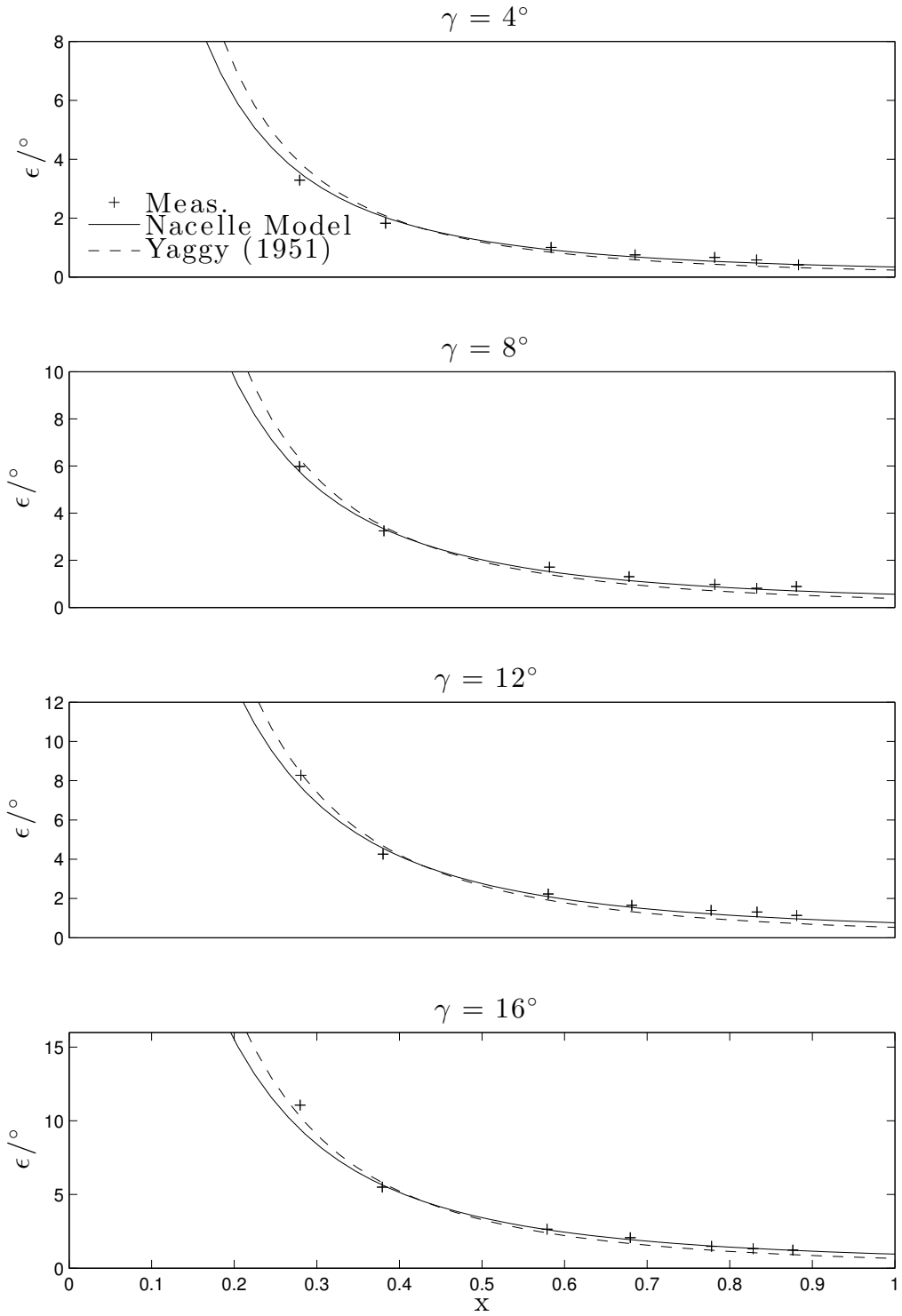

FIGURE C.3: VARIATION OF ϵ ALONG X_D VS. MEASUREMENTS FROM YAGGY (1951). CONICAL SPINNER.

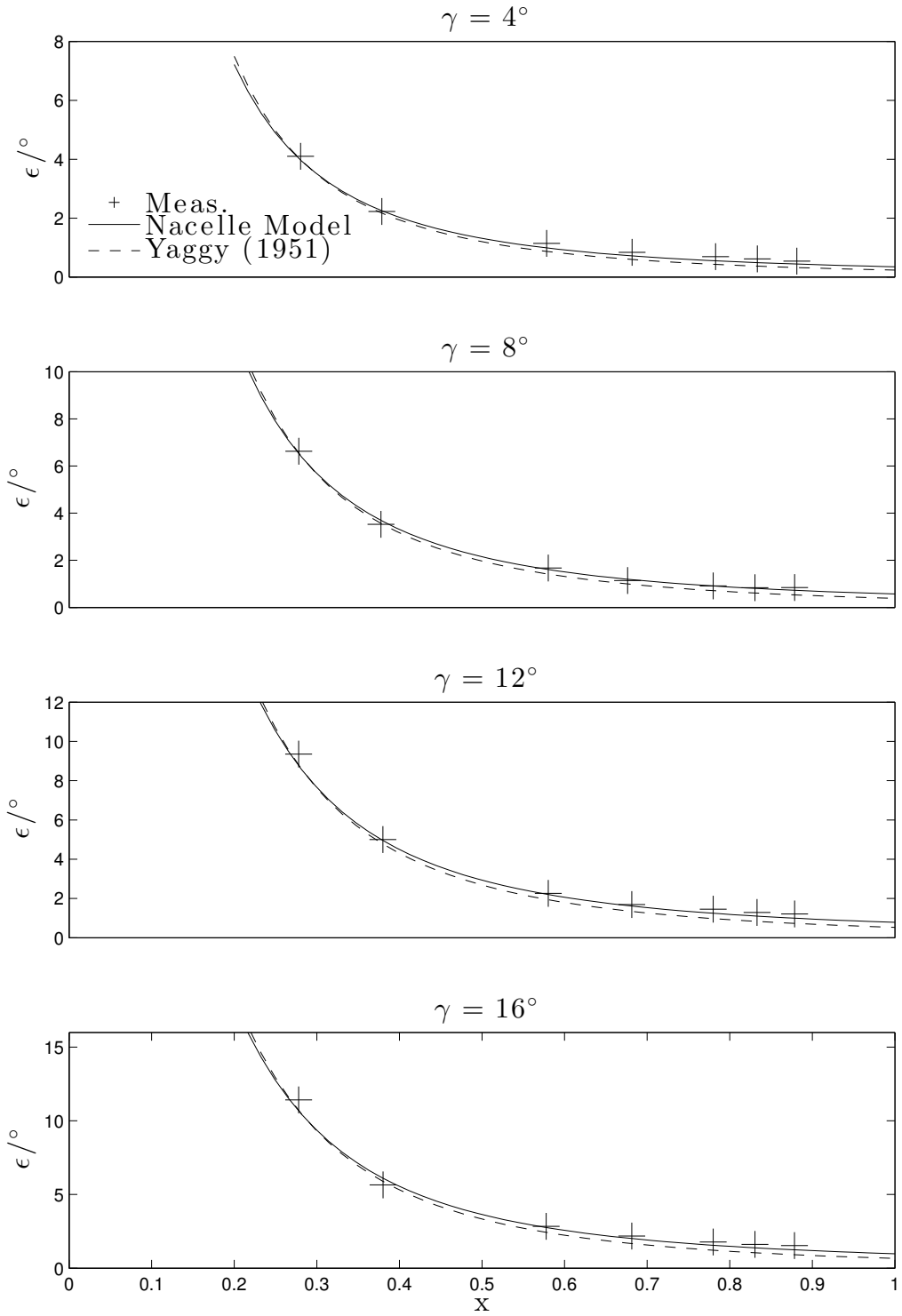

FIGURE C.4: VARIATION OF ϵ ALONG X_D VS. MEASUREMENTS FROM YAGGY (1951). CONICAL FAIRED SPINNER.

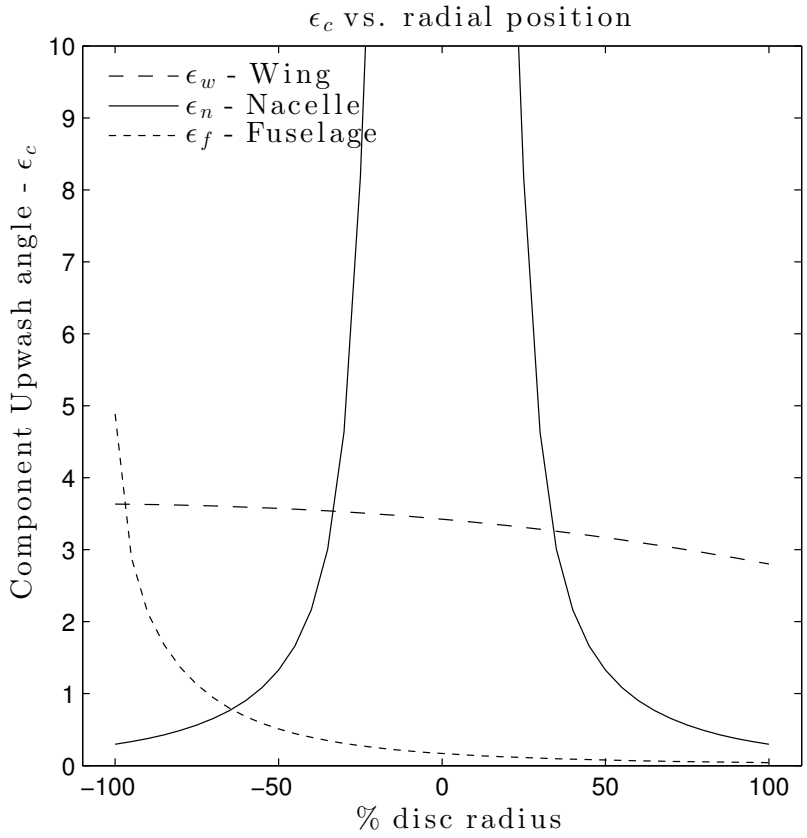

(A) UPWASH ANGLE DUE TO INDIVIDUAL COMPONENTS.

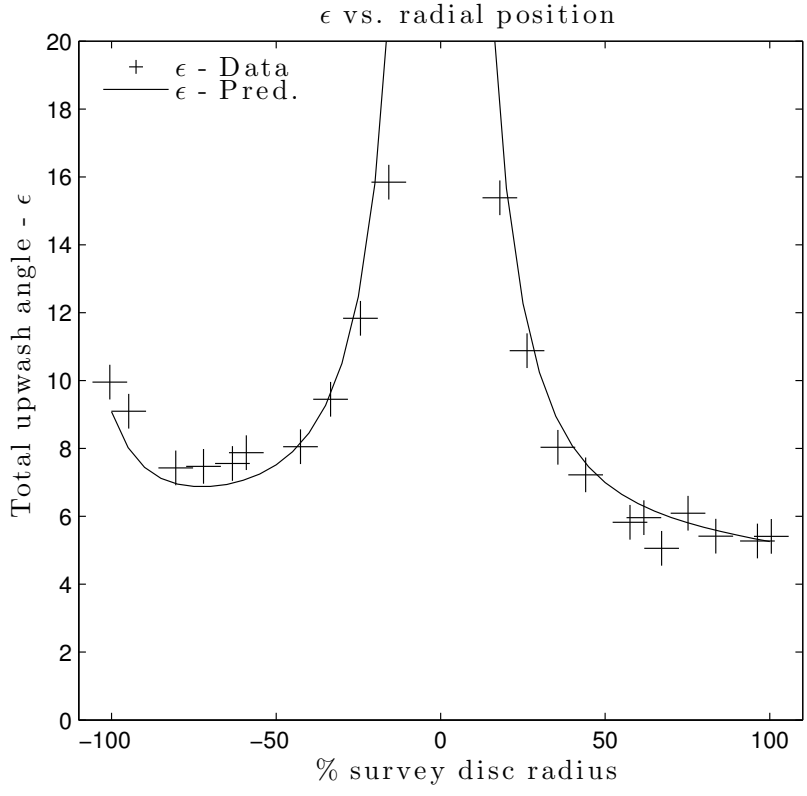

(B) UPWASH ANGLE DUE TO WHOLE AIRCRAFT VS. DATA FROM YAGGY (1951).

FIGURE C.5: UPWASH ANGLE AT DISC PLANE DUE TO COMBINED WING, FUSELAGE AND SPINNER/NACELLE. $\alpha_{A/C} = 10°$.